View metadata, citation and similar papers at core.ac.uk
brought to you by CORE
provided by EPub Bayreuth

New Carbazole Based Materials for Optoelectronic Applications

Dissertation

for the award of the academic degree of
Doctor of Natural Science (Dr. rer. nat.)
from the Faculty of Biology, Chemistry and Geosciences
University of Bayreuth

submitted by
Martin Sonntag
born in Hof / Saale

Bayreuth, 2006

Die vorliegende Arbeit wurde in der Zeit von Januar 2003 bis Juli 2006 am Lehrstuhl für Makromolekulare Chemie I der Universität Bayreuth angefertigt.

Vollständiger Abdruck der von der Fakultät für Biologie, Chemie und Geowissenschaften der Universität Bayreuth genehmigten Dissertation zur Erlangung des akademischen Grades Doktor der Naturwissenschaften (Dr. rer. Nat.)

Datum der Einreichung der Arbeit: 26.07.2006

Datum des wissenschaftlichen Kolloquiums: 13.11.2006

Prüfungsausschuß:

Vorsitzender:	*Prof. Dr. Hans-Werner Schmidt*
Erstgutachter:	*Prof. Dr. Peter Strohriegl*
Zweitgutachter:	*Prof. Dr. Karlheinz Seifert*
	Prof. Dr. Gerhard Platz

Für meine
lieben Eltern

„Je mehr wir können,
desto weniger dürfen wir.
Je weniger wir dürfen,
desto mehr müssen wir wissen.“

MANFRED EIGEN
dt. Chemiker und Nobelpreisträger
(geboren 1927)

Danksagung

Die vorliegende Doktorarbeit wurde unter der Anleitung von Herrn Prof. Dr. Peter Strohriegl, am Lehrstuhl für Makromolekulare Chemie I der Universität Bayreuth, angefertigt. Ihm gilt mein besonderer Dank für die interessante Themenstellung, die Möglichkeit der Teilnahme an internationalen Fachtagungen und vor allem für seine große Diskussionsbereitschaft.

Herrn Prof. Dr. Hans-Werner Schmidt danke ich für die Überlassung eines sehr gut ausgestatteten Laborplatzes an seinem Lehrstuhl.

Mein Dank gilt auch den Mitarbeitern der Philips Research Laboratories für die freundliche Aufnahme bei meinen zahlreichen Aufenthalten in Eindhoven. Ganz besonders hervorheben möchte ich dabei Dr. Dago de Leeuw und Dr. Sepas Setayesh für ihre unermüdliche Diskussionsbereitschaft und die Messung der Transistorcharakteristiken.

Für die hervorragende Zusammenarbeit im Rahmen des EUROFET/TMR-Programms der Europäischen Union möchte ich mich vor allem bei Dr. Thomas Anthopoulos (Philips Eindhoven), Juan Cabanillas-Gonzales (Polytecnico Milano), Jakub Mezyk (Universita Milano-Bicocca), und Kurt Pernstich (ETH Zürich) bedanken. Besonders hervorzuheben ist dabei Dr. Sigurt Schrader (TU Wildau) für die ausgezeichnete Organisation und Betreuung des Projekts.

Ich möchte mich bei allen Mitarbeitern des Lehrstuhls MC 1 bedanken, die durch ihre fachliche Unterstützung zum Gelingen dieser Arbeit beigetragen haben. Besonders hervorzuheben sind hierbei Dr. Klaus Kreger und Dr. Christian Neuber für ihre Hilfestellung bei der Lösung von Problemen jedweder Art. Ganz herzlich möchte ich mich vor allem bei denjenigen bedanken, die durch verschiedene Aktivitäten ein sehr angenehmes Arbeitsklima geschaffen haben und inzwischen zu guten Freunden geworden sind. Dabei sind vor allem Dr. Katja Fischer, Stefan Lindner, Frank Abraham, Nils Mohmeyer, Doris Hanft und Dr. Heiko Thiem zu nennen. Bei dieser Gelegenheit möchte ich meinen beiden Laborkollegen Esther Scheler und Michael Rothmann viel Erfolg bei der Erstellung ihrer Doktorarbeiten wünschen.

Für die finanzielle Unterstützung möchte ich mich bei dem Bundesministerium für Bildung und Forschung (BMBF), der Philips GmbH und der Merck KGaA im Rahmen des POLITAG Programms, sowie bei der Deutschen Forschungsgemeinschaft, Sonderforschungsbereich 481, bedanken.

Meinen Eltern möchte ich für ihre Unterstützung während des gesamten Studiums und der Anfertigung dieser Doktorarbeit ganz herzlich danken, da sie dies alles überhaupt erst ermöglicht haben.

Meiner Freundin Gabi danke ich für ihr großes Verständnis und ihre Geduld bei all den größeren und kleineren Problemen, die mir während meiner Promotion widerfahren sind.

List of Abbreviations

δ	chemical shift
λ	wavelength
ν	wave number [cm^{-1}]
a.u.	arbitrary unit
abs.	absolute
CV	cyclic voltammetry
DSC	differential scanning calorimetry
EL	electroluminescence
ETL	electron transport layer
eV	electronvolt
Fc	ferrocene
FTIR	Fourier-Transform-Infrared spectroscopy
HMDS	hexamethyldisilazane
HOMO	highest occupied molecular orbital
HTL	hole transport layer
HTM	hole transport material
ITO	Indium tin oxide
LUMO	lowest unoccupied molecular orbital
MPLC	medium pressure liquid chromatography
MS	mass spectrometrie
NMR	nuclear magnetic resonance
OFET	organic field-effect transistor
OLED	organic light emitting diode
PEDOT:PSS	poly(3,4-ethylenedioxythiophene) / polystyrene sulfonate
PL	photoluminescence
ppm	parts per million
PTC	phase transfer catalyst
RT	room temperature
SAXS	small angle X-ray scattering

SEC	size exclusion chromatography
$TBAPF_6$	tetrabutylammoniumhexafluorophosphate
T_g	glass transition temperature
TGA	thermogravimetric analysis
THF	tetrahydrofuran
T_m	melting point
UV/vis	ultraviolet/visible

Table of Contents

1. Introduction

1.1. Organic Electronics

For a long time it was a matter of fact that polymers and low molar mass organic materials do not conduct electricity. Therefore these materials were used as insulators in the electronic industry. This point of view changed in 1977 when Alan J. Heeger, Alan G. MacDiarmid and Hideki Shirakawa found that the conductivity of poly(acetylene) can be increased by eleven orders of magnitude when it is doped with halogens.[1, 2] For the discovery and development of conductive polymers they received the Nobel Prize for Chemistry in 2000.[3, 4] Since then the possibility of using organic semiconducting materials for applications in optoelectronics and the semiconductor industry has been of great scientific and technological interest.[5-7] Easy processability, i.e. from solution, large area coverage and the possibility to use flexible substrates make organic semiconductors ideal candidates for low cost electronic applications. During the last 15 years rapid progress took place in the field of materials development, device design, deposition processes and molecular modeling.[8] In the area of organic thin film devices very active research is going on spanning many subjects such as organic light emitting diodes (OLEDs)[9], organic field-effect transistors (OFETs)[10], sensors[11] and organic photovoltaics.[12]

Organic light emitting diodes have undergone the fastest development. Several companies have already brought consumer products based on OLED technology to the market. In 1998 Pioneer launched the first car radio with a monochrome OLED display. Already five years later Kodak introduced a digital camera featured with a full color active matrix OLED display. Today a variety of mobile phones and MP3 players with low resolution OLED panels are commercially available. All of the small displays that are available today are prepared by evaporation techniques. In Figure 1-1 a selection of commercial consumer electronics with organic light emitting diode displays is shown. An important advantage of these displays is the low power consumption, as no additional backlight is required for illumination of the screen. Furthermore there is no viewing angle dependence observed what is a known problem from flat screens based on common liquid crystal (LC) technology.

Figure 1-1. *Kodak digital camera with full color OLED display (left, www.kodak.com) and Sony mobile MP3 player with monochrome OLED display (right, www.sony.de).*

Recently Samsung and Epson announced new prototypes of full color OLED displays that are made from ink jet printed polymers.[13, 14] With a size of 40 inches these screens are the largest OLED devices up to now (Figure 1-2). The displays feature a brightness of about 600 cd/m^2 and a resolution of 1200x800 pixels. It is expected that a large scale production of such screens in a cost-effective manner can only be realized by solution process techniques, and that vacuum evaporation of the active materials would be too expensive.

Figure 1-2. *40 inch prototype OLED display from Samsung made from solution processed polymers.*[14]

At the moment further applications like white light emitting OLEDs as the next solid-state light source[15] and novel print heads for copiers and laser printers using an OLED as light source (Epson)[16] are developed. Most of the 15 million OLED panels sold in 2003 were used for mobile phone displays. One year later the sales figures were already twice as high.[17]
Although huge progress has been made in the are of organic electronics, all OLED devices that were produced so far are still driven by traditional Si-based backplanes and control electronics.[8] In the last years, Philips has made considerable progress in developing backplanes from organic semiconductors. In 2005 the company presented a prototype of a flexible display that is completely driven by organic field-effect transistors (OFETs). The so-called e-reader which is shown in Figure 1-3 (left) has a rollable display, is up to 5 inches large and has a resolution of 320x240 pixels (Q-VGA).

Figure 1-3. *E-reader with rollable display and Q-VGA resolution from Philips (left) and a design study of an organic RFID tag, prepared by roll-to-roll printing technique from PolyIC (right, www.polyic.com).*

Another interesting field of application for OFETs are so-called radio frequency identification (RFID) tags widely used in logistics and security applications. On such chips information can be stored and read out contactless with a wireless reading/writing device. The driving voltage for the RDIF tag is supplied by the radio waves form the reading/writing unit. The “smart label” receives the radio waves with its built in antenna and therefore does not require an internal power supply. Nowadays RFID tags are based on silicon circuits and hence are quite expensive. Prices of about 20 cents per tag make them still uneconomical for many applications. This problem could be solved with RFID tags based on organic semiconductors. Prices might drop below one cent per unit as the production costs are much lower in this case. Liquid phase techniques like roll-to-roll printing are developed in order to get access to a

cheap mass production of RFID tags.[18] Recently PolyIC has presented a pre-production line for roll-to-roll printing on flexible substrates.[19] Figure 1-3 (right) shows a transponder chip that was prepared by using this new printing technique. Organic RFID tags might be the price labels in the supermarket of the future and are able to replace the barcodes that are used today.

1.2. Organic field-effect transistors (OFETs)

The invention of the first “transistor” (transfer/resistor) in 1947 by John Bardeen, William Shockley and Walter Brattain revolutionized the whole electronic industry.[20] Since then Si-based electronic devices and their application in microelectronics started to dominate our everyday life. Charge carrier mobilities in field-effect transistors made from single crystalline silicon reach values up to 1500 cm^2/Vs.[21] Such high mobilities allow the production of highly integrated circuits requiring very little space. In a modern central processing unit (CPU) of a personal computer, 125 million transistors are accommodated in a volume of only 8 cm^3 The average distance between the single transistors is 65 nm.[22]

The first FET for which organic materials were used as semiconducting material was reported in 1986.[23] Although only low charge carrier mobilities of about 10^{-5} cm^2/Vs were achieved, a lot of research effort was put in the development of new materials and processing techniques.[24, 25] The possibility to use flexible substrates together with liquid phase deposition methods were the motivation for a number of ambitious research projects.[26, 27]

1.2.1. OFET device operation

In principle an OFET consists of three different electrodes: source, drain and gate. Ideally the source and drain contacts should behave as ohmic contacts for the majority carrier type in the organic semiconductor. These two contacts can be considered as one plate of a capacitor. The second capacitor plate is the so-called gate contact. These two capacitor plates are separated by an insulator layer. The semiconducting material is then deposited between the source and drain contacts. Between drain and gate different driving voltages can be applied whereas the source electrode is grounded.[28] The principle operation modes of an OFET are depicted in Figure 1-4. Usually organic FETs are primarily operated as accumulation mode enhancement transistors.

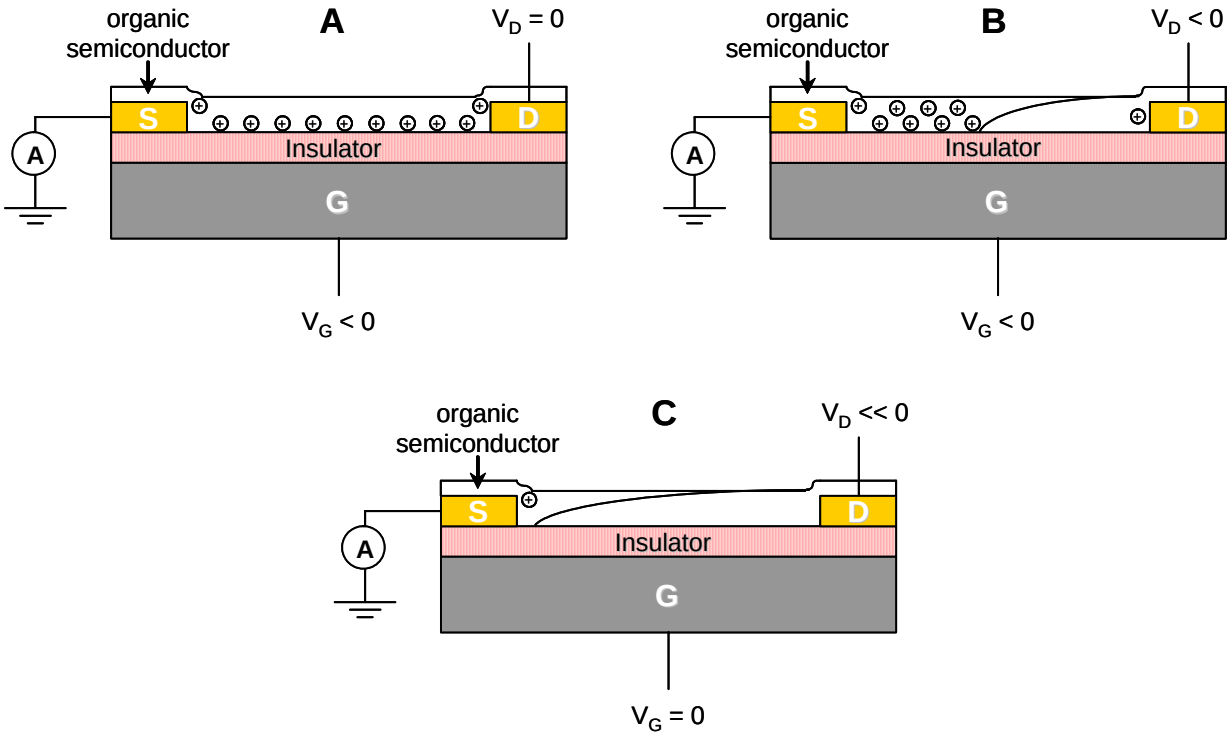

Figure 1-4. *Schematic operation modes of a organic field-effect transistor, using a p-type semiconducting material (from [28], modified).*

In the following paragraph the basic device operation of an OFET will be described for a p-type material, what means that the charge carriers are holes. This operating principle can be adopted for n-type semiconductors with electrons as charge carriers.

In Figure 1-4 A, a schematic of a transistor is shown where a negative gate bias but no drain voltage is applied. This leads to an increased concentration of positive charge carriers at the interface between insulator and semiconductor[28], and a conducting channel between the source and drain electrodes is formed.[29] The additional positive charges accumulated in this region are provided by the ohmic source and drain contacts. When a negative bias is applied to the gate as well as to the drain electrodes (Figure 1-4 B), the charge carriers start to move along the conducting channel. Now a current between source and drain can be measured with the electric field as driving force. If the drain voltage is increased, a depletion zone is formed at the drain electrode. At a sufficiently high drain voltage the depletion zone finally reaches the source electrode what results in saturation current between source and drain. That means that the transistor is driven in the saturation regime what is shown in Figure 1-4 C.

1.2.2. OFET characteristics

The operation modes that were described before can be measured and plotted in two different ways. If a gate voltage sweep is carried out and the source drain voltage is kept constant, a transfer characteristic of the FET device is obtained (Figure 1-5). In this case the source drain current is plotted versus the gate voltage. From this kind of evaluation the turn on voltage and the on/off-ratio of a transistor can be extracted. Turn on voltages of only a few volts are desired to be able to use batteries as power supply. This is essential when it comes to mobile electronic applications. For integrated circuits, high on/off-ratios of about 10^6 are required in order to distinguish between the on and off status of the transistor. If a gate sweep is carried out in two directions hysteresis effects of the device can be investigated. Hysteresis means that the source drain current of the backward sweep is lower that that from the forward sweep. This phenomenon gives information about the purity of the semiconducting material and reveals interface effects between semiconductor and insulator. Ideally, no or only little hysteresis effects should be observed. In this context it is important to mention that the charge carrier transport takes place in the conducting channel which is only a few monolayers thick.[30]

From the transfer characteristics, the field-effect mobility of the semiconducting material (μ_{FET}) can be calculated by Equation 1-1.[25]

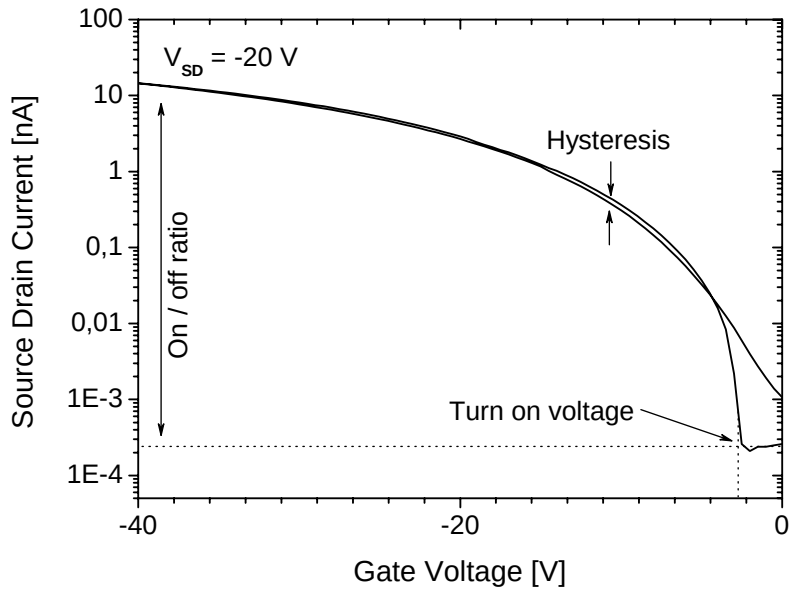

Figure 1-5. *Typical transfer characteristics of an organic FET: Gate voltage versus source drain current at a constant source drain bias with a star-shaped triphenylamine as semiconductor on a bottom gate FET substrate from Philips.*[31]

$$\mu_{FET} = \left(\frac{L}{W \cdot C \cdot V_D} \right) \frac{\partial I_{SD}}{\partial V_G}$$

Equation 1-1. *Calculation of the field-effect mobility (μ_{FET}). L is the channel length, W the channel width and C is the capacitance of the insulator per unit area. V_D is the drain voltage, I_{SD} the drain current and V_G is the gate voltage.*

In order to obtain the output characteristics of an organic FET, the source drain voltage is plotted versus the source drain current. The measurements are carried out with different (constant) gate voltages. Typical output characteristics are presented in Figure 1-6.

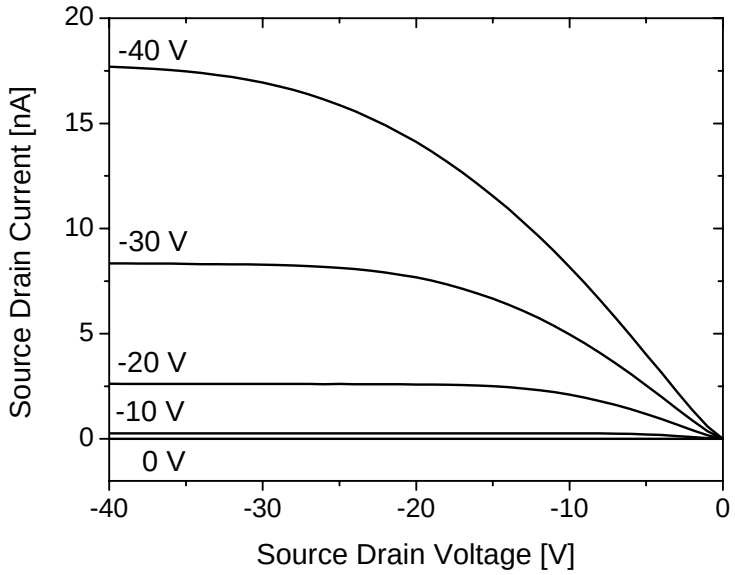

Figure 1-6. *Typical output characteristics of an organic FET at different gate voltages (0 V, -10 V, -20 V, -30 V, -40 V).*

The output characteristics can be divided in two different regimes. If the gate voltage is higher than the source drain bias, the device runs in the linear regime. In this region the source drain current should increase linearly. Otherwise the semiconducting material exhibits an ohmic contact resistance at the source drain electrodes. The saturation regime is reached as soon as the source drain voltage exceeds the gate voltage. At this point the source drain current becomes constant.[32] The characteristics shown in Figure 1-5 and Figure 1-6 were measured from a triphenylamine based molecular glass which is described in Paper 1.

1.2.3. OFET architectures

For the application of organic materials in FETs, two different device architectures were developed. The bottom gate OFET structure (Figure 1-7 left) is based on a heavily doped n^{++} silicon wafer that is used as gate contact. An insulating layer of silicon dioxide (200 nm) is thermally grown on top of the gate contact. Gold is evaporated and photolithographically patterned to form the source and drain contacts.[28] Finally the organic semiconductor is deposited, i.e. by spin-coating or drop casting, on top of the substrate. This kind of setup allows a quick and efficient material screening. The fact that the non-polar organic material is in direct contact with the highly polar SiO_2 insulator is a drawback of this device architecture. A variety of interface effects may occur due to the drastic change of polarity.[27, 33] In order to reduce the dipole-dipole interactions, different surface treatments can be applied to the SiO_2.[34] This technique will be described in detail in the following paragraph.

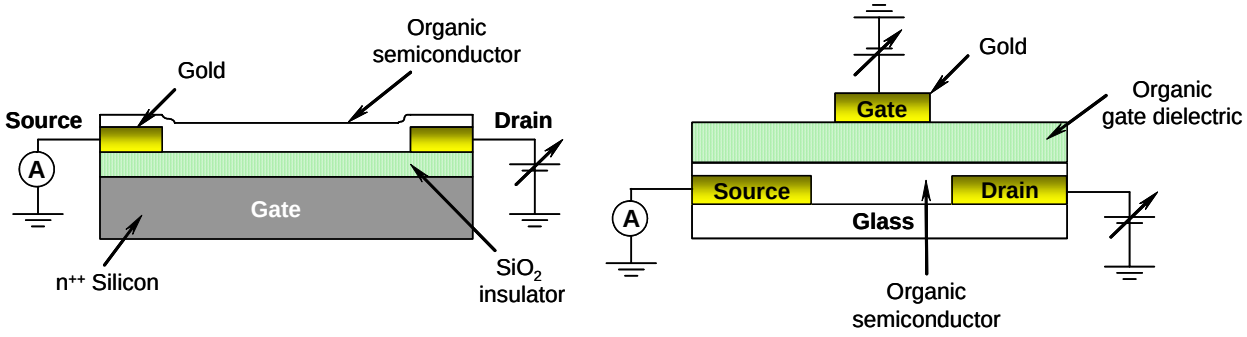

Figure 1-7. *Schematic of two different FET device architectures. Left: bottom gate setup, right: top gate architecture.*

Figure 1-7 (right) shows the so-called top gate device architecture. In this case an organic gate dielectric can be used. It is deposited on top of the semiconducting layer before the gate electrode is deposited by evaporating gold through a shadow mask. The preparation of these FET substrates is more complex and time consuming but a variety of different organic gate insulators can be utilized.[27, 35, 36] Furthermore the sensitive organic semiconductor is protected by the gate dielectric layer in this FET setup.

1.2.4. Materials for OFET applications

In the past years, intensive effort has been spent on developing new polymeric or low molar mass semiconducting materials with mobilities approaching the 1 cm^2/Vs of amorphous silicon.[25, 32] It turned out that such high mobilities, which are on the edge of band transport, can only be obtained from organic compounds that show a high degree of molecular order.[37, 38] Consequently, the highest charge carrier mobilities are obtained from single crystalline materials. Acenes like pentacene and rubrene have been investigated intensively during the last years (Figure 1-8). Purification and single crystal growth from these materials is the topic of many publications. With field-effect mobilities of about 15 cm^2/Vs, single crystalline rubrene has set the benchmark among organic semiconductors.[39] The second highest mobility value of about 5 cm^2/Vs was obtained from pentacene single crystals.[40] Although these acenes show excellent OFET performances, it is very unlikely that theses molecules will finally be used in organic electronics.[41, 42] In fact, the preparation of single crystals from soft organic materials is an expensive and painstaking process and not suitable for device production in a large scale. Furthermore the acenes are sensitive towards light and suffer from degradation when they are stored under ambient conditions.[43, 44]

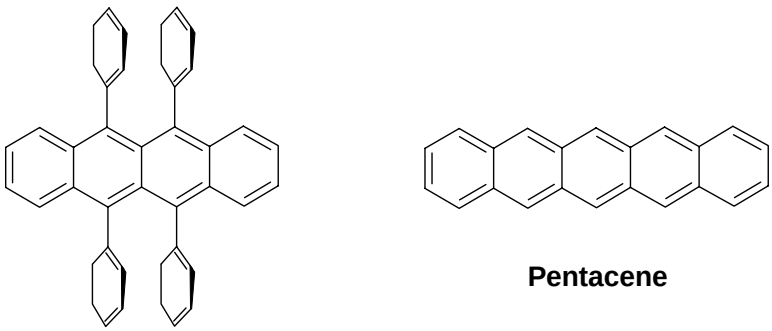

Figure 1-8. *Structures of acenes for high mobility single crystalline OFETs.*

Vacuum-deposition of small molecules offers a more simplified approach to prepare organic FETs exhibiting fairly high carrier mobilities. Especially with thiophene derivatives impressive improvements have been made. If sexithiophenes are evaporated, thin films with a polycrystalline order can be obtained. In the case of sexithiophene[45] (Figure 1-9), mobilities of $2x10^{-3}$ cm^2/Vs have been recorded.[46] If the sexithiophene core is substituted with hexyl

side chains (DH6T, Figure 1-9) field-effect mobilities up to 0.13 cm^2/Vs were reported.[47] The increased mobility of DH6T can be explained by an improved packing of the single molecules what leads to a smaller intermolecular distance.

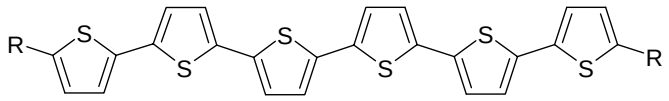

6T (R = H)
DH6T (R = C_6H_{13})

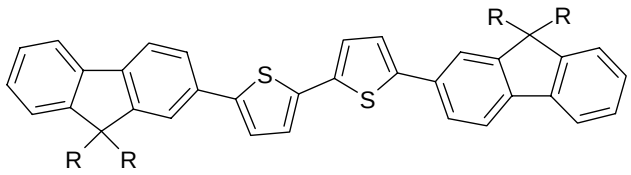

FTTF (R = H)
DHFTTF (R = C_6H_{13})

Figure 1-9. *Structure of thiophene based materials for OFET applications. Above: sexithiophene (6T) and α,ϖ-dihexylsexithiophene (DH6T). Below: 5,5'-bis-(9H-fluoren-2-yl)-2,2'-bithiophene (FTTF) and 5,5'-bis-(7-hexyl-9H-fluoren-2-yl)-2,2'-bithiophene (DHFTTF)*

Bao et al have reached field-effect mobilities of $2x10^{-2}cm^2/Vs$[48] by vacuum depositing a polycrystalline layer of a bithiophene which is substituted with two fluorene units (FTTF, Figure 1-9).[49] By introducing hexyl chains to the fluorene side groups in the 7-positions (DHFTTF, Figure 1-9) the mobility was increased up to 0.14 cm^2/Vs due to a closer packing of the core molecules.[41]

All the low molar mass compounds that were mentioned before can only be processed by vacuum deposition, what makes large scale device fabrication ineffective. For this reason liquid phase processing is the key to low price organic electronics. One possible approach to reach this target is the usage of polymeric compounds. Today, poly(3-hexylthiophene) (P3HT, Figure 1-10) is one of the best investigated polymers concerning its performance in organic FETs.[50, 51] Thin films of regioregular P3HT exhibit a highly microcrystalline and anisotropic lamellar morphology what leads to two-dimensional conjugated layers with strong π-π interchain interactions. These thiophene layers are separated from each other by the alkyl side chains which act as a kind of insulating layer. This microstructure allows a fast in-plane charge transport.[52] The charge carrier mobility of P3HT strongly depends on the degree of regioregularity. P3HT with a head-to-tail regioregularity of 81% shows mobilities of about

$2x10^{-4}$ cm^2/Vs whereas 0.1-0.3 cm^2/Vs can be obtained if the regioregularity is increased to 96%.[52] Big disadvantages of these thiophene based materials are a poor photostability and the high sensitivity towards oxygen.[53] Exposure to sunlight in the presence of air causes formation of carbonyl defects in the polymer with an associated loss of conjugation and mobility.[54]

A step towards higher environmental stability of thiophene based materials was made by Koezuka et al who have prepared poly(thiophenevinylene) (PTV, Figure 1-10) from which mobility values of 0.22 cm^2/Vs were obtained.[55] McCulloch et al reached 0.15 cm^2/Vs together with a reasonable atmospheric stability from poly(2,5-bis(3-decylthiophen-2yl)-thieno-[2,3-b]thiophene (PTT, Figure 1-10).[56]

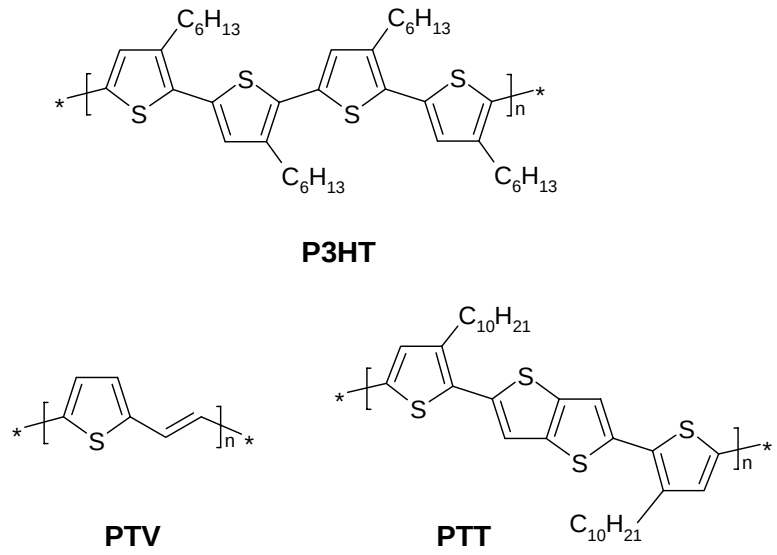

Figure 1-10. *Chemical structures of thiophene based polymers: poly(3-hexylthiophene) (P3HT), poly(thiophenevinylene) (PTV) and poly(2,5-bis(3-decylthiophen-2yl)-thieno-[2,3-b]thiophene (PTT).*

An alternative approach to obtain highly ordered thin films are large monodomains formed by liquid crystals (LC). The molecules can be aligned in the LC-phase at elevated temperatures. The orientation is then frozen in either by quenching the LC-phase to room temperature or by photopolymerization of liquid crystalline compounds with photoreactive endgroups, which are known as reactive mesogens (RM). A well-established liquid crystalline material from which good charge carrier mobilities can be obtained is poly-(9,9'-dioctylfluoren-2-yl)-co-bithiophene (F8T2, Figure 1-11). Sirringhaus et al have shown mobilities of about 0.01 cm^2/Vs from solution processed F8T2. Alignment of the F8T2 molecules was carried out

in the nematic phase above 265 °C on rubbed polyimide perpendicular to the FET electrodes. The orientation was frozen in by quenching the substrate to room temperature.[57] In such supercooled LC-phases the orientation will fade over the time what is a drawback concerning field-effect mobilities. Broer et al were the first to solve this problem. They introduced photopolymerizable endgroups to the LC-core molecule in order to fix the orientation of the mesophase by chemically crosslinking the mesogens.[58] With this reactive mesogen approach the group of McCulloch reached mobilities of $4x10^{-4}$ cm^2/Vs after photopolymerizing the methacrylate endgroups of a quaterthiophene derivative (quarterthiophene RM)[59] which is shown in Figure 1-11.

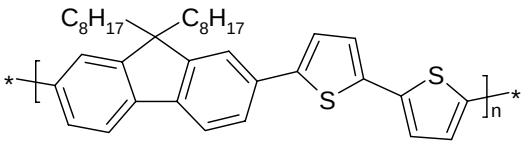

F8T2

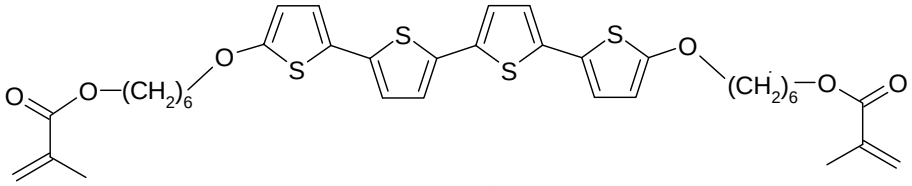

Quarterthiophene RM

Figure 1-11. *Chemical structures of poly-(9,9'-dioctylfluoren-2-yl)-co-bithiophene (F8T2) and the reactive mesogen with photocrosslinkable endgroups 2-methacrylic acid 6-{5'''-[5-(2-methylacryloyloxy)hexyloxymethyl][2,2';5',2'';5'',2''']-quarterthiophen-5-yl-ethoxy}hexyl ester (quarterthiophene RM).*

The introduction of aromatic amines as active material in OFETs was an important step towards environmental stability. Compounds like poly-(triarylamine) (PTAA, Figure 1-12) do not suffer from atmospheric degradation and are not sensitive towards moisture. Due to vitrification they exhibit excellent film forming properties when they are processed from solution. The drawback of the amorphous state is a decrease of the hole mobility due to the isotropic behaviour of the material. By using organic dielectric layers with low polarities, charge carrier mobilities up to 10^{-2} cm^2/Vs could be reached in PTAA transistors.[27]

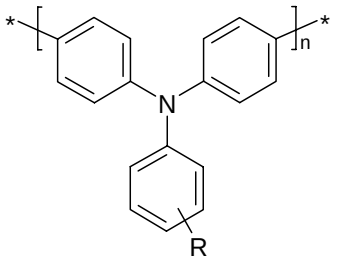

PTAA

Figure 1-12. *Chemical structure of a glass forming poly-(triphenylamine) derivative (PTAA).*

1.3. Organic light emitting diodes (OLEDs)

1.3.1. Electroluminescence

The emission of electromagnetic radiation in the UV, visible and infrared region is called luminescence. The different kinds of luminescence can be distinguished by different ways of excitation. If a material is excited optically, an electron from the highest occupied molecular orbital (HOMO, S_0) is excited to the lowest unoccupied molecular orbital (LUMO, S_1). The excited electron rapidly relaxes to the vibrational ground state. Under emission of light the excited electron returns to the S_0 state again. Due to an energy loss in the excited state, the wavelength of the emitted light is longer than the absorption wavelength. The principle of photoluminescence (PL) is shown in the Jablonski diagram (Figure 1-13).

Applying a voltage to an organic semiconducting material is another possibility to obtain luminescence. This kind of light generation is called electroluminescence (EL) and was discovered by Pope[60] (1963) and Helfrich et al[61] (1965). An emission of blue light was observed by applying voltages around 400 V to an anthracene single crystal. Since Tang and van Slyke found electroluminescence from a thin, evaporated two layer OLED consisting of tris(8-hydroxyquinoline)aluminium (AlQ_3, Figure 1-18) and an aromatic amine in 1987, huge progress was made in this area of research. At that time Tang et al used a stable Mg/Al alloy as cathode and reached a brightness of 1000 Cd/m^2 at low operating voltages of about 10 V.[62]

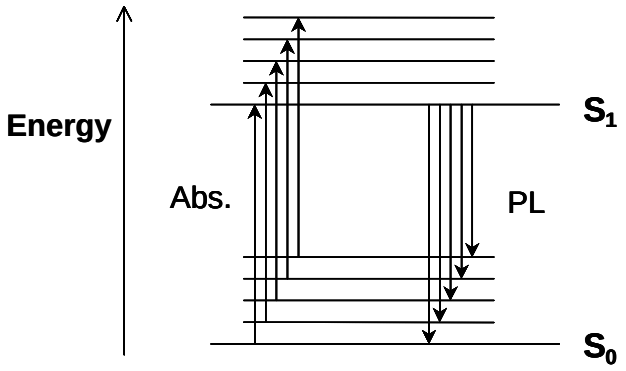

Figure 1-13. *Term scheme of optical excitation and photoluminescence (Jablonski diagram).*

1.3.2. Principle of organic LEDs

A single layer device architecture is the simplest OLED structure. In this case the organic emitter is deposited between two metal electrodes. In a single layer setup the organic semiconductor acts as emitter and charge transport material (holes and electrons) at the same time. As material for the anode indium-tin-oxide (ITO) is used in most cases. A thin, semitransparent ITO layer is sputtered onto a glass substrate. Afterwards, the emitting layer is deposited either by liquid phase or evaporation techniques onto the ITO anode. Finally, an electropositive metal like Al, Ca and Mg is evaporated on top of the OLED substrate as cathode. A suitable cathode material has a low work function in order to ensure efficient electron injection into the organic semiconductor. A typical single layer OLED setup is shown in Figure 1-14.

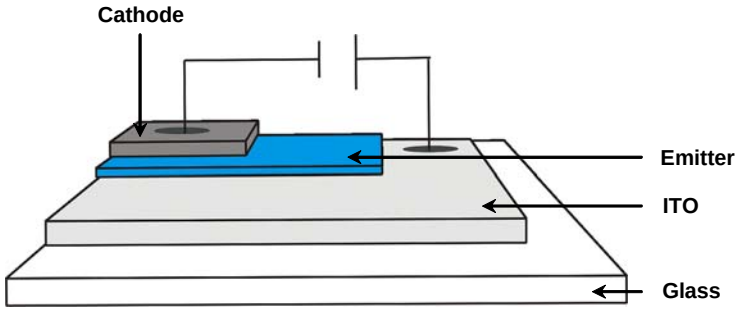

Figure 1-14. *Schematic of a single layer OLED setup.*

If a voltage is applied to the electrodes of an OLED device as depicted in Figure 1-14, electrons from the cathode and holes from the anode are injected into the organic

semiconductor. Due to the electric field between the two electrodes, the positive and negative charge carriers move through the organic layer. As soon as they recombine in the emitting material, light is generated. The energy level diagram of a single layer organic LED is shown in Figure 1-15.

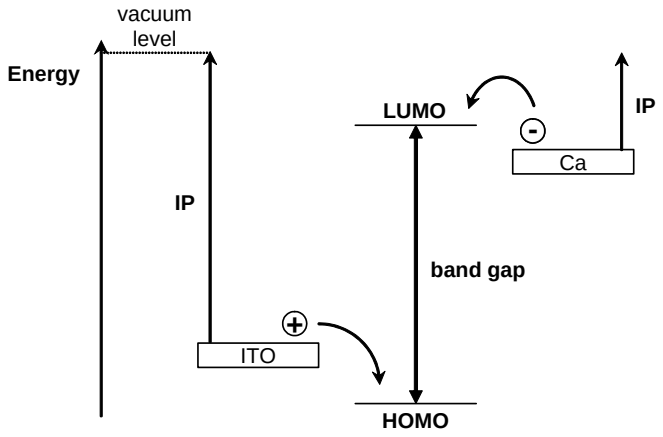

Figure 1-15. *Energy level diagram of a single layer OLED device architecture.*

The efficiency of an OLED is determined by the number of charge carriers that are injected and the number of holes and electrons that actually recombine under emission of light. The materials used in single layer devices are usually better hole than electron conductors.[63] As the holes are moving faster through the emitting layer than the electrons, the recombination zone is shifted towards the cathode what usually leads to a non-radiative loss of energy.[64] Consequently, the efficiency of the device decreases.[65]

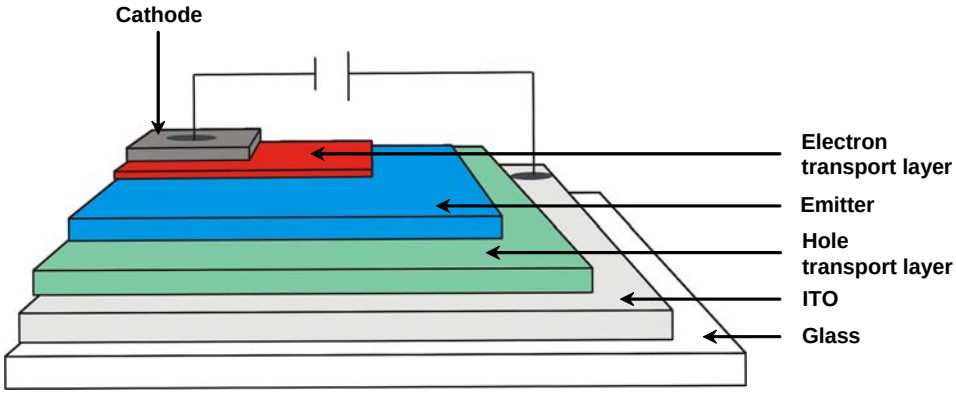

Figure 1-16. *Schematic of a multi layer OLED setup.*

In order to improve device efficiency, the multi layer OLED architecture was introduced which is shown in Figure 1-16. Additional hole (HTL) and electron transport layers (ETL) are introduced in order to balance the different charge carrier mobilities. By varying transport properties and thickness of those supporting layers, the recombination zone can be shifted towards the emission layer.

The advantages concerning a multi layer device setup, is the possibility to adapt the HOMO and LUMO levels of the used materials. A good overlap of the corresponding energy levels is essential to obtain a maximum carrier injection into the different layers.[63]

1.3.3. Materials for OLED applications

Active materials in OLEDs have to fulfil a variety of requirements. First of all they have to emit light with suitable color coordinates of the CIE-system (Commission International de L' Eclairage) and have to ensure a sufficient transport of charge carriers. A good chemical and electrochemical stability as well as a high thermal stability are also important prerequisites for OLED materials.[66, 67] Furthermore the compounds should exhibit good film forming properties. Crystallization of the thin films may lead to a decrease of charge carrier mobilities and finally to a short in the device.[68, 69] For this issue small molecules with bulky side groups are well suited. From low molar mass compounds homogeneous thin films can be prepared by vacuum deposition. As the bulky substituents prevent crystallization, molecular glasses are formed by these non-polymeric compounds.[70] Materials used as HTL have to exhibit HOMO levels in the order of -5.3 eV and therefore low ionization potentials. Aromatic amines like NPB, CBP and TCTA (Figure 1-17) are typical hole conductor materials for OLED applications.[71]

Substances used for electron transport are often metal complexes like AlQ_3 and BAlQ[72] or electron poor heterocycles like BPhen[73] (Figure 1-18).

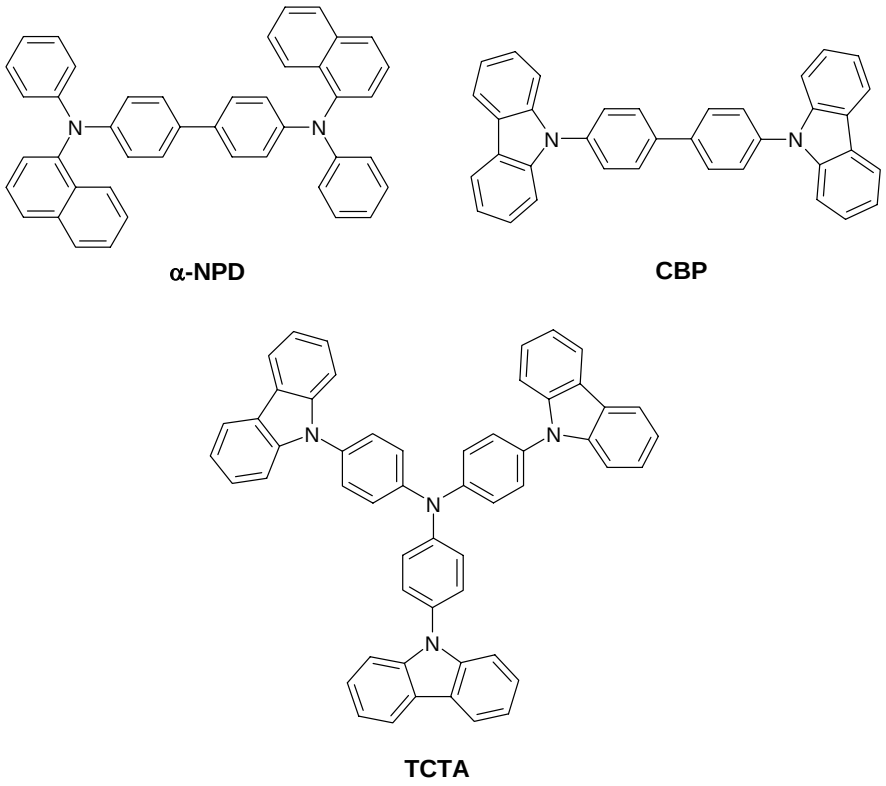

Figure 1-17. *Typical aromatic amines that are used for hole transport in OLED devices: N,N'-di(naphthalen-1-yl)-N,N'-diphenyl-biphenyl-4,4'-diamine (α-NPD), bis-(4-carbazol-9-yl)-biphenyl (CBP) and tris-(4-carbazol-9-yl-phenyl)-amine (TCTA).*

In 1990 the group of Richard Friend was the first who used a conjugated polymer as emitter in a solution processed single layer OLED.[74] As the highly fluorescent poly(p-phenylene-vinylene) (PPV, Figure 1-19) is insoluble, they had to work with a precursor material which was converted into PPV by a thermal treatment. A few years later soluble PPV derivatives like MEH-PPV[75] and OC_1C_{10}-PPV were developed (Figure 1-19). By the introduction of different alkoxy substituents the solubility of the new polymers could be increased. It turned out that the emission color of the polymeric materials can also be influenced by the side chain substitution pattern. PPV for example is a green emitter, whereas with MEH-PPV orange light can be generated. OC_1C_{10}-PPV emits red light.

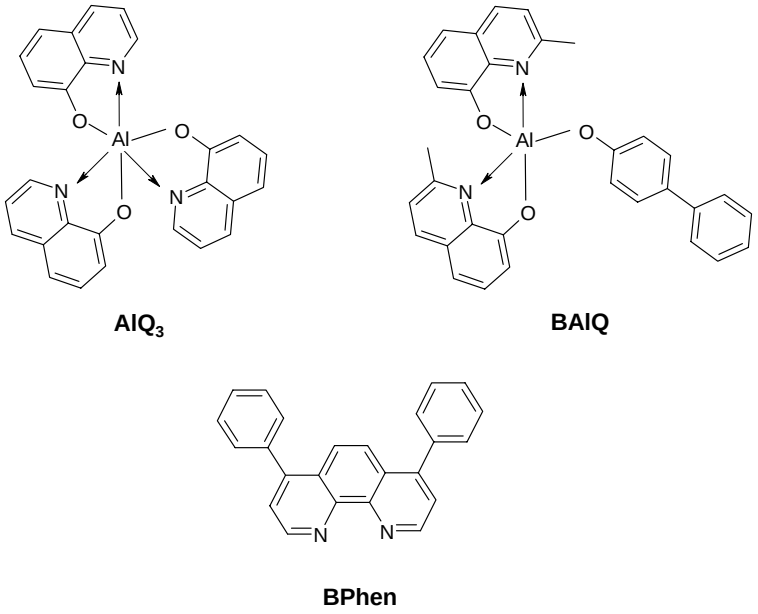

Figure 1-18. *Typical examples for ETL materials: tris(8-hydroxyquinoline) aluminium (AlQ_3), bis-(2-dimethyl-8 quinoxalato)-4-(phenyl-phenoxalto) aluminium(III) (BAlQ) and 4,7-Diphenyl-[1,10]phenanthroline (BPhen).*

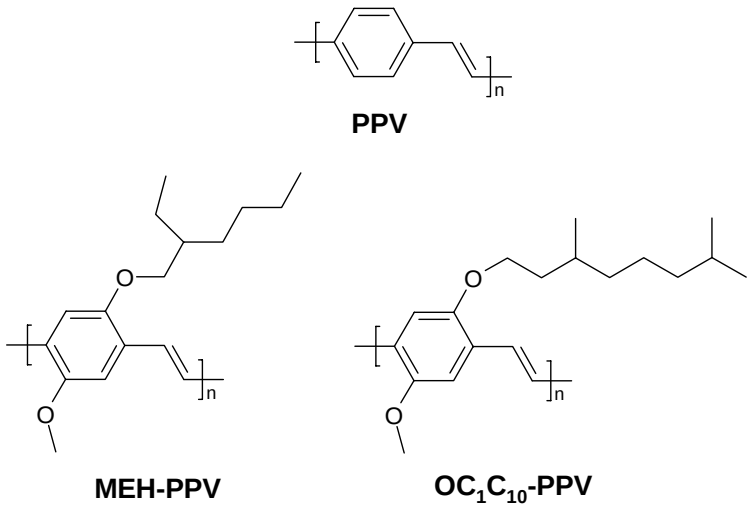

Figure 1-19. *Chemical structure of PPV and its soluble derivatives.*

For the emission of blue light, materials with a large energy gap between HOMO and LUMO level are required. Today, 9,9-dialkylated polyfluorenes[76] and so-called ladder-type polymers (LPPP)[77] which are also based on fluorene chromophores, are frequently used as blue emitters. The chemical structures of these polymers are shown in Figure 1-20.

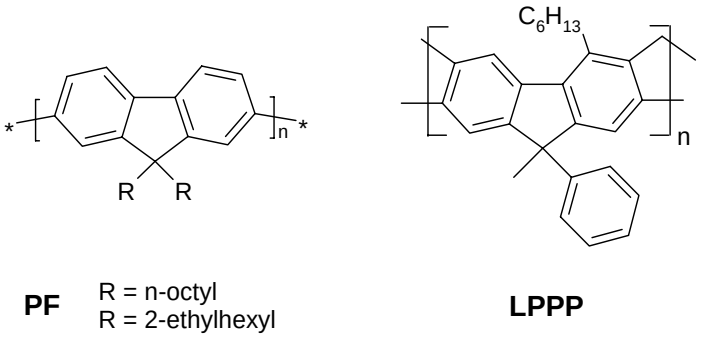

Figure 1-20. *Chemical structures of fluorene based blue light emitting polymers for OLED applications: 9,9-dialkylated poly(2,7-fluorene) (PF) and ladder-type poly(p-phenylene) (LPPP).*

Due to the large energy gap between HOMO and LUMO level in blue emitters, the long term stability of blue OLED devices is still a serious problem.

2. Aim of the thesis

In recent years the development of novel organic semiconductors for optoelectronic applications has attracted a lot of interest both in industry and academics. Especially in the area of organic field-effect transistors (OFETs) and organic light emitting diodes (OLEDs) huge progress has been made. One of the main technological attractions of organic electronics is that the active layers can be deposited at low temperatures by liquid phase techniques. This makes organic semiconductors ideal candidates for low-cost, large-area electronic applications on flexible substrates.[7, 78]

Among the large number of materials investigated, single crystals from fused aromatics like pentacene and rubrene exhibit the highest charge carrier mobilities that have been recorded so far.[25, 39] As these materials suffer from rapid atmospheric degradation and sensitivity to daylight, it is very unlikely that they will be used on a large scale in organic electronics.[41, 42] Therefore, novel organic semiconductors combining high environmental stability, easy processability and appropriate charge carrier mobilities are still a challenge.

The key parameters that describe the performance of an OLED display are efficiency, color and lifetime.[79] While red and green OLEDs with adequately long lifetimes have been developed for some consumer electronic products, the lifetime of blue OLEDs is still much shorter. The development of a stable blue emitter for OLED applications with a high efficiency is still a key issue in the area of material research.

This thesis addresses two different research issues in the field of organic electronics. New materials based on aromatic amines for OFET and OLED applications are described in this work. First of all aromatic amines with a star-shaped architecture were synthesized and characterized. Their performance as organic p-type semiconductor in OFETs is reported as well as the preparation and optimization of the FET devices. Furthermore a series of novel fused aromatics with carbazole units was prepared. These so-called bisindenocarbazoles were successfully tested as blue emitter in OLEDs. By introducing aromatic side groups to the core molecule, a liquid crystalline derivative was obtained. The influence of these different molecular architectures on morphology, electrochemical stability, HOMO/LUMO levels, thermal and optical properties of the materials will be discussed in detail.

2.1. Aromatic amines with a star-shaped molecular architecture

The first part of the thesis deals with the synthesis and characterization of novel star-shaped molecules based on triphenylamine. Due to their star-shaped architecture, these compounds have almost no tendency to crystallize and therefore form so-called molecular glasses. Today this class of materials is widely used in photocopiers and laser printers. These low molar mass compounds can be processed both from the gas phase and from solution. In both cases homogeneous amorphous films can be obtained from the new star-shaped materials (Figure 2-1, left). In all cases, triphenylamine has been used as core molecule and different carbazole and fluorene side arms were introduced as side arms in order to study the influence on the HOMO and LUMO levels of the target compounds. For efficient charge carrier injection from the gold electrodes of the transistor, a HOMO level of about -5.2 eV is required. The novel materials have been characterized in detail and their OFET performance was investigated.

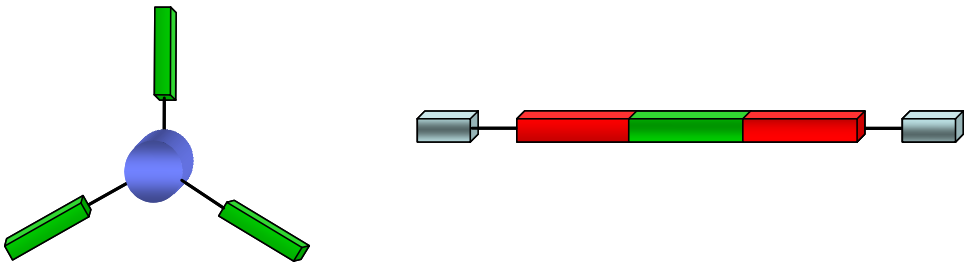

Figure 2-1. *Different molecular architectures: star-shaped design, leading to molecular glasses (left); annelated core molecule with different side group substituents leading to liquid crystalline (LC) phases (right).*

2.2. Fused aromatic compounds based on carbazole units

The second part of the thesis describes the development of a new class of fused heterocycles based on 2,7-substituted carbazole units. One of the major outcomes of my diploma thesis is that 2,7-carbazole based compounds are electrochemically unstable and undergo dimerization reactions in the 3- and 6-positions of the carbazole unit. Therefore an appropriate substitution pattern has to be found which could solve this problem. Beside the electrochemical stability, a high environmental stability is required for application in organic electronics. The molecular design should allow the preparation of thin films from the gas phase as well as from solution. In this thesis, bisindenocarbazoles are introduced as a new class of fused heterocycles (Figure

2-2). The thermal properties of the bisindenocarbazole can be tailored by introducing different alkyl side chains in the very last step of the synthesis. As the targed compounds exhibit a stong blue fluorescence they were tested as blue emitter in OLEDs.

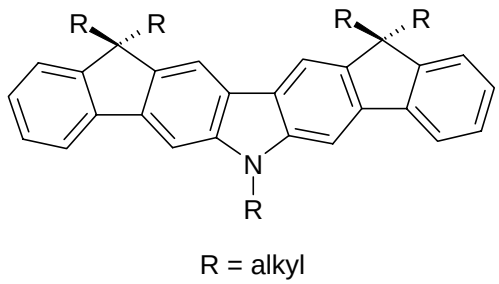

Figure 2-2. *Chemical structure of the bisindenocarbazole core molecule.*

Furthermore a new bisindenocarbazole building block was prepared from which a series of side-chain-substituted derivatives (Figure 2-1, right) were synthesized in order to study the influence on morphology and electrochemical properties.

As described in the introductory chapter, a possible approach to ordered thin films for optoelectronic devices are solution processable liquid crystalline (LC) monodomains. In the case of organic FETs the orientation of liquid crystalline materials has been used to increase the charge carrier mobilities.[56, 57, 80] By adopting this concept to organic LEDs, it is possible to generate polarized electroluminescence as it was already shown from liquid crystalline polyfluorenes.[81, 82] Due to the rigid rod-like core of the bisindenocarbazole, novel liquid crystalline compounds were obtained by substituting the bisindenocarbazole building block with aromatic side groups (Figure 2-3).

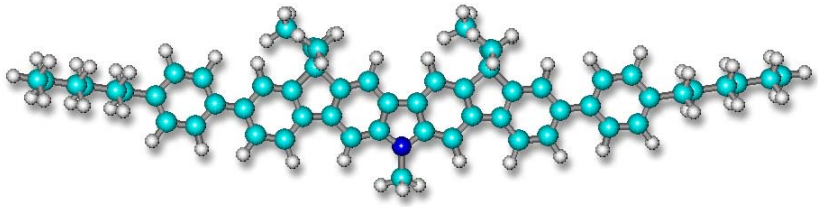

Figure 2-3. *MOPAC calculation of a rigid rod-like bisindenocarbazole which exhibits a liquid crystalline phase.*

3. Novel star-shaped triphenylamine based molecular glasses and their use in OFETs *(Paper 1)*

3.1. Amorphous molecular glasses

For a long time it was believed that vitrification can only be obtained from polymeric compounds. However, recent extensive studies have revealed that an amorphous morphology can also be obtained from small molecules if their molecular structure is designed properly.[66] Low molar mass organic compounds that form stable amorphous phases above room temperature are so-called "molecular glasses".[71] Molecular glasses are of great interest because of several aspects. As they are in a state of thermodynamic nonequilibrium, they undergo structural relaxation, exhibiting glass-transition phenomena which are usually only known from polymers. The amorphous state shows isotropic and homogeneous properties without any grain boundaries. It is characterized by the presence of free volume and disorder in both molecular distance and orientation. Molecular glasses are able to form uniform amorphous films both from the gas phase and from solution. In contrast to polymers, molecular glasses are monodisperse compounds and therefore can be highly purified by column chromatography or sublimation techniques. Slight impurities may already have a negative influence on charge carrier mobilities as well as on the device stability. Therefore a high purity is an essential prerequisite for the application of a material in organic electronics. Today, especially amorphous molecular materials with conjugated π-electron systems have constituted a new class of functional organic materials for use in various applications. They are widely used as hole conductors in photocopiers,[83] laser printers and organic light-emitting diodes (OLEDs).[66]

During the last years we figured out that small organic molecules with a star-shaped molecular architecture including three sidearms show excellent glass-forming properties.[84, 85] These compounds form stable amorphous phases and their tendency to crystallize is very low.

3.2. Synthesis and characterization of star-shaped molecular glasses based on triphenylamine

Six novel star-shaped molecules with a triphenylamine core substituted with carbazole and fluorene sidearms were prepared (Figure 3-1). The synthesis of the triiodotriphenylamine core and of the different sidearms is described in detail in paper 1. The key step in the synthetic

route towards the molecular glasses is a trifold Suzuki cross coupling reaction. The Suzuki reaction was chosen, as it is an excellent tool for unsymmetrical aryl-aryl couplings.[86]

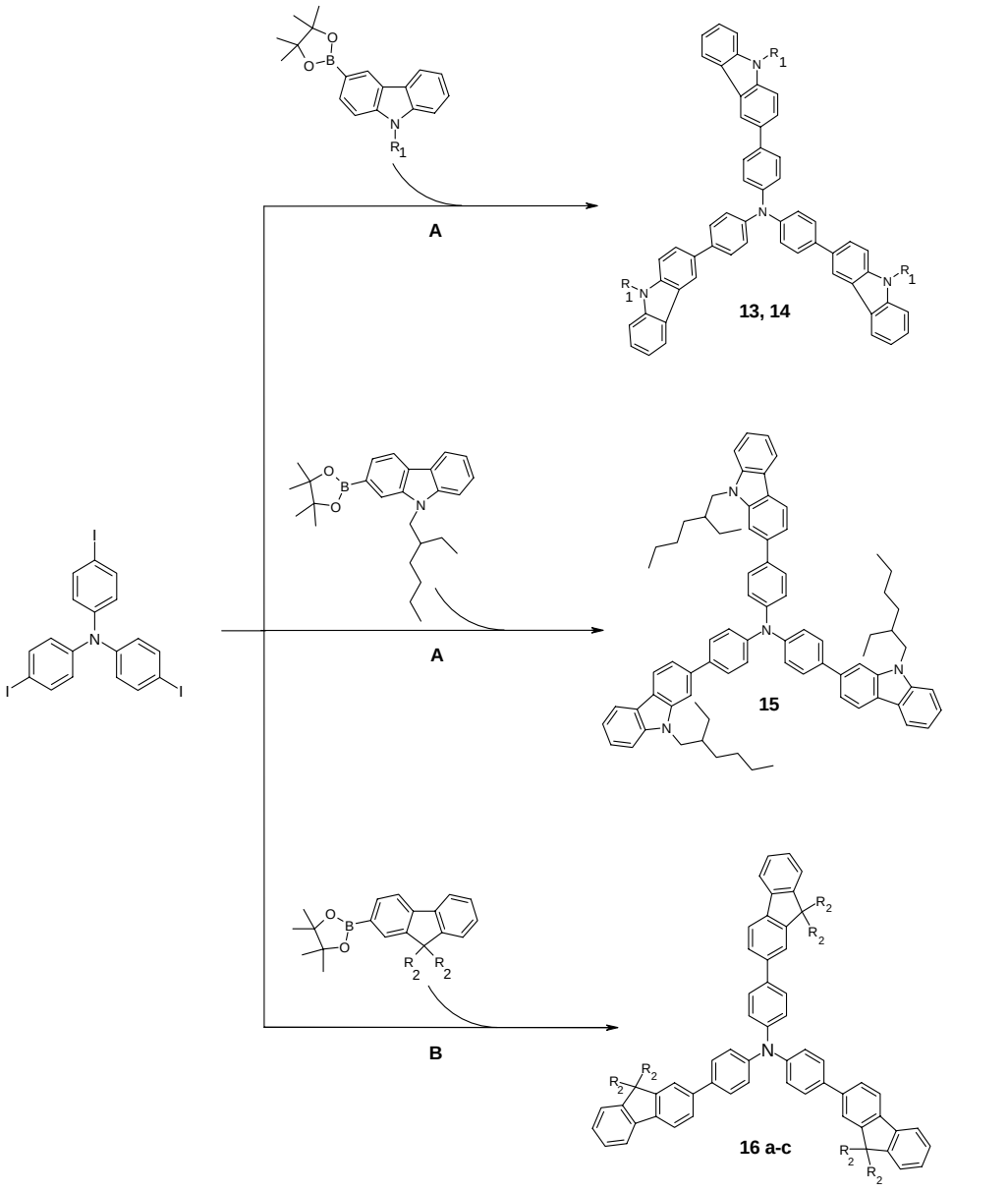

A = $P(o\text{-}tol)_3$, $Pd(OAc)_2$, toluene, 2N K_2CO_3, PTC, 60 °C, 2 h

B = $Pd(PPh_3)_4$, toluene, 2N K_2CO_3, PTC, 50 - 80 °C, 1 d

	R_1		R_2
13	3,4-dimethyl-phenyl	**16a**	ethyl
14	ethyl-hexyl	**16b**	butyl
		16c	hexyl

Figure 3-1. *Synthesis of the star-shaped compounds* ***13-16*** *by Suzuki cross coupling (numbering according to paper 1).*

Since the materials were prepared for the application as semiconductor in OFET devices, they have to exhibit a very high purity. Therefore all target molecules were purified by medium pressure liquid chromatography (MPLC). By using this purification technique, the target compounds **13-16** were obtained with an exceptional high degree of purity what was proven by size exclusion chromatography (SEC) and elemental analysis.

Thermal analysis of **13-16** revealed excellent thermal stabilities up to 495 °C and showed that all compounds with the exception of **15** form molecular glasses. In the case of **15**, where the carbazole sidearms are substituted in the 2-positions to the core molecule, only a melting point at 223 °C was detected in the differential scanning calorimetry (DSC) experiment. Nevertheless, thin amorphous films can be obtained from **15** when the material is spin-coated from solution. The thermal data are summarized in Table 3-1.

Table 3-1. *Thermal properties of the star-shaped compounds* ***13-16****.*

	T_{dec} [°C][1]	T_g [°C][2]	T_m [°C][2]
13	495	167	---
14	413	68	---
15	424	---	223
16a	407	118	248[3]
16b	384	96	---
16c	392	57	---

[1] Onset of decomposition determined by TGA, heating rate 10 K/min, N_2 atmosphere

[2] Determined by DSC, scan rate 10 K/min, N_2 atmosphere, 2nd run

[3] Melting point only detected during the first heating; the compound vitrified on cooling to room temperature with 10 K/min

Similar absorption and fluorescence spectra from THF solutions were obtained from all six molecules. The maxima of absorption are found about 360 nm, the maxima of fluorescence is close to 400 nm.

Cyclic voltammetry measurements revealed that the compounds **13, 14** and **16a-c** are electrochemically stable. In case of **15**, where the carbazole sidearms are substituted in the 2-position, the oxidation is not reversible. For the fluorene containing compounds **16a-c**, HOMO values of -5.2 eV were obtained from the CV experiments, whereas the HOMO levels of the carbazole based target molecules are about 0.2 eV higher at -5.0 eV.

3.3. Preparation and measurement of organic FETs

The transistor performance of the new star-shaped compounds was investigated with bottom gate OFET substrates from Philips. The devices consist of a heavily doped n^{++} silicon wafer as gate contact. On top of the gate electrode an insulating layer of silicon dioxide is grown thermally. Afterwards gold is evaporated and photolithographically patterned to form the source and drain contacts (Figure 3-2).[28] In order to obtain the best possible FET performance of the new materials, several surface treatments of the polar SiO_2 gate insulator were carried out. As these preliminary tests are very important for the transistor results presented in paper 1, the surface treatment procedures are described in more detail at this point.

It is a well known fact that the device characteristics can be influenced by covering the gate insulator with a self assembled monolayer (SAM) of organosilane compounds.[87] For this concern we decided to use hexamethyldisilazane (HMDS) as it the most suitable silanizing agent in connection with with aromatic amine based semiconducting materials.[35]

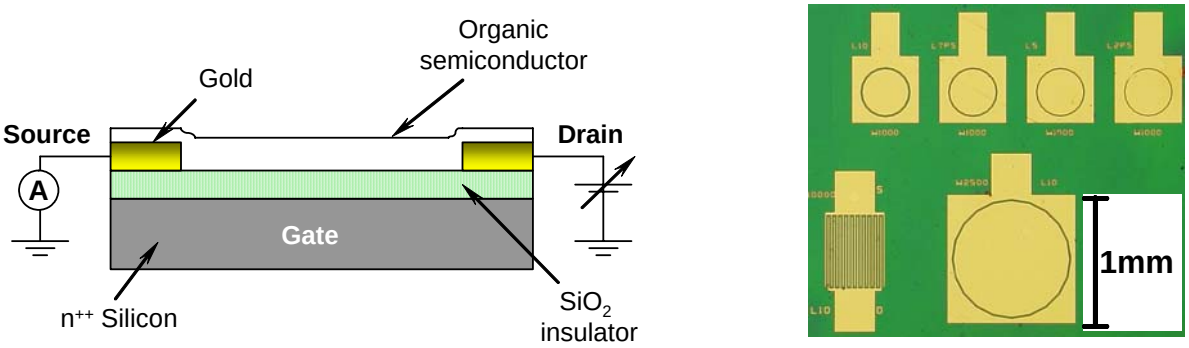

Figure 3-2. *Schematic of the used bottom gate OFET device architecture (left) and microscopic image of a Philips bottom gate OFET substrate containing several transistors with different channel lengths (right).*

First of all the bottom gate FET substrates were cleaned with fuming HNO_3 for 30 min at room temperature. After rinsing the substrates thoroughly with distilled water the silane coupling agent was vapor deposited at 80 °C. In order to check the influence of the evaporation time, the FET devices were kept in the HMDS vapor for 3 and 24 h, respectively. The experimental setup for vapor deposition of the HMDS is shown in Figure 3-3.

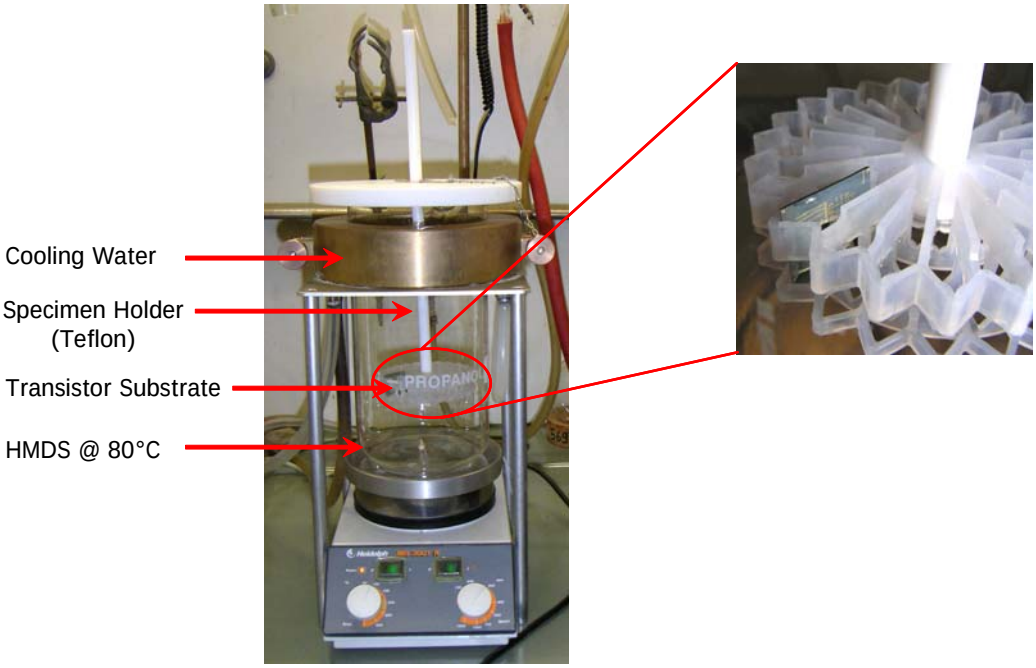

Figure 3-3. *Experimental setup for HMDS vapor deposition onto the OFET substrates.*

Afterwards the substrates were flushed with isopropanol before the organic semiconductor (**13**) was deposited onto the FET substrates. This was either done by spin-coating from 2-wt% toluene solution or by evaporation from the gas phase. The spin-coated films were dried under argon atmosphere at 130 °C for 30 min. An average film thickness of 40 nm was determined. For the sake of comparison, additional FET devices without HMDS treatment were prepared. All devices were annealed for 15 min at 90 °C under vacuum before the transistor characteristics were measured.

The preliminary measurements showed that the field-effect mobilities from the HMDS treated substrates are one order of magnitude higher than from the untreated FET devices. The turn-on voltage could be reduced from -5 V (untreated substrate) to -2 V by silanization with HMDS (24 h evaporation). Shorter HMDS treatment results in an insignificant drop of the turn-on voltage (-4 V). It was found that hysteresis effects can be eliminated almost completely by surface modification with the organosilane. Contact resistance could be tremendously reduced and on/off-ratios of the devices were increased by two orders of magnitude up to 10^5. Concerning hysteresis, contact resistance and on/off-ratio, no significant changes could be observed with of different HMDS deposition times. Furthermore it was found that the deposition of the amine glass **13** by spin-coating or vacuum evaporation has no influence on the FET performance.

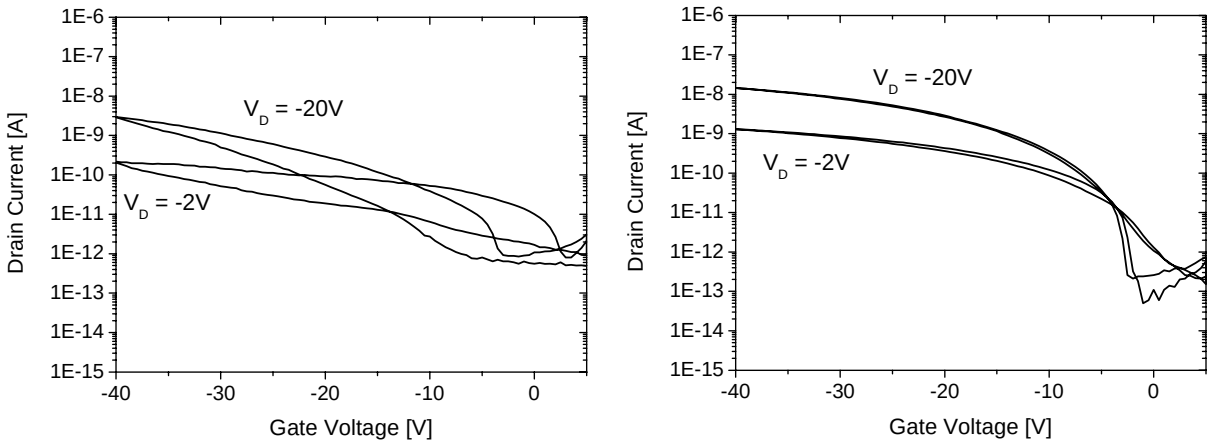

Figure 3-4. *Transfer characteristics of OFET devices with untreated (left) and HMDS silanized (24 h) gate insulator surfaces (right). In both cases the triphenylamine based star-shaped compound **13** was used as semiconducting material. The untreated OFET substrate shows significant hysteresis effects, a 3 V higher turn-on voltage and a lower on/off-ratio.*

The transfer characteristics in Figure 3-4 clearly show the improvements that were achieved concerning hysteresis effects, turn-on voltages and on/off-ratios by treating the gate insulator surface with HMDS. Comparison of the output characteristics in Figure 3-5 clearly shows that the effect of contact resistance was reduced remarkably by introducing this substrate treatment. This means that the charge carrier injection from the gold electrodes into the organic semiconductor was improved significantly. Concerning the additional reduction of the turn-on voltage by evaporating HMDS for 24 h, we decided to adopt this substrate preparation procedure for all future OFET measurements.

From this series of molecular glasses the highest charge carrier mobilities were obtained from compound **15** with 3×10^{-4} cm^2/Vs. The other star-shaped materials **13**, **14** and **16b** exhibit mobilities in the range of 10^{-4} cm^2/Vs. Furthermore on/off-ratios of about 10^5 and remarkably low turn-on voltages between -5 and -1 V could be achieved with the new compounds.

The most promising result is the high environmental stability of the OFETs under ambient conditions. Storage of the devices for more than four months in air and daylight had no influence on the device performance. Merely the field-effect mobility dropped slightly. Figure 3-6 shows the transistor characteristics of the pristine device and after storing it for four months, using **13** as semiconductor.

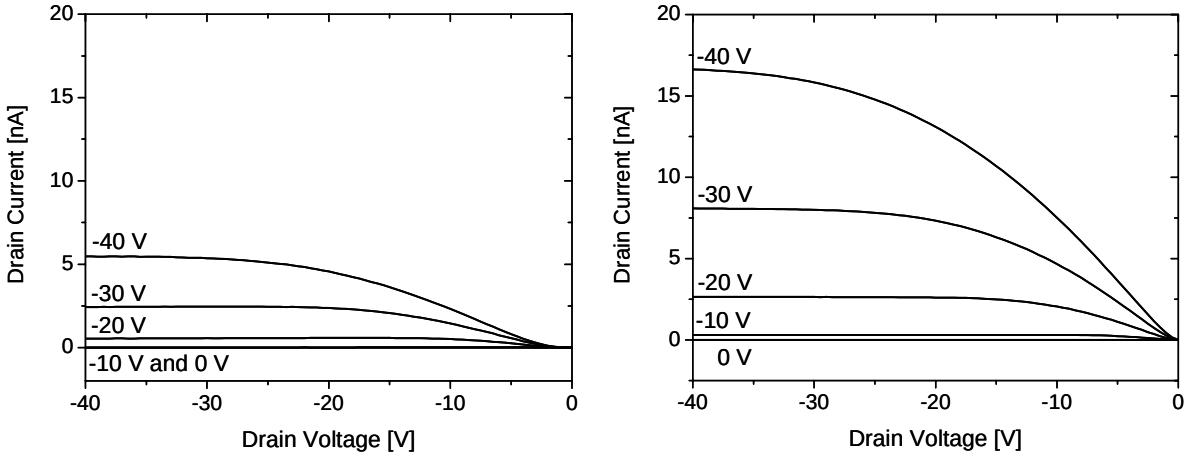

Figure 3-5. *Output characteristics of OFET devices with untreated (left) and HMDS silanized (24 h evaporation) gate insulator surfaces (right). The untreated OFET substrate shows a non-linear increase of the drain current between 0 and -15 V. This is clear evidence for contact resistance between the organic semiconductor and the gold electrodes. This effect could be reduced significantly by the surface modification with HMDS.*

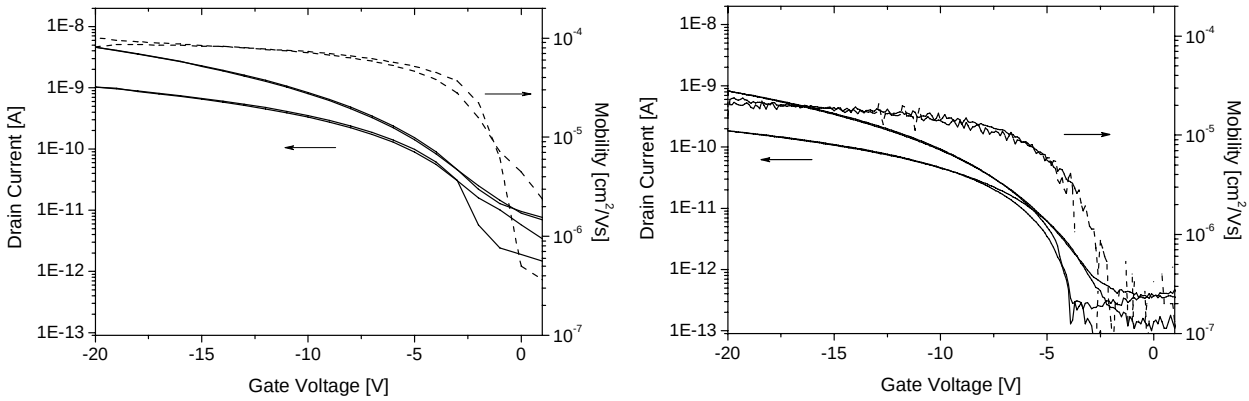

Figure 3-6. *Transfer characteristics of* ***13****. The drain potentials were –20 V and –2 V in the upper and lower traces, respectively (solid lines). Left: pristine device. Right: device performance after storage under ambient conditions and daylight for 4 months.*

In conclusion five out of six star-shaped triphenylamines which were prepared by the Suzuki cross-coupling form stable molecular glasses. Thin amorphous films can be obtained from these compounds when they are spin-coated or evaporated. It was also shown that the HOMO levels can be tailored by exchanging the sidearm substituents. The star-shaped molecules with fluorene side groups (**16a-c**) exhibit HOMO levels of -5.2 eV which can be increased by 0.2 eV if carbazole units are introduced to the triphenylamine core (**13-15**).

Furthermore a suitable surface treatment procedure was developed for the bottom gate OFET substrates. Hole carrier mobilities up to 3×10^{-4} cm^2/Vs and on/off-ratios in the range 10^5 were achieved form the novel star-shaped materials. The excellent longterm stability of the FET devices under ambient conditions is the most promising result of this work.

4. Synthesis and characterization of novel conjugated bis-indenocarbazoles *(Paper 2)*

In recent years a variety of 3,6-linked carbazole oligomers and polymers have been described in literature.[88] It is a well known fact that from 3,6-linked carbazole derivatives no conjugation of the π-electrons over large distances can be obtained.[89, 90] The conjugated segment of such compounds can probably be best described as a substituted 1,4-diamino-biphenyl structure.[91] In a previous work we have described a new synthetic route for N-alkylated carbazole trimers linked in the 2- and 7-positions.[90] Those carbazole oligomers exhibit an almost linear molecular architecture and were developed in order to compare them to the corresponding fluorene trimers with identical alkyl substitution. In case of the 2,7-linked carbazole trimers the conjugation of the π-electron system is now extended over six phenyl rings. Among other things we found that the 2,7-linked trimers exhibit a strong blue fluorescence as it is known from conjugated fluorene oligomers (Figure 4-1).

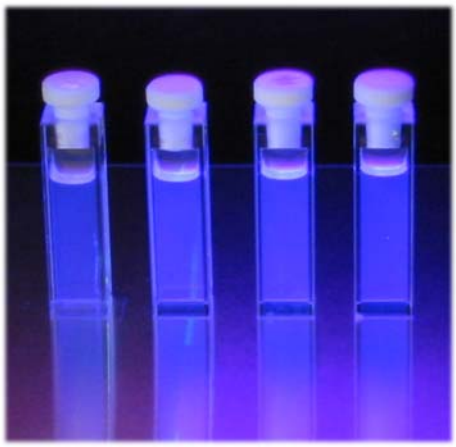

Figure 4-1. *Saturated blue fluorescence of fluorene trimers (left) and the corresponding 2,7-linked carbazole trimers (right).*[90]

Concerning the electrochemical stability, different results were obtained from the fluorene and the 2,7-linked carbazole trimers. Cyclic voltammetry (CV) proved the electrochemical stability of the fluorene compounds whereas the carbazole trimers were irreversibly oxidized. An explanation for the different electrochemical behavior of these compounds is that in case

of the 2,7-linked carbazole trimers the radical cation is extended over the whole molecule. Due to the donor effect of the carbazole nitrogen, the 3,6-positions are highly activated and therefore undergo dimerization reactions.[92]

The main aim of the further research work was to prepare a novel, electrochemically stable material on the basis of 2,7-carbazole units. At the same time it should exhibit a strong blue fluorescence as observed from the 2,7-linked carbazole trimer. The basic idea was to block the activated 3- and 6-positions of the carbazole that obviously are sensitive towards electrochemical oxidation. The protection of these electrochemically sensitive positions can be achieved by a ring closure reaction between the carbazole unit and a functionalized phenyl substituent. By doing so, fused aromatic system was obtained. In paper 2 the synthesis of the resulting bisindenocarbazoles is described in full detail. The different steps of the synthesis towards this new class of fused heterocycles are presented in Figure 4-2.

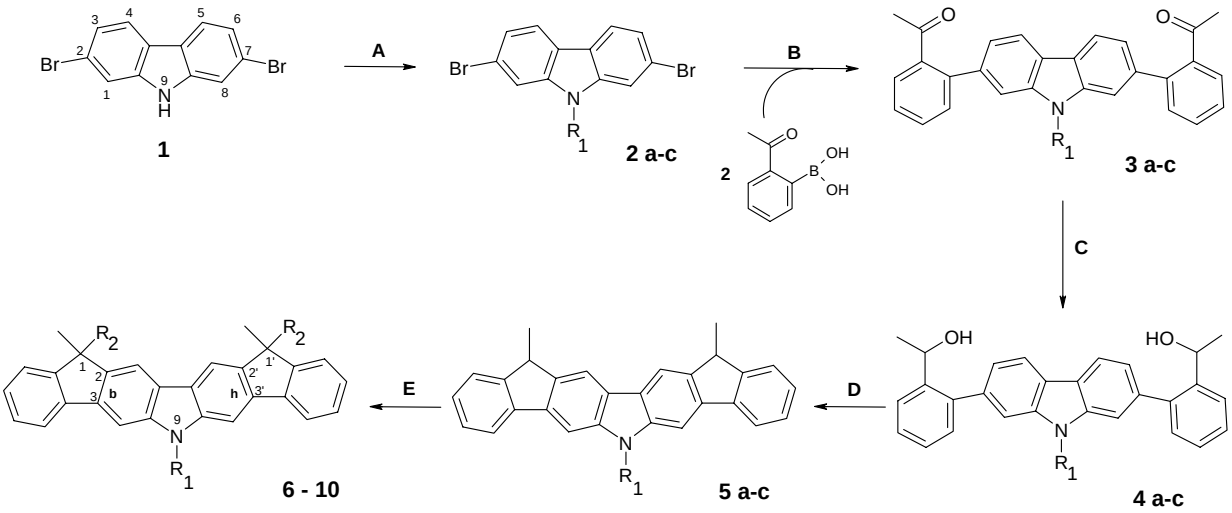

2a,b: A = alkyl bromide, acetone, KOH, PTC, 70 °C, 5 h

2c: A = Me_2SO_4, acetone, 10N KOH, 50 °C, 30 min

B = $P(otol)_3$, $Pd(OAc)_2$, 2N KOH, toluene, PTC, 90 °C, 2 h

C = lithium triethylborohydride, THF, 0 °C, 1 h

D = BF_3*$O(C_2H_5)_2$, CH_2Cl_2, RT, 30 min

E = 1.6 M n-BuLi, alkyl bromide, THF, -78 °C, 1 h

compd	R_1	R_2
2-5a	*sec*-butyl	---
2-5b	2-ethylhexyl	---
2-5c	methyl	---
6	*sec*-butyl	methyl
7	*sec*-butyl	n-butyl
8	*sec*-butyl	ethyl
9	2-ethylhexyl	ethyl
10	methyl	ethyl

Figure 4-2. *Synthesis of the bisindenocarbazoles* ***6-10****.*

Again, the Suzuki reaction was chosen in order to couple the phenyl substituents to a 2,7-dibromocarbazole starting compound (step B in Figure 4-2). Afterwards the keto groups of **3a-c** have to be reduced to the corresponding secondary alcohols. This was done with lithium triethylborohydride in absolute THF (super-hydride). The reduction with super-hydride solution works fast and quantitatively and requires no further purification of the intermediate. The crucial step of the bisindenocarbazole synthesis is the ring closure reaction with boron trifluoride etherate as Lewis-acid catalyst in order to obtain an annelated aromatic system in which the electrochemically sensitive 3- and 6-positions of the carbazole are protected. Finally different alkyl side chains can be introduced to the planar bisindenocarbazole core with n-BuLi and the corresponding alkyl halide. The big advantage of this synthetical approach is that the thermal properties as well as the morphology of the target compounds can be tailored in the very last step of the synthesis. After optimization of the different synthetic steps shown in Figure 4-2, the bisindenocarbazoles **6-10** are obtained in a five step synthesis with an overall yield of 50 % starting from 2,7-dibromocarbazole **1**.

The bisindenocarbazoles **6-10** are mixtures of stereoisomers. In case of **10** it was possible to separate the two diastereomers by medium pressure liquid chromatography (MPLC). The first fraction is the meso form with *(R,S)* configuration. The second fraction consists of the *(R,R)* and *(S,S)* enantiomers (Figure 4-3). The *(R,R/S,S)* and the *(R,S)*-isomers are formed in a ratio of 2:1. The melting points of the two isomers differ by 19 °C. The *(R,S)*-isomer melts at 292 °C, the *(R,R/S,S)* racemate at 273°C.

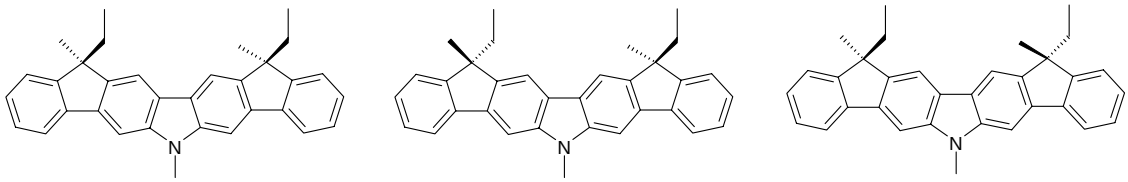

(R,S)-isomer of **10** *(S,S)*-isomer of **10** *(R,R)*-isomer of **10**

Figure 4-3. *Isomers of bisindenocarbazole **10** and their different configurations.*

In concern of optical and electrochemical properties there were no differences found between the three isomers of **10**, shown in Figure 4-3.

CV measurements proved the electrochemical stability of new bisindenocarbazole compounds. A representative CV curve of **6** is shown in Figure 4-4. By taking a HOMO level of -4.8 eV for the standard ferrocene/ferrocenium redox system[93], HOMO values in the range of -5.4 eV were calculated for the bisindenocarbazoles.

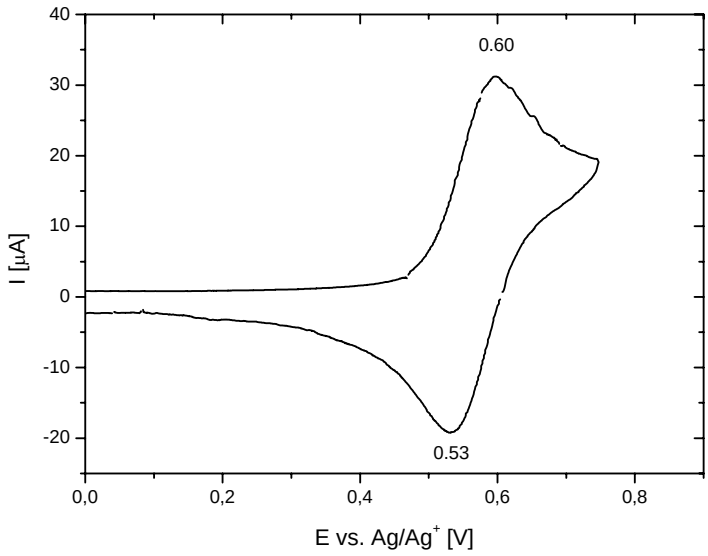

Figure 4-4. *CV curve of **6**, measured at 25 °C at a scan rate of 50 mV/s vs. Ag/Ag^+ in CH_2Cl_2 with $TBAPF_6$ as supporting electrolyte.*

As expected, the UV-Vis spectra of the different bisindenocarbazoles are identical. A strong blue fluorescence is obtained from solution with emission maxima around 410 nm. In order to estimate the fluorescence quantum yield of the new bisindenocarbazoles they were compared to the blue laser dye Exalite 428 [7,7''-bis(4-t-amylphenyl)-9,9,9',9',9'',9''-hexapropyl-2,2':7'2''-terfluorene] from which the quantum yield is known.[94, 95] Fluorescence spectra were taken from cyclohexane solutions and by integration, fluorescence quantum yields of 63 % were calculated.

The strong blue fluorescence and good quantum yields together with the excellent electrochemical stability make the new bisindenocarbazoles attractive candidates as blue emitter in OLEDs. Since the low molar mass bisindenocarbazoles can be sublimed quantitatively at temperatures below 320 °C (atmospheric pressure), they are well suited for deposition from the gas phase. The preparation of OLEDs with a bisindenocarbazole as blue emitter will be described in the next chapter.

In conclusion, we have developed a new versatile synthetic route for conjugated bisindenocarbazoles. By substitution with a variety of alkyl substituents in the very last step of the synthesis, their morphology can be varied from highly crystalline materials (**6**) to amorphous molecular glasses (**7**). Excellent thin films can be prepared by vacuum evaporation of the novel materials. CV experiments have shown that the bisindenocarbazoles exhibit a high electrochemical stability with HOMO values around -5.4 eV. Furthermore a strong blue fluorescence is obtained from the fused aromatic ring system with quantum yields up to 63 %.

5. Synthesis of a novel liquid crystalline bisindenocarbazole derivative *(Paper 3 and 4)*

From the research on organic field-effect transistors (OFET) it is a well known fact that the charge carrier mobility strongly depends on the degree of order in an organic semiconductor.[38] As mentioned before, the highest charge carrier mobilities are achieved in single crystalline materials like rubrene and pentacene.[39, 96] Nevertheless growing single crystals from organic compounds is a painstaking and expensive process.

Liquid crystals provide an alternative route to highly ordered thin films. If the organic material is oriented on organic alignment layers at elevated temperatures, large monodomains together with improved charge carrier mobilities can be obtained.[97-99] Concerning OLED applications, it was shown that linearly polarized light can be generated by using highly efficient emitter materials which exhibit LC mesophases.[81, 100]

As the bisindenocarbazoles described in paper 3 exhibit a strong blue fluorescence together with a high electrochemical stability, we decided to extend the core molecule with different aryl substituents in order to obtain liquid crystalline bisindenocarbazoles. The main target was to study the structure-property relationship of the new bisindenocarbazole derivatives concerning morphology, photoluminescence emission and the influence of the substituents on HOMO and LUMO levels.

First of all bromine was introduced as leaving group to the bisindenocarbazole core molecule in position 7 and 7'. For this purpose the symmetric *(R,S)*-isomer of *(1R, 1'S)*-diethyl-*(1S, 1'R)*-dimethyl-bisindeno[3,2-b:2'3'-h]-9-methylcarbazole was halogenated using alumina-supported copper(II) bromide in carbon tetrachloride.[101] The selective bromination of the bisindenocarbazole core compound to the dibrominated bisindenocarbazole **2** was verified by 2D-NMR spectroscopy. Suzuki cross coupling was used to couple the different side groups to the new building block. The reaction scheme including the different side arms is shown in Figure 5-1. After purification by MPLC the novel bisindenocarbazole derivatives **13-16** were obtained in good yields.

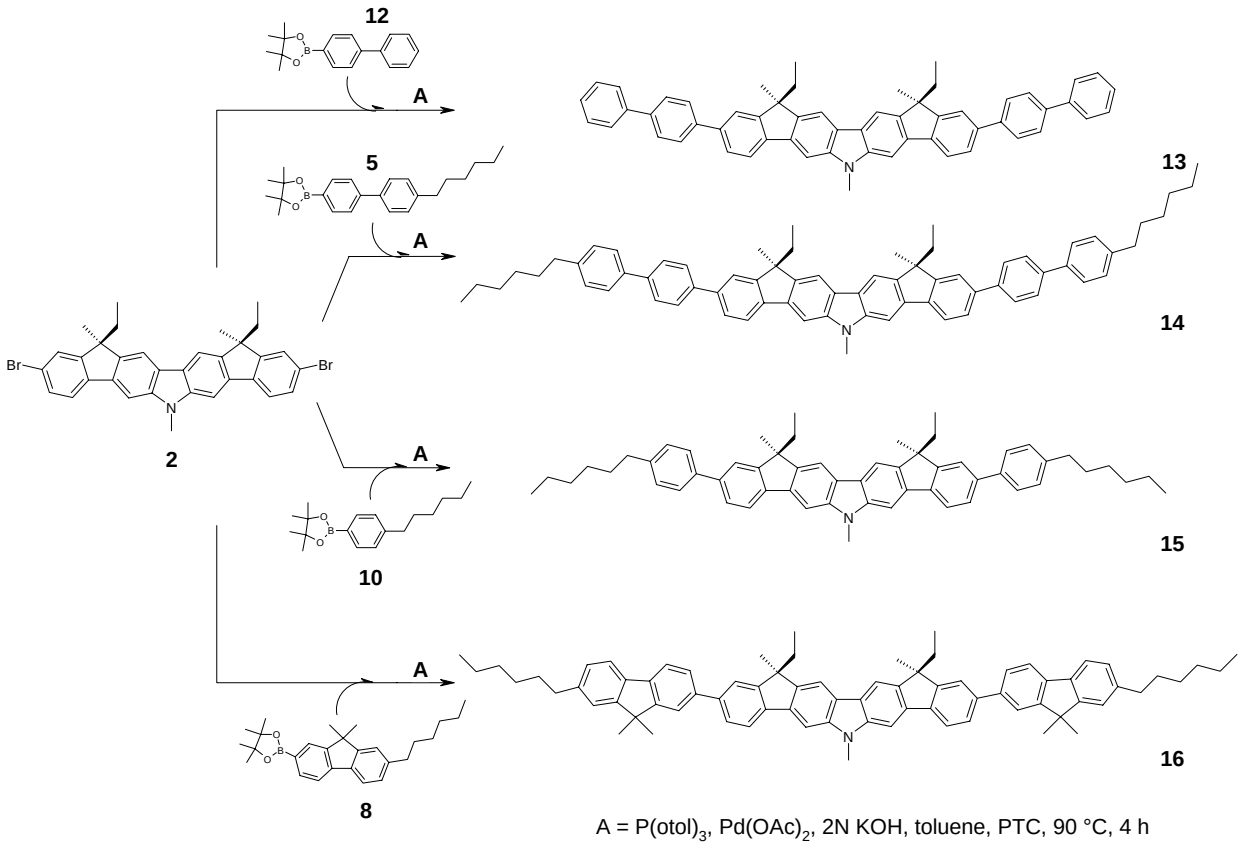

Figure 5-1. *Synthesis of the bisindenocarbazole derivatives by Suzuki cross coupling (numbering according to paper 4).*

Polarized optical microscopy (POM) showed that the bisindenocarbazole derivative with the 4-hexylphenyl side groups (**15**) exhibits a liquid crystalline phase above 180 °C. The transition into the isotropic phase is observed at a temperature of 251 °C. Upon cooling the typical Schlieren texture appears at 250 °C and crystallization started at about 165 °C. POM images are shown in Figure 5-2.

Further analysis by small angle X-ray scattering (SAXS) at a temperature of 220 °C confirmed the existence of a nematic LC phase. In the small angle region a Bragg peak was observed from which an average end-to-end distance of 34.5 Å is obtained. This distance is about 1.5 Å shorter than the calculated length of the extended molecules which is consistent with a slightly tilted arrangement of the bisindenocarbazole molecules in the nematic mesophase. From the broad wide angle Bragg peak a spacing of 5.6 Å is obtained. This peak reflects the average side-to-side distance of the rod-like molecules and is a typical value for a nematic LC phase. While **15** shows a liquid crystalline phase, the bisindenocarbazole

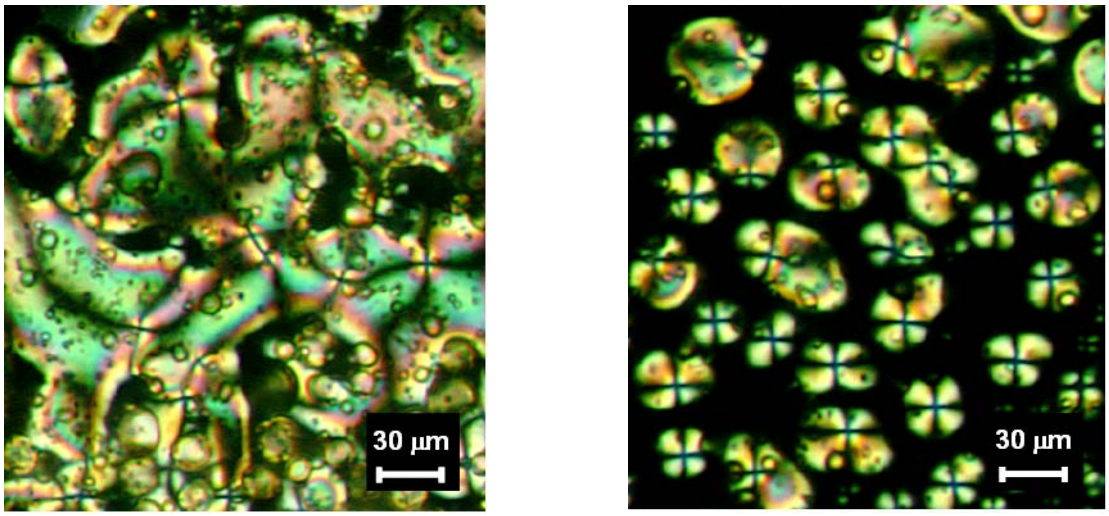

Figure 5-2. *Polarizing microscopy images of* ***15*** *on heating 220 °C (left) and upon cooling at 248 °C (right).*

derivatives **14** and **16** form molecular glasses with glass transition temperatures (T_g) of 103 and 105 °C, respectively. In contrast, **13** is crystalline and melts under decomposition at 331 °C.

CV measurements revealed excellent electrochemical stabilities of all bisindenocarbazole derivatives. As expected the different side group substituents have no influence on the HOMO levels. For all four bisindenocarbazole derivatives the same HOMO value of -5.4 eV was obtained.

Table 5-1. *Optical properties of the bisindenocarbazole derivatives*

comp.	λ_{abs} [nm][1]	$\lambda_{max,flur}$ [nm][2]	Stokes shift [nm]	Φ_f [%][3]
13	378	397	19	56
14	378	397	19	54
15	395	403	8	49
16	374	400	26	34

[1] Longest wavelength absorption maximum, measured in 10^{-5} M cyclohexane solution

[2] Fluorescence spectra taken from 10^{-6} M cyclohexane solution

[3] Fluorescence quantum yield

As expected the optical properties of the new materials are very similar. A strong blue fluorescence and quantum yields up to 56 % were recorded for **13-16**. In Table 5-1 the

maxima of absorption and fluorescence are summarized together with the corresponding Stokes shifts and quantum yields. The very small Stokes shifts of the bisindenocarbazole derivatives can be explained by the rigid π-electron system which allows no major geometrical changes in the transition from the ground to the excited state.[77, 102] It is noteworthy that the liquid crystalline compound **15** exhibits the smallest Stoke shift (8 nm) among all the bisindenocarbazole derivatives. In Figure 5-3 the combined absorption and fluorescence spectra of **15** are shown.

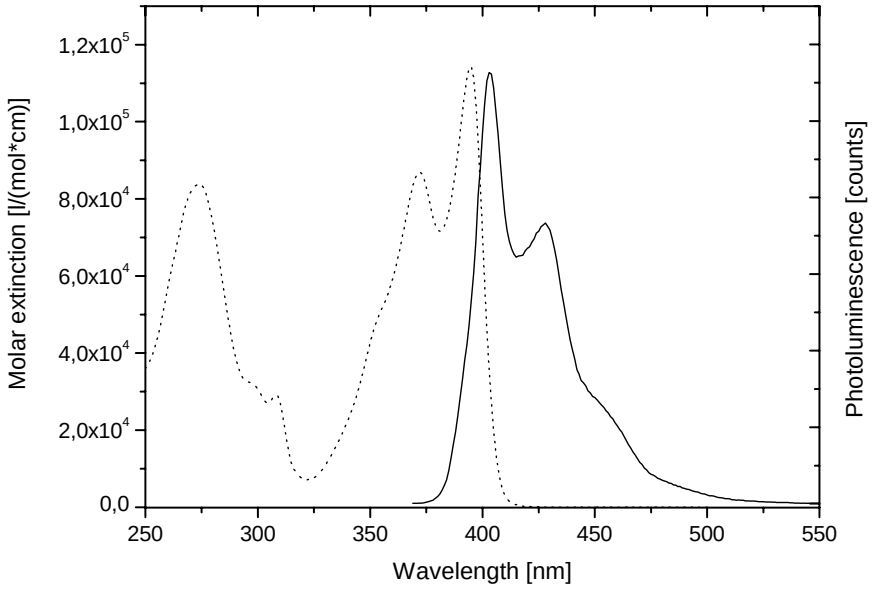

Figure 5-3. *Absorption and fluorescence spectrum of the liquid crystalline bis-indenocarbazole **15**. The absorption spectrum was taken from 10^{-5} M cyclohexane solution and the fluorescence spectrum was measured from 10^{-6} M cyclohexane solution with an excitation wavelength of 395 nm.*

In conclusion four novel bisindenocarbazole derivatives were synthesized and characterized concerning their thermal, optical and electrochemical properties. Compound **15** exhibits a broad nematic mesophase which was characterized by POM and SAXS. Furthermore fluorescence quantum yields up to 56 % were obtained from the new compounds. The excellent electrochemical and environmental stability together with the strong blue fluorescence make the new compounds attractive candidates for optoelectronic applications. As this is the first liquid crystalline compound from this new class of fused aromatics, we decided to summarize these results in a short communication (paper 3). In a full paper (paper 4) the novel bisindenocarbazole derivatives **13-16** are discussed in detail.

6. Bisindenocarbazole as new deep-blue emitter for OLED applications *(Paper 5)*

Since the first organic light-emitting diode (OLED) was reported in 1987 by Tang and VanSlyke[9] great efforts have been made to optimize both materials and OLED devices. This has led to the first commercial full-color flat panel displays of the next generation.[103, 104] For this issue new red, green and blue emitter materials had to be developed. Until today the preparation of efficient red[105] and green[106] electroluminescent OLED devices has been described in literature. However the production of pure blue light-emitting devices is still a big challenge. External quatum yields of about 2.4 % and lifetimes of ca. 10 000 h have been reported so far from blue fluorescent emitters.[107] In order to achieve quantum efficiencies of 10.4 %, so-called phosphorescent emitters like iridium (III)bis[(4,6-di-fluoropheny)-pyridinato-N,$C^{2'}$]picolinate (FIrpic) have been introduced.[108] However the device lifetimes are shorter and it has not been possible to obtain a deep-blue light emission from devices based on phosphorescent dyes. Since current blue light emitting devices still have some drawbacks, there is still a strong demand for the development of new high performance blue emitters.

Recently we have reported on novel bisindenocarbazoles from which a strong blue fluorescence together with quantum yields up to 63 % were obtained. For this reason we have tested the new material as blue emitter in OLED devices. In typical setups for blue OLEDs the blue fluorophore is often doped into a wide band gap host material in order to avoid quenching of the EL emission and to adjust the HOMO energy levels of the different materials used in the OLED setup. For this issue we decided to test 4,4'-dicarbazolyl-1,1'-biphenyl (CBP), 1,3-bis(9-carbazolyl)benzene (mCP) and 4,4',4''-tri(N-carbazolyl)-triphenylamine (TCTA) as host materials.

Before OLEDs could be prepared, the host/guest energy transfer had to be investigated. This was done by fluorescence spectroscopy and in the case of the CBP matrix, additionally by time resolved photoluminescence (PL). These preliminary experiments proved an efficient energy transfer between the matrix materials and the blue bisindenocarbazole dye. Furthermore it was found that doping concentrations of 1 % yielded the highest fluorescene intensity. Higher amounts of the dopant lead to a quenching of the PL intensity. The results are discussed in detail in paper 5.

For the preparation of the OLED devices a combinatorial evaporation setup was used in order to dope the different host systems by co-evaporation of the guest material. By using this technique it was also possible to evaporate step gradients of the hole blocking layers in a single experiment. In conclusion it was found that a pure, deep-blue emission at CIE coordinates of x = 0.19 and y = 0.17 can be obtained from the bisindenocarbazole emitter by using TCTA as host material doped with 1 % of 1,1-Dimethyl-1', 1'-dimethyl-bisindeno[3,2-b:2'3'-h]-9-sec-butyl-carbazole (Figure 6-2, inset) as emitter. At a hole blocking layer (BCP) thickness below 40 nm, a shoulder at 500 nm is detected in the EL spectra. The intensity of the shoulder increases with decreasing thickness of the BCP layer. This can be explained by the fact that the excitons are not confined in the TCTA/emitter layer if the blocking layer is too thin and therefore are able to diffuse into the Alq_3 layer which leads to a green emission. The corresponding EL spectra are shown in Figure 6-2.

Luminance values of 200 cd/m^2 at a current density of 100 mA/cm^2 and a maximum luminance efficiency of 1.60 cd/A were obtained from the TCTA containing OLEDs at a BCP layer thickness of 40 nm. The turn on voltage was recorded at 5 V. The energy level diagram and the setup of the device using TCTA as matrix material are shown in Figure 6-1.

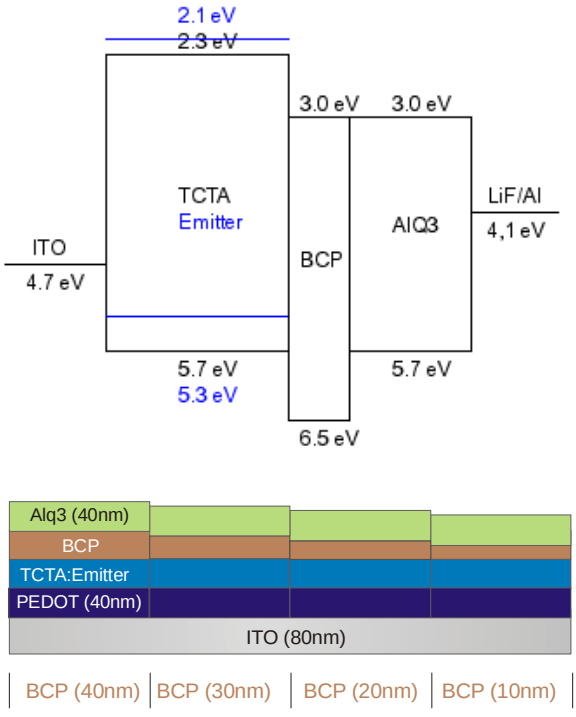

Figure 6-1. *Energy level diagram of the OLED containing TCTA as host material doped with 1 % of the blue bisindenocarbazole emitter (above) and device architecture with different BCP layer thicknesses (below).*

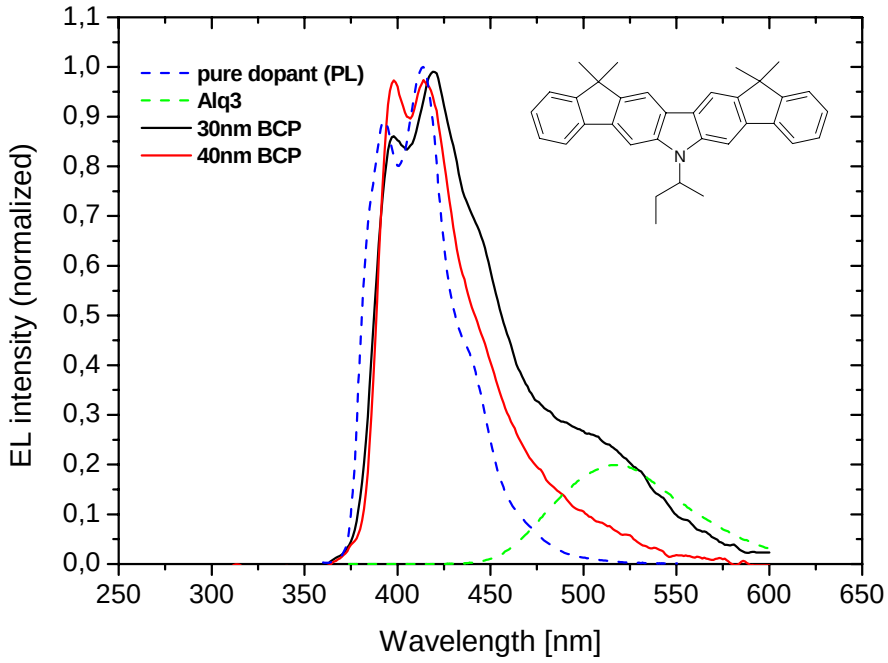

Figure 6-2. *EL spectra of the TCTA containing OLEDs with different BCP blocking layer thicknesses. For comparison the PL spectrum of the pure bisindenocarbazole emitter is added (blue dashed curve). The inset shows the chemical structure of the bisindenocarbazole emitter molecule.*

The current-voltage characteristics of the TCTA containing OLEDs (Figure 6-3) show a saturation of the luminescence values at driving voltages higher than 10 V. This could be explained by the fact that the TCTA/emitter layer was solution processed and therefore no HTL could be used. Thus a huge mismatch of the HOMO energy levels of the ITO anode and the TCTA layer occurs and therefore an efficient charge carrier injection is no longer ensured. In future experiments the emitting layer will be prepared by evaporation what might solve the problem of the low brightness values.

The application of CBP and mCP as host materials resulted in the emission of green light with a maximum around 500 nm. Therefore the emission can be exclusively assigned to Alq_3. In conclusion it was found that TCTA is the most suitable matrix for the novel emitter. These experiments have shown that the bisindenocarbazole is a promising candidate to be used as blue light emitting material in OLED applications.

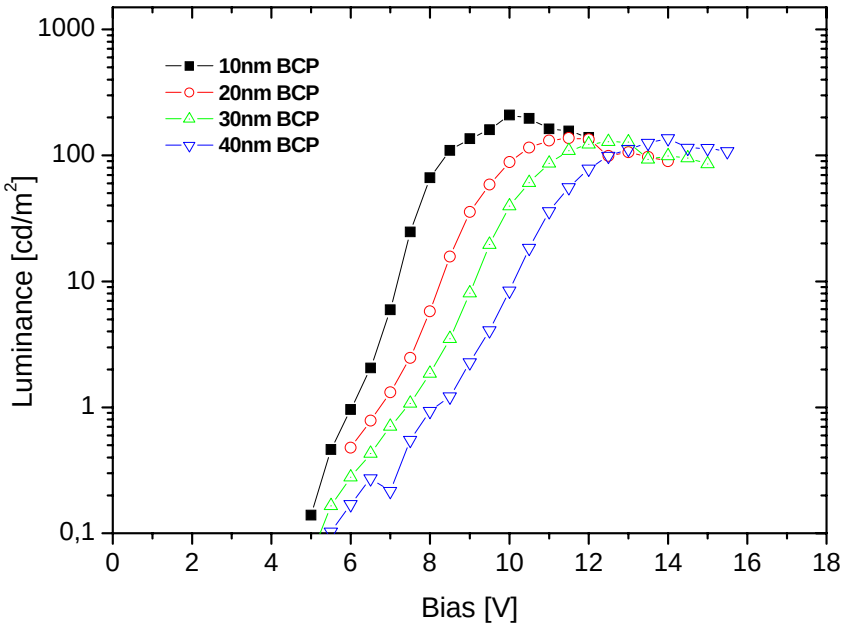

Figure 6-3. *Current-voltage characteristics of the OLEDs with TCTA matrix containing 1 % of the bisindenocarbazole dopant. Device setup: ITO/PEDOT (40 nm)/TCTA:bisindeno-carbazole (40 nm)/BCP (10, 20, 30 and 40 nm)/Alq$_3$ (40 nm)/LiF (1 nm)/Al (150 nm).*

7. Summary

The motivation for this thesis was the synthesis, characterization and the testing of new, environmentally stable materials based on aromatic amines for OFET and OLED applications. The preparation of high quality thin films from solution as well as from the gas phase was an another important issue.

The first part of this thesis deals with star-shaped molecular glasses with triphenylamine as core molecule. Substituted fluorene and carbazole units were attached to the core molecule as side arms via trifold Suzuki cross coupling reaction. The target compounds were highly purified by medium pressure liquid chromatography (MPLC) as purity is an important prerequisite for organic materials to be used for optoelectronic applications. The novel star-shaped compounds exhibit high thermal stabilities up to 500 °C and form stable amorphous phases. HOMO values of -5.2 eV were determined for the fluorene containing compounds from CV experiments. The HOMO levels of the carbazole based molecules are 0.2 eV higher at -5.0 eV. As these values fit perfectly to the HOMO levels of the gold or poly(3,4-ethylenedioxythiophene (PEDOT) electrodes used in organic field-effect transistors, a good charge carrier injection is expected. From all star-shaped molecules high quality thin films can be prepared both from solution, i. e. by spin-coating, and from the gas phase. The target molecules are depicted in Figure 7-1.

Before the new materials were finally tested in transistor devices, a suitable surface treatment of the OFET substrates was developed. By introducing self-assembled monolayers, prepared from hexamethyldisilazane (HMDS), on top of the SiO_2 insulator layer of the FET substrates, the field-effect mobility was increased by at least one order of magnitude. Furthermore it was possible to improve on/off-ratios as well as turn on voltages. In conclusion hole carrier mobilities up to 3×10^{-4} cm^2/Vs and on/off-ratios of 10^5 were achieved from the new star-shaped compounds. The performance of the devices was not affected by a four month storage period in air and daylight. Merely a slight drop of the field-effect mobility was observed. The exceptional long term stability of the FET devices under ambient conditions and the excellent solution processability are the most promising results of this work.

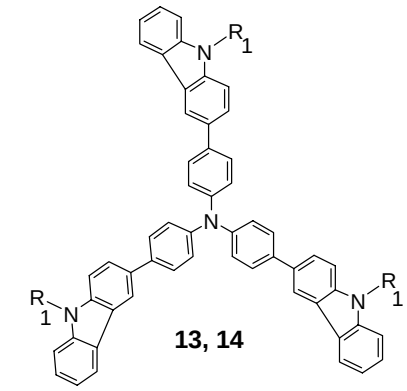

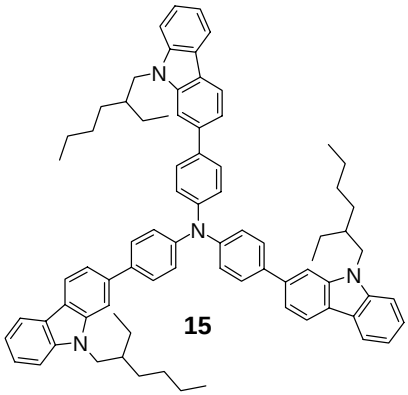

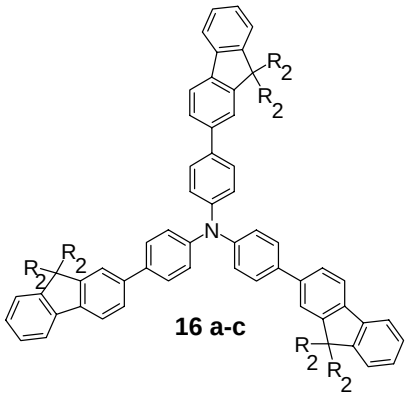

	R_1		R_2
13	3,4-dimethyl-phenyl	**16a**	ethyl
14	ethyl-hexyl	**16b**	butyl
		16c	hexyl

Figure 7-1. *Star-shaped compounds with a triphenylamine core and carbazole and fluorene side arms (numbering according to paper 1).*

The second part of this thesis describes the synthesis and characterization of a new class of fused heterocycles based on carbazole units. In my diploma thesis 2,7-linked carbazole trimers were characterized in great detail. Among other things it was found that these compounds are not electrochemically stable. It turned out that the trimers are very sensitive towards electrochemical oxidation and subsequent dimerization at the highly activated 3- and 6-positions. Nevertheless those carbazole trimers exhibit a strong blue fluorescence and their energy levels fit perfectly to the electrodes which are frequently used in OFET devices. Furthermore the trimers show an excellent environmental stability. As these are important prerequisites for optoelectronic applications, an appropriate substitution pattern had to be found to solve the problem of electrochemical instability. A new synthetic approach towards stable 2,7-linked carbazoles is presented in this thesis. For this issue a series of bisindenocarbazoles is introduced as a new class of fused heterocycles. A synthetical procedure was designed which allows to tailor the thermal properties of the target compounds by introducing different alkyl substituents in the very last step of the synthesis. Yields up to 50 % can be obtained after six synthetical steps including purification of the intermediates.

Figure 7-2 shows the chemical structure of bisindenocarbazole **6** and the corresponding CV curve which proves the electrochemical stability of this new class of fused aromatics.

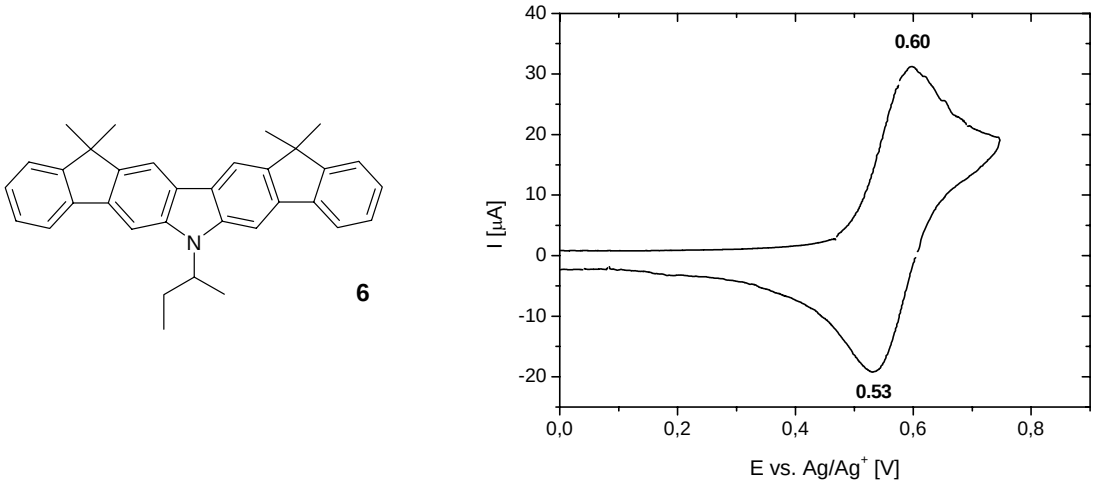

Figure 7-2. *Chemical structure of bisindenocarbazole* ***6*** *(left, numbering according to paper 2). The CV curve proves the electrochemical stability of this new class of fused heterocycles (right).*

Five bisindenocarbazoles with different alkyl substitution patterns have been prepared and characterized. Their morphology varies from highly crystalline materials with short alkyl side chains to amorphous molecular glasses if longer or branched alkyl groups are attached to the core. The compounds sublime quantitatively at temperatures around 320 °C and excellent thin films can be prepared by vacuum evaporation. HOMO values of -5.3 eV and fluorescence quantum yields as high as 63 % are obtained.

As the bisindenocarbazoles exhibit a bright blue fluorescence together with high quantum yields, they were tested as blue emitter for OLED applications. In typical setups for blue light emitting LEDs, the blue emitter is doped into a wide band gap host material in order to avoid quenching of the electroluminescence and to adjust the energy levels of the different materials used in the setup. For this issue 4,4'-dicarbazolyl-1,1'-biphenyl (CBP), 1,3-bis(9-carbazolyl)benzene (mCP) and 4,4',4"-tri(N-carbazolyl)triphenylamine (TCTA) were tested as matrix materials and 1,1-Dimethyl-1', 1'-dimethyl-bisindeno[3,2-b:2'3'-h]-9-*sec*-butyl-carbazole was used as emitter. Before the OLED devices could be prepared, the host/guest energy transfer was checked. For this purpose thin films of the host compounds containing

different dopant concentrations were prepared which were characterized by fluorescence spectroscopy and in the case of the CBP matrix, additionally by time resolved PL spectroscopy. The preliminary experiments proved an efficient energy transfer from the matrix to the emitter and showed a maximum of the PL intensity at a doping concentration of 1 %.

A combinatorial evaporation setup was used for the preparation of the OLED devices in order to dope the different host systems by co-evaporation of the bisindenocarbazole dye. This deposition method also allows the variation of the film thicknesses of the charge transport layers in a single experiment. Figure 7-3 (right) shows the OLED architecture containing TCTA as matrix together with different layer thicknesses of the 2,9-dimethyl-4,7-diphenyl-1,10-phenanthroline (BCP) hole blocker. The corresponding energy level diagram is also shown in Figure 7-3.

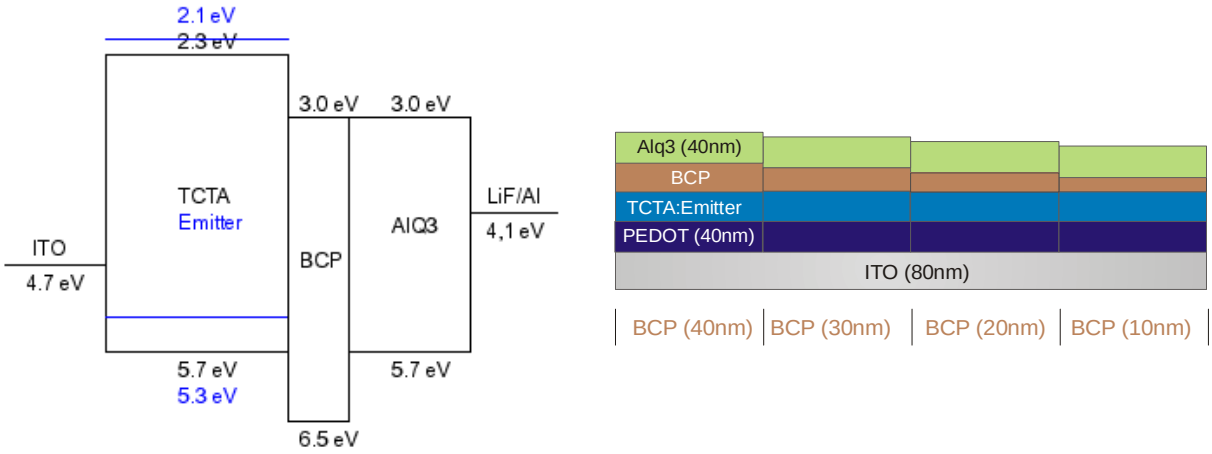

Figure 7-3. *Energy level diagram of the OLED containing TCTA as host material doped with 1 % of the blue dye (left) and device architecture with different film thicknesses of the BCP hole blocking layer (right).*

By using this device architecture a deep-blue emission from the bisindenocarbazole dye at CIE color coordinates of x = 0.19 and y = 0.17 was obtained at a hole blocking layer thickness of 40 nm. Luminance values up to 200 cd/m^2 at a current density of 100 mA/cm^2 and a luminance efficiency of 1.60 cd/A were achieved with this series of devices. The turn on of the light emission was observed at 5 V. These very first results show that the bisindenocarbazole is a promising new blue fluorescent emitter for organic LEDs.

From the research on organic field-effect transistors (OFETs) it is a well known fact that the charge carrier mobility strongly depends on the degree of order in an organic semiconductor. A possible approach to well ordered thin films are large monodomains formed by liquid crystals (LC). The molecules can be aligned in the LC-phase at elevated temperatures. The orientation is then frozen in, i. e. by quenching the LC-phase to room temperature. By adopting this concept to organic LEDs, it is possible to generate polarized electroluminescence. Due to the rigid rod-like core of the bisindenocarbazole it was possible to obtain a novel derivative exhibiting a broad nematic mesophase by extending the core with aromatic side groups. A new bisindenocarbazole building block was prepared by selective bromination of the core molecule in the 7- and 7'-position. Afterwards alkyl substituted phenyl, biphenyl and fluorene side groups were attached to the bisindenocarbazole core. The chemical structures of the bisindenocarbazole derivatives together with their thermal properties are presented in Figure 7-4. The nematic mesophase of 7,7'-di-(4-hexyl-phenyl)-(*1R, 1'S*)-diethyl-(*1S, 1'R*)-dimethyl-bisindeno[3,2-b:2'3'-h]-9-methyl-carbazole (**15**) was characterized by polarizing microscopy (POM) and small angle X-ray scattering (SAXS). A broad nematic mesophase phase between 180 °C and 251 °C was found in case of the hexylphenyl substituted bisindenocarbazole derivative. A polarizing microscopy image of the nematic LC phase at 220 °C and the corresponding X-ray difractogram are shown in Figure 7-5.

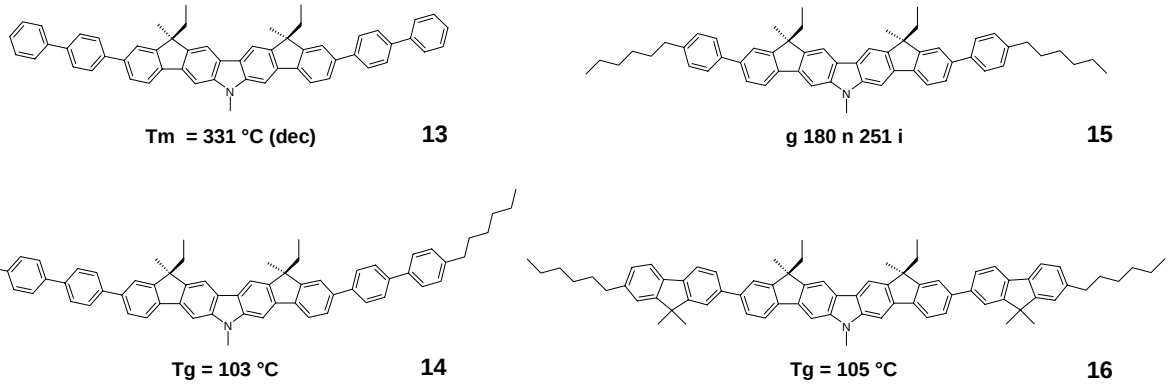

Figure 7-4. *Chemical structures and thermal properties of the novel bisindenocarbazole derivatives (numbering according to paper 4).*

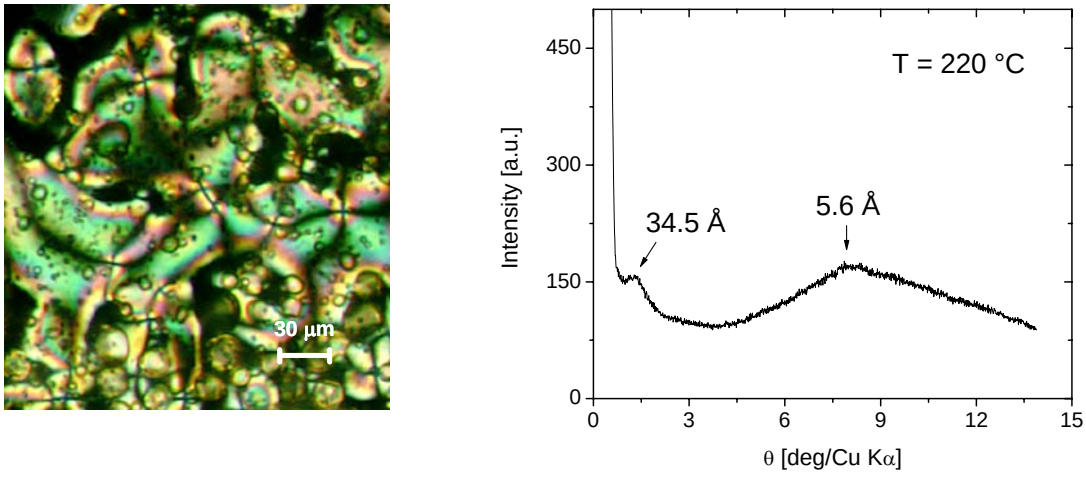

Figure 7-5. *Polarizing microscopy image of the nematic mesophase at 220 °C under crossed polarizers (left) and X-ray difractogram at 220 °C (right) of* ***15****.*

All bisindenocarbazole derivatives exhibit high thermal stabilities up to 300 °C and show excellent electrochemical stabilities in the CV experiments. HOMO and LUMO levels of -5.4 eV and -2.3 eV were determined. Just like the bisindenocarbazoles, the novel derivatives also display a strong blue fluorescence with solution quantum yields up to 56 %.

In conclusion two classes of carbazole containing materials for optoelectronic applications are described in this thesis. On the one hand the synthesis and characterization of amorphous, star-shaped molecular glasses was reported. These compounds exhibit an excellent environmental stability and were successfully tested as semiconductor in OFETs. On the other hand bisindenocarbazoles were prepared which represent a new class of fused heterocycles. Furthermore the first liquid crystalline derivative based on bisindenocarbazole as core molecule is reported. The derivative with the broad nematic mesophase has to be tested in an OFET in the near future. Improved field-effect mobilities can be expected from the compound when an orientation layer is used for increasing the degree of order in the device. Furthermore it was shown that a deep-blue electroluminescence can be obtained from OLEDs by using bisindenocarbazole as emitter molecule. The first experiments with the novel fluorescent dye are the starting point for further investigations concerning the development of a suitable device architecture with a higher brightness and luminescence efficiency.

8. Zusammenfassung

Ziel dieser Dissertation war die Synthese, Charakterisierung sowie die Erprobung neuer Materialien auf Basis aromatischer Amine für die Anwendung in organischen Leuchtdioden (OLED) und Feld-Effekt Transistoren (OFET). Neben der Stabilität gegenüber Luftfeuchtigkeit und Sauerstoff war auch die Möglichkeit der Herstellung qualitativ hochwertiger dünner Filme sowohl aus Lösung als auch aus der Gasphase ein wichtiges Kriterium bei der Entwicklung dieser Materialien.

Der erste Teil dieser Arbeit beschäftigt sich mit molekularen Gläsern, die eine sternförmige Architektur aufweisen und aus einem Triphenylaminkern aufgebaut sind. Mittels einer dreifachen Kupplungsreaktion nach Suzuki wurde der Kern mit substituierten Fluoren- und Carbazoleinheiten verknüpft. Da organische Materialien für den Einsatz in optoelektronischen Bauteilen von hoher Reinheit sein müssen, wurden die Zielverbindungen mit Hilfe der Mitteldruckchromatographie (MPLC) aufgereinigt. Die sternförmigen Verbindungen zeigen sehr hohe thermische Stabilitäten bis zu Temperaturen von 500 °C und bilden stabile amorphe Phasen. Die HOMO Niveaus der fluorensubstituierten Verbindungen wurden cyclovoltammetrisch (CV) zu -5.2 eV bestimmt. Das HOMO der carbazolhaltigen Moleküle liegt dagegen um 0.2 eV höher, also bei -5.0 eV. Nachdem die Lage der HOMO Niveaus energetisch genau zu denen der Gold- bzw. Poly(3,4-ethylendioxythiophen) (PEDOT)-Elektroden passt, welche häufig in organischen Feldeffekttransistoren zum Einsatz kommen, kann von einer guten Ladungsträgerinjektion ausgegangen werden. Von allen sternförmigen Verbindungen lassen sich ausgezeichnete dünne Filme sowohl aus Lösung, z. B. durch Spin-coaten, als auch aus der Gasphase herstellen. Die chemischen Strukturen der Zielmoleküle sind in Abbildung 8-1 dargestellt.

Bevor die neuen Substanzen in Transistoren getestet werden konnten, musste zunächst eine geeignete Oberflächenbehandlung für die OFET Substrate entwickelt werden. Durch die Abscheidung von selbstorganisierten Monoschichten aus Hexamethyldisilazan (HMDS) auf der SiO_2 Isolatoroberfläche konnten die Feld-Effekt Mobilitäten der Transistoren um mehr als eine Größenordnung gesteigert werden. Des weiteren konnten mit Hilfe dieser Methode das On/Off-Verhältnis sowie die Einschaltspannungen erheblich verbessert werden. Mit den neuen sternförmigen Verbindungen konnten Lochleitermobilitäten bis zu 3×10^{-4} cm^2/Vs und On/Off-Verhältnisse von 10^5 erreicht werden. Die Leistungsfähigkeit der Transistoren wurde selbst durch eine vierwöchige Lagerung an Licht und Luft nicht beeinträchtigt. Lediglich ein

leichter Abfall der Ladungsträgermobilitäten konnte beobachtet werden. Die hervorragende Langzeitstabilität der FET Substrate und die ausgezeichnete Verarbeitbarkeit der Materialien aus Lösung sind wohl die vielversprechendsten Ergebnisse aus diesem Teil der Arbeit.

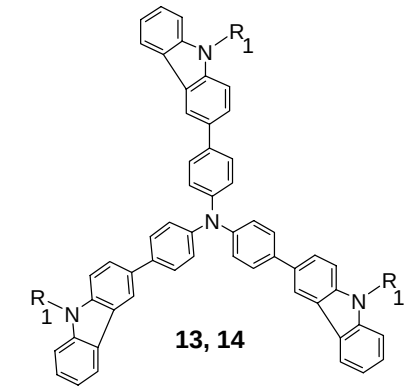

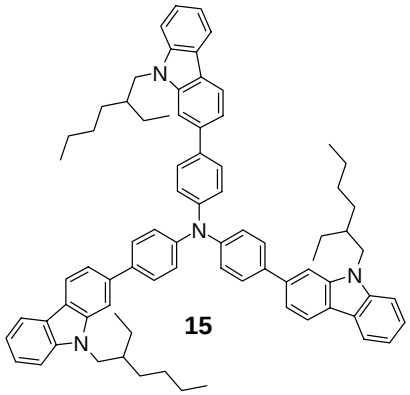

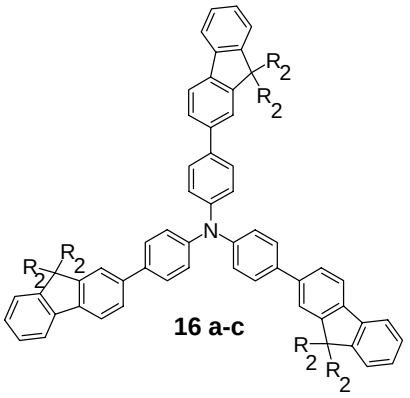

	R_1		R_2
13	3,4-dimethyl-phenyl	**16a**	ethyl
14	ethyl-hexyl	**16b**	butyl
		16c	hexyl

Abbildung 8-1. *Chemische Strukturen der sternförmigen Verbindungen mit Triphenylamin-kern und Carbazol- bzw. Fluorenseitengruppen (Nummerierung entsprechend Paper 1).*

Der zweite Teil dieser Dissertation beschäftigt sich mit der Synthese und Charakterisierung einer neuen Klasse von annelierten Heterozyklen auf der Basis von Carbazoleinheiten. In meiner Diplomarbeit wurden 2,7-verknüpfte Carbazoltrimere eingehend untersucht. Dabei zeigte sich, dass diese Verbindungen elektrochemisch nicht stabil sind. Die Trimere sind empfindlich gegenüber elektrochemischer Oxidation und dimerisieren an den stark aktivierten 3- und 6-Positionen. Jedoch wiesen diese Carbazoltrimere eine starke blaue Fluoreszenz auf und ihre HOMO Energieniveaus entsprachen denen der in OFETs häufig eingesetzten Elektrodenmaterialien. Die Trimere zeigten auch ein hervorragende Stabilität an Licht und Luft. Nachdem diese Eigenschaften wichtige Voraussetzungen für elektronische Anwendungen sind, musste ein geeignetes Substitutionsmuster gefunden werden, um elektrochemisch stabile Carbazolverbindungen zu erhalten. In dieser Arbeit wurde eine neuartige Synthese entwickelt, die es ermöglicht 2,7-substituierte Carbazole in eine stabile

Struktur zu integrieren. Zu diesem Zweck wurde eine Reihe von Bisindenocarbazolen synthetisiert, die zu einer neuen Klasse von annelierten Heterozyklen gehören. Es wurde eine Synthesestrategie erarbeitet, die es ermöglicht die thermischen Eigenschaften der Zielmoleküle durch Einführung verschiedener Alkylgruppen im letzten Syntheseschritt zu steuern. Nach sechs Schritten und der Aufreinigung aller Zwischenstufen konnten mit dieser Synthese Ausbeuten von bis zu 50 % erzielt werden. Abbildung 8-2 zeigt die chemische Struktur des Bisindenocarbazols **6** sowie das zugehörige CV Spektrum, welches die elektrochemische Stabilität dieser neuen Materialklasse belegt.

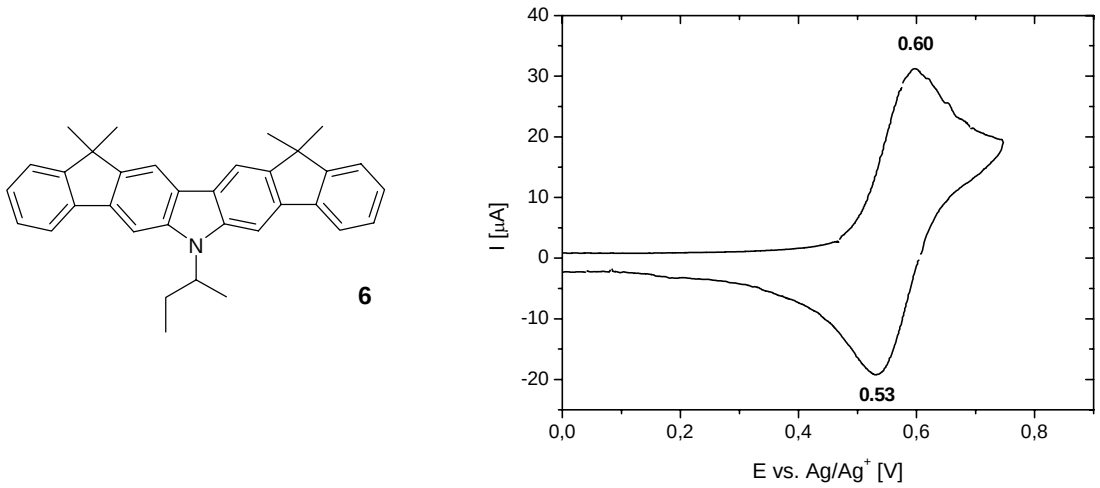

Abbildung 8-2. *Strukturformel des Bisindenocarbazols* ***6*** *(links, Nummerierung nach Paper 2). Das Cyclovoltamogramm belegt die elektrochemische Stabilität der neuen Materialklasse (rechts).*

Insgesamt wurden fünf neue Bisindenocarbazole mit unterschiedlichen Alkylsubstituenten synthetisiert und charakterisiert. Durch gezielte Alkylierung konnten unterschiedlichste Morphologien realisiert werden. Kurze Alkylsubstituenten führten zu kristallinen Verbindungen, wohingegen mit langen bzw. verzeigten Ketten amorphe Gläser erhalten wurden. Die Substanzen sublimieren bereits ab Temperaturen von 320 °C quantitativ. Durch Verdampfen der Substanzen im Vakuum können deshalb hervorragende dünne Filme präpariert werden. Die HOMO Niveaus liegen bei -5.3 eV und es wurden Fluoreszenquantenausbeuten von bis zu 63 % in Lösung gemessen. Nachdem die Bisindenocarbazole stark blau fluoreszieren und hohe Quantenausbeuten aufweisen, wurden sie als blauer Emitter in OLEDs getestet. Normalerweise wird in einer OLED der blaue Fluoreszenzfarbstoff in ein Matrixmaterial mit großer Bandlücke eindotiert, um ein Quenchen

der Elektrolumineszenz zu verhindern und um die unterschiedlichen Energieniveaus der verwendeten LED-Materialien angleichen zu können. Für diesen Zweck wurden 4,4'-dicarbazolyl-1,1'-biphenyl (CBP), 1,3-bis(9-carbazolyl)benzol (mCP) und 4,4',4''-tri(N-carbazolyl)triphenylamin (TCTA) als Matrixmaterialien getestet und mit 1,1-Dimethyl-1’,1’-dimethyl-bisindeno[3,2-b:2’3’-h]-9-*sec*-butyl-carbazol als Farbstoff dotiert. Bevor die LEDs gebaut werden konnten, musste zunächst der Energieübertrag von der Matrix auf den Emitter untersucht werden. Dafür wurden dünne Filme von den Matrixmaterialien präpariert, die unterschiedliche Konzentrationen des Fluoreszenzfarbstoffs enthielten. Die dünnen Schichten wurden mit Hilfe der Fluoreszenzspektroskopie analysiert. Im Falle der CBP Matrix wurden zusätzlich noch zeitaufgelöste PL Spektren aufgenommen. Die Experimente zeigten, dass der Energieübertrag von der Matrix zum Emitter sehr effizient verläuft und dass bereits ab einer Dotierungskonzentration von 1 % die maximale PL Intensität erreicht wird.

Für die Herstellung der OLEDs wurde ein kombinatorisches Aufdampfverfahren verwendet, welches ein gleichzeitiges Verdampfen der Matrixmaterialien zusammen mit dem Bisindenocarbazol Emitter ermöglichte. Mit Hilfe dieser Methode war es auch möglich die Dicken der Lochtransportschicht in einem einzigen Aufdampfzyklus zu variieren. Abbildung 8-3 (rechts) zeigt die Architektur der OLEDs mit TCTA als Matrix und unterschiedlichen Filmdicken des Lochblockers 2,9-dimethyl-4,7-diphenyl-1,10-phenanthrolin (BCP). Das entsprechende Energieniveauschema ist ebenfalls in Abbildung 8-3 (links) dargestellt.

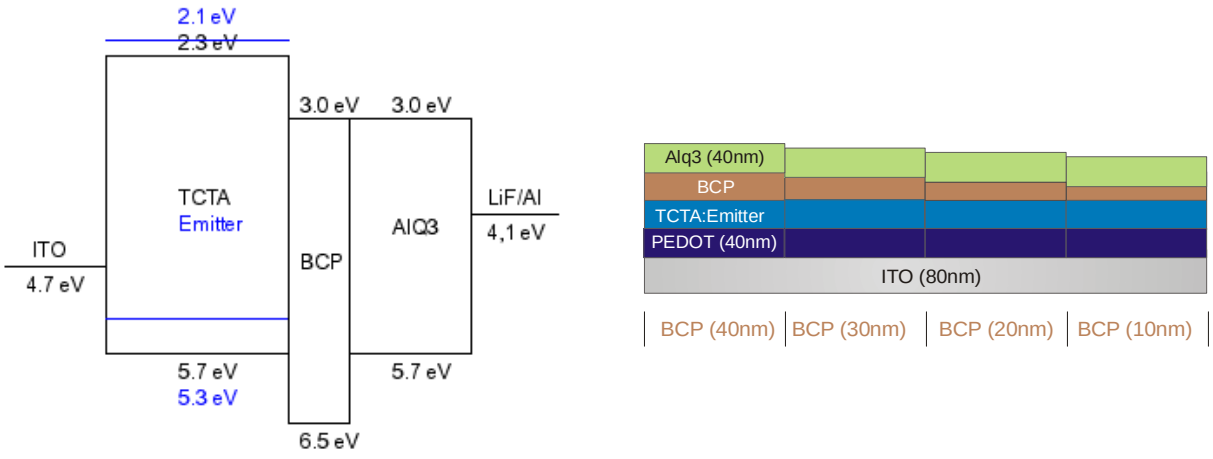

Abbildung 8-3. *Energieniveauschema der OLED mit TCTA als Matrixmaterial und einer Dotierungskonzentration des blauen Emitters (**6**) von 1 % (links). OLED Aufbau mit unterschiedlichen Filmdicken des Lochblockers BCP (rechts).*

Durch die Verwendung dieser OLED Architektur konnte eine tief blaue Emission des Bisindenocarbazols mit CIE Farbkoordinaten von x = 0.19 und y = 0.17 erzielt werden. Die Dicke der Lochblockerschicht betrug dabei 40 nm. Die maximale Leuchtkraft der OLED wurde zu 200 cd/m^2 bei einer Stromdichte von 100 mA/cm^2 bestimmt. Die Effizienz des Devices liegt bei 1.60 cd/A. Die Einschaltspannung ab der eine Lichtemission wahr genommen wurde, lag bei 5 V. Diese Ergebnisse sind sehr viel versprechend und zeigen, dass die neuen Bisindenocarbazole als blaue Fluoreszenzemitter für die Verwendung in organischen Leuchtdioden gut geeignet sind.

Die Forschung auf dem Gebiet der organische Feld-Effekt Transistoren hat gezeigt, dass die Ladungsträgerbeweglichkeit eng mit dem Ordnungsgrad des organischen Halbleiters verknüpft ist. Die Verwendung von flüssigkristallinen Materialien (LC), die in der Lage sind große Monodomänen zu bilden, stellen eine gute Möglichkeit dar, dünne Filme mit einem hohen Ordnungsgrad herzustellen. Die Moleküle werden bei erhöhter Temperatur in der flüssigkristallinen Phase mit Hilfe einer Orientierungsschicht ausgerichtet. Anschließend wird ihre Orientierung z. B. durch schnelles Abschrecken auf Raumtemperatur fixiert. Wird dieses Konzept auf die Fertigung von organischen Leuchtdioden übertragen, ist es möglich polarisierte Elektrolumineszenz zu erzeugen. Aufgrund der stäbchenförmigen Struktur der Bisindenocarbazole war es durch eine Verlängerung des Grundkörpers mit aromatischen Seitengruppen möglich, ein neuartiges, flüssigkristallines Derivat mit einer breiten nematischen Phase herzustellen. Hierzu wurde zunächst ein neuer Bisindenocarbazol Baustein durch selektive Bromierung der 7- und 7'-Position synthetisiert. Anschließend wurden dann alkylierte Phenyl-, Biphenyl- und Fluorenseitengruppen an den Bisindenocarbazol Grundkörper gekuppelt. Die chemischen Strukturen der neuen Bisindenocarbazolderivate und deren thermische Eigenschaften sind in Abbildung 8-4 zusammengefasst. Das hexylphenyl substituierte Bisindenocarbazolderivat weist eine breite nematische Phase zwischen 180 °C und 251 °C auf. Die nematische LC-Phase des 7,7'-di-(4-hexyl-phenyl)-(*1R,1'S*)-diethyl-(*1S,1'R*)-dimethyl-bisindeno[3,2-b:2'3'-h]-9-methylcarbazols (**15**) wurde mit Hilfe der Polarisationsmikroskopie und mit Kleinwinkelröntgenstreuung (SAXS) charakterisiert. Abbildung 8-5 zeigt neben dem Röntgendiffraktogramm auch ein polarisations-mikroskopisches Bild des flüssigkristallinen Derivates. Die Aufnahmen wurden jeweils bei einer Temperatur von 220 °C gemacht.

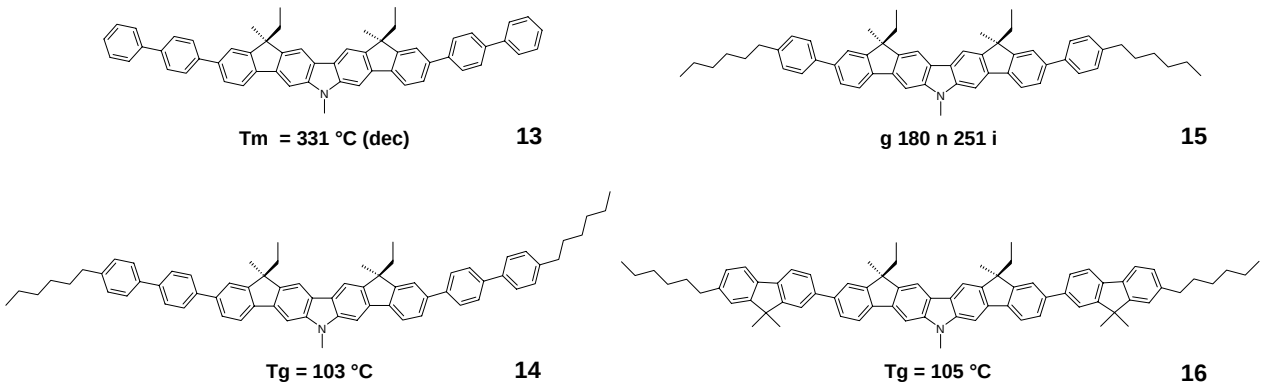

Abbildung 8-4. *Strukturformeln und thermische Daten der neuartigen Bisindenocarbazol-derivate (Nummerierung nach Paper 4).*

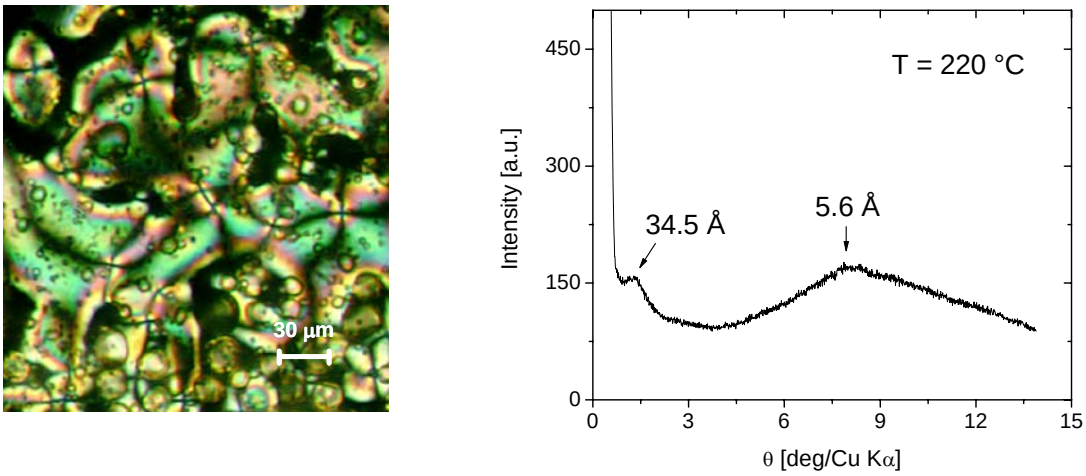

Abbildung 8-5. *Polarisationsmikroskopische Aufnahme der nematischen Mesophase von* ***15*** *bei 220 °C zwischen zwei gekreuzten Polarisatoren (links) und Röntgendiffraktogramm bei 220 °C (rechts).*

Alle Bisindenocarbazolderivate weisen hohe thermische Stabilitäten von bis zu 300 °C auf. CV Messungen zeigen ihre ausgezeichnete elektrochemische Stabilität. Die HOMO bzw. LUMO Niveaus wurden jeweils zu -5.4 eV und -2.3 eV bestimmt. Genau wie die Bisindenocarbazole selbst, zeigen auch deren Derivate eine stark blaue Fluoreszenz mit Quantenausbeuten von bis zu 56 % in Lösung.

In dieser Dissertation werden zwei neue Materialklassen auf Carbazolbasis für die Anwendung in optoelektronischen Bauteilen beschrieben. Der erste Teil der Arbeit handelt von der Synthese und Charakterisierung sternförmiger Verbindungen, die stabile amorphe Gläser bilden. Diese Verbindungen zeichnen sich vor allem durch ihre außerordentliche Stabilität gegenüber Einflüssen wie Feuchtigkeit und Sauerstoff aus. Sie sind außerdem erfolgreich als organische Halbleiter in OFETs getestet worden. Im zweiten Teil wird die Synthese und Charakterisierung von Bisindenocarbazolen, einer neuen Klasse von annelierten Heterozyklen, beschrieben. Auf der Basis dieser Bisindenocarbazole wurde ein neues flüssigkristallines Derivat hergestellt. Dieses Derivat, das eine breite nematische LC-Phase aufweist, soll in naher Zukunft in einem organischen Feld-Effekt Transistor untersucht werden. Durch die Verwendung einer Orientierungsschicht im Transistorsubstrat kann eine geordnete, flüssigkristalline Monodomäne erzeugt werden. Dies lässt eine Steigerung der Ladungsträgerbeweglichkeit erwarten. Ferner wurde gezeigt, dass mit Bisindenocarbazolen als Emitter in OLEDs eine tief blaue Elektrolumineszenz erzeugt werden kann. Die ersten Tests mit dem neuen Fluoreszenzemitter sind der Ausgangspunkt für die Entwicklung einer geeigneten OLED Architektur, mit der noch höhere Leuchtstärken und Quantenausbeuten erreicht werden sollen.

9. Statement

Parts of the work presented in this thesis were carried out in collaboration with other scientists and technicians. In the following paragraphs my own contribution to the different publications and manuscripts is specified.

Paper 1

Novel star-shaped triphenylamine based molecular glasses and their use in OFETs

Martin Sonntag, Klaus Kreger, Doris Hanft, Peter Strohriegl,

Sepas Setayesh and Dago de Leeuw

Chemistry of Materials **2005**, *17*, 3031-3039.

I carried out the synthesis of the tris-{4-[9-(3,4-dimethyl-phenyl)-carbazol-3-yl]-phenyl}-amine (**13**) including the carbazole side arms (**2, 5, 8**). Afterwards I characterized the star-shaped compound **13** concerning its thermal (TGA, DSC), optical (UV-Vis, fluorescence) and electrochemical (CV) properties. The remaining target compounds were synthesized and characterized by Klaus Kreger and Doris Hanft. The preparation of the OFET substrates (surface treatment and deposition of organic semiconductors) and all FET measurements were carried out and evaluated by myself. Dago de Leeuw and Sepas Setayesh gave me the opportunity to use the FET probe stations at the Philips Research Laboratories in Eindhoven (NL) and helped me with the interpretation of the transistor measurements. I have written the draft of the manuscript before it was finalized jointly with my thesis advisor Prof. Dr. Peter Strohriegl.

Paper 2

Synthesis and characterization of novel conjugated bisindenocarbazoles

Martin Sonntag and Peter Strohriegl

Tetrahedron **2006**, *62*, 8103-8108.

All synthetic and characterisation work (NMR, DSC, TGA, UV-Vis, fluorescence, CV) for this publication was carried out by myself. I have written the draft of the manuscript before it was finalized jointly with my thesis advisor Prof. Dr. Peter Strohriegl.

Paper 3

Novel Bisindenocarbazole Derivative Exhibiting a Nematic Mesophase

Martin Sonntag and Peter Strohriegl

Tet. Lett., **2006**, *47*, 8313-8317.

I have prepared and characterized (NMR, DSC, TGA, UV-Vis, fluorescence, CV, POM) all compounds presented in this publication. The SAXS measurement was done by Andreas Timme. Sample preparation and evaluation of the X-ray data was carried out by myself. I have written the draft of the manuscript before it was finalized jointly with my thesis advisor Prof. Dr. Peter Strohriegl.

Paper 4

Synthesis of a novel liquid crystalline bisindenocarbazole derivative

Martin Sonntag and Peter Strohriegl

Liquid Crystals, **2006**, *in press.*

I have prepared and characterized (NMR, DSC, TGA, UV-Vis, fluorescence, CV, POM) all compounds presented in this publication. The results of the SAXS measurement carried out by Andreas Timme are included in this publication. I have written the draft of the manuscript before it was finalized jointly with my thesis advisor Prof. Dr. Peter Strohriegl.

Paper 5

Bisindenocarbazole as new blue emitter for OLEDs

Martin Sonntag, Michael M. Rothmann and Peter Strohriegl

Intended for submission

The time resolved photoluminescence spectra were measured by Jakub Mezyk (Universita Milano-Bicocca). All samples used for these measurements were prepared by myself. The preparation of the OLEDs by vacuum evaporation was carried together with Michael Rothmann. I have written the draft of the manuscript before it was finalized jointly with my thesis advisor Prof. Dr. Peter Strohriegl.

10. Literature

[1] Shirakawa, H., Louis, E. J., MacDiarmid, A. G., Chiang, C. K., Heeger, A. J., *J. Chem. Soc. Chem. Commun.*, **1977**, 578-580.

[2] Chiang, C. K., Fincher, C. R., Jr., Park, Y. W., Heeger, A. J., Shirakawa, H., Louis, E. J., Gau, S. C., MacDiarmid, A. G., *Phys. Rev. Lett.*, **1977**, *39*, 1098-1101.

[3] http://nobelprize.org/chemistry/laureates/2000/index.html.

[4] Shirakawa, H., *Angew. Chem. Int. Ed.*, **2001**, *40*, 2575-2580.

[5] Miller, L. S., Mullin, J. B., Editors, *Electronic Materials: From Silicon to Organics*, **1991**.

[6] Farchioni, R., Grosso, G., Editors, *Organic Electronic Materials: Conjugated Polymers and Low Molecular Weight Organic Solids. [In: Springer Ser. Mater. Sci., 2001; 41]*, **2001**.

[7] Forrest, S. R., *Nature*, **2004**, *428*, 911-918.

[8] Kelley, T. W., Baude, P. F., Gerlach, C., Ender, D. E., Muyres, D., Haase, M. A., Vogel, D. E., Theiss, S. D., *Chem. Mater.*, **2004**, *16*, 4413-4422.

[9] Tang, C. W., VanSlyke, S. A., *Appl. Phys. Lett.*, **1987**, *51*, 913-915.

[10] Drury, C. J., Mutsaers, C. M. J., Hart, C. M., Matters, M., de Leeuw, D. M., *Appl. Phys. Lett.*, **1998**, *73*, 108-110.

[11] Horowitz, G., *Adv. Mater*, **1990**, *2*, 287-292.

[12] Tang, C. W., *Appl. Phys. Lett.*, **1986**, *48*, 183-185.

[13] www.epson.co.jp/e/newsroom.

[14] http://samsung.com/PressCenter/PressRelease.asp?seq=20050519_0000123644.

[15] Murano, S., Burghart, M., Birnstock, J., Wellmann, P., Vehse, M., Werner, A., Canzler, T., Stuebinger, T., He, G., Pfeiffer, M., Boerner, H., *Proceedings of SPIE-The International Society for Optical Engineering*, **2005**, *5937*, 59370H/59371-59370H/59378.

[16] http://www.epson.co.jp/e/newsroom/2006/news_20060314.htm.

[17] http://www.heise.de/newsticker/.

[18] Clemens, W., Fix, W., *Physik Journal*, **2003**, *2*, 31-36.

[19] http://www.polyic.de/de/index.php.

[20] Bardeen, J., *Phys. Rev.*, **1947**, *71*, 717.

[21] Gertsen, C., Kneser, H. O., Vogel, H., *Physik*, Springer Verlag, Berlin Heidelberg, **1986**.

[22] www.intel.com.

[23] Tsumura, A., Koezuka, H., Ando, T., *Appl. Phys. Lett.*, **1986**, *49*, 1210-1212.

[24] Garnier, F., *Chem. Phys.*, **1998**, *227*, 253-262.

[25] Dimitrakopoulos, C. D., Malenfant, P. R. L., *Adv. Mater.*, **2002**, *14*, 99-117.

[26] Ling, M. M., Bao, Z., *Chem. Mater.*, **2004**, *16*, 4824-4840.

[27] Veres, J., Ogier, S., Lloyd, G., de Leeuw, D., *Chem. Mater.*, **2004**, *16*, 4543-4555.

[28] Brown, A. R., Jarrett, C. P., de Leeuw, D. M., Matters, M., *Synth. Met.*, **1997**, *88*, 37-55.

[29] Horowitz, G., Hajlaoui, R., Bouchriha, H., Bourguiga, R., Hajlaoui, M., *Adv. Mater*, **1998**, *10*, 923-927.

[30] Batlogg, B., *European conference on organic electronics and related phenomena*, **2001**, Potsdam, Germany.

[31] de Leeuw Dago, M., *personal communication*.

[32] Dimitrakopoulos, C. D., Mascaro, D. J., *IBM J. Res. & Dev.*, **2001**, *45*, 11-27.

[33] Pernstich, K. P., Goldmann, C., Krellner, C., Oberhoff, D., Gundlach, D. J., Batlogg, B., *Synth. Met.*, **2004**, *146*, 325-328.

[34] Zen, A., Neher, D., Silmy, K., Hollaender, A., Asawapirom, U., Scherf, U., *Jap. J. Appl. Phys.*, **2005**, *44*, 3721-3727.

[35] Veres, J., Ogier, S., Leeming, S., Brown, B., Cupertino, D., *Materials Research Society Symposium Proceedings*, **2002**, *708*, 243-250.

[36] Veres, J., Ogier, S. D., Leeming, S. W., Cupertino, D. C., Khaffaf, S. M., *Adv. Funct. Mater.*, **2003**, *13*, 199-204.

[37] Karl, N., *Synth. Met.*, **2003**, *133-134*, 649-657.

[38] Sirringhaus, H., *Adv. Mater.*, **2005**, *17*, 2411-2425.

[39] Sundar Vikram, C., Zaumseil, J., Podzorov, V., Menard, E., Willett Robert, L., Someya, T., Gershenson Michael, E., Rogers John, A., *Science*, **2004**, *303*, 1644-1646.

[40] Kelley, T. W., Muyres, D. V., Baude, P. F., Smith, T. P., Jones, T. D., *Mat. Res. Soc. Proc.*, **2003**, *771*, 169-179.

[41] Meng, H., Zheng, J., Lovinger, A. J., Wang, B.-C., Van Patten, P. G., Bao, Z., *Chem. Mater.*, **2003**, *15*, 1778-1787.

[42] Miao, Q., Nguyen, T.-Q., Someya, T., Blanchet, G. B., Nuckolls, C., *J. Am. Chem. Soc.*, **2003**, *125*, 10284-10287.

[43] Laquindanum, J. G., Katz, H. E., Lovinger, A. J., *J. Am. Chem. Soc.*, **1998**, *120*, 664-672.

[44] Katz, H. E., Bao, Z., Gilat, S. L., *Acc. Chem. Res.*, **2001**, *34*, 359-369.

[45] Garnier, F., Yassar, A., Hajlaoui, R., Horowitz, G., Deloffre, F., Servet, B., Ries, S., Alnot, P., *J. Am. Chem. Soc.*, **1993**, *115*, 8716-8721.

[46] Dodabalapur, A., Torsi, L., Katz, H. E., *Science*, **1995**, *268*, 270-271.

[47] Dimitrakopoulos, C. D., Furman, B. K., Graham, T., Hegde, S., Purushothaman, S., *Synth. Met.*, **1998**, *92*, 47-52.

[48] Noh, Y.-Y., Azumi, R., Goto, M., Jung, B.-J., Lim, E., Shim, H.-K., Yoshida, Y., Yase, K., Kim, D.-Y., *Chem. Mater.*, **2005**, *17*, 3861-3870.

[49] Meng, H., Bao, Z., Lovinger, A. J., Wang, B. C., Mujsce, A. M., *J. Am. Chem. Soc.*, **2001**, *123*, 9214-9215.

[50] Bao, Z., Dodabalapur, A., Lovinger, A. J., *Appl. Phys. Lett.*, **1996**, *69*, 4108.

[51] Sirringhaus, H., Tessler, N., Friend, R. H., *Science*, **1998**, *280*, 1741.

[52] Sirringhaus, H., Brown, P. J., Friend, R. H., Nielsen, M. M., Bechgaard, K., Langeveld-Voss, W., Spiering, A. J. H., Janssen, R. A. J., Meijer, E. W., Herwig, P., de Leeuw, D. M., *Nature*, **1999**, *401*, 685.

[53] Yu, W., Meng, H., Pei, J., Huang, W., *J. Am. Chem. Soc.*, **1998**, *120*, 11808-11809.

[54] Ficker, J., von Seggern, H., Rost, H., Fix, W., Clemens, W., McCulloch, I., *Appl. Phys. Lett.*, **2004**, *85*, 1377.

[55] Fuchigami, H., Tsumura, A., Koezuka, H., *Appl. Phys. Lett.*, **1993**, *63*, 1372-1374.

[56] McCulloch, I., Heeney, M., Bailey, C., Genevicius, K., MacDonald, I., Shkunov, M., Sparrowe, D., Tierney, S., Wagner, R., Zhang, W., Chabinyc, M. L., Kline, R. J., McGehee, M. D., Toney, M. F., *Nature Materials*, **2006**, *5*, 328-333.

[57] Sirringhaus, H., Wilson, R. J., Friend, R. H., Inbasekaran, M., Wu, W., Woo, E. P., Grell, M., Bradley, D. D. C., *Appl. Phys. Lett.*, **2000**, *77*.

[58] Broer, D. J., Lub, J., Mol, G. N., *Nature*, **1995**, *378*, 467-469.

[59] McCulloch, I., Zhang, W., Heeney, M., Bailey, C., Giles, M., Graham, D., Shkunov, M., Sparrowe, D., Tierney, S., *J. Mater. Chem.*, **2003**, *13*, 2436-2444.

[60] Pope, M., Kallmann, H. P., Magnante, P., *J. Chem. Phys.*, **1963**, *38*, 2042-2043.

[61] Helfrich, W., Schneider, W. G., *Phys. Rev. Lett.*, **1965**, *14*, 229-231.

[62] Tang, C. W., van Slyke, S. A., *Appl. Phys. Lett.*, **1987**, *51*, 913-915.

[63] Bradley, D. D. C., *Adv. Mater*, **1992**, *4*, 756-758.

[64] Rothberg, L. J., Lovinger, A. J., *J. Mater. Res.*, **1996**, *12*, 3174-3186.

[65] Sheats, J. R., Antoniadis, H., Hueschen, M., Leonard, W., Miller, J., Moon, R., Roitman, D., Stocking, A., *Science*, **1996**, *273*, 884-888.

[66] Shirota, Y., *J. Mater. Chem.*, **2000**, *10*, 1-25.

[67] D'Andrade, B. W., Datta, S., Forrest, S. R., Djurovich, P., Polikarpov, E., Thompson, M. E., *Org. Electr.*, **2005**, *6*, 11-20.

[68] Forrest, S. R., Burrows, P. E., *Org. El. Mater. Dev.*, **1997**, 415-458.

[69] Deussen, M., Bässler, H., *Chiuz*, **1997**, *31*, 76-86.

[70] Shirota, Y., *Opt. Eng.*, **2005**, *94*, 147-178.

[71] Shirota, Y., *J. Mater. Chem.*, **2005**, *15*, 75-93.

[72] Kulkarni, A. P., Tonzola, C. J., Babel, A., Jenekhe, S. A., *Chem. Mater.*, **2004**, *16*, 4556-4573.

[73] Kishigami, Y., Tsubaki, K., Kondo, Y., Kido, J., *Synth. Met.*, **2005**, *153*, 241-244.

[74] Burroughes, J. H., Bradley, D. D. C., Brown, A. R., Marks, R. N., MacKay, K., Friend, R. H., Burn, P. L., Holmes, A. B., *Nature*, **1990**, *347*, 539-541.

[75] Heeger, A. J., Braun, D., *J. Chem. Soc., Abstr.,*, **1993**, *118*, 157401.

[76] Bernius, M. T., Inbasekaran, M., O'Brien, J., Wu, W., *Adv. Mater*, **2000**, *23*, 1737.

[77] Scherf, U., *J. Mater. Chem.*, **1999**, *9*, 1853-1864.

[78] Sirringhaus, H., Buergi, L., Kawase, T., Friend, R. H., *Thin Film Transistors*, Marcel Dekker, New York, **2003**.

[79] http://www.cdtltd.co.uk/press/archive_press_release_index/2004/338.asp.

[80] Huisman, B.-H., Valeton, J. J. P., Nijssen, W., Lub, J., ten Hoeve, W., *Adv. Mater.*, **2003**, *15*, 2002-2005.

[81] Grell, M., Knoll, W., Lupo, D., Meisel, A., Miteva, T., Neher, D., Nothofer, H.-G., Scherf, U., Yasuda, A., *Adv. Mater.*, **1999**, *11*, 671-675.

[82] Whitehead, K. S., Grell, M., Bradley, D. D. C., Jandke, M., Strohriegl, P., *Appl. Phys. Lett.*, **2000**, *76*, 2946-2948.

[83] Borsenberger, P. M., Weiss, D. S., *Organic Photoreceptors for Xerography*, Marcel Dekker, Inc., **1998**.

[84] Jandke, M., Strohriegl, P., Berleb, S., Werner, E., Brütting, W., *Macromolecules*, **1998**, *31*, 6436-6443.

[85] Pfeuffer, T., Hanft, D., Strohriegl, P., *Liq. Cryst.*, **2002**, *29*, 1555-1564.

[86] Schlüter, A. D., *J. Polym. Sci. Part A: Polym. Chem.*, **2001**, *39*, 1533-1556.

[87] Pernstich, K. P., Goldmann, C., Krellner, C., Oberhoff, D., Gundlach, D. J., Batlogg, B., *Synthetic Metals*, **2004**, *146*, 325-328.

[88] Sigwalt, P., Wegner, G., Morin, J.-F., Leclerc, M., Ades, D., Siove, A., *Macromol. Rapid Commun.*, **2005**, *26*, 761-778.

[89] Romero, D. B., Schaer, M., Leclerc, M., Ades, D., Siove, A., Zuppiroli, L., *Synth. Met.*, **1996**, *80*, 271.

[90] Sonntag, M., Strohriegl, P., *Chem. Mater.*, **2004**, *16*, 4736-4742.

[91] Geissler, U., Hallensleben, M. L., Rienecker, A., Rohde, N., *Polym. Adv. Tech.*, **1997**, *8*, 87-92.

[92] Zotti, G., Schiavon, G., Zecchin, S., Morin, J.-F., Leclerc, M., *Macromolecules*, **2002**, *35*, 2122-2128.

[93] Pommerehne, J., Vestweber, H., Guss, W., Mahrt, R. F., Bässler, H., Porsch, M., Daub, J., *Adv. Mater.*, **1995**, *7*, 551-554.

[94] Kauffman, J. M., Litak, P. T., Novinski, J. A., Kelley, C. J., Ghiorghis, A., Qin, Y., *J. Fluorescence*, **1995**, *5*, 295-305.

[95] Crosby, G. A., Demas, J. N., *J. Phys. Chem.*, **1971**, *75*, 991-1024.

[96] Baude, P. F., Ender, D. A., Haase, M. A., Kelley, T. W., Muyres, D. V., Theiss, S. D., *Appl. Phys. Lett.*, **2003**, *82*, 3964-3966.

[97] van Breemen, A. J. J. M., Herwig, P. T., Chlon, C. H. T., Sweelssen, J., Schoo, H. F. M., Setayesh, S., Hardeman, W. M., Martin, C. A., de Leeuw, D. M., Valeton, J. J. P., Bastiaansen, C. W. M., Broer, D. J., Popa-Merticaru, A. R., Meskers, S. C. J., *J. Am. Chem. Soc.*, **2006**, *128*, 2336-2345.

[98] Adam, D., Schuhmacher, P., Simmerer, J., Haeussling, L., Siemensmeyer, K., Etzbach, K. H., Ringsdorf, H., Haarer, D., *Nature*, **1994**, *371*, 141-143.

[99] Fechtenkötter, A., Saalwächter, K., Harbison, M. A., Müllen, K., Spiess, H. W., *Angew. Chem. Int. Ed.*, **1999**, *38*, 3039-3042.

[100] Aldred, M. P., Eastwood, A. J., Kelly, S. M., Vlachos, P., Contoret, A. E. A., Farrar, S. R., Mansoor, B., O'Neill, M., Tsoi, W. C., *Chem. Mater.*, **2004**, *16*, 4928-4936.

[101] Kodomari, M., Satoh, H., Yoshitomi, S., *J. Org. Chem.*, **1988**, *53*, 2093-2094.

[102] Lemmer, U., Heun, S., Mahrt, R. F., Scherf, U., Hopmeier, M., Siegner, U., Goebel, E. O., Müllen, K., Baessler, H., *Chem. Phys. Lett.*, **1995**, *240*, 373-378.

[103] Kido, J., Ikeda, W., Kimura, M., Nagai, K., *Jpn. J. Appl. Phys., Part 2*, **1996**, *35*, L394-L396.

[104] Montes, V. A., Li, G., Pohl, R., Shinar, J., Anzenbacher, P., Jr., *Adv. Mater*, **2004**, *16*, 2001-2003.

[105] Baldo, M. A., O'Brien, D. F., You, Y., Shoustikov, A., Sibley, S., Thompson, M. E., Forrest, S. R., *Nature*, **1998**, *395*, 151-154.

[106] Kawamura, Y., Goushi, K., Brooks, J., Brown, J. J., Sasabe, H., Adachi, C., *Appl. Phys. Lett.*, **2005**, *86*, 0711041-0711043.

[107] Kwong, R. C., Nugent, M. R., Michalski, L., Ngo, T., Rajan, K., Tung, Y.-J., Weaver, M. S., Zhou, T. X., Hack, M., Thompson, M. E., Forrest, S. R., Brown, J. J., *Appl. Phys. Lett.*, **2002**, *81*, 162-164.

[108] Tokito, S., Iijima, T., Suzuri, Y., Kita, H., Tsuzuki, T., Sato, F., *Appl. Phys. Lett.*, **2003**, *83*, 569-571.

Novel Star-shaped Triphenylamine Based Molecular Glasses and their Use in OFETs

Martin Sonntag, Klaus Kreger, Doris Hanft, Peter Strohriegl*

Universität Bayreuth, Lehrstuhl für Makromolekulare Chemie I, Universitätsstraße 30, 95440 Bayreuth, Germany

Sepas Setayesh, Dago de Leeuw

Philips Research Laboratories, Prof. Holstlaan 4, 5656 AA Eindhoven, The Netherlands

Chemistry of Materials, **2005,** *17*, 3031-3039.

Summary

Six novel star-shaped compounds with a triphenylamine core and carbazole or fluorene side arms have been synthesized by Suzuki cross coupling. The star-shaped molecules are able to form molecular glasses. They were characterized regarding their thermal, optical and electrochemical properties. The new compounds were tested as organic semiconductors in solution processed organic field-effect transistors (OFETs). Mobilities of 3×10^{-4} cm^2/Vs, high on/off-ratios of up to 10^5 and low threshold voltages were obtained. The new materials show very small hysteresis and an exceptionally high stability under ambient conditions.

Keywords: molecular glass, Suzuki cross coupling, carbazole, triphenylamine, OFET

*To whom correspondence should be addressed. E-mail: peter.strohriegl@uni-bayreuth.de

1. Introduction

Among organic materials, vitrification was regarded for a long time to be mainly a privilege of polymers. Today a large number of amorphous low molar mass materials, so-called organic glasses, are known. Especially those with conjugated π-electron systems have attracted the interest of many research groups[1, 2]. Due to their remarkable electronic and optical properties, such amorphous compounds have a high potential as materials in optoelectronic devices. In fact, molecular glasses are widely used in photocopiers[3], laser printers and organic light-emitting diodes (OLEDs)[4].

In electronic and optoelectronic devices organic materials are usually used as thin films. From molecular glasses such films can be prepared both from solution, e.g. drop casting, spin coating and ink jet printing[5] or by vapor deposition from the gas phase. Compared to polymers, amorphous molecular materials have a number of advantages. Molecular glasses are monodisperse compounds and therefore can be highly purified by column chromatography or sublimation. This is very important for optoelectronic materials since a small amount of impurities is often detrimental for the electrical properties, e. g. the charge carrier mobility.

In the past, we have studied a number of organic glasses with star-shaped architectures.[6-10] We found that star-shaped molecules with three side arms have excellent glass forming properties[8, 9]. Amorphous phases from such molecules showed excellent long-term stability under ambient conditions, which means that the tendency to crystallize is very low. The glass transitions of these compounds are at sufficiently high temperatures to allow their application in electronic devices.

An upcoming field of application is organic electronics where π-conjugated molecular glasses are used as active material in organic field effect transistors (OFETs). In this paper we describe the synthesis of six novel star-shaped molecules with a triphenylamine core and carbazole or fluorene side arms. The molecules are shown in Scheme 1. **13-16** form molecular glasses which have been successfully tested as semiconductors in organic field-effect transistors (OFETs).

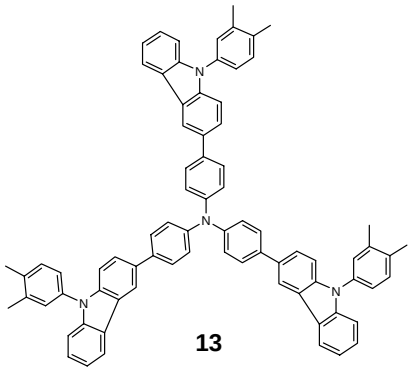

13

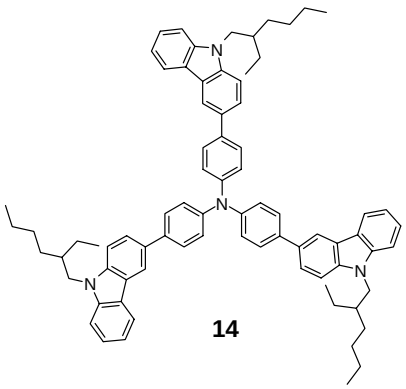

14

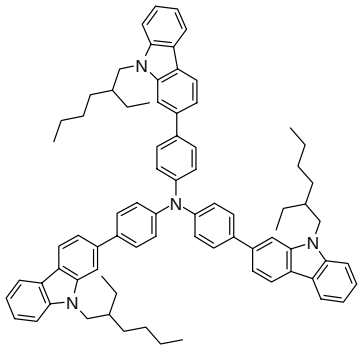

15

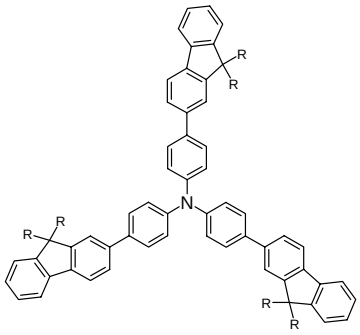

16 a-c

	R
16 a	ethyl
16 b	butyl
16 c	hexyl

Scheme 1. *Structures of the star-shaped molecules.*

2. Results and Discussion

Synthesis of the carbazole and fluorene side arms and the triphenylamine core

Monofunctional carbazoles and fluorenes were used as side arms for our star-shaped molecules (Scheme 2). Bromination of carbazole with Br_2 usually leads to a variety of brominated carbazole compounds. Due to the electronic structure of the carbazole molecule, the activated 3- and 6-positions are substituted first. By using only one equivalent of bromine and careful control of the reaction temperature at 0 °C it is possible to obtain 3-bromocarbazole (**1**) in good yield.

The synthesis of 2-bromocarbazole (**2**) is more complicated. In this case, the bromine has to be introduced before the carbazole skeleton is generated. For this purpose we used the ring closure reaction of 4-bromo-2'-nitro-biphenyl which has been reported elsewhere [11].

In the next step, the bromocarbazoles **1** and **2** were N-alkylated with 2-ethyl-hexyl bromide in order to achieve solubility and good film forming properties of the target compounds (Scheme 2). For the synthesis of the phenylsubstituted carbazole derivative **5**, 3-bromocarbazole (**1**)

was N-phenylated with 4-iodo-1,2-dimethyl-benzene and CuI in a modified Goldberg reaction[12].

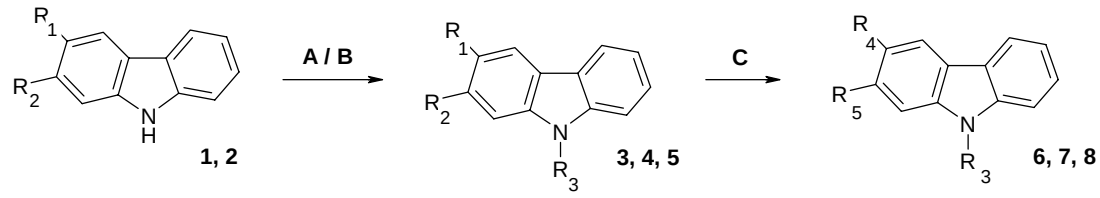

1, 2 **3, 4, 5** **6, 7, 8**

A = 2-ethyl-hexylbromide, acetone, KOH-powder, PTC, reflux, 12 h

B = 4-Iodo-1,2-dimethyl-benzene, trans-cyclohexane-1,2-diamine, CuI, DMF, toluene, K_2CO_3, 115 °C, 2.5 h

C = n-BuLi, THF (abs.), 2-isopropoxy-4,4,5,5-tetramethyl-1,3,2-dioxaborolane, -78 °C, 12 h

	R_1	R_2	R_3	R_4	R_5
1	Br	H	---	---	---
2	H	Br	---	---	---
3	H	Br	ethyl-hexyl	---	---
4	Br	H	ethyl-hexyl	---	---
5	Br	H	3,4-dimethyl-phenyl	---	---
6	---	---	ethyl-hexyl	borolane	H
7	---	---	ethyl-hexyl	H	borolane
8	---	---	3,4-dimethyl-phenyl	borolane	H

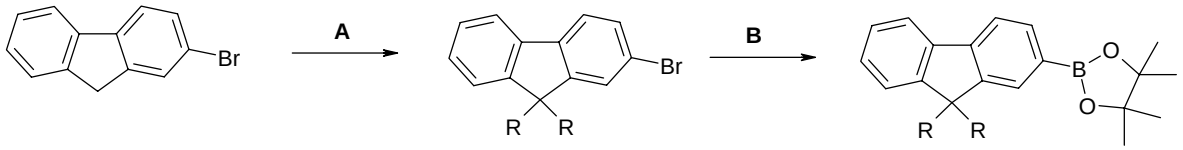

9 **10 a-c** **11 a-c**

A = alkyl bromide, 50% NaOH, PTC, DMSO, 80 °C, 16 h

B = n-BuLi, THF, 2-isopropoxy-4,4,5,5-tetramethyl-1,3,2-dioxaborolane, -78 °C, 12 h

10 / 11	R
a	ethyl
b	butyl
c	hexyl

Scheme 2. *Synthesis of the carbazole and fluorene side arms.*

The bromocarbazoles **3**, **4** and **5** were then converted to the corresponding borolane compounds **6**, **7**, and **8**, respectively. **3-5** were first lithiated at -78 °C and then reacted with 2-isopropoxy-4,4,5,5-tetramethyl-1,3,2-dioxaborolane.

The alkylations of commercially available 2-bromofluorene (**9**) were carried out in a two-phase system of DMSO and 50 % NaOH according to a literature procedure[13]. Subsequently the fluorene compounds **10a-c** were converted to the borolanes **11a-c** in the same way as described for the carbazoles.

All the molecular glasses described in this paper have a triphenylamine core. Therefore, triphenylamine was iodinated with KI/KIO_3 in a mixture of glacial acid and water under reflux to yield tris-(4-iodo-phenyl)-amine (**12**).[14]

Preparation of the star-shaped compounds

The key step of our synthesis is a trifold Suzuki cross coupling reaction which was carried out in a two-phase system of toluene and aqueous potassium carbonate. Due to the different reactivity of the side arms, two different catalyst systems were chosen. For the more reactive fluorene side arms, the reactivity of $Pd(PPh_3)_4$ is sufficient, whereas for the carbazoles a more reactive combination of $Pd(OAc)_2$ and $P(o\text{-}tol)_3$ was used. (Scheme 3).

The target compounds **13-16** were first purified by column chromatography on silica gel. Size exclusion chromatography (SEC) measurements with a column set suitable for the separation of oligomers revealed that the materials still contained small amounts of impurities (Figure 1). Since materials for applications in organic electronics must exhibit a very high purity, we decided to carry out further purification by medium pressure liquid chromatography (MPLC, for details see experimental section). With that method, the star-shaped compounds **13**, **14** and **16 a-c** were obtained in a very high purity. **15** was purified by preparative thin layer chromatography. As an example, Figure 1 shows the SEC chromatogram of **16b** before and after purification by MPLC. It can be seen that after the first purification using column chromatography some byproducts are still present. After MPLC-purification no impurities are detected in the magnified SEC scan.

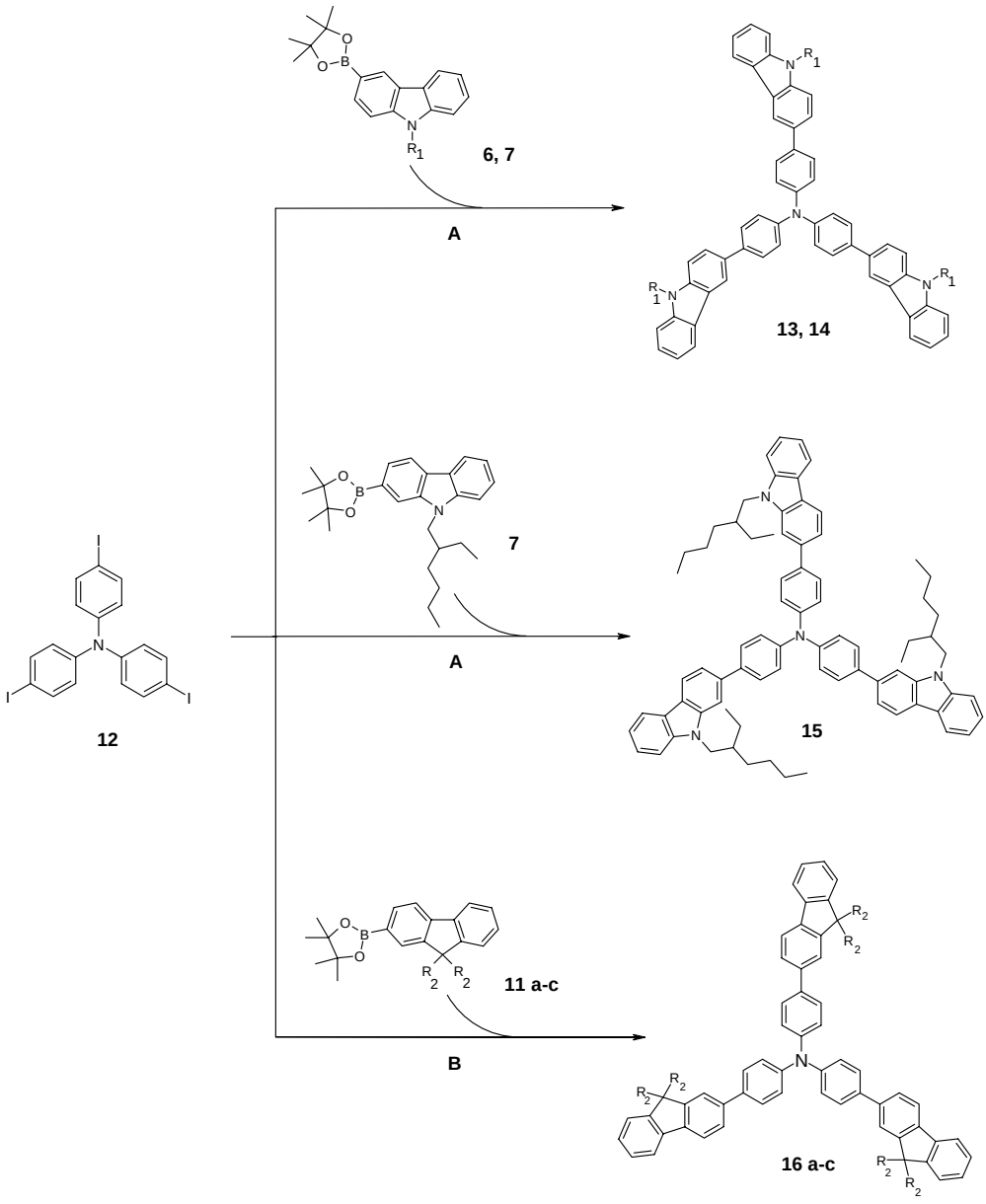

A = $P(o\text{-}tol)_3$, $Pd(OAc)_2$, toluene, 2N K_2CO_3, PTC, 60 °C, 2 h

B = $Pd(PPh_3)_4$, toluene, 2N K_2CO_3, PTC, 50 - 80 °C, 1 d

	R_1		R_2
13	3,4-dimethyl-phenyl	**16a**	ethyl
14	ethyl-hexyl	**16b**	butyl
		16c	hexyl

Scheme 3. *Synthesis of the star-shaped compounds* ***13-16*** *by Suzuki cross coupling.*

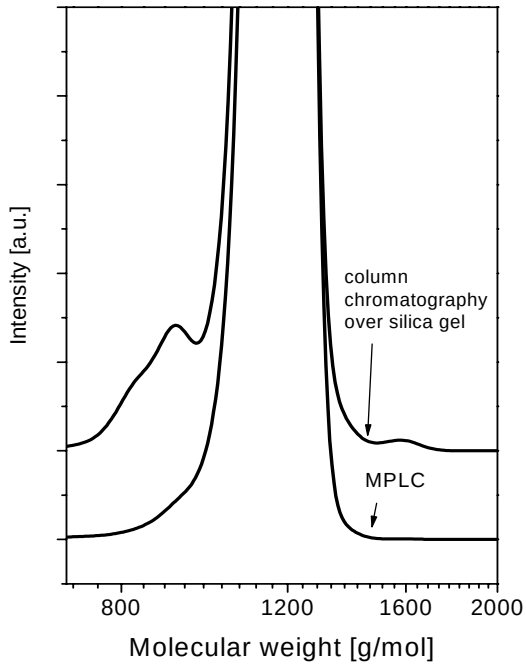

Figure 1. *Magnified section of SEC chromatograms of* ***16b*** *after conventional column chromatography and after MPLC (lower curve). Eluent: THF, calibration with oligostyrene standards.*

Properties of the star-shaped molecules

The thermal properties were determined by thermogravimetric analysis (TGA) and differential scanning calorimetry (DSC). TGA experiments in nitrogen atmosphere revealed that all of the novel star-shaped molecules exhibit a high thermal stability up to 495 °C (**13**) (Table 1).

DSC measurements showed that the two carbazole-containing molecules **13** and **14** and the fluorene compounds **16 a-c** form molecular glasses with glass transition temperatures (T_g) between 57 °C and 167 °C. It is interesting that **14** (carbazole linked in *3-position* to the core) forms a molecular glass (T_g = 68 °C) whereas **15** (carbazole building block linked in *2-position* to the core) crystallizes upon cooling and shows a melting point (T_m) at 223 °C. Nevertheless, amorphous films are also obtained from **15** when the material is processed from solution.

Table 1: *Thermal characteristics of the star-shaped molecules* ***13-16****.*

	T_{dec} [°C][1]	T_g [°C][2]	T_m [°C][2]
13	495	167	---
14	413	68	---
15	424	---	223
16a	407	118	248[3]
16b	384	96	---
16c	392	57	---

[1] Onset of decomposition determined by TGA, heating rate 10 K/min, N_2 atmosphere

[2] Determined by DSC, scan rate 10 K/min, N_2 atmosphere, 2nd run

[3] Melting point was only detected during the first heating; the compound vitrified on cooling to room temperature with 10 K/min

The absorption and fluorescence spectra of **14**, **15** and **16a** are presented in Figure 2. It turns out that the longest wavelength absorption of the fluorene-2-yl-compound **16a** and the carbazole-2-yl- compound **15** are very similar (Table 2). Furthermore, the emission spectra of **15** and **16a** are also almost identical. In the case of the carbazole-3-yl-compound **14**, the absorption and fluorescence maxima are shifted to shorter wavelengths.

The conjugated system is best represented by a benzidine-like structure in the star-shaped compounds where the carbazole side arms are linked in the 3-position, whereas in the 2-linked compounds **15** and **16a**, the conjugation is extended over a terphenyl-like structure. (Figure 2)

Table 2. *Optical properties of the star-shaped molecules* ***13-16****.*

	λ_{abs} [nm][1]	$\lambda_{max,fluo}$ [nm][2]	λ_{ae} [nm][3]
13	348	405	390
14	344	394	385
15	360	409	398
16a	365	408	401
16b	365	408	401
16c	365	408	401

[1] Longest wavelength absorption maximum, measured in 10^{-6} M THF solution

[2] Fluorescence spectra measured in 10^{-4} M THF solution, excitation wavelength 350 nm

[3] Absorption edge

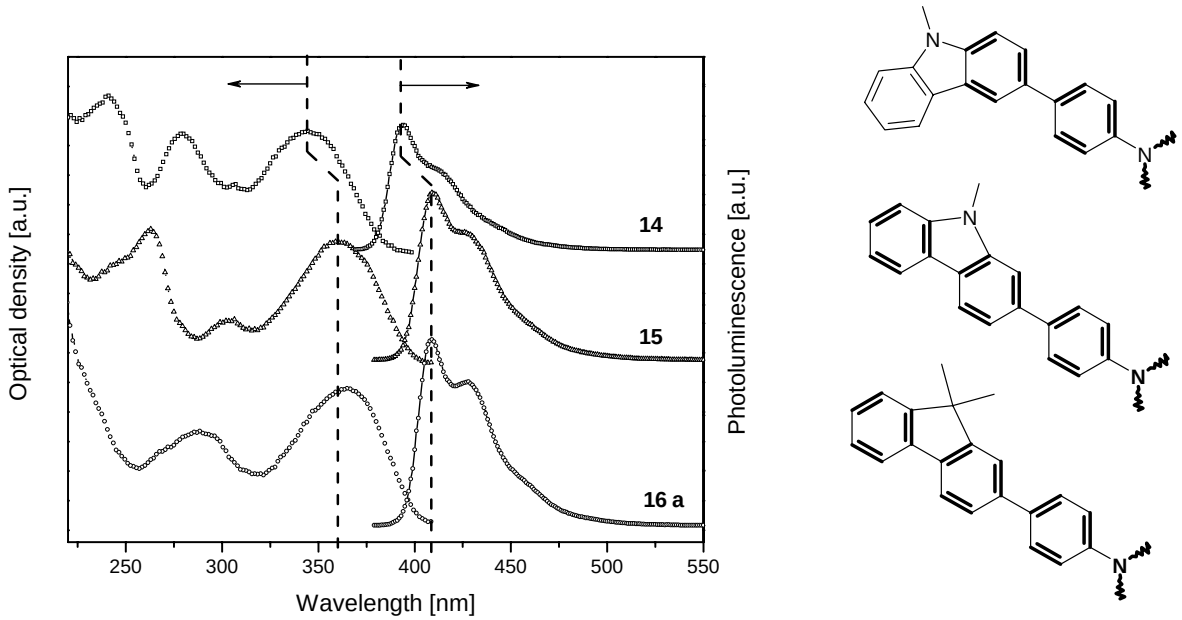

Figure 2. *Comparison of the absorption and fluorescence spectra of star-shaped compounds with 2- / 3-linked carbazole and fluorene side arms. Absorption spectra were measured from* 10^{-6} *M THF solutions. The fluorescence spectra were taken from* 10^{-4} *M THF solutions (excitation wavelength: 350 nm). Right: schematic of the conjugated segments in* ***14****,* ***15*** *and* ***16a****.*

The electrochemical stability of the star-shaped compounds was examined by cyclic voltammetry (CV). All measurements were carried out at 25 °C in CH_2Cl_2 solution containing 0.1 M tetrabutylammonium hexafluorophosphate ($TBAPF_6$) as supporting electrolyte with a glassy carbon working electrode. The oxidation potentials were measured vs. Ag/AgCl as the reference electrode. The experiments were calibrated with the standard ferrocene/ferrocenium redox system. Taking –4.8 eV as HOMO level for the ferrocene redox system[17], the HOMO values of the star-shaped molecules were calculated. The LUMO values were obtained from the optical gap (ΔE), which in turn can be calculated from the absorption edge (ref. Table 2). The results of the CV measurements are shown in Table 3.

Table 3. *Oxidation potentials, HOMO and LUMO values of the star-shaped molecules* ***13-16.***

	Ox_1 vs. Ag/Ag^+[V][1]	Ox_2 vs. Ag/Ag^+[V][1]	reversible	HOMO [eV]	ΔE [eV][2]	LUMO [eV]
13	0.27	0.66	yes	-5.0	3.2	-1.8
14	0.30	0.52	yes	-5.0	3.2	-1.8
15	(0.44)	(0.59)	no	(-5.2)	3.1	(-2.1)
16a-c	0.50	1.04	yes	-5.2	3.1	-2.1

[1] CV measured in CH_2Cl_2 solution with $TBAPF_6$ and ferrocene / ferrocenium

[2] Optical gap taken from the absorption spectra

To check if the new compounds are electrochemically stable, 10 subsequent redox cycles were measured. The fluorene-containing compounds **16a-c** do not show any change during the 10 measurements. Two fully reversible oxidations at about 0.5 eV and 1.0 eV are detected. HOMO values of –5.2 eV were calculated for **16a-c**. The carbazole based molecules **13** and **14** also showed reversible oxidations during the 10 redox cycles. Only compound **15**, in which the carbazole units are connected in the 2-positions to the triphenylamine core, is electrochemically unstable. We suppose that the electron rich and therefore highly activated 3- and 6-positions of the carbazole rings in **15** are very sensitive towards electrochemical oxidation, which may lead to dimerization reactions[18]. As the 3- and 6-positions in fluorenes are not activated, **16a-c** exhibit fully reversible oxidations. In contrast to the electrochemically unstable compound **15**, the carbazole-containing molecules **13** and **14** in which the carbazole rings are linked in 3-position to the triphenylamine core exhibit a reversible redox behavior. As already described with the optical spectra, we attribute this to the fact that the 'chromophore' in **13** and **14** is a benzidine-like structure whereas in the case of **15** it is more like an amino-substituted terphenyl. This leads to a smaller activation of the 6-positions in **13** and **14** compared to **15** and hence to a higher electrochemical stability. For the electrochemically stable compounds **13** and **14** HOMO values of –5.0 eV were determined.

Material screening in OFET devices.

Today, aromatic amines are frequently used as xerographic materials and in OLEDs,[3, 19] whereas reports on their use as semiconducting material in OFETs are seldom. Only very recently triarylamine oligomers have been used in organic field effect transistors, and high field effect mobilities combined with exceptionally high stabilities have been reported[20].

The transistor architecture we have used for testing our new materials is shown in Figure 3[21]. The drain current was measured as a function of the gate bias (forward sweep from +5 V to

–20 V / backward sweep from –20 V to + 5V). The devices were tested with two fixed drain potentials of –2 V and –20 V, respectively.

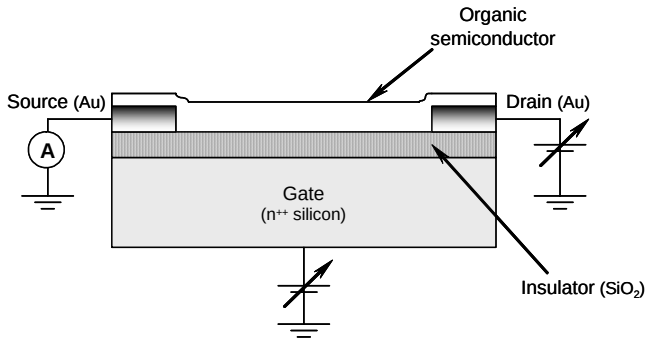

Figure 3. *Schematic of the organic field-effect transistors.*

The mobility was calculated from the gate sweep according to the following equation[22]:

$$\mu_{FET} = (L/W\ C_i\ V_D)\ (\partial I_D/\partial V_G) \qquad \textbf{eq. 1}$$

Where L is the channel length, W is the channel width, C_i the capacitance of the insulator per unit area, V_D is the drain voltage, I_D is the drain current and V_G is the gate voltage. All measurements were performed in air.

The transfer characteristics of an OFET prepared from the carbazole-containing molecular glass **14** is presented in Figure 4. **14** exhibits a field-effect mobility of $10^{-4}\,cm^2V^{-1}s^{-1}$, an on/off-ratio of 10^4 and a very low turn-on voltage of about -2 V. The results of the transistor measurements with the other molecular glasses are summarized in Table 4. It turns out that the three carbazole-containing compounds (**13**, **14**, **15**) and the fluorene glass **16b** all have field-effect mobilities in the range of $10^{-4}\,cm^2V^{-1}s^{-1}$. Their on/off-ratios vary from 10^3 for **13** to 10^5 for **16b**. Since both the carbazole glasses **13-15** and the fluorene glass **16b** have HOMO levels between -5.0 and -5.2 eV, holes are efficiently injected from the gold electrodes which leads to very low onset voltages between -1 and -5 V.

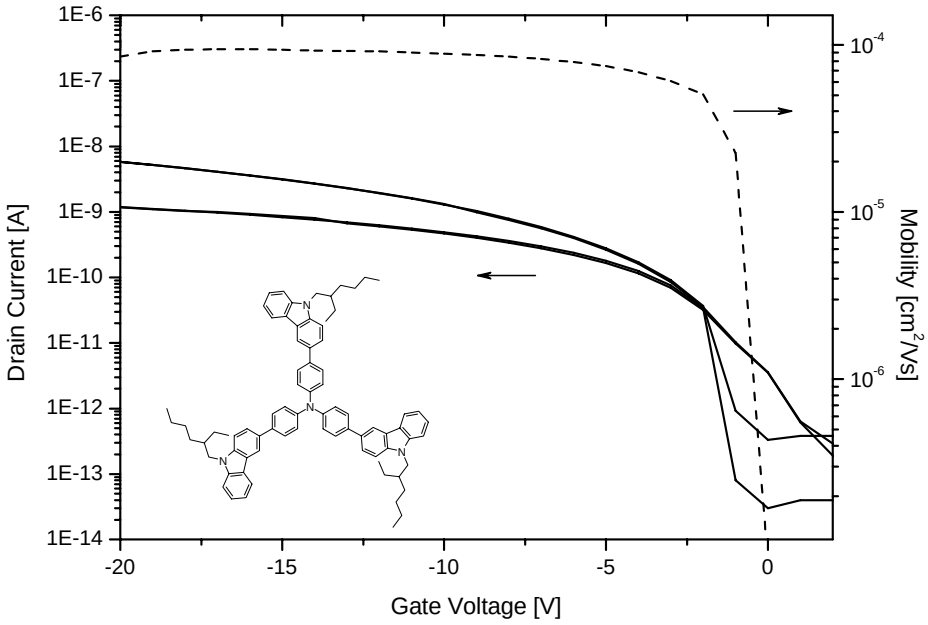

Figure 4. *OFET characteristics of* ***14****. The drain potentials were -20 V and -2 V in the upper and lower traces, respectively (solid lines). The dashed curve shows the mobility values (for* V_D *= -2 V).*

A very important property of organic materials to be used in OFETs is their stability under ambient conditions. A field-effect transistor from the star-shaped compound **13** was stored for 4 months under ambient conditions and light in the laboratory and then tested again, with no observed change in the onset voltage or on/off-ratio. Only the field-effect mobility dropped to a value of 2 x 10^{-5} $cm^2V^{-1}s^{-1}$. The transistor characteristics of **13** before and after storage are presented in Figure 5.

Table 4. *Properties of the OFET devices.*

	Onset [V] [1]	μ_{FET} [$cm^2V^{-1}s^{-1}$] [2]	I_{on}/I_{off} [3]
13	-3	1×10^{-4}	10^3
14	-2	1×10^{-4}	10^4
15 [4]	-5	3×10^{-4}	10^4
16b	-1	1×10^{-4}	10^5

[1] Determined at a drain potential of -2 V

[2] Mobility calculated using equation 1

[3] On/off-ratio calculated from the drain currents at gate voltages of 0 and -20 V and V_D = -20 V

[4] amorphous film processed from solution

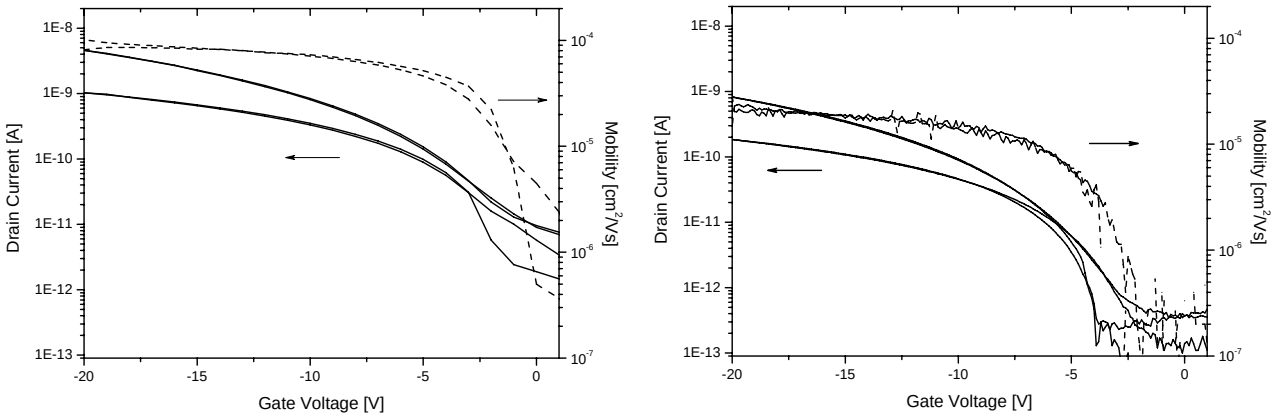

Figure 5. *Transfer characteristics of* ***13****. The drain potentials were –20 V and –2 V in the upper and lower traces, respectively (solid lines). The transistor shows only very small hysteresis in the forward/backward sweeps. The dashed curve shows that the mobility (calculated from equation 1) reaches its maximum almost directly after turning on the FET device. Left: freshly prepared device. Right: device performance after storage under ambient conditions and daylight for 4 months.*

3. Conclusions

We have synthesized six novel star-shaped molecules with a triphenylamine core and tested them in organic field-effect transistors. By using alkylfluorenes and N- alkylated or N-phenylated carbazole units as side arms of the novel molecular glasses we obtained electrochemically stable materials with a high solubility in common organic solvents and good film-forming properties. The materials were highly purified by medium pressure liquid chromatography (MPLC). We have tested the new materials as semiconductors in solution processed organic field effect transistors. Compounds **13-15** and **16b** exhibit mobilities in the range of 10^{-4} $cm^2V^{-1}s^{-1}$. The highest mobility of 3×10^{-4} cm^2/Vs was obtained in a device prepared from **15**. Probably the most promising result is the very good long term stability of the OFETs under ambient conditions. The fact that the molecular glasses can be easily processed from solution helps to simplify device preparation.

We have shown that the triphenylamine based molecular glasses, both with carbazole and fluorene side arms are well suited as semiconductors in organic FETs. We believe that improvements in surface treatment and the use of insulators with a low dielectric constant[20] may lead to a further increase of the field-effect mobility and thus make the materials attractive for applications in organic electronics.

4. Experimental

Material Synthesis. All chemicals and reagents were used as received from Aldrich. Tetrahydrofuran (THF) and toluene were distilled over potassium before use. The synthesis of 2-bromocarbazole (**2**) has been reported elsewhere[11].

Synthesis of the side arms

3-Bromocarbazole (1). To a solution of 33.5 g (0.2 mol) carbazole in 800 ml pyridine, a mixture of 10.3 ml (0.2 mol) bromine in 30 ml pyridine was added slowly from a dropping funnel at 0 °C. After the addition was completed, the reaction mixture was stirred for 2 h at 0 °C. The pyridine was removed by distillation and 300 ml water, 60 ml ethanol and 5 ml HCl were added to the residue. The mixture was heated to reflux and stirred vigorously for 20 minutes. After cooling to room temperature, the residue was separated, dissolved in toluene and filtered over neutral aluminium oxide. Recrystallization from toluene yielded

32.11 g (65 %) 3-bromocarbazole (**1**) as white powder. ^{1}H-NMR (250 MHz, d_6-DMSO): δ(ppm) 7.15(t, 1H), 7.43(m, 4H), 8.12(d, 1H), 8,33(d, 1H), 11.40(s, 1H). ^{13}C-NMR (62.5 MHz, d_6-DMSO) 110.9, 111.2, 113.2, 119.3, 120.5, 121.0, 121.8, 123.1, 125.8, 128.2, 138.7, 140.5. IR (KBr): $\tilde{\nu}$ (cm^{-1}): 3404, 1753, 1622, 1600, 1469, 1445, 1332, 1240, 1109, 1054, 879, 724. Mass spectrum: m/z ([M$^+$]): 245/247.

3-Bromo-9-(2-ethyl-hexyl)carbazole (4). To a solution of 3 g (12 mmol) 3-bromocarbazole (**2**) in 30 ml acetone, 1.35 g (24 mmol) KOH powder, 4.26 ml (24 mmol) 2-ethyl-hexyl-bromide, and 0.2 g of tetrabutylammonium hydrogensulfate as phase-transfer catalyst were added. The reaction mixture was heated to reflux for 12 h before the solvent was evaporated. The residue was poured into water and extracted with diethyl ether. The organic layer was washed with water and dried over Na_2SO_4 before the solvent was evaporated. The crude product was purified by column chromatography on silica gel with hexane:ethyl acetate (10:1) as eluent yielding 3.86 g (85 %) 3-Bromo-9-(2-ethyl-hexyl)carbazole (**4**) as a colorless oil. ^{1}H-NMR (250 MHz, $CDCl_3$): δ(ppm) 0.87(t, 3H), 0.91(t, 3H), 1.20-1.49(m, 8H), 1.95(septet, 1H), 4.01(m, 2H), 7.15(m, 1H), 7.23(dd, 1H), 7.28(m, 1H), 7.37(m, 1H), 7.42(d, 1H), 7.84(d, 1H), 7.96(d, 1H). ^{13}C-NMR (62.5 MHz, $CDCl_3$): δ(ppm) 11.3, 14.4, 23.4, 24.8, 29.1, 31.3, 39.6, 47.9, 108.7, 109.4, 119.6, 119.7, 120.9, 121.7, 122.9, 122.2, 122.7, 126.4, 141.4, 142.1. IR (NaCl): $\tilde{\nu}$ (cm^{-1}) 3063, 2958, 2929, 2871, 1624, 1591, 1472, 1451, 1437, 1322, 1246, 1218, 1126, 721. Mass spectrum: m/z ([M$^+$]): 357/359.

2-Bromo-9-(2-ethyl-hexyl)carbazole (**3**) was prepared according to the same procedure.

3-Bromo-9-(3,4-dimethylphenyl)-carbazole (5). The reaction mixture consisting of 3-bromocarbazole (**2**) (1 g, 4 mmol), 0.25 ml (4 mmol) trans-cyclohexane-1,2-diamine, 0.7 ml (5.0 mmol) 4-iodo-1,2-dimethyl-benzene, 1.3 g (9.2 mmol) K_2CO_3, 76 mg (0.4 mmol) CuI, 30 ml DMF and 15 ml toluene was stirred under argon at 115 °C. After 2.5 h the mixture was poured into 300 ml water and was extracted three times with hexane:ethyl acetate (4:1). The organic layer was washed with water and concentrated sodium thiosulfate solution and filtered over neutral aluminium oxide. After the solvent was evaporated, the crude product was purified by column chromatography on silica gel using hexane:ethyl acetate (16:1) as eluent to yield 2.5 g (50 %) 3-Bromo-9-(3,4-dimethylphenyl)-carbazole (**5**) as a white solid. ^{1}H-NMR (250 MHz, d_6-DMSO): δ(ppm) 2.24(s, 3H), 2.26(s, 3H), 7.24(m, 3H), 7.33(m, 2H), 7.40(m, 2H), 7.50(m, 1H), 8.27(m, 1H), 8.47(m, 1H). ^{13}C-NMR (62.5 MHz, d_6-DMSO): δ(ppm) 21.3, 22.4, 110.1, 111.4, 112.5, 120.1, 120.4, 122.2, 125.0, 126.48, 126.53, 128.5, 134.4, 136.1, 139.7, 141.3 IR (KBr): $\tilde{\nu}$ (cm^{-1}) 3056, 2958, 2866, 1515, 1467, 1446, 1364, 1325, 1270, 1231, 1054, 746. Mass spectrum: m/z ([M$^+$]): 349/351.

9-(2-Ethyl-hexyl)-2-(4,4,5,5-tetramethyl-[1,3,2]dioxaborolan-2-yl)-carbazole (7). 1.5 g (4.2 mmol) 2-Bromo-9-(2-ethyl-hexyl)carbazole (**4**) were dissolved in 50 ml absolute THF under argon. The solution was cooled to –78 °C before 2.9 ml (4.6 mmol) n-BuLi (1.6M solution in hexane) were added drop-wise. The reaction mixture was stirred for 20 min before 1.0 ml (5.0 mmol) 2-isopropoxy-4,4,5,5-tetramethyl-1,3,2-dioxaborolane were added. The reaction mixture was allowed to warm to room temperature and stirred for another 12 h before it was poured into ice water. The solution was extracted with diethyl ether, the organic phase washed with brine and dried with Na_2SO_4 before the solvent was evaporated. Purification was carried out by column chromatography on silica gel with hexane:acetic ester (20:1) as eluent. The reaction yielded 1.12 g (66 %) 9-(2-Ethyl-hexyl)-2-(4,4,5,5-tetramethyl-[1,3,2]dioxaborolan-2-yl)-carbazole (**7**) as yellowish oil. ^{1}H-NMR (250 MHz, $CDCl_3$): δ (ppm): 0.80(t, 3H), 0.83(t, 3H), 1.12-1.37(m, 8H), 1,32(s, 12H), 2.02(m, 1H), 4.12 (m, 2H), 7.14(m, 1H), 7.32(d, 1H), 7.40(m, 1H), 7.61(dd, 1H), 7.79(s, 1H), 8.02(d, 1H), 8.05(d, 1H). ^{13}C-NMR (62.5 MHz, $CDCl_3$): δ (ppm): 11.0, 14.1, 23.0, 24.4, 25.0, 28.6, 30.8, 39.3, 47.2, 83.8, 109.1, 115.4, 118.6, 119.5, 120.7, 122.6, 124.8, 125.2, 126.1, 140.5, 141.3. IR (NaCl): $\tilde{\nu}$ (cm^{-1}): 3053, 2961, 2859, 1623, 1561, 1476, 1360, 1330, 1141, 964,. Mass spectrum: m/z ($[M^+]$): 405.

9-(2-ethyl-hexyl)-3-(4,4,5,5-tetramethyl-[1,3,2]dioxaborolan-2-yl)-carbazole (6).

The synthesis was carried out as described before for (**7**).The reaction yielded 80 % of **6** as yellowish oil. ^{1}H-NMR (250 MHz, $CDCl_3$): δ (ppm): 0.87(t, 3H), 0.91(t, 3H), 1.20-1.49(m, 8H), 1,41(s, 12H), 2.07(m,1H), 4.18 (m, 2H), 7.26(m, 1H), 7.38-7.42(m, 2H), 7.47(m, 1H), 7.93(d, 1H), 8.15(d, 1H), 8.62(s, 1H). ^{13}C-NMR (62.5 MHz, $CDCl_3$): δ (ppm): 11.3, 14.4, 23.4, 24.7, 25.3, 29.2, 31.3, 39.7, 47.8, 83.9, 108.7, 109.4, 119.5, 120.9, 122.9, 124.5, 125.9, 128.1, 132.4, 141.3, 143.5 . IR (NaCl): $\tilde{\nu}$ (cm^{-1}): 3042, 3013, 2972, 2855, 1623, 1596, 1458, 1429, 1354, 1223, 1073, 963, 863, 747. Mass spectrum: m/z ($[M^+]$): 405.

9-(3,4-dimethylphenyl)-3-(4,4,5,5-tetramethyl-[1,3,2]dioxaborolan-2-yl)-carbazole (8).

The synthesis was carried out as described before for (**7**).The reaction yielded 86 % of **8** as white solid. ^{1}H-NMR (250 MHz, $CDCl_3$): δ (ppm): 1.32(s, 12H), 2.32(s, 3H), 2.34(s, 3H), 7.17-7.26(m, 7H), 7.76(d, 1H), 8.10(d, 1H), 8.56(s, 1H). ^{13}C-NMR (62.5 MHz, $CDCl_3$): δ (ppm): 24.9, 31.4, 83.6, 109.3, 109.9, 120.1, 120.4, 123.0, 123.4, 125.8, 126.6, 126.7, 127.7, 132.3, 134.7, 141.2, 143.1, 150.6. IR (NaCl): $\tilde{\nu}$ (cm^{-1}): 3042, 2972, 2867, 1623, 1595, 1481, 1428, 1353, 1301, 1233, 1141, 1073, 962, 863, 748. Mass spectrum: m/z ($[M^+]$): 397.

2-Bromo-9,9-diethylfluorene (10a). 10 g (41 mmol) of the commercially available 2-bromofluorene (**9**) were dissolved in 85 ml DMSO. To the solution 0.85 g triethylbenzyl-ammonium chloride and 0.85 g tetra-n-butyl-ammonium chloride were added as phase-

transfer catalysts. After the addition of 50 ml 25 N NaOH solution, 16.8 ml (230 mmol) of bromo-ethane were added. The reaction mixture was stirred at 100 °C. After 12h, water was added until the two phases mixed. The solution was extracted with diethyl ether, washed with water and dried with Na_2SO_4 before the solvent was evaporated. The crude product was purified by column chromatography on silica gel with hexane/ethyl acetate 15:1 as eluent, yielding 12 g (97 %) 2-Bromo-9,9-diethylfluorene (**10 a**) as white crystals. ^{1}H-NMR (250 MHz, $CDCl_3$): δ (ppm): 0.32(t, 6H), 2.00(q, 4H), 7.30(m, 3H), 7.45(m, 2H), 7.55(m, 1H), 7.66(m, 1H). ^{13}C-NMR (62.5 MHz, $CDCl_3$): δ(ppm) 8.4, 32.6, 56.4, 119.7, 121.7, 122.9, 126.2, 127.0, 127.4, 129.9, 140.4, 140.5, 149.4, 152.1. Mass spectrum: m/z ([M^+]): 300/302. IR (KBr): $\tilde{\nu}$ (cm^{-1}): 3059, 2960, 2910, 2847, 1440, 1375, 1256, 1130, 1003, 874, 731.

2-Bromo-9,9-dibutylfluorene (10b).

The synthesis for **10b** was carried out as described before for **10a**. The reaction yielded 91 % of **10b** as white powder. ^{1}H-NMR (250 MHz, $CDCl_3$): δ (ppm): 0.55(m, 4H), 0.67(t, 6H), 1.03(m, 4H), 1.95(m, 4H), 7.33(m, 3H), 7.44(m, 2H), 7.55(m, 1H), 7.63(m, 1H). ^{13}C-NMR (62.5 MHz, $CDCl_3$): δ(ppm) 13.8, 23.0, 25.9, 40.1, 55.3, 119.7, 120.9, 121.0, 122.9, 126.2, 126.9, 127.4, 129.9, 140.0, 140.1, 150.3, 152.9. Mass spectrum: m/z ([M^+]): 356/358. IR (KBr): $\tilde{\nu}$ (cm^{-1}): 3059, 2960, 2910, 2874, 1440, 1375, 1256, 1130, 1003, 874, 731.

2-Bromo-9,9-dihexylfluorene (10c).

11c was prepared according to the procedure described above for **10a**. The reaction yielded 93 % of **10c** as colorless oil. ^{1}H-NMR (250 MHz, $CDCl_3$): δ (ppm): 0.55(m, 4H), 0.67(t, 6H), 1.00-1.21(m, 12H), 1.94(m, 4H), 7.32(m, 3H), 7.45(m, 2H), 7.54(m, 1H), 7.67(m, 1H). ^{13}C-NMR (62.5 MHz, $CDCl_3$): δ(ppm) 14.0, 22.6, 23.6, 29.6, 31.5, 40.3, 55.3, 119.7, 120.9, 121.0, 122,9, 126.1, 126.9, 127.4, 129.9, 140.0, 140.1, 150.3, 153.0. IR (KBr): $\tilde{\nu}$ (cm^{-1}): 3063, 3024, 2954, 2856, 1599, 1465, 1442, 1405, 1377, 1132, 1062, 876. Mass spectrum: m/z ([M^+]): 412/414.

2-(9,9-Diethyl-fluoren-2-yl)-4,4,5,5-tetramethyl-[1,3,2]dioxaborolane (11a).

8 g (26.6 mmol) of 2-bromo-9,9-diethylfluorene (**10a**) were dissolved in 100 ml absolute THF under argon. The solution was cooled to -78°C before 11.7 ml (29.2 mmol) n-BuLi (2.5M solution in hexane) were added drop-wise. The reaction mixture was stirred for 20 min before 6.5 ml (31.9 mmol) 2-isopropoxy-4,4,5,5-tetramethyl-1,3,2-dioxaborolane were added. The reaction mixture was allowed to warm to room temperature and stirred for 12 h before it was poured into ice water. The solution was extracted with diethyl ether, the organic phase washed with brine and dried with Na_2SO_4 before the solvent was evaporated. Purification was carried out by column chromatography on silica gel with hexane:acetic ester (10:1) as eluent. The

reaction yielded 7.3 g (79 %) 2-(9,9-Diethyl-fluoren-2-yl)-4,4,5,5-tetramethyl-[1,3,2]-dioxaborolane (**11a**) as white solid. ^{1}H-NMR (250 MHz, $CDCl_3$): δ (ppm): 0.29(t, 6H), 1.38(s, 12H), 2.05(m, 4H), 7.33(m, 3H), 7.69(d, 1H), 7.71(m, 1H), 7.73(d, 1H), 7.79(dd, 1H). ^{13}C-NMR (62.5 MHz, $CDCl_3$): δ (ppm): 8.5, 24.9, 32.6, 56.1, 83.7, 118.9, 120.0, 122.9, 126.7, 127.5, 128.0, 128.9, 133.7, 141.3, 144.5, 149.0, 152.4. IR (KBr): $\tilde{\nu}$ (cm^{-1}): 3064, 3038, 2999, 2926, 2875, 1608, 1456, 1418, 1356, 1141, 831. Mass spectrum: m/z ([M^+]): 348.

2-(9,9-Dibutyl-fluoren-2-yl)-4,4,5,5-tetramethyl-[1,3,2]-dioxaborolane (11b).

11b was prepared according to the same procedure as described for **11a**. The reaction yielded 72 % of **11b** as white solid. ^{1}H-NMR (250 MHz, $CDCl_3$): δ (ppm): 0.52(m, 4H), 0.65(t, 6H), 1.05(m, 4H), 1.39(s, 12H), 1.98(m, 4H), 7.27-7.37(m, 3H), 7.70(d, 1H), 7.72(m, 1H), 7.74(d, 1H), 7.81(dd, 1H). ^{13}C-NMR (62.5 MHz, $CDCl_3$): δ (ppm): 13.8, 23.0, 24.9, 25.9, 40.1, 55.0, 83.7, 118.9, 120.1, 122.9, 126.6, 127.5, 128.0, 128.8, 133.7, 140.9, 144.1, 149.8, 151.3. IR (KBr): $\tilde{\nu}$ (cm^{-1}): 3031, 2964, 2928, 1611, 1419, 1357, 1145, 741. Mass spectrum: m/z ([M^+]): 404.

2-(9,9-dihexyl-fluoren-2-yl)-4,4,5,5-tetramethyl-[1,3,2]-dioxaborolane (11c).

11c was prepared according to the same procedure as described for **11a**. The reaction yielded 75 % of **11c** as colorless oil. ^{1}H-NMR (250 MHz, $CDCl_3$): δ (ppm): 0.60(m, 4H), 0.75(t, 6H), 1.00-1.13(m, 12H), 1.38(s, 12H), 1.97(m, 4H), 7.27-7.36(m, 3H), 7.70(d, 1H), 7.72(m, 1H), 7.75(d, 1H), 7.81(dd, 1H). ^{13}C-NMR (62.5 MHz, $CDCl_3$): δ (ppm): 13.9, 22.6, 23.6, 24.9, 29.6, 31.5, 40.2, 55.1, 83.7, 118.9, 120.1, 122.9, 126.6, 127.4, 128.0, 128.8, 133.7, 140.9, 144.1, 149.9, 151.3. IR (KBr): $\tilde{\nu}$ (cm^{-1}): 3051, 2977, 2955, 2927, 1610, 1570, 1456, 1354, 1145, 963, 741. Mass spectrum: m/z ([M^+]): 460.

Synthesis of the core molecule

Tris-(4-iodophenyl)-amine (12). To a mixture of triphenylamine (12.3 g, 50 mmol) and potassium iodide (16.6 g, 100 mmol), 200 ml of glacial acetic acid and 20 ml water were added. The reaction mixture was refluxed under argon until a clear, yellow solution was obtained. 21.4 g of KIO_3 (100 mmol) were added in small portions and the mixture was refluxed for 1 h. Thereafter 20 ml of water were added to precipitate the crude product. The residue was filtered off, dissolved in toluene and washed several times with concentrated sodium thiosulfate solution. The organic layer was then washed with water, dried over Na_2SO_4 and the solvent evaporated. Recrystallization from ethyl acetate yielded 28.7 g (92 %) tris-(4-iodophenyl)-amine (**12**) as light brown crystals. ^{1}H-NMR (250 MHz, $CDCl_3$): δ(ppm)

6.81(d, 6H), 7.54(d, 6H). ^{13}C-NMR (63.5 MHz, $CDCl_3$): δ(ppm) 86.6, 126.0, 138.4, 146.4. IR (KBr): $\tilde{\nu}$ (cm^{-1}) 1574, 1483, 1312, 1283, 1058, 1003, 815, 709, 509. Mass spectrum: m/z ($[M^+]$): 623.

Synthesis of the star-shaped molecules

Tris-{4-[9-(3,4-dimethyl-phenyl)-carbazol-3-yl]-phenyl}-amine (13). 0.27 g (0.43 mmol) of tris-(4-iodo-phenyl)-amine (**12**) and 3.2 equivalents of 9-(3,4-dimethylphenyl)-3-(4,4,5,5-tetramethyl-[1,3,2]dioxaborolan-2-yl)-carbazole (**8**) (0.55 g, 1.38 mmol) were dissolved in 15 ml toluene. 8 ml of a 2M K_2CO_3 solution and 10 mg of trimethylbenzylammonium chloride were added before the reaction mixture was degassed by three subsequent freeze/thaw cycles. Thereafter 5.8 mg (2.6 x 10^{-5} mol) $Pd(AcO)_2$ and 23.7 mg (7.8 x 10^{-5} mol) tri-o-tolylphosphine were added under argon. The mixture was stirred for 10 h at 75 °C before it was poured into ice water, extracted with diethyl ether and dried with Na_2SO_4. After evaporation of the solvent the product was purified by column chromatography on silica gel with hexane:toluene (3:2) as eluent. Finally the product was purified a second time with MPLC. Hexane:tetrahydrofuran (15:1) was used as eluent at a pressure of 18 bar. The reaction yielded 0.28 g (62 %) tris-{4-[9-(3,4-dimethyl-phenyl)-carbazol-3-yl]-phenyl}-amine (**13**) as white solid. ^{1}H-NMR (250 MHz, $CDCl_3$): δ (ppm): 2.32(d, 18H), 7.17-7.38(m, 27H), 7.60(m, 9H), 8.10(m, 3H), 8.28(m, 3H). ^{13}C-NMR (62.5 MHz, $CDCl_3$): δ (ppm): 18.5, 18.9, 108.9, 117.2, 118.7, 119.3, 122.3, 122.7, 123.4, 123.5, 124.0, 124.9, 126.9, 127.3, 129.9, 131.8, 134.2, 135.0, 137.3, 139.4, 140.5. IR (KBr): $\tilde{\nu}$ (cm^{-1}): 3027, 2919, 2854, 1601, 1506, 1474, 1287, 1254, 1160, 1012, 883, 744. $\lambda_{max,abs.}$ (10^{-6} M THF solution) 348 nm; $\lambda_{max,flu.}$ (10^{-4} M THF solution) 405 nm. Mass spectrum: m/z ($[M^+]$): 1052. Isotopic clusters of M^+[g/mol] (rel. int.): 1052(100 %), 1053(89 %), 1054(39 %), 1055(12 %), 1056(3 %). Anal. Calcd for $C_{78}H_{60}N_4$ (1053.4): C, 88.94; H, 5.74; N, 5.32. Found: C, 89.14; H, 5.96; N, 4.99.

Tris-{4-[9-(2-ethyl-hexyl)-carbazol-3-yl]-phenyl}-amine (14). The synthesis was carried out as described for star-shaped compound **13**. MPLC-purification was carried out with hexane:toluene (3:1) as eluent at a pressure of 20 bar yielding 58% of **14** as white solid. ^{1}H-NMR (250 MHz, $CDCl_3$): δ (ppm): 0.80(t, 9H), 0.85(t, 9H), 1.11-1.41(m, 24H), 2.01(m, 3H), 4.10(m, 6H), 7.15(m, 6H), 7.32(m, 6H), 7.39(m, 6H), 7.61(m, 9H), 8.07(d, 3H), 8.25(m, 3H). ^{13}C-NMR (62.5 MHz, $CDCl_3$): δ (ppm): 11.4, 14.5, 23.5, 24.9, 29.3, 31.5, 39.9, 47.9, 109.5, 109.6, 118.8, 119.2, 120.8, 123.4, 123.7, 124.7, 125.2, 126.1, 128.3, 132.2, 140.7, 141.8. IR (KBr): $\tilde{\nu}$ (cm^{-1}): 3055, 3028, 2955, 2926, 1627, 1600, 1514, 1488, 1476, 1315, 1218, 1155, 745. $\lambda_{max,abs.}$ (10^{-6} M THF solution) 344 nm; $\lambda_{max,flu.}$ (10^{-4} M THF solution) 394 nm.

Mass spectrum: m/z ([M^+]): 1076. Isotopic clusters of M^+[g/mol] (rel. int.): 1076(100 %), 1077(90 %), 1078(40 %), 1079(12 %), 1080(3 %). Anal. Calcd for $C_{78}H_{87}N_4$ (1077.6): C, 86.94; H, 7.86; N, 5.20. Found: C, 86.40; H, 7.96; N, 5.59.

Tris-{4-[9-(2-ethyl-hexyl)-carbazol-2-yl]-phenyl}-amine (15). The synthesis was carried out as described for star-shaped compound **13**. In this case the product (**15**) was purified by preparative TLC with hexane:CH_2Cl_2 (5:2) as eluent yielding 52% of **15** as white solid. ^{1}H-NMR (250 MHz, $CDCl_3$): δ (ppm): 0.79(t, 9H), 0.86(t, 9H), 1.16-1.36(m, 24H), 2.05(m, 3H), 4.14(d, 6H), 7.16(m, 3H), 7.27(m, 6H), 7.33-7.43(m, 9H), 7.51(s, 3H), 7.61(m, 6H), 8.01-8.07(m, 6H). ^{13}C-NMR (62.5 MHz, $CDCl_3$): δ (ppm): 11.4, 14.4, 23.5, 24.8, 29.2, 31.4, 39.8, 47.8, 107.3, 109.4, 118.5, 119.3, 120.6, 120.9, 122.2, 123.0, 124.9, 125.9, 128.7, 137.1, 138.8, 141.8, 142.0, 147.1. IR (KBr): $\tilde{\nu}$ (cm^{-1}): 3061, 3031, 2957, 2927, 1599, 1515, 1456, 1317, 1287, 744. $\lambda_{max,abs.}$ (10^{-6} M THF solution) 360 nm; $\lambda_{max,flu.}$ (10^{-4} M THF solution) 409 nm. Mass spectrum: m/z ([M^+]): 1076. Isotopic clusters of M^+[g/mol] (rel. int.): 1076(100 %), 1077(90 %), 1078(40 %), 1079(12 %), 1080(3 %). Anal. Calcd for $C_{78}H_{87}N_4$ (1077.6): C, 86.94; H, 7.86; N, 5.20. Found: C, 87.02; H, 7.44; N, 5.54.

Tris-[4-(9,9-diethyl-fluoren-2-yl)-phenyl]-amine (16a).

1.0 g (1.58 mmol) of tris-(4-iodo-phenyl)-amine (**12**) and 2.2 g (6.32 mmol) of 2-(9,9-diethyl-fluoren-2-yl)-4,4,5,5-tetramethyl-[1,3,2]-dioxaborolane (**11a**) were dissolved in 16 ml toluene. 10 ml of a 2M Na_2CO_3 solution and 10 mg of trimethyl-benzylammonium chloride were added before the reaction mixture was degassed by three subsequent freeze/thaw cycles. After that, 40 mg (3.5 x 10^{-5} mol) tetrakis-(triphenyl-phosphine)palladium [$Pd(PPH_3)_4$] were added under argon. The mixture was stirred for 24 h at 85 °C before it was poured into ice water, extracted with diethyl ether and dried with Na_2SO_4. After evaporation of the solvent the product was purified by column chromatography on silica gel with hexane:tetrahydrofurane (15:1) as eluent. Finally the product was purified by MPLC. Hexane:tetrahydrofuran (30:1) was used as eluent at a pressure of 20 bar. The reaction yielded 0.95 g (66 %) tris-[4-(9,9-diethyl-fluoren-2-yl)-phenyl]-amine (**16a**) as yellowish solid. ^{1}H-NMR (250 MHz, $CDCl_3$): δ (ppm): 0.37(t, 18H), 2.10(q, 12H), 7.27-7.37(m, 15H), 7.56-7.63(m, 12H), 7.75(m, 6H). ^{13}C-NMR (62.5 MHz, $CDCl_3$): δ (ppm): 8.6, 32.8, 56.1, 119.6, 119.9 , 121.0, 122.9, 124.4, 125.5, 126.8, 126.9, 127.9, 136.0, 139.4, 140.5, 141.2, 146.7, 150.1, 150.6. IR (KBr): $\tilde{\nu}$ (cm^{-1}): 3032, 2962, 2918, 1598, 1513, 1451, 1321, 1284, 821, 737. $\lambda_{max,abs.}$ (10^{-6} M THF solution) 365 nm; $\lambda_{max,flu.}$ (10^{-4} M THF solution) 408 nm. Mass spectrum: m/z ([M^+]): 905. Isotopic clusters of M^+[g/mol] (rel. int.): 905(100 %), 906(78 %),

907(30 %), 908(7 %), 909(2 %). Anal. Calcd for $C_{69}H_{63}N$ (906.3): C, 91.45; H, 7.01; N, 1.55. *Found: C, 91.26; H, 6.98; N, 1.76.*

Tris-[4-(9,9-dibutyl-fluoren-2-yl)-phenyl]-amine (16b). The synthesis was carried out as described for star-shaped compound **16a**. MPLC made with hexane:tetrahydrofurane (30:1) as eluent at a pressure of 18 bar yielding 80% of **16b** as white solid. ^{1}H-NMR (250 MHz, $CDCl_3$): δ (ppm): 0.63(m, 12H), 0.66(t, 18H), 1.09(m, 12H), 2.01(m, 12H), 7.29-7.37(m, 15H), 7.60(m, 12H), 7.75(m, 6H). ^{13}C-NMR (62.5 MHz, $CDCl_3$): δ (ppm): 13.8, 23.1, 26.0, 40.3, 55.0, 119.7, 119.9, 120.9, 122.9, 124.4, 125.5, 126.8, 126.9, 127.9, 136.1, 139.4, 140.1, 140.8, 146.7, 150.9, 151.4. IR (KBr): $\tilde{\nu}$ (cm^{-1}): 3055, 3031, 2955, 2927, 1599, 1483, 1451, 1320, 740. $\lambda_{max,abs.}$ (10^{-6} M THF solution) 365 nm; $\lambda_{max,flu.}$ (10^{-4} M THF solution) 408 nm. Mass spectrum: m/z ([M^+]): 1073. Isotopic clusters of M^+[g/mol] (rel. int.): 1073(100 %), 1074(93 %), 1075(43 %), 1076(12 %), 1077(2 %). Anal. Calcd for $C_{81}H_{87}N$ (1074.6): C, 90.54; H, 8.16; N, 1.30. Found: C, 90.23; H, 8.28; N, 1.33.

Tris-[4-(9,9-dihexyl-fluoren-2-yl)-phenyl]-amine (16c). The synthesis was carried out as described for star-shaped compound **16a**. MPLC was made with hexane:tetrahydrofurane (35:1) as eluent at a pressure of 20 bar yielding 73% of **16c** as white solid. ^{1}H-NMR (250 MHz, $CDCl_3$): δ (ppm): 0.69(m, 12H), 0.76(t, 18H), 1.06-1.16(m, 36H), 2.00(m, 12H), 7.23(m, 15H), 7.57-7.64(m, 12H), 7.74(m, 6H). ^{13}C-NMR (62.5 MHz, $CDCl_3$): δ (ppm): 14.0, 22.6, 23.7, 29.7, 31.5, 40.4, 55.1, 119.6, 119.9, 120.9, 122.8, 124.4, 125.5, 126.7, 126.9, 127.9, 136.1, 139.4, 140.1, 140.8, 146.7, 150.9, 151.4. IR (KBr): $\tilde{\nu}$ (cm^{-1}): 3032, 2953, 2926, 1599, 1483, 1465, 1451, 1320, 739. $\lambda_{max,abs.}$ (10^{-6} M THF solution) 365 nm; $\lambda_{max,flu.}$(10^{-4} M THF solution) 408 nm. Mass spectrum: m/z ([M^+]): 1241. Isotopic clusters of M^+[g/mol] (rel. int.): 1241(95 %), 1242(100 %), 1243(52 %), 1244(18 %), 1245(5 %), 1246(2 %). Anal. Calcd for $C_{93}H_{111}N$ (1242.9): C, 89.87; H, 9.00; N, 1.13. Found: C, 90.03; H, 8.59; N, 1.37.

The purity of all star-shaped compounds was additionally checked by SEC using a column set suitable for separation of oligomers with THF as eluent.

Measurements

^{1}H-NMR spectra were recorded with a Bruker AC 250 (250 MHz) apparatus. All data are given as chemical shifts δ [ppm] downfield from $Si(CH_3)_4$. The IR spectra were recorded using a Bio-Rad Digilab FTS-40. The UV-VIS spectra were recorded with a Hitachi U-3000 spectrophotometer. Emission spectra were obtained from a Shimadzu spectrofluoro-photometer RF-5301PC. Conventional mass spectra (MS) were recorded with a Finnigan MAT 8500 (70 eV) spectrometer. Thermogravimetric analysis (TGA) was performed on a

Perkin Elmer TAS-409 at a heating rate of 10 K/min under N_2. For differential scanning calorimetry measurements (DSC) a Perkin Elmer DSC-7 apparatus was used (heating/cooling rate: 10 K/min). The purity of the target compounds was checked with a Waters size exclusion chromatography system (SEC) for oligomers (analytical columns: crosslinked polystyrene gel (Polymer Laboratories), length: 2 x 60 cm, width: 0.8 cm, particle size: 5 μm, pore size 100 Å, eluent THF (0.5 ml/min, 80 bar), polystyrene standard). The system included a Waters 410 differential refractometer and a Waters 486 UV-detector (254 nm). Cyclic voltammetry measurements (CV) were performed with a glassy carbon working electrode (0.2 mm) in a three-electrode potentiostat configuration from EG&G Princeton Applied Research.

Device fabrication and testing

The organic field effect transistor devices were prepared on heavily doped n^{++} silicon wafers as gate contact on top of which an insulating layer of silicon dioxide was thermally grown. Gold was evaporated and photolithographically patterned to form the source and drain contacts[22]. The devices were completed by deposition of the starburst molecules which functioned as the organic semiconducting material. The films were prepared by using the drop casting technique. The average film thickness of the semiconductor layer was about 150 nm. For dissolving the triphenylamine based compounds, toluene or methylene chloride were used as solvent. The electrical measurements were carried out either in air or in vacuum (10^{-4} Torr) using a Hewlett-Packard semiconductor parameter analyzer Agilent 4155C. The reported transistors had a ring configuration with a channel length of 40 μm and a channel width of 1000 μm.

Acknowledgements:

We thank J. Ostrauskaite for the CV measurements and are grateful to the BMBF (POLITAG programme) for financial support.

5. References

[1] Y. Shirota, T. Kobata, N. Noma, *Chem. Lett.* **1989**, 1145.

[2] P. Strohriegl, J. V. Grazulevicius, *Adv. Mater.* **2002**, *14*, 1439.

[3] P. M. Borsenberger, D. S. Weiss, *Organic Photoreceptors for Xerography*, Marcel Dekker, Inc., **1998**.

[4] Y. Shirota, *J. Mater. Chem.* **2000**, *10*, 1.

[5] S. E. Burns, P. Cain, J. Mills, J. Wang, H. Sirringhaus, *MRS Bulletin* **2003**, *28*, 829.

[6] J. Bettenhausen, P. Strohriegl, *Adv. Mater.* **1996**, *8*, 507.

[7] J. Bettenhausen, P. Strohriegl, *Macromol. Rapid Commun.* **1996**, *17*, 623.

[8] M. Jandke, P. Strohriegl, S. Berleb, E. Werner, W. Brütting, *Macromolecules* **1998**, *31*, 6436.

[9] T. Pfeuffer, D. Hanft, P. Strohriegl, *Liq. Cryst.* **2002**, *29*, 1555.

[10] K. Kreger, M. Jandke, P. Strohriegl, *Synthetic Metals* **2001**, *119*, 163.

[11] M. Lux, P. Strohriegl, H. Hoecker, *Makromol. Chem.* **1987**, *188*, 811.

[12] A. Klapars, J. C. Antilla, X. Huang, S. L. Buchwald, *J. Am. Chem. Soc.* **2001**, *123*, 7727.

[13] E. P. Woo, M. Inbasekaran, W. Shiang, G. R. Roof, US Patent 5,708,130, **1998**.

[14] Y. Kuwabara, H. Ogawa, H. Inada, Y. Shirota, *Adv.Mater.* **1994**, *6*, 677.

[15] W. Schmidt, *Optische Spectroskopie, VCH Verlagsgesellschaft, Weinheim* **1994**.

[16] E. Conwell, *Trends Polym. Sci.* **1997**, *5*, 218.

[17] J. Pommerehne, H. Vestweber, W. Guss, R. F. Mark, H. Bässler, M. Porsch, J. Daub, *Adv. Mater.* **1995**, *7*, 55.

[18] G. Zotti, G. Schiavon, S. Zecchin, J.-F. Morin, M. Leclerc, *Macromolecules* **2002**, *35*, 2122.

[19] C. W. Tang, S. A. VanSlyke, *Appl. Phys. Lett.* **1987**, *51*, 913.

[20] J. Veres, S. Ogier, G. Lloyd, D. de Leeuw, *Chem. Mater.* **2004**, *16*, 4543.

[21] A. R. Brown, A. Pomp, D. M. de Leeuw, D. B. M. Klaassen, E. E. Havinga, P. Herwig, K. Muellen, *J. Appl. Phys.* **1996**, *79*, 2136.

[22] A. R. Brown, C. P. Jarrett, D. M. de Leeuw, M. Matters, *Synth. Met.* **1997**, *88*, 37.

Synthesis and characterization of novel conjugated bisindenocarbazoles

Martin Sonntag, Peter Strohriegl*

Lehrstuhl Makromolekulare Chemie I, Universität Bayreuth, 95440 Bayreuth, Germany

Tetrahedron, **2006**, *62*, 8103-8108.

Keywords

Bisindenocarbazole, carbazole, Suzuki cross coupling

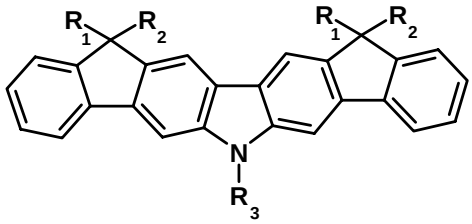

Abstract

We present the synthesis of 5 new bisindenocarbazoles with different alkyl substituents. The synthesis starts from 2,7-dibromocarbazole and leads to the bisindenocarbazoles **6-10** in five steps with an overall yield of about 50 %. By substitution of the core with different alkyl chains in the last step of the synthesis, the morphology of the bisindenocarbazoles can be varied from crystalline materials to molecular glasses. The bisindenocarbazoles are electrochemically stable and exhibit a strong, saturated blue emission with a quantum yield of 63 % in solution.

*To whom correspondence should be addressed. E-mail: peter.strohriegl@uni-bayreuth.de

1. Introduction

Fused aromatics like pentacene and rubrene are attractive materials for organic electronics. Both pentacene single crystals[1] and thin, polycrystalline pentacene films exhibit carrier mobilities above 1 cm^2/Vs in organic field effect transistors (OFETs).[2] Single crystalline rubrene shows carrier mobilities up to 15 cm^2/Vs in OFETs.[3] In addition, rubrene has been used as efficient yellow dopant in organic light emitting diodes (OLEDs).[4]

Besides pure hydrocarbons like pentacene, materials containing fused heterocycles have attracted increasing interest as materials for organic electronics during the last years. For example indolo- and bisindolocarbazoles have been synthesized and successfully tested in OFETs.[5-8]

In this paper we present the synthesis of 5 new bisindenocarbazoles, a class of fused heterocycles that has not yet been described in the literature. We have developed a new and versatile strategy for the preparation of these materials which makes it possible to introduce different alkyl substituents to the core in the very last step of the synthesis. This allows us to tailor the properties of this new class of materials. For example, **6** with four small methyl substituents in the 1 and 1' position is highly crystalline whereas **7** with two butyl and two methyl groups is an amorphous molecular glass.

2. Results and discussion

2.1. Preparation of the bisindenocarbazoles

Scheme 1 shows the synthetic route to the new bisindenocarbazoles. The preparation of 2,7-dibromocarbazole (**1**) and the *N*-alkylated carbazole monomers (**2a-c**) has been reported elsewhere.[9-13]

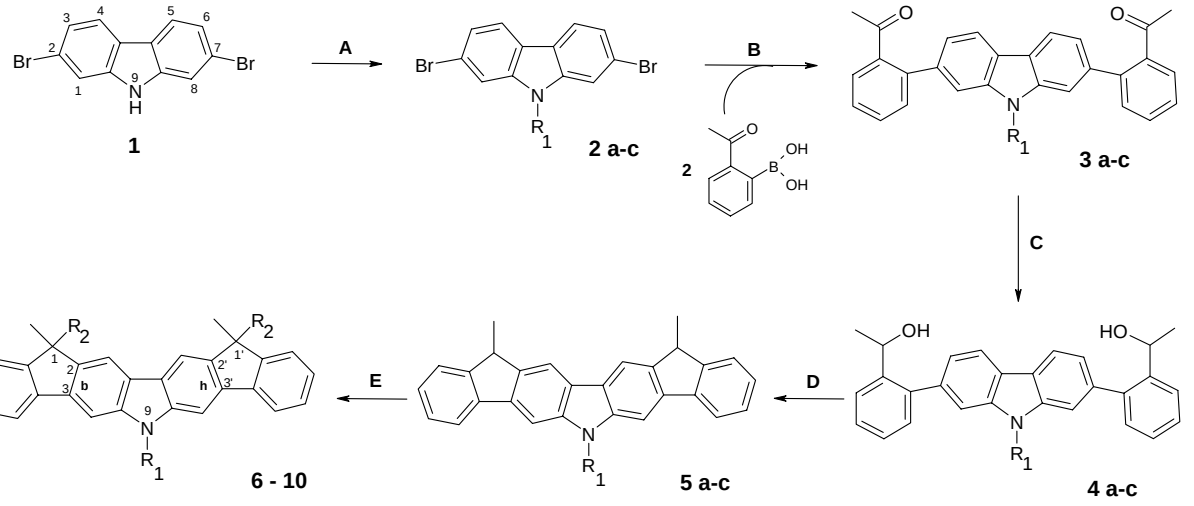

2a,b: A = alkyl bromide, acetone, KOH, PTC, 70 °C, 5 h

2c: A = Me_2SO_4, acetone, 10N KOH, 50 °C, 30 min

B = $P(otol)_3$, $Pd(OAc)_2$, 2N KOH, toluene, PTC, 90 °C, 2 h

C = lithium triethylborohydride, THF, 0 °C, 1 h

D = $BF_3*O(C_2H_5)_2$, CH_2Cl_2, RT, 30 min

E = 1.6 M n-BuLi, alkyl bromide, THF, -78 °C, 1 h

compd	R_1	R_2
2-5a	*sec*-butyl	---
2-5b	2-ethylhexyl	---
2-5c	methyl	---
6	*sec*-butyl	methyl
7	*sec*-butyl	n-butyl
8	*sec*-butyl	ethyl
9	2-ethylhexyl	ethyl
10	methyl	ethyl

Scheme 1. *Synthesis of bisindenocarbazoles with different alkyl substituents.*

For the phenylation (**B**) of the N-alkyl carbazoles **2a-c** in position 2 and 7, the Suzuki cross coupling reaction was chosen, as it is an excellent tool for unsymmetrical aryl-aryl couplings.[14] The reactions were carried out in a two-phase system of toluene and aqueous potassium carbonate, with trimethylbenzylammonium chloride as phase-transfer catalyst (PTC). For the Suzuki coupling of 2-acetylphenylboronic acid and the N-alkylated 2,7-dibromocarbazoles **2a-c**, a mixture of $Pd(OAc)_2$ and P(*o*-tol)$_3$ was used as catalyst. Excellent yields of up to 91 % of **3a-c** were achieved. In the next step the keto groups were reduced to the corresponding secondary alcohols **4a-c** by reaction with lithium triethylborohydride (super-hydride) in absolute THF. In the case of the bisindenocarbazoles the reduction with super-hydride solution works fast and quantitatively.

The ring closure reaction of **4a-c** to the bisindenocarbazoles **5a-c** was carried out with boron trifluoride etherate as Lewis-acid catalyst in dichloromethane at room temperature. Ring closure occurs exclusively in the 3- and 6-positions of the carbazole which are highly activated.

Finally different alkyl side chains can be introduced to the planar bisindenocarbazole core with n-BuLi and the corresponding alkyl halide. The alkylation of the bisindenocarbazoles in the very last step is a big advantage of this synthetic approach. As we will show in the next chapter, the morphology and the thermal properties of the target molecules can be tailored by adding alkyl groups of different length without changing the optical and electrical properties.

The bisindenocarbazoles **6-10** are mixtures of stereoisomers. **6** is a mixture of 2 enantiomers, **7-9** have 3 stereocenters and hence 8 enantiomers and 4 diastereomers. **10** with two stereocenters in the 1 and 1' position is a mixture of 2 enantiomers and 2 diastereomers. Only in the case of **10** we were able to separate the 2 diastereomers by medium pressure liquid chromatography (MPLC). The first fraction is the meso form with *(R,S)* configuration. The second fraction consists of the *(R,R)* and *(S,S)* enantiomers (Scheme 2). The *(R,R/S,S)* and the *(R,S)*-isomers are formed in a ratio of 2:1. The melting points of the two isomers differ by 19 °C. The *(R,S)*-isomer melts at 292 °C, the *(R,R/S,S)* racemate melts at 273°C. In contrast, it was not possible to separate the bisindenocarbazoles **7-9** which are a mixture of 4 diastereomers. Therefore the NMR and thermal data refer to the isomeric mixtures.

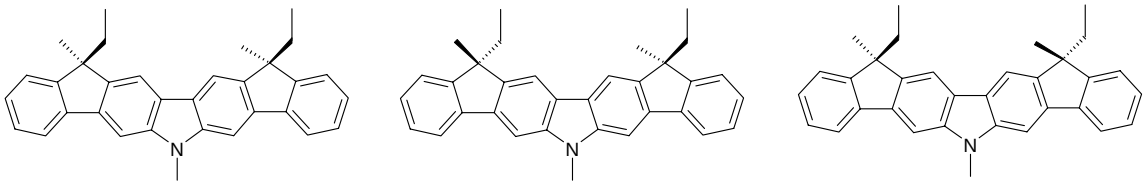

(R,S)-isomer of **10** *(S,S)*-isomer of **10** *(R,R)*-isomer of **10**

*Scheme 2: Different isomers and configurations of **10**.*

All bisindenocarbazoles show good solubility in common organic solvents (e.g., THF, toluene, chloroform). The structures of the bisindenocarbazoles were confirmed by IR, ^{1}H- and ^{13}C-NMR, mass spectrometry and elemental analysis. The synthetic procedures and the analytical data of all compounds are given in the experimental part.

2.2. Thermal properties

The thermal properties of the bisindenocarbazoles were determined by thermogravimetric analysis (TGA) and differential scanning calorimetry (DSC) and are summarized in Table 1. TGA experiments in nitrogen showed that the bisindenocarbazoles **6-10** start to sublime at temperatures above 260 °C. Between 300 °C and 350 °C quantitative weight loss was detected in all cases. The fact that the molecules can be sublimed quantitatively at ≈ 320 °C at normal pressure allows to prepare high quality films of the materials by vapor deposition.

DSC measurements clearly show how the morphology of the molecules can be tailored by changing the alkyl side groups. Compound **6** with four methyl substituents in the 1- and 1'-position is crystalline (T_m = 265 °C), whereas **7** with two butyl and two methyl side chains is amorphous and exhibits only a glass transition at 106 °C. In contrast to **6** which recrystallizes upon cooling, the ethyl/methyl substituted molecule **8** can be transferred into a glassy state upon cooling in the DSC experiment. A melting point of **8** is only observed in the first heating cycle at 250 °C. In the second and third run only the glass transition at 103 °C is detected. In the bisindenocarbazole **9**, the N-*sec*-butyl substituent of the central carbazole unit is replaced by a longer 2-ethylhexyl chain. This leads to a low glass transition temperature of 74 °C and a melting point at 164 °C.

In the case of **10**, we were able to separate the two diastereomers. Both the *(R,R/S,S)* and the *(R,S)*-isomer of **10** are crystalline and melt at 273 °C and 292 °C, respectively. Upon cooling, both compounds show recrystallization in the DSC-experiment. The mixture of the two diastereomers is also crystalline. In contrast to the two pure isomers, the mixture does not recrystallize upon cooling but forms a glass which recrystallizes during the subsequent heating cycle. This shows that the mixture has a higher tendency to form a molecular glass than the pure diastereomers.

Table 1. *Thermal properties of the bisindenocarbazoles* ***6-9****.*

compd	T_g [°C][1]	T_m [°C][1]	T_{subl} [°C][2]
6	---	265	310
7	106[3]	---	320
8	103[3]	250[3,4]	305
9	74[3]	164[3]	330
10 *(R,S)*	---	292	260
10 *(R,R/S,S)*	---	273	260

[1] Determined by DSC, scan rate 10 K/min, 2nd run, N_2 atmosphere

[2] Onset of sublimation determined by TGA, heating rate 10 K/min, N_2 atmosphere

[3] T_g and T_m refer to mixtures of 4 diastereomers

[4] Melting point only detected in the first heating cycle

2.3. Optical Properties

As expected, identical UV-Vis spectra are obtained from the bisindenocarbazoles. The change of the alkyl side chains has no influence on the absorption of the bisindenocarbazole chromophore. The absorption and fluorescence spectra of **6** (Figure 1) are representative for the bisindenocarbazoles **6-10**. The absorption maximum is at 380 nm. The bisindenocarbazoles exhibit a strong, saturated blue fluorescence with an emission maximum at 410 nm. The small Stokes shift of 6 nm is typical for the rigid structure of the bisindenocarbazoles.[15]

The fluorescence spectrum of **6** shows characteristic vibronic structures. The separation between the peaks at 388 and 410 nm is 1382 cm^{-1}, and between 410 and the shoulder at 435 nm is 1461 cm^{-1}. These values correspond to two discrete carbazole skeleton vibrations in the IR-spectrum.

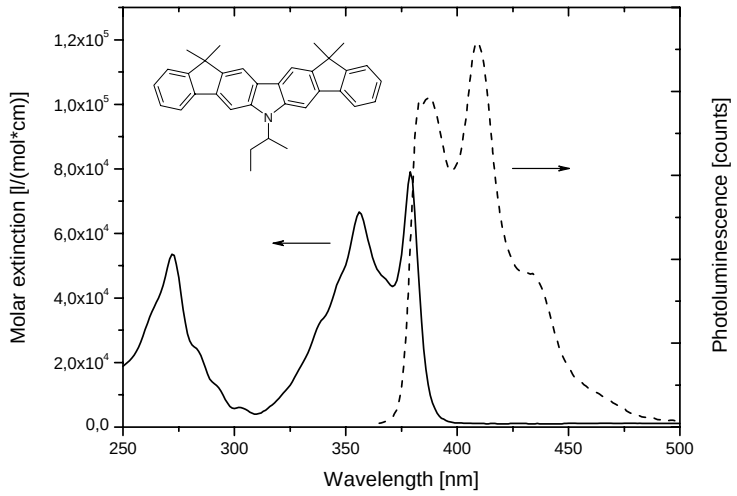

Figure 1. *Absorption and fluorescence spectra of the bisindenocarbazole* ***6****. The absorption spectra were taken from* 10^{-5} *M cyclohexane solutions and the fluorescence spectra from* 10^{-6} *M cyclohexane solutions with an excitation wavelength of 350 nm.*

In order to estimate the fluorescence quantum yield (Φ_f) of the bisindenocarbazoles, the fluorescence of **6** was compared to the well known blue laser dye Exalite 428 [7,7''-bis(4-*t*-amylphenyl)-9,9,9',9',9'',9''-hexapropyl-2,2':7'2''-terfluorene]. Exalite 428 has a quantum efficiency of 90 % in cyclohexane solution.[16] 10^{-5} M solutions of **6** and Exalite 428 in cyclohexane were prepared and diluted to an optical density of ≈ 0.1 in order to minimize self-absorption.[17] From these solutions fluorescence spectra were taken and by integration, a fluorescence quantum yield of 63 % was calculated for **6**.

2.4. Electrochemical properties

The electrochemical stability of the bisindenocarbazoles was examined by cyclic voltammetry (CV). All measurements were carried out at 25 °C in CH_2Cl_2 solution containing 0.1 M tetrabutylammonium hexafluorophosphate ($TBAPF_6$) as supporting electrolyte with a glassy carbon working electrode. The oxidation potentials were measured vs. Ag/AgCl as the reference electrode.[18] The CV curve of **6** (Figure 2) shows one oxidation peak at 0.60 V which is fully reversible. Repeated oxidation and reduction cycles had no influence on the CV curve. The same results are obtained for the other bisindenocarbazoles **7-10**. This is a proof for the electrochemical stability of the new bisindenocarbazoles. It has been reported that the electrochemical oxidation of compounds based on 2,7-linked carbazoles is not fully reversible

and that such materials undergo dimerization reactions in the activated 3- and 6-positions of the carbazole rings.[6, 10] The high electrochemical stability of the bisindenocarbazoles **6-10**, in which these positions are blocked by ring closure, strongly supports this argument and shows that the activated 3- and 6-positions in 2,7-linked carbazole compounds have to be blocked in order to obtain electrochemically stable materials.

The HOMO levels of the bisindenocarbazoles **6-10** can be estimated from the CV-measurement. For this purpose, the CV was calibrated with the standard ferrocene/ferrocenium redox system. Taking -4.8 eV as HOMO level for the ferrocene redox system[19], HOMO values of -5.3 eV were obtained. With an optical band gap of 3.2 eV, calculated from the absorption edge at 391 nm, LUMO values of -2.1 eV are calculated for compounds **6-10**.

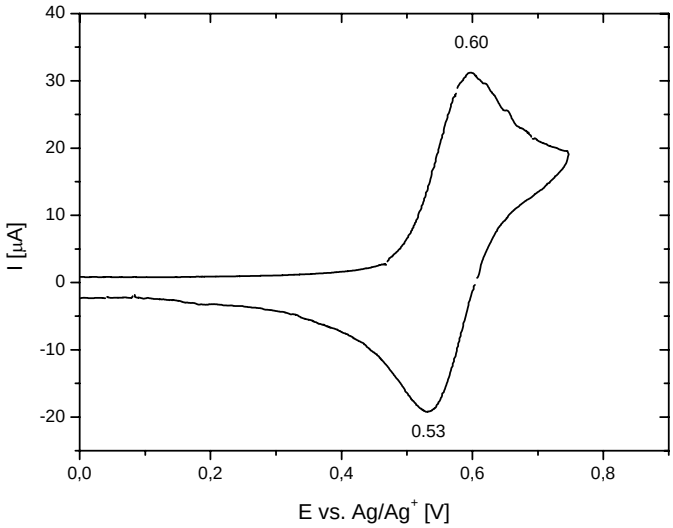

Figure 2. *CV measurement of* ***6****, measured at 25 °C at a scan rate of 50 mV/s vs. Ag/Ag*$^+$ *in acetonitrile with TBAPF*$_6$ *as supporting electrolyte.*

3. Conclusions

In conclusion, we have developed a new versatile synthetic route to conjugated bisindenocarbazoles. The title compounds **6-10** are obtained in five steps from 2,7-dibromocarbazole **1** with an overall yield of 50 %. By substitution with a variety of alkyl substituents in the very last step of the synthesis, their morphology can be varied from highly crystalline materials (**6**) to amorphous molecular glasses (**7**). The compounds sublime quantitatively at temperatures around 320 °C and excellent films can be prepared by evaporation. In CV experiments the bisindenocarbazoles showed a high electrochemical stability. This is in contrast to the 2,7-carbazole trimers, which have been reported before.[10] These trimers show irreversible electrochemical oxidation due to dimerization reactions in the highly activated 3- and 6-positions of the carbazole ring. In the bisindenocarbazoles **6-10** the reactive 3- and 6-positions in the central carbazole unit are blocked by the ring closure. From the CV measurements and the optical band gap, HOMO levels of -5.3 eV and LUMO values of -2.1 eV were calculated. All bisindenocarbazoles **6-10** exhibit a strong, saturated blue emission with a quantum yield of 63 % in solution and will be tested as blue dopants in organic light emitting diodes in the near future.

4. Experimental

4.1. General

^{1}H-NMR spectra were recorded with a Bruker AC 250 (250 MHz) apparatus. All data are given as chemical shifts δ [ppm] downfield from $Si(CH_3)_4$. The IR spectra were recorded using a Bio-Rad Digilab FTS-40. The UV-VIS spectra were recorded with a Hitachi U-3000 spectrophotometer. Emission spectra were obtained from a Shimadzu spectrofluoro-photometer RF-5301PC. Conventional mass spectra (MS) were recorded with a Finnigan MAT 8500 (70 eV) with a MAT 112S Varian. Thermogravimetric analysis (TGA) was performed on a Perkin Elmer TAS-409 at a heating rate of 10 K/min under N_2. For differential scanning calorimetry measurements (DSC) a Perkin Elmer DSC-7 apparatus was used (heating/cooling rate: 10 K/min). Cyclic voltammetry measurements (CV) were performed with a glassy carbon working electrode (0.2 mm) in a three-electrode potentiostat configuration from EG&G Princeton Applied Research.

All chemicals and reagents were used as received from Aldrich. Tetrahydrofuran (THF) was distilled over potassium before use. The synthesis of 2,7-dibromocarbazole (**1**) and of N-alkylated 2,7-dibromocarbazoles (**2a-c**) has been reported elsewhere.[9-13]

2,7-Bis-(2-acetylphenyl)-9-*sec*-butyl-carbazole (3a).

1.3 g (3.5 mmol) 2,7-Dibromo-9-*sec*-butyl-carbazole (**2a**) and 1.3 g (7.7 mmol) 2-acetylphenylboronic acid were dissolved in 45 ml of toluene. A 2 M solution of K_2CO_3 (25 ml) and 0.2 g of trimethylbenzylammonium chloride were added. The reaction mixture was degassed by three freeze/thaw cycles before 31.3 mg (0.14 mmol) of $Pd(OAc)_2$ and 127.0 mg (0.42 mmol) of tri-*o*-tolylphosphine (P(*o*-tol)$_3$) were added under argon. The mixture was stirred for 15 h at 90 °C before it was poured into ice-water and extracted with diethyl ether. After evaporation of the solvent, the product was purified by column chromatography on silica gel with hexane/THF (6:1) as eluent yielding 1.42 g (89 %) of **3a** as a colorless solid. ^{1}H-NMR (250 MHz, $CDCl_3$): δ(ppm) 0.71(t, 3H), 1.58(d, 3H), 1.86(s, 6H), 1.95(m, 1H), 2.21(m, 1H), 4.53-4.67(m, 1H), 7.20(m, 2H), 7.37(m, 4H), 7.52(m, 6H), 8.13(d, 2H). MS (70 eV): *m/z* = 459 (M^+)

2,7-Bis-(2-acetylphenyl)-9-(2-ethylhexyl)-carbazole (3b) was prepared according to the procedure described above (yield: 91 %). ^{1}H-NMR (250 MHz, $CDCl_3$): δ(ppm) 0.78-0.87(m, 6H), 1.12-1.40(m, 8H), 1.48(s, 6H), 2.07(m, 1H), 4.16(m, 2H), 7.17(d 2H), 7.34(m, 6H), 7.36(m, 2H), 7.70(d, 2H), 8.14(d, 2H). MS (70 eV): *m/z* = 515 (M^+).

2,7-Bis-(2-acetylphenyl)-9-methyl-carbazole (3c) was prepared according to the procedure described above (yield: 83 %). ^{1}H-NMR (250 MHz, $CDCl_3$): δ(ppm) 1.99(s, 6H), 3.88(s, 3H), 7.24(d, 1H), 7.27(d, 1H), 7.40(m, 2H), 7.39-7.48(m, 2H), 7.54-7.58(m, 6H), 8.16(d, 2H).
MS (70 eV): *m/z* = 417 (M^+).

2,7-Bis-[2-(2-hydroxyethylphenyl)-9-*sec*-butyl-carbazole (4a).

0.37 g (0.80 mmol) of **3a** were dissolved in 25 ml abs. THF. The solution was flushed with argon and cooled to 0 °C before 2.3 ml (2.40 mmol) of a 1M lithium triethylborohydride solution in THF (super-hydride) were added slowly. The reaction mixture was stirred at 0 °C for 1 h and 15 ml of an aqueous NH_4Cl solution were added. Thereafter the reaction batch was poured into 150 ml water and extracted with diethyl ether. The organic layer was washed with water and the solvent removed. The product was purified by column chromatography on silica gel with hexane/ethyl acetate (1.5:1) as eluent yielding 0.35 g (95 %) of **4a** as a colorless solid. ^{1}H-NMR (250 MHz, DMSO): δ(ppm) 0.74(t, 3H), 1.29-1.33(m, 6H), 1.67(m,

3H), 2.01(m, 1H), 2.24(m, 1H), 4.93(m, 3H), 5.14(m, 2H), 7.20(d, 2H), 7.35-7.51(m, 6H), 7.68(d, 2H), 7.73(d, 2H), 8.29(d, 2H). MS (70 eV): *m/z* = 463 (M^+)

2,7-Bis-[2-(2-hydroxyethylphenyl)-9-(2-ethylhexyl)-carbazole (4b) was prepared according to the procedure described above (yield: 96 %). ^{1}H-NMR (250 MHz, $CDCl_3$): δ(ppm) 0.71-0.88(m, 6H), 1.14-1.46(m, 11H), 1.49(d, 3H), 2.07(m, 1H), 4.16(d, 2H), 5.09(m, 2H), 7.17(d, 2H), 7.36-7.49(m, 8H), 7.71(d, 2H), 8.12(d, 2H). MS (70 eV): *m/z* = 519 (M^+).

2,7-Bis-[2-(2-hydroxyethylphenyl)-9-methyl-carbazole (4c) was prepared according to the procedure described above (yield: 98 %). ^{1}H-NMR (250 MHz, $CDCl_3$): δ(ppm) 1.45(d, 6H), 3.90(s, 3H), 5.10 (q, 2H), 7.18(d, 1H), 7.35-7.40(m, 6H), 7.43-7.51(m, 3H), 7.73(d, 2H), 8.15(d, 2H). MS (70 eV): *m/z* = 421 (M^+).

1,1'-Dimethyl-bisindeno[3,2-b:2'3'-h]-9-*sec*-butyl-carbazole (5a).

To a solution of 0.1 g (0.22 mmol) **4a** in 10 ml dichloromethane, 0.1 ml (0.65 mmol) boron trifluoride etherate were added. The mixture was stirred for 30 min at room temperature before 15 ml ethanol and 20 ml water were added. The reaction batch was extracted with dichloromethane, washed with water and dried with Na_2SO_4 before the solvent was evaporated. Purification by column chromatography on silica gel with hexane/THF (3:1) as eluent yielded 83 mg (92 %) of **5a** as colorless solid. ^{1}H-NMR (250 MHz, DMSO): δ(ppm) 0.81(t, 3H), 1.64(d, 6H), 1.80(d, 3H), 2.12(m, 1H), 2.49(m, 1H), 4.10(q, 2H), 5.05(m, 1H), 7.35-7.46(m, 4H), 7.64(d, 2H), 8.12(d, 2H), 8.21(s, 2H), 8.39(d, 2H). MS (70 eV): *m/z* = 427 (M^+).

1,1'-Dimethyl-bisindeno[3,2-b:2'3'-h]-9-(2-ethylhexyl)-carbazole (5b) was prepared as described above (yield: 90 %). ^{1}H-NMR (250 MHz, $CDCl_3$): δ(ppm) 0.84(m, 6H), 1.51-1.46(m, 8H), 1.49(d, 6H), 2.05(m, 1H), 3.96(q, 2H), 4.86(m, 2H), 7.33-7.44(m, 4H), 7.60(d, 2H), 8.10(d, 2H), 8.19(s, 2H), 8.35(d, 2H). MS (70 eV): *m/z* = 483 (M^+).

1,1'-Dimethyl-bisindeno[3,2-b:2'3'-h]-9-methyl-carbazole (5c) was prepared as described above (yield: 88 %). ^{1}H-NMR (250 MHz, $CDCl_3$): δ(ppm) 1.56(d, 6H), 4.13(q, 2H), 4.51(s, 3H), 7.32-7.40(m, 4H), 7.55(d, 2H), 7.72(s, 2H), 7.86(d, 2H), 8.20(s, 2H). MS (70 eV): *m/z* = 385 (M^+).

1,1'-Di-*n*-butyl-1,1'dimethyl-bisindeno[3,2-b:2'3'-h]-9-*sec*-butyl-carbazole (7).

60 mg (0.14 mmol) of **5a** were dissolved in 15 ml THF (abs.) under argon. The solution was cooled to -78 °C before 0.19 ml (0.3 mmol) n-BuLi (1.6M solution in hexane) were added slowly. After 15 min stirring 0.2 ml (0.4 mmol) 1-bromobutane were added. The solution was allowed to warm to room temperature and stirred for another hour before it was poured into 50 ml ice water. The reaction batch was extracted with diethyl ether, the organic phase

washed with water and the solvent evaporated. Purification was carried out by column chromatography on silica gel with hexane/THF (10:1) as eluent. In addition **7** was purified by MPLC with hexane/THF (15:1) at a pressure of 18 bar. The reaction yielded 51 mg (75 %) of **7** as white solid. ^{1}H-NMR (250 MHz, $CDCl_3$): δ(ppm): 0.62(m, 9H), 0.87(t, 4H), 1.01-1.10(m, 4H), 1.51(m, 6H), 1.74(d, 3H), 1.96-2.17(m, 5H), 2.28-2.47(m, 1H), 4.76(m, 1H), 7.27-7.37(m, 6H), 7.69(s, 2H), 7.76(d, 2H), 8.01(s, 2H). ^{13}C-NMR (62.5 MHz, $CDCl_3$): δ(ppm): 12.2, 14.3, 19.6, 23.5, 26.9, 28.1, 28.6, 41.8, 50.4, 53.6, 114.1, 119.9, 123.2, 123.3, 123.6, 127.1, 127.3, 128.5, 141.2, 143.7, 153.4. IR (Si-wafer): $\tilde{\nu}$ (cm^{-1}): 3011, 2958, 2972, 1488, 1452, 1378, 1342, 1240, 740. MS (70 eV): *m/z* = 539 (M^+). Anal. Calcd for $C_{40}H_{45}N$ (539.8): C, 89.00; H, 8.40; N, 2.59. Found: C, 89.09; H, 8.31; N, 2.58.

1,1-Dimethyl-1', 1'-dimethyl-bisindeno[3,2-b:2'3'-h]-9-*sec*-butyl-carbazole (6).

Compound **6** was prepared according to the procedure described for **7**. For the alkylation iodomethane was used (yield: 70 %). **6** was purified by MPLC with hexane/THF (10:1) at a pressure of 18 bar. ^{1}H-NMR (250 MHz, $CDCl_3$): δ(ppm): 0.90(t, 3H), 1.61(m, 12H), 1.78(d, 3H), 2.05-2.21(m, 1H), 2.35-2.53(m, 1H), 4.81(m, 1H), 7.28-7.49(m, 6H), 7.82(s, 2H), 7.89(d, 2H), 8.15(s, 2H). ^{13}C-NMR (62.5 MHz, $CDCl_3$): δ(ppm): 12.2., 19.6, 26.8, 28.5, 46.5, 53.6, 101.4, 114.0, 120.8, 123.1, 123.7, 127.4, 132.1, 137.6, 140.3, 145.3, 154.9. IR (Si-wafer): $\tilde{\nu}$ (cm^{-1}): 3014, 2961, 2926, 1489, 1452, 1377, 1342, 1241, 740. MS (70 eV): *m/z* = 455 (M^+). Anal. Calcd for $C_{34}H_{33}N$ (455.7): C, 89.63; H, 7.30; N, 3.07. Found: C, 89.56; H, 7.33; N, 3.12.

1,1'-Diethyl-1,1'-dimethyl-bisindeno[3,2-b:2'3'-h]-9-*sec*-butyl-carbazole (8).

Compound **8** was prepared according to the procedure described for **7**. For the alkylation bromoethane was used. **8** was purified by MPLC with hexane/THF (15:1) at a pressure of 18 bar (yield: 80 %). ^{1}H-NMR (250 MHz, $CDCl_3$): δ(ppm): 0.41(m, 6H), 0.90(m, 3H), 1.58(s, 6H), 1.78(d, 3H), 2.05-2.22(m, 5H), 2.34-2.41(m, 1H), 4.78(m, 1H), 7.26-7.41(m, 6H), 7.78(s, 2H), 7.82(d, 2H), 8.05(s, 2H). ^{13}C-NMR (62.5 MHz, $CDCl_3$): δ(ppm): 9.0, 11.8, 19.2, 27.3, 28.2, 34.1, 50.4, 53.2, 113.7, 115.0, 119.4, 122.9, 124.1, 126.4, 138.3, 141.0, 142.9, 152.6. IR (Si-wafer): $\tilde{\nu}$ (cm^{-1}): 3049, 2963, 2929, 1488, 1452, 1378, 1342, 1240, 741. MS (70 eV): *m/z* = 483 (M^+). Anal. Calcd for $C_{36}H_{37}N$ (483.7): C, 89.39; H, 7.71; N, 2.90. Found: C, 89.54; H, 7.69; N, 2.85.

1,1'-Diethyl-1,1'-dimethyl-bisindeno[3,2-b:2'3'-h]-9-(2-ethylhexyl)-carbazole (9).

Compound **9** was prepared according to the procedure described for **7**. For the alkylation, **5b** was treated with bromoethane. **9** was purified by MPLC with hexane/THF (20:1) at a pressure of 18 bar (yield: 76 %). ^{1}H-NMR (250 MHz, $CDCl_3$): δ(ppm): 0.33(m, 6H), 0.80-0.96(m,

6H), 1.18-1.48(m, 8H), 1.52(s, 6H), 1.98-2.16(m, 5H), 4.20(m, 2H), 7.21-7.39(m, 6H), 7.58(s, 2H), 7.75(d, 2H), 7.98(s, 2H). ^{13}C-NMR (62.5 MHz, $CDCl_3$): δ(ppm): 7.8, 9.8, 12.9, 21.8, 23.4, 26.0, 27.6, 29.8, 32.9, 38.2, 46.5, 49.2, 98.6, 112.5, 118.2, 121.6, 125.6, 125.7, 137.3, 139.7, 141.8, 151.4. IR (Si-wafer): $\tilde{\nu}$ (cm^{-1}): 3046, 2960, 2928, 1491, 1460, 1354, 1330, 1265, 739. MS (70 eV): *m/z* = 539 (M^+). Anal. Calcd for $C_{40}H_{45}N$ (539.8): C, 89.00; H, 8.40; N, 2.59. Found: C, 89.03; H, 8.46; N, 2.59.

1,1'-Diethyl-1,1'-dimethyl-bisindeno[3,2-b:2'3'-h]-9-methyl-carbazole (10).

Compound **10** was prepared according to the procedure described for **7**. For the alkylation, **5c** was treated with bromoethane. **10** was purified by MPLC with hexane/THF (25:1) at a pressure of 18 bar (yield: 76 %). In case of **10** it was possible to separate the two isomers by this technique. 200 mg of the *(R,S)*-isomer and 400 mg of the *(S,S/R,R)*-isomer were obtained after vacuum freeze drying. *(R,S)*-isomer: ^{1}H-NMR (250 MHz, $CDCl_3$): δ(ppm): 0.28-0.45(m, 6H), 1.59(s, 3H), 1.88(s, 3H), 2.15(q, 2H), 2.29-2.45(m, 1H), 2.51-2.68(m, 1H), 4.32(s, 3H), 7.28-7.44(m, 6H), 7.71-7.76(m, 2H), 7.78(d, 1H), 7.86(d, 1H), 8.05(s, 1H), 8.17(d, 1H). ^{13}C-NMR (62.5 MHz, $CDCl_3$): δ(ppm): 9.41, 27.74, 27.83, 28.04, 34.19, 34.48, 50.96, 52.91, 100.29, 112.33, 113.82, 119.56, 119.80, 119.94, 122.35, 123.30, 123.994, 124.64, 127.21, 127.30, 127.35, 127.39, 132.41, 139.34, 139.64, 140.47, 141.22, 141.29, 142.38, 144.25, 152.96. IR (Si-wafer): $\tilde{\nu}$ (cm^{-1}): 3049, 2962, 2923, 1495, 1457, 1378, 1307, 1225, 743. MS (70 eV): *m/z* = 441 (M^+). Anal. Calcd for $C_{33}H_{31}N$ (441.6): C, 89.75; H, 7.08; N, 3.17. Found: C, 89.54; H, 6.95; N, 3.20.

S,S/R,R isomer: ^{1}H-NMR (250 MHz, $CDCl_3$): δ(ppm): 0.37-0.40(m, 6H), 1.63(s, 6H), 2.08-2.16(m, 4H), 4.00(s, 3H), 7.30-7.45(m, 6H), 7.69(s, 2H), 7.85(d, 2H), 8.06(s, 2H). ^{13}C-NMR (62.5 MHz, $CDCl_3$): δ(ppm): 9.42, 27.79, 29.82, 34.56, 50.50, 99.81, 114.22, 119.94, 123.20, 123.26, 127.34, 139.08, 141.36, 142.07, 143.59, 152.96. IR (Si-wafer): $\tilde{\nu}$ (cm^{-1}): 3050, 2961, 2920, 1494, 1458, 1349, 1307, 1264, 739. MS (70 eV): *m/z* = 441 (M^+). Anal. Calcd for $C_{33}H_{31}N$ (441.6): C, 89.75; H, 7.08; N, 3.17. Found: C, 89.73; H, 7.09; N, 3.09.

Acknowledgments

The authors would like to thank Prof. K. Seifert for helpful discussions and Prof. M. Thelakkat for the introduction to the CV measurements and the BMBF (POLITAG program) and the EU (EUROFET Network) for financial support.

5. References and notes

1. Baude, P. F.; Ender, D. A.; Haase, M. A.; Kelley, T. W.; Muyres, D. V.; Theiss, S. D., *Appl. Phys. Lett.* **2003,** 82, (22), 3964-3966.
2. Dimitrakopoulos, C. D.; Malenfant, P. R. L., *Adv. Mater.* **2002,** 14, (2), 99-117.
3. Sundar Vikram, C.; Zaumseil, J.; Podzorov, V.; Menard, E.; Willett Robert, L.; Someya, T.; Gershenson Michael, E.; Rogers John, A., *Science* **2004,** 303, (5664), 1644-1646.
4. Chen, C. H.; Shi, J.; Tang, C. W., *Macromol. Symp.* **1998,** 125, 1-48.
5. Wakim, S.; Bouchard, J.; Blouin, N.; Michaud, A.; Leclerc, M., *Org. Lett.* **2004,** 6, 3413-3416.
6. Zotti, G.; Schiavon, G.; Zecchin, S.; Morin, J.-F.; Leclerc, M., *Macromolecules* **2002,** 35, (6), 2122-2128.
7. Wu, Y.; Li, Y.; Gardner, S.; Ong, B. S., *J. Am. Chem. Soc.* **2005,** 127, (2), 614-618.
8. Li, Y.; Wu, Y.; Gardner, S.; Ong, B. S., *Adv. Mater.* **2005,** 17, (7), 849-853.
9. Dierschke, F.; Grimsdale, A. C.; Muellen, K., *Synthesis* **2003**, (16), 2470-2472.
10. Sonntag, M.; Strohriegl, P., *Chem. Mater.* **2004,** 16, (23), 4736-4742.
11. Lux, M.; Strohriegl, P.; Höcker, H., *Makromol. Chem.* **1987,** 188, 811-820.
12. Beginn, C.; Grazulevicius, J. V.; Strohriegl, P.; Simmerer, J.; Haarer, D., *Macromol. Chem. Phys.* **1994,** 195, (7), 2353-2370.
13. Patrick, D. A.; Boykin, D. W.; Wilson, D. A.; Tanious, F. A.; Spychala, J.; Bender, B. C.; Hall, J. E.; Dykstra, C. C.; Ohemeng, K. A.; Tidwell, R. R., *Eur. J. Med. Chem.* **1997,** 32, 781-793.
14. Schlüter, A. D., *J. Polym. Sci. Part A: Polym. Chem.* **2001,** 39, (10), 1533-1556.
15. Scherf, U., *J. Mater. Chem.* **1999,** 9, (9), 1853-1864.
16. Kauffman, J. M.; Litak, P. T.; Novinski, J. A.; Kelley, C. J.; Ghiorghis, A.; Qin, Y., *J. Fluorescence* **1995,** 5, (3), 295-305.
17. Crosby, G. A.; Demas, J. N., *J. Phys. Chem.* **1971,** 75, (8), 991-1024.
18. Heinze, J., *Angew. Chem.* **1984,** 96, 823-840.
19. Pommerehne, J.; Vestweber, H.; Guss, W.; Mahrt, R. F.; Bässler, H.; Porsch, M.; Daub, J., *Adv. Mater.* **1995,** 7, (6), 551-554.

Novel Bisindenocarbazole Derivative Exhibiting a Nematic Mesophase

Martin Sonntag, Peter Strohriegl*

Lehrstuhl Makromolekulare Chemie I, Universität Bayreuth, 95440 Bayreuth, Germany

*To whom correspondence should be addressed. E-mail: peter.strohriegl@uni-bayreuth.de

Tetrahedron Letters, **2006**, *47*, 8313-8317.

(Published with minor revisions)

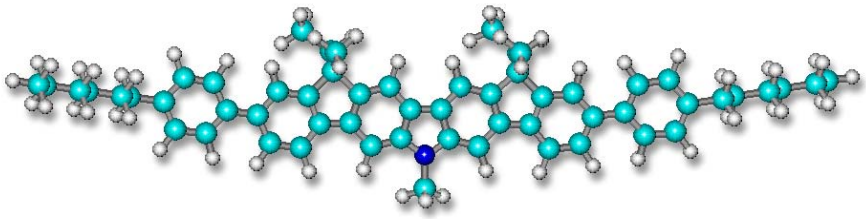

Abstract

In this paper we describe the synthesis of the first liquid crystalline bisindenocarbazole derivative. The novel bisindenocarbazole exhibits a broad nematic mesophase between 180 and 250 °C which was characterized by polarizing microscopy and small angle x-ray scattering. The material shows an excellent electrochemical stability and a strong blue fluorescence.

Communication

During the last decade considerable progress has been made in the development of new organic semiconductors. Among these materials fused aromatics like pentacene and rubrene have received special attention due to their high charge carrier mobilities. In single crystals of pentacene[1] and rubrene[2] mobilities up to 15 cm^2/Vs have been demonstrated. In recent years, some fused heterocycles with improved stability towards oxidation have been synthesized.[3-6] Polycrystalline thin films were obtained by evaporation of selected indolocarbazole derivatives on heated substrates. Such microcrystalline films exhibit charge carrier mobilities up to 0.1 cm^2/Vs in organic field-effect transistors.[5, 6] Nevertheless, in polycrystalline films the mobility strongly depends on the morphology, e. g. the grain size and packing of the microcrystals and therewith is very sensitive towards the deposition conditions.

An alternative approach to well ordered thin films are large monodomains formed by liquid crystals (LC). The molecules can be aligned in the LC-phase at elevated temperatures. The orientation is then frozen in either by quenching the LC-phase to room temperature or by photopolymerization of liquid crystalline compounds with photoreactive groups, known as reactive mesogens. High mobilities in discotic liquid-crystal phases from 2,3,6,7,10,11-hexahexylthiotriphenylene were reported by Haarer et al in 1999. Photoinduced charge carrier mobilities up to 0.1 cm^2/Vs were obtained in the helical columnar mesophase.[7] The group of Müllen reported the synthesis of discotic hexabenzocoronene derivatives from which carrier mobilities up to 1 cm^2/Vs were determined by a pulse-radiolysis time-resolved microwave conductivity technique (PR-TRMC).[8, 9] Besides discotic materials, rod-like calamitic molecules are also able to form highly ordered mesophases. In the smectic G phase of an α,ω-dialkylterthiophene, carrier mobilities of $2x10^{-2}$ cm^2/Vs for both holes and electrons were reported by Hanna in 2000.[10] Furthermore the orientation of calamitic LC-phases has been adopted to increase charge carrier mobilities in organic field-effect transistors (OFETs). Here liquid crystalline fluorene-bithiophene copolymers like F8T2[11] have been used as well as low molar mass oligothiophenes[12, 13] and reactive mesogens.[14] A second field in which ordered LC-phases have already been successfully used, are organic light emitting diodes (OLEDs). Polyfluorenes and fluorene model compounds with nematic mesophases have been used to generate linearly polarized light.[15-19]

Recently we have introduced a series of bisindenocarbazoles which are a new class of fused aromatic heterocycles. By introduction of different alkyl side chains the thermal properties of the bisindenocarbazoles can be tailored from crystalline materials to amorphous molecular

glasses.[20] In order to obtain a liquid crystalline bisindenocarbazole derivative, the core molecule has to be extended to increased the length/width ratio. In this article we present the synthetic access to a novel rod-like bisindenocarbazole derivative which exhibits a nematic LC phase together with a saturated blue photoluminescence.

The synthesis of the bisindenocarbazole starting compound **1** is reported elsewhere.[20] The new building block **2** was prepared by reaction of **1** with two equivalents of bromine. For this purpose we used a halogenation reaction with alumia-supported copper(II) bromide in carbon tetrachloride.[21] The bromination was carried out with the *(R,S)*-bisindenocarbazole isomer shown in Scheme 1. 2D-NMR spectroscopy revealed that the bromine was introduced selectively in the 7- and 7'-position of the bisindenocarbazole core (Figure S1, Supporting Information). The conversion of 1-bromo-4-hexyl-benzene into the corresponding borolane compound **3** was carried out in with n-BuLi and 2-isopropoxy-4,4,5,5-tetramethyl-1,3,2-dioxaborolane in dry THF. Finally the bisindenocarbazole derivative **4** was prepared by a palladium catalyzed Suzuki cross-coupling reaction as depicted in Scheme 1.

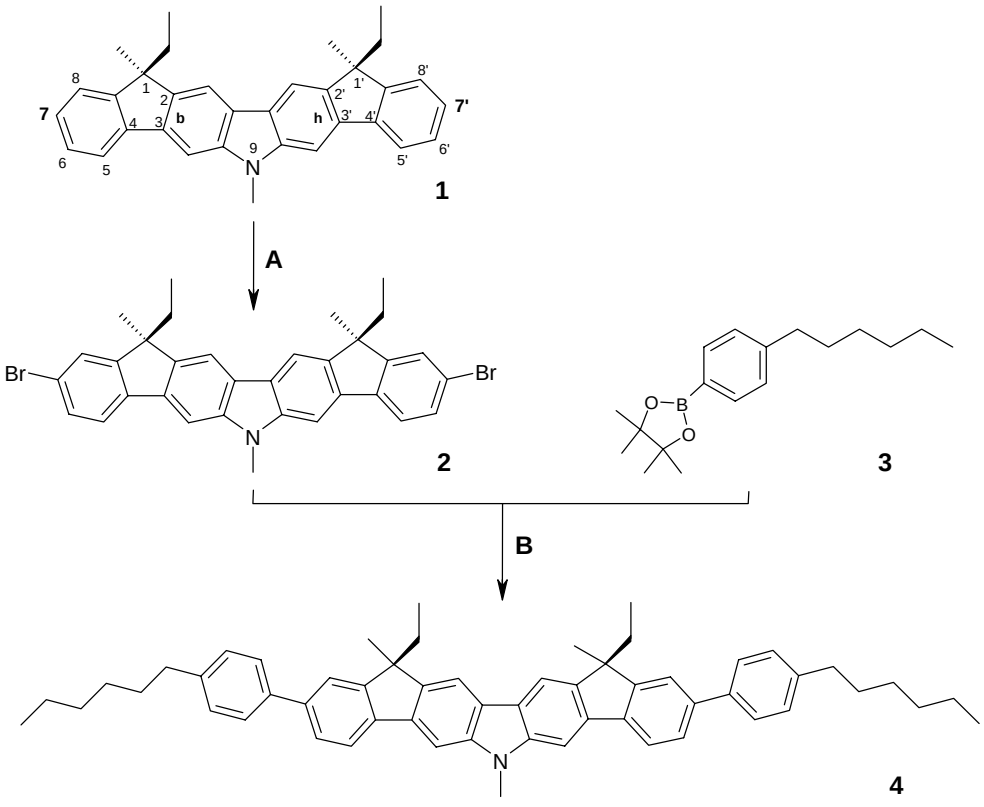

Scheme 1. *Synthesis of the nematic bisindenocarbazole derivative* ***4.***

The product shows excellent solubility in common organic solvents which facilitates purification and processing of the material. The target compound **4** was purified by medium pressure liquid chromatography (MPLC) and characterized by IR, ^{1}H- and ^{13}C-NMR, mass spectrometry and elemental analysis (Supporting Information).

Thermogravimetric analysis (TGA) proved the high thermal stability of the novel bisindenocarbazole derivative. In nitrogen atmosphere decomposition starts at about 310 °C at a heating rate of 10 K/min. Above 180 °C a nematic mesophase is observed by polarizing microscopy (POM) up to a clearing temperature at 251 °C. Upon cooling the typical Schlieren texture of the nematic mesophase appeares at 250 °C and crystallization starts at about 165 °C. Polarizing microscope images are shown in Figure 1. In the DSC measurement **4** exhibits a melting transition at around 180 °C with an enthalpy of 12.4 kJ/mol and shows recrystallization at 165 °C (8.1 kJ/mol).

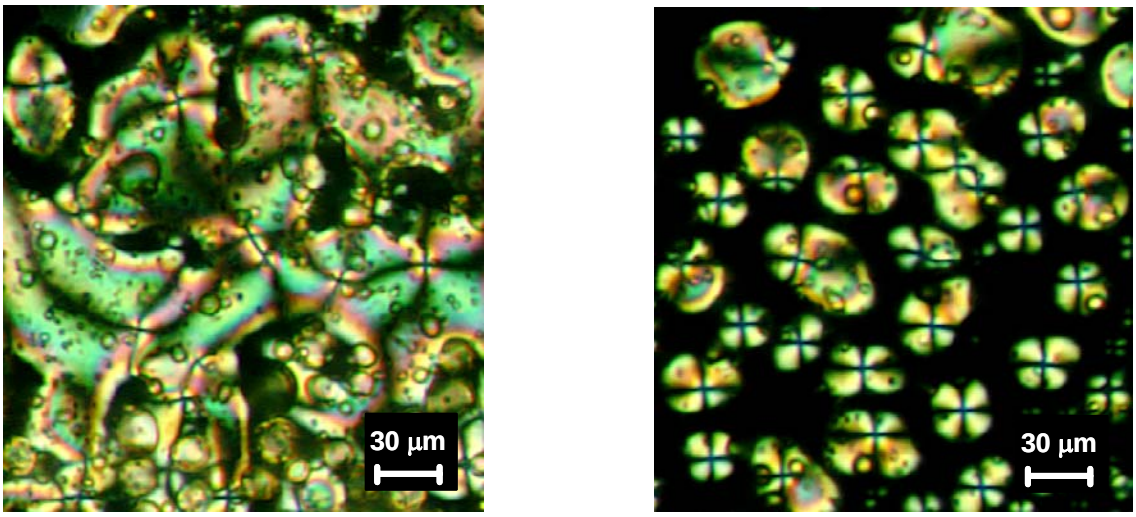

Figure 1. *Polarizing microscopy images of* ***4*** *upon heating at 220 °C (left) and upon cooling at 248 °C (right) under crossed polarizers.*

Further analysis by small angle X-ray scattering (SAXS) at a temperature of 220 °C confirmed the existence of a nematic LC phase (Figure 2). In the small angle region a Bragg peak was observed from which an average end-to-end distance of 34.5 Å at 220 °C can be calculated. This distance is a little bit shorter than the calculated length of the extended molecules (ca. 36 Å) which is consistent with a slightly tilted arrangement of the rigid-rod like bisindenocarbazole molecules in the nematic mesophase. From the broad wide angle Bragg peak a spacing of 5.6 Å is obtained. This peak reflects the average side-to-side distance of the rod-like molecules and is a typical value for a nematic LC phase.

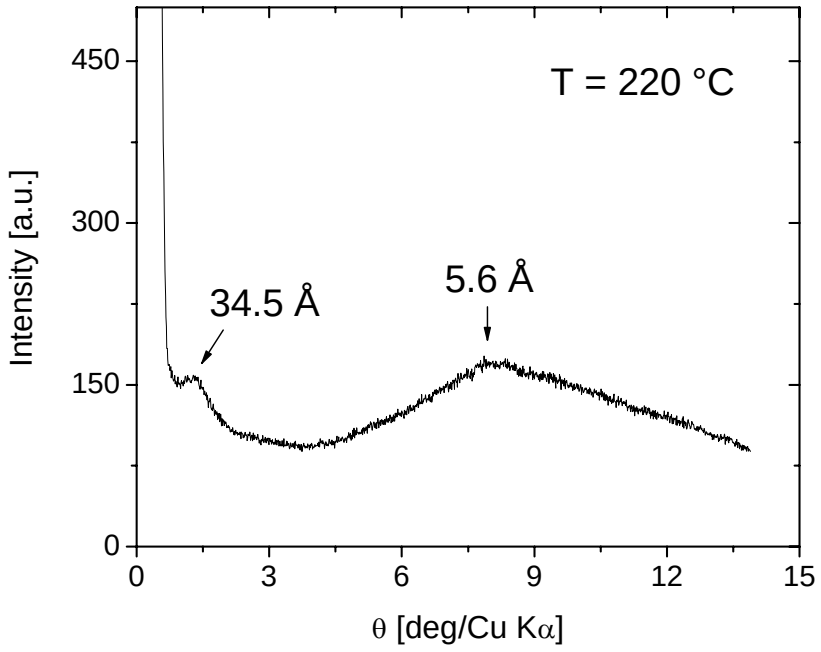

Figure 2. *X-ray diffractogram of the bisindenocarbazole derivative* ***4*** *at 220 °C.*

Absorption and photoluminescence (PL) spectra of **4** were taken from diluted cyclohexane solutions (Supporting Information, Fig. S2). The absorption maximum is detected at 395 nm and the maximum of photoluminescence emission at 403 nm (excitation wavelength 390 nm). The very small Stokes shift of only 8 nm can be explained by the rigid π-electron system of the new material which allows no major geometrical changes in the transition from the ground to the excited state.[22, 23] For comparison, the bisindenocarbazole core itself has a Stokes shift of 6 nm.[20] The strong blue fluorescence of the liquid crystalline bisindenocarbazole **4** makes it an attractive candidate as blue emitter in polarized organic light emitting devices (OLEDs).

For the investigation of the electrochemical properties we have used cyclic voltammetry (CV). The CV curve of **4** measured vs. Ag /AgCl shows only one oxidation peak at 443 mV which is quasireversible (Figure S3). Repeated oxidation and reduction cycles did not change the CV curve what demonstrates the high electrochemical stability of **4**. Taking -4.8 eV as the HOMO level for the standard ferrocene / ferrocenium redox system[24] a HOMO level of -5.4 eV was calculated for **4**. With the optical band gap of 3.0 eV from the absorption spectrum, a LUMO value of -2.4 eV can be estimated.

Conclusion

We present a new synthetic route to a novel bisindenocarbazole derivative with a broad nematic mesophase between 180 and 250 °C. Bisindenocarbazoles represent a class of fused aromatics from which no liquid crystalline derivatives have been described before. The material is thermally stable and exhibits excellent electrochemical stability. From the CV measurements a HOMO value of -5.3 eV was calculated. At the moment the synthesis of a number of bisindenocarbazole derivatives is in progress in order to get a better understanding of the structure-property relationship in this new class of materials.

Acknowledgments:
The authors would like to thank Andreas Timme for the SAXS measurement and Günter Lattermann for fruitful discussions. We are grateful to the Deutsche Forschungsgemeinschaft (SFB 481) and the BMBF (POLITAG programme) for financial support.

References

(1) Baude, P. F.; Ender, D. A.; Haase, M. A.; Kelley, T. W.; Muyres, D. V.; Theiss, S. D., *Appl. Phys. Lett.* **2003,** *82*, 3964.
(2) Sundar Vikram, C.; Zaumseil, J.; Podzorov, V.; Menard, E.; Willett Robert, L.; Someya, T.; Gershenson Michael, E.; Rogers John, A., *Science* **2004,** *303*, 1644.
(3) Wakim, S.; Bouchard, J.; Simard, M.; Drolet, N.; Tao, Y.; Leclerc, M., *Chem. Mater.* **2004,** *16*, 4386.
(4) Wakim, S.; Bouchard, J.; Blouin, N.; Michaud, A.; Leclerc, M., *Org Lett.* **2004,** *6*, 3413.
(5) Li, Y.; Wu, Y.; Gardner, S.; Ong, B. S., *Adv. Mater.* **2005,** *17*, 849.
(6) Wu, Y.; Li, Y.; Gardner, S.; Ong, B. S., *J. Am. Chem. Soc.* **2005,** *127*, 614.
(7) Adam, D.; Schuhmacher, P.; Simmerer, J.; Haeussling, L.; Siemensmeyer, K.; Etzbach, K. H.; Ringsdorf, H.; Haarer, D., *Nature* **1994,** *371*, 141.
(8) Van De Craats, A. M.; Warman, J. M.; Fechtenkotter, A.; Brand, J. D.; Harbison, M. A.; Müllen, K., *Adv. Mater.* **1999,** *11*, 1469.
(9) Fechtenkötter, A.; Saalwächter, K.; Harbison, M. A.; Müllen, K.; Spiess, H. W., *Angew. Chem. Int. Ed.* **1999,** *38*, 3039.
(10) Funahashi, M.; Hanna, J., *Appl. Phys. Lett.* **2000,** *76*, 2574.

(11) Sirringhaus, H.; Wilson, R. J.; Friend, R. H.; Inbasekaran, M.; Wu, W.; Woo, E. P.; Grell, M.; Bradley, D. D. C., *Appl. Phys. Lett.* **2000**, 406.

(12) McCulloch, I.; Heeney, M.; Bailey, C.; Genevicius, K.; MacDonald, I.; Shkunov, M.; Sparrowe, D.; Tierney, S.; Wagner, R.; Zhang, W.; Chabinyc, M. L.; Kline, R. J.; McGehee, M. D.; Toney, M. F., *Nature Materials* **2006,** *5*, 328.

(13) van Breemen Albert, J. J. M.; Herwig Peter, T.; Chlon Ceciel, H. T.; Sweelssen, J.; Schoo Herman, F. M.; Setayesh, S.; Hardeman Willie, M.; Martin Christian, A.; de Leeuw Dago, M.; Valeton Josue, J. P.; Bastiaansen Cees, W. M.; Broer Dirk, J.; Popa-Merticaru Andreea, R.; Meskers Stefan, C. J., *J. Am. Chem. Soc.* **2006,** *128*, 2336.

(14) Huisman, B.-H.; Valeton, J. J. P.; Nijssen, W.; Lub, J.; ten Hoeve, W., *Adv. Mater.* **2003,** *15*, 2002.

(15) Grell, M.; Knoll, W.; Lupo, D.; Meisel, A.; Miteva, T.; Neher, D.; Nothofer, H.-G.; Scherf, U.; Yasuda, A., *Adv. Mater.* **1999,** *11*, 671.

(16) Geng, Y.; Chen, A. C. A.; Ou, J. J.; Chen, S. H.; Klubek, K.; Vaeth, K. M.; Tang, C. W., *Chem. Mater.* **2003,** *15*, 4352.

(17) Culligan, S. W.; Geng, Y.; Chen, S. H.; Klubek, K.; Vaeth, K. M.; Tang, C. W., *Adv. Mater.* **2003,** *15*, 1176.

(18) Aldred, M. P.; Eastwood, A. J.; Kelly, S. M.; Vlachos, P.; Contoret, A. E. A.; Farrar, S. R.; Mansoor, B.; O'Neill, M.; Tsoi, W. C., *Chem. Mater.* **2004,** *16*, 4928.

(19) Whitehead, K. S.; Grell, M.; Bradley, D. D. C.; Jandke, M.; Strohriegl, P., *Appl. Phys. Lett.* **2000,** *76*, 2946.

(20) Sonntag, M.; Strohriegl, P., *Tetrahedron*, **2006**, *62*, 8103.

(21) Kodomari, M.; Satoh, H.; Yoshitomi, S., *J. Org. Chem.* **1988,** *53*, 2093.

(22) Scherf, U., *J. Mater. Chem.* **1999,** *9*, 1853.

(23) Lemmer, U.; Heun, S.; Mahrt, R. F.; Scherf, U.; Hopmeier, M.; Siegner, U.; Goebel, E. O.; Muellen, K.; Baessler, H., *Chem. Phys. Lett.* **1995,** *240*, 373.

(24) Pommerehne, J.; Vestweber, H.; Guss, W.; Mahrt, R. F.; Bässler, H.; Porsch, M.; Daub, J., *Adv. Mater.* **1995,** *7*, 551.

Supporting Information

Martin Sonntag, Peter Strohriegl*

Lehrstuhl Makromolekulare Chemie I, Universität Bayreuth, 95440 Bayreuth, Germany

*To whom correspondence should be addressed. E-mail: peter.strohriegl@uni-bayreuth.de

Experimental

General

^{1}H-NMR spectra were recorded with a Bruker AC 250 (250 MHz) apparatus. 2D-NMR spectra were recorded with a Bruker AC 300 (300 MHz). All data are given as chemical shifts δ [ppm] downfield from $Si(CH_3)_4$. The IR spectra were recorded using a Bio-Rad Digilab FTS-40. The UV-VIS spectra were recorded with a Hitachi U-3000 spectrophotometer. Emission spectra were obtained from a Shimadzu spectrofluoro-photometer RF-5301PC. Mass spectra (MS) were recorded with a Finnigan MAT 8500 (70 eV) with a MAT 112S Varian. Thermogravimetric analysis (TGA) was performed on a Perkin Elmer TAS-409 at a heating rate of 10 K/min under N_2. For differential scanning calorimetry measurements (DSC) a Perkin Elmer Diamond DSC apparatus was used (heating/cooling rate: 10 K/min). Polarized microscopy was carried out with the Nikon Diaphot 300 equipped with a Linkon hotstage. Cyclic voltammetry measurements (CV) were performed with a glassy carbon working electrode (0.2 mm) in a three-electrode potentiostat configuration from EG&G Princeton Applied Research. All CV experiments were carried out at 25 °C in CH_2Cl_2 solution containing 0.1 M tetrabutylammonium hexafluorophosphate ($TBAPF_6$) as supporting electrolyte. Oxidation potentials were measured vs. Ag/AgCl as the reference electrode.[1] X-ray analysis was carried out with a Huber/Seifert Iso-Debyeflex 3003, using a Guinier diffractometer system (Cu K_α: 1,5418 Å) with a sealed tube for temperature dependent measurements.

All chemicals and reagents were used as received from Aldrich. Neutral alumina was purchased from ICN Biomedicals (MP Alumina N, Akt. I). Carbon tetrachloride (p. a.) was received from Merck. Tetrahydrofuran (THF) was distilled over potassium before use. The

synthesis of *(1R, 1'S)*-Diethyl-*(1S, 1'R)*-dimethyl-bisindeno[3,2-b:2'3'-h]-9-methyl-carbazole (**1**) has been reported elesewhere.[2]

Preparation of Alumina Supported Copper(II) Bromide [3]

To a solution of copper (II) bromide (10 g) in distilled water (30 ml) neutral alumina (20 g) was added at room temperature. The water was evaporated at 80 °C under reduced pressure with a rotary evaporator. The resulting reagent was dried under high vacuum at 100 °C for 24 h and stored under argon.

Synthesis of 7,7'-dibromo-*(1R, 1'S)*-diethyl-*(1S, 1'R)*-dimethyl-bisindeno[3,2-b:2'3'-h]-9-methyl-carbazole (2).

A mixture of the *(R,S)*-binsindenocarbazole isomer **1**[2] (0.38 mg, 0.86 mmol), Al_2O_3-$CuBr_2$ (2.9 g) and carbon tetrachloride (80 ml) was stirred at 70 °C for 3 h. Afterwards the product mixture was filtered and the spent reagent was washed with dichloromethane (30 ml) before the solvents from the combined filtrates were evaporated under reduced pressure. Purification by column chromatography on silica gel with hexane/THF (10:1) as eluent yielded 0.4 g (78 %) of **2** as pale yellow solid. The NOESY-NMR spectrum of **2** is shown in Figure S1. ^{1}H-NMR (250 MHz, $CDCl_3$): δ(ppm): 0.38(t, 6H, 2xMe, J = 7.3 Hz), 1.61(s, 6H, 2xMe) 2.15(q, 4H, 2xCH_2, J = 7.3 Hz), 3.93(s, 3H, NMe), 7.48(dd, 2H, J = 8.0 Hz and J = 1.5 Hz), 7.53(d, 2H, J = 1.5 Hz), 7.64(s, 2H) 7.68(d, 2H, J = 8.0 Hz), 8.04(s, 2H); ^{13}C-NMR (62.5 MHz, $CDCl_3$): δ(ppm): 8.93, 27.23, 29.41, 34.05, 50.88, 99.55, 113.95, 120.82, 120.89, 123.05, 126.27, 130.03, 137.72, 139.92, 141.77, 142.90, 154.73; *m/z* = 597/599/601 (M^+, 50/100/50 %); Anal. Calc for $C_{33}H_{29}Br_2N$ (599.4): C, 66.13; H, 4.88; N, 2.34. Found: C, 66.11; H, 4.87; N, 2.36.

Synthesis of 2-(4-hexyl-phenyl)-4,4,5,5-tetramethyl-[1,3,2]dioxaborolane (3).

1.0 g (4.1 mmol) of 1-Bromo-4-hexyl-benzene were dissolved in absolute THF under argon. The solution was cooled to -78 °C before 3.1 ml (5.0 mmol) n-BuLi (1.6 M solution in hexane) were added dropwise. The reaction mixture was stirred for 10 min, before 1.0 ml (5.0 mmol) of 2-isopropoxy-4,4,5,5-tetramethyl-1,3,2-dioxaborolane were added. The reaction mixture was allowed to warm to room temperature and stirred for another 12 h before it was poured into ice water. The solution was extracted with diethyl ether, the organic phase washed with brine and dried with Na_2SO_4 before the solvent was removed. Purification by column chromatography on silica gel with hexane/THF (15:1) as eluent yielded 1.0 g (85 %) of **3** as

colorless oil. ^{1}H-NMR (250 MHz, $CDCl_3$): δ(ppm): 0.86(t, 3H, Me, J = 7.0 Hz), 1.18-1.26(m, 8H, 4xCH_2), 1.33(s, 12H, 4xMe), 2.62(t, 2H, CH_2, J = 7.6 Hz), 7.20(d, 2H, J = 7.6 Hz), 7.73(d, 2H, J = 7.6 Hz); m/z = 288 (M^+, 100 %), 217 (46), 189 (29), 107 (23).

Synthesis of 7,7'-di-(4-hexyl-phenyl)-*(1R, 1'S)*-diethyl-*(1S, 1'R)*-dimethyl-bisindeno[3,2-b:2'3'-h]-9-methyl-carbazole (4).

0.1 g (0.17 mmol) of the dibromo bisindenocarbazole **2** and 0.1 g (0.35 mmol) of the borolane compound **3** were dissolved in 25 ml toluene. A 2M K_2CO_3 solution (6 ml) and 0.1 g of trimethylbenzylammonium chloride were added. The reaction mixture was degassed by three freeze/thaw cycles before 1.7 mg (7.3 x 10^{-6} mol) of palladium(II) acetate and 6.7 mg (2.2 x 10^{-5} mol) of tri-o-tolylphosphine were added under argon. The mixture was stirred for 4 h at 90 °C. The reaction mixture was poured into ice water, extracted with diethyl ether and dried with Na_2SO_4. After evaporation of the solvent, the product was purified by MPLC with hexane/THF (30:1) as eluent at a pressure of 18 bar. 98 mg (79 %) of **4** were obtained as white solid. ^{1}H-NMR (250 MHz, $CDCl_3$): δ(ppm): 0.37(t, 6H, 2xMe, J = 7.3 Hz), 0.83(t, 6H, 2xMe, J = 6 Hz), 1.18-1.32(m, 10H, 5xCH_2), 1.49-1.65(m, 12H, 2xMe, 3xCH_2), 2.09(q, 4H, 2x CH2, J = 7.3 Hz), 2.56(t, 4H, J = 7.7 Hz), 3.89(s, 3H, NMe), 7.18(d, 4H, J = 8.1 Hz), 7.50-7.57(m, 8H), 7.61(s, 2H), 7.79(d, 2H, J = 7.6 Hz), 8.00(s, 2H). ^{13}C-NMR (62.5 MHz, $CDCl_3$): δ(ppm): 8.01, 13.10, 21.63, 26.42, 28.04, 28.38, 30.51, 30.75, 33.21, 34.63, 49.62, 98.37, 112.77, 118.73, 120.39, 121.77, 124.90, 125.96, 127.82, 137.40, 138.01, 138.95, 138.99, 140.74, 140.93, 142.53, 152.15; m/z = 761 (M^+, 100 %), 732 (30), 703 (10), 330 (33); IR (KBr): $\tilde{\nu}$ (cm^{-1}): 2959, 2926, 2854, 1559, 1495,1345, 1260, 841; Anal. Calc. for $C_{57}H_{63}N$ (762.1): C, 89.83; H, 8.33; N, 1.84. Found: C, 89.40; H, 8.30; N, 2.10.

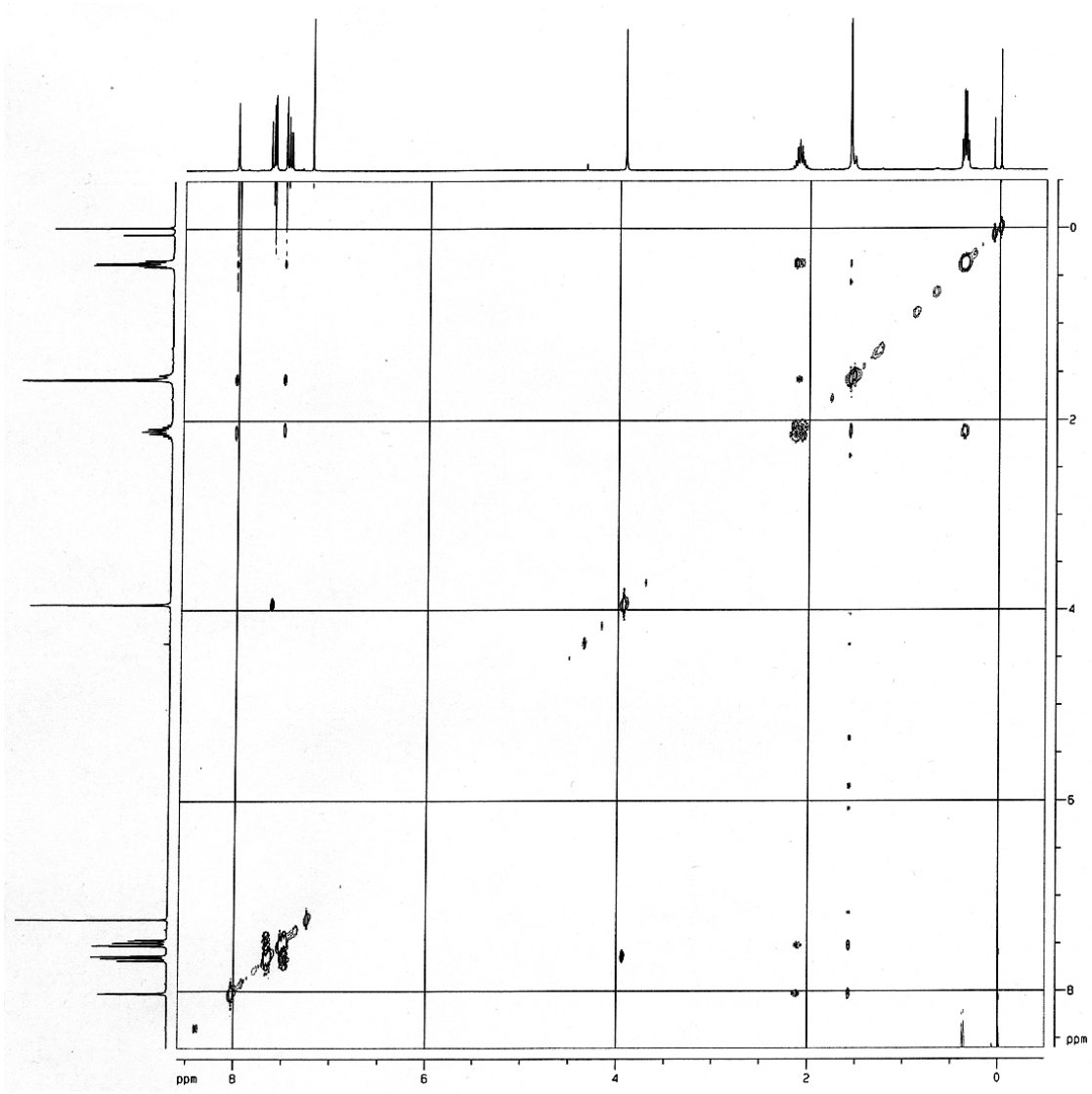

Figure S1. *^{1}H-^{1}H NMR NOESY spectrum of dibromo bisindenocarbazole (**2**) in $CDCl_3$.*

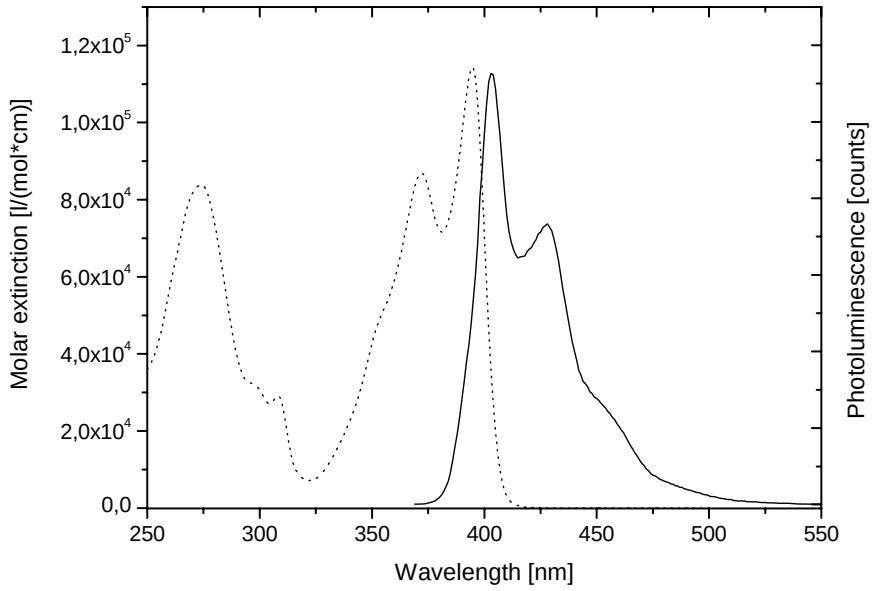

Figure S2. *Absorption and fluorescence spectra of the phenylated bisindenocarbazole* ***15****. The absorption spectrum was taken from* 10^{-5} *M cyclohexane solution and the fluorescence spectrum was measured from* 10^{-6} *M cyclohexane solution with an excitation wavelength of 395 nm.*

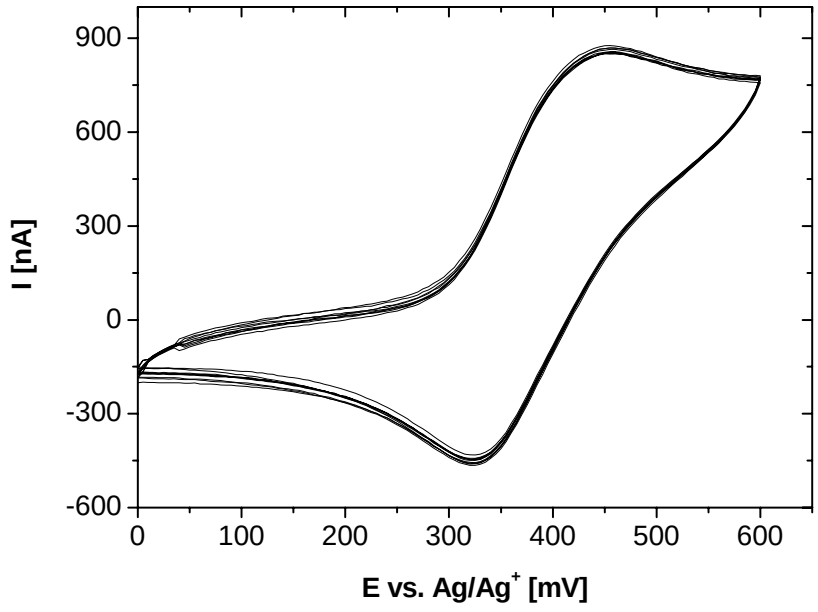

Figure S3. *Cylic voltammetry of* ***4*** *in* CH_2Cl_2 / $TBAPF_6$, υ = 50 mV/s. *Ten subsequent redox cycles were carried out in order to check the electrochemical stability of the bisindenocarbazole derivative* ***4****.*

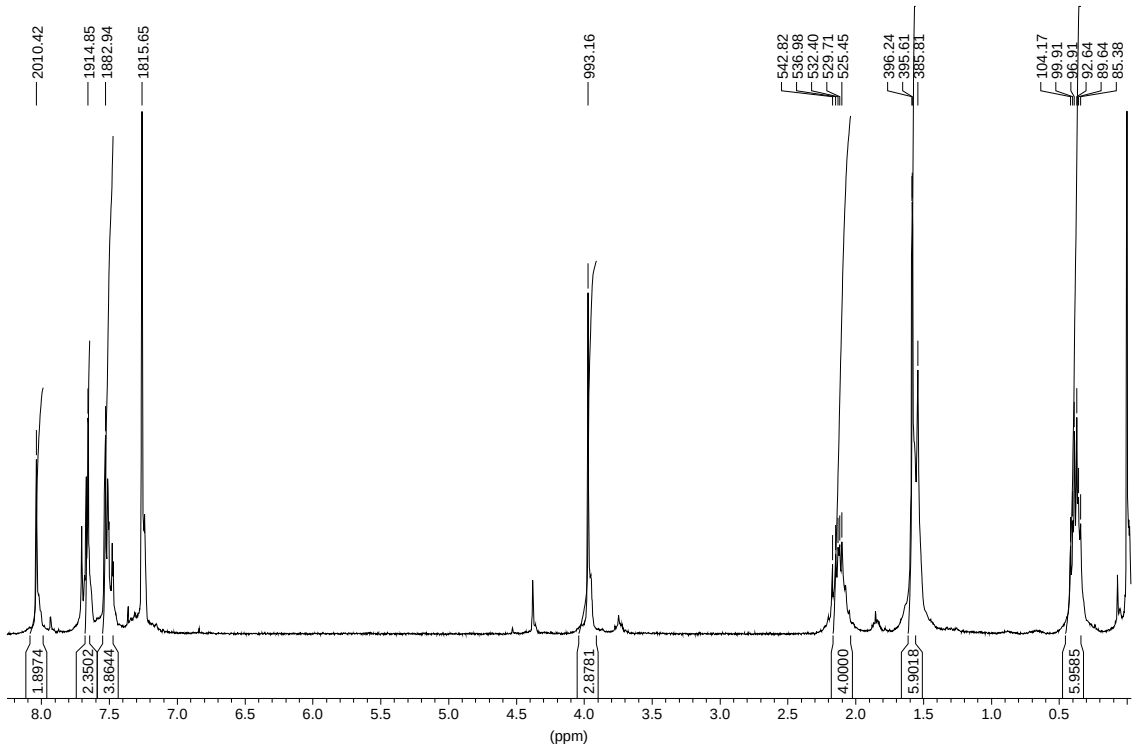

Figure S4. *^{1}H-NMR spectrum of **2** (coupling constants in Hz).*

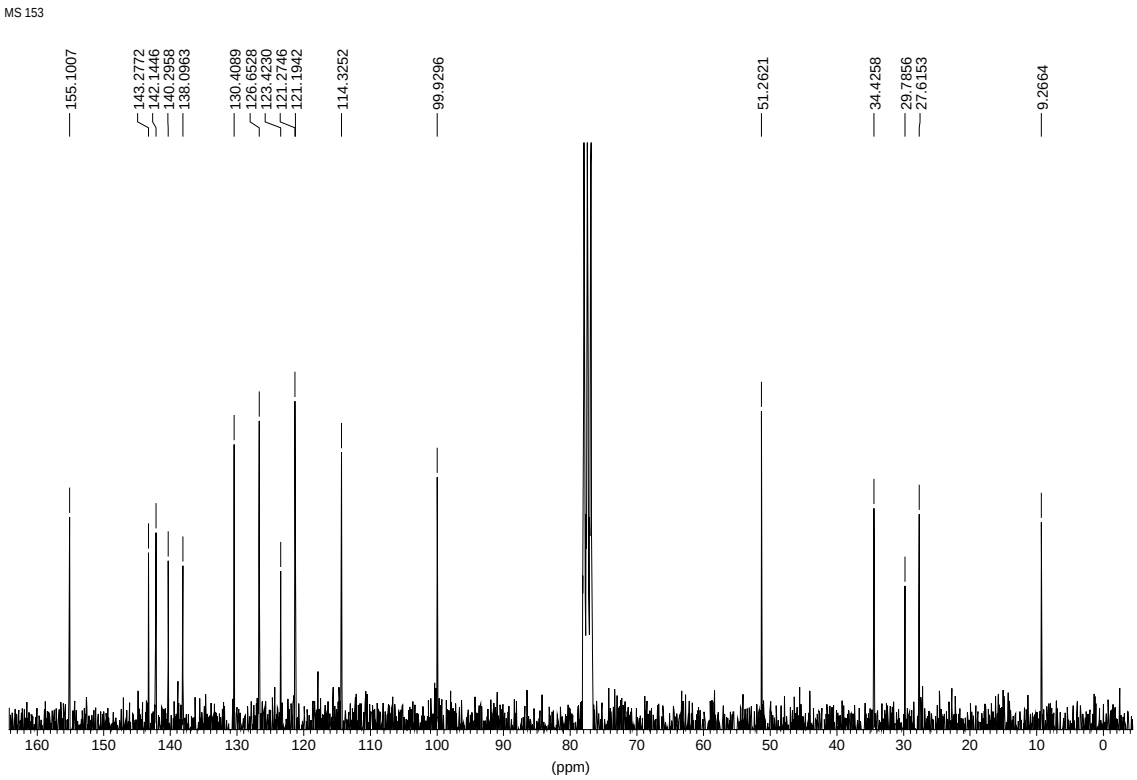

Figure S5. *^{13}C-NMR spectrum of **2** (chemical shifts in ppm).*

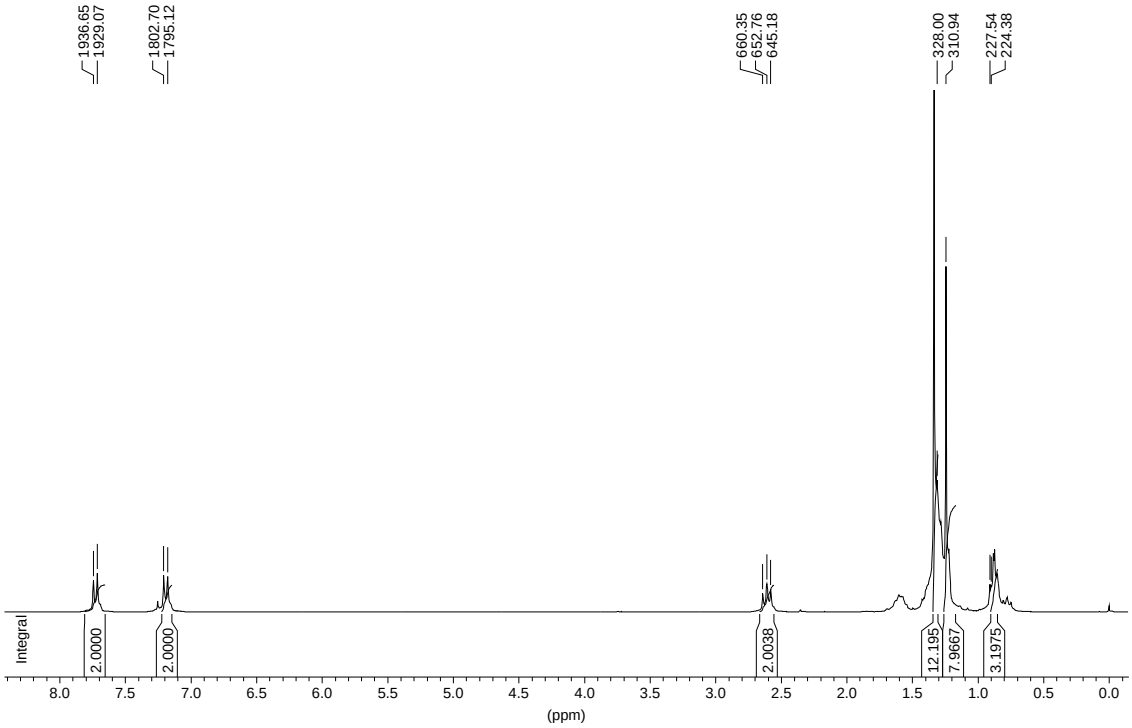

Figure S6. *^{1}H-NMR spectrum of **3** (coupling constants in Hz).*

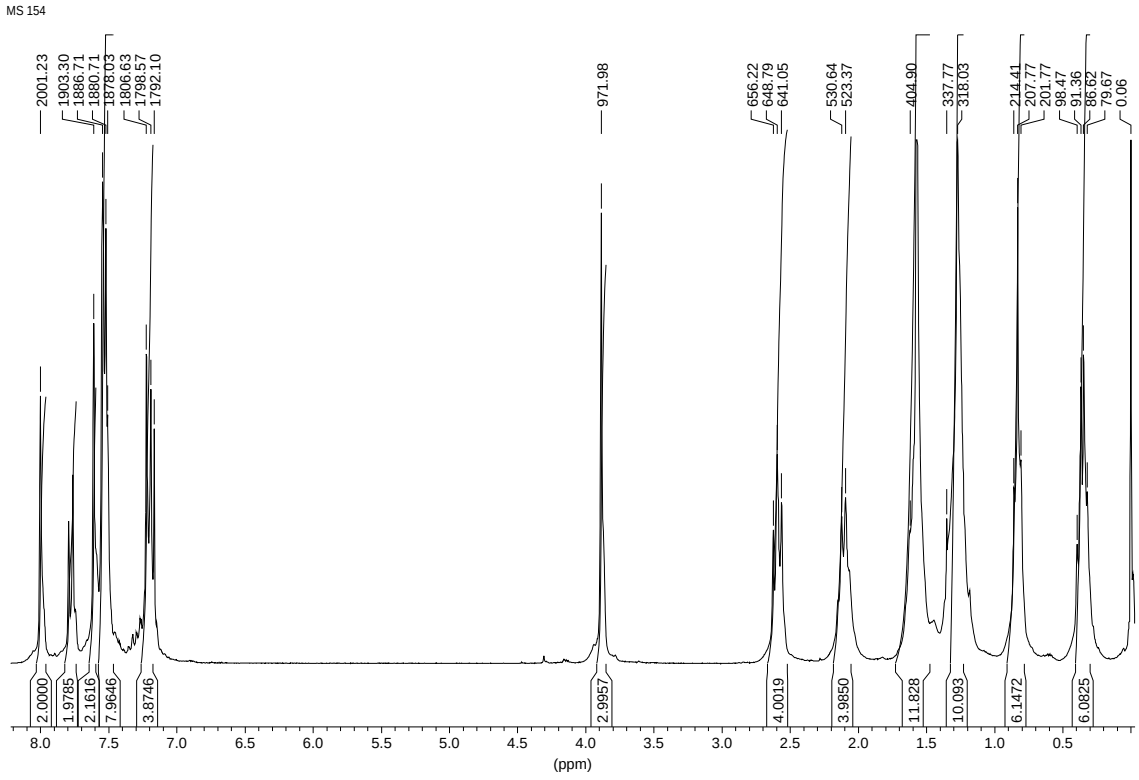

Figure S7. *^{1}H-NMR of **4** (coupling constants in Hz).*

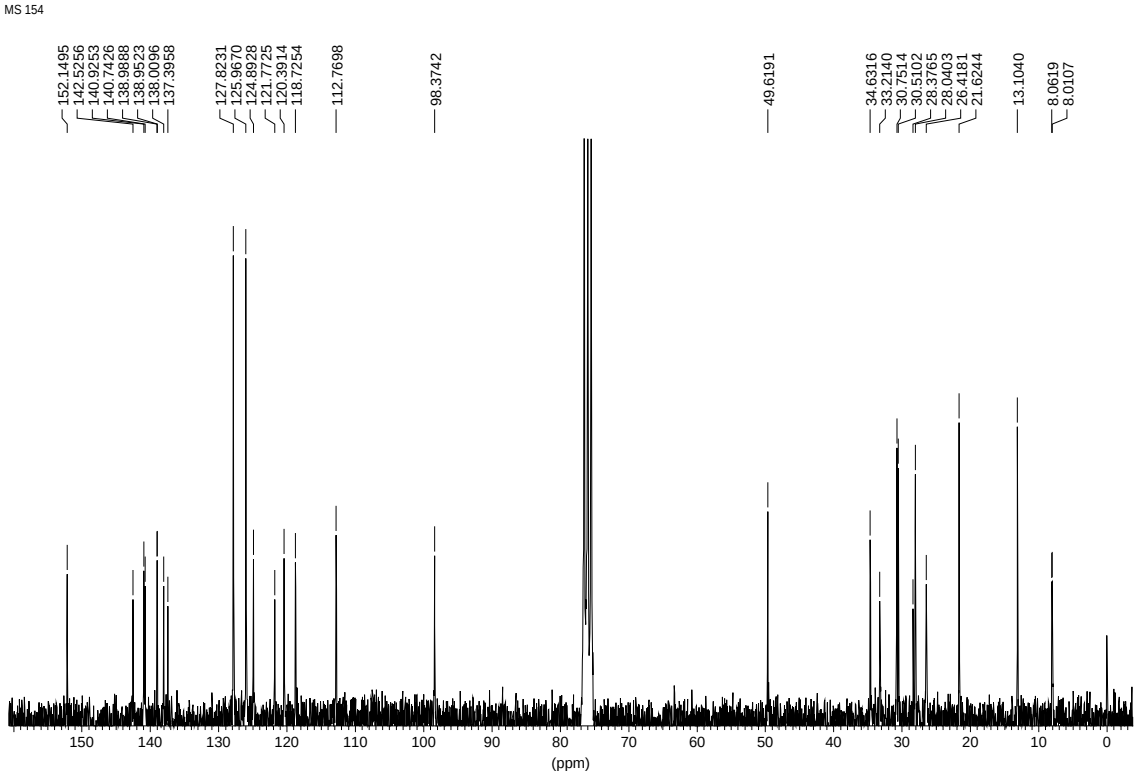

Figure S8. *^{13}C-NMR of **4** (chemical shifts in ppm).*

(1) Heinze, J., *Angew. Chem.* **1984,** *96*, 823.

(2) Sonntag, M.; Strohriegl, P., *Tetrahedron*, **2006**, *62*, 8103.

(3) Kodomari, M.; Satoh, H.; Yoshitomi, S., *J. Org. Chem.* **1988,** *53*, 2093.

Synthesis of a novel liquid crystalline bisindenocarbazole derivative

Martin Sonntag, Peter Strohriegl*

Macromolecular Chemistry I, University of Bayreuth, 95440 Bayreuth, Germany

Liquid Crystals, **2006,** *in press*.

Keywords

Bisindenocarbazole, nematic mesophase, Suzuki cross coupling, alumina supported halogenation

Abstract

In this paper we describe the synthesis of four new bisindenocarbazole derivatives, prepared by selective bromination of bisindenocarbazole in 7- and 7'-position. Followed by Suzuki cross coupling with alkyl substituted phenyl, biphenyl and fluorene units. From this new class of fused aromatics a liquid crystalline derivative is reported for the first time. The bisindenocarbazole with two 4-hexylphenyl side groups exhibits a broad nematic phase between 180 and 250 °C. Whereas the other derivatives are crystalline or form molecular glasses. All bisindenocarbazoles exhibit high thermal stabilities above 300 °C and show excellent electrochemical stability. HOMO and LUMO levels of -5.4 eV and -2.3 eV were determined by cyclic voltammetry and optical spectroscopy. The bisindenocarbazoles display a strong blue fluorescence with up to 56 % quantum yield in solution.

*To whom correspondence should be addressed. E-mail: peter.strohriegl@uni-bayreuth.de

1. Introduction

During the last years the development of new organic semiconductors made huge progress. Among these materials fused aromatics like pentacene and rubrene have received special attention due to their high charge carrier mobilities. In single crystals of pentacene [1] and rubrene [2] mobilities up to 15 cm^2/Vs have been demonstrated. In recent years, also fused heterocycles like indeno- and indolocarbazoles with improved stability towards oxidation have been synthesized [3-6]. Polycrystalline thin films were obtained by evaporation of selected indolocarbazole derivatives on heated substrates. In these microcrystalline films charge carrier mobilities up to 0.1 cm^2/Vs were achieved in organic field-effect transistors [5, 6]. In polycrystalline films the mobility strongly depends on the film morphology, e. g. the grain size and packing of the micro crystals and therewith is very sensitive towards the deposition conditions.

An alternative approach to well ordered thin films are large monodomains formed by liquid crystals (LC). The molecules can be aligned in the LC-phase at elevated temperatures. The orientation is then frozen in either by quenching the LC-phase to room temperature or by photopolymerization of liquid crystalline compounds with photoreactive groups, known as reactive mesogens. High mobilities in discotic liquid-crystal phases from 2,3,6,7,10,11-hexahexylthiotriphenylene were reported by Haarer et al in 1999. Photoinduced charge carrier mobilities up to 0.1 cm^2/Vs were obtained in the helical columnar mesophase [7]. The group of Müllen reported the synthesis of discotic hexabenzocoronene derivatives. In these materials, carrier mobilities up to 1 cm^2/Vs were determined by a pulse-radiolysis time-resolved microwave conductivity technique (PR-TRMC) [8, 9]. Besides discotic materials, rod-like calamitic molecules are also able to form highly ordered mesophases with high carrier mobilities. In the smectic G phase of a α,ω-dialkylterthiophene, mobilities of $2x10^{-2}$ cm^2/Vs for both holes and electrons were reported by Hanna [10]. The orientation of calamitic LC-phases has also been used to make organic field-effect transistors (OFETs) with high charge carrier mobilities. Here liquid crystalline fluorene-bithiophene copolymers like F8T2 [11] have been used as well as low molar mass oligothiophenes [12, 13] and reactive mesogens [14].

A second field in which ordered LC-phases have been successfully applied are organic light emitting diodes (OLEDs). In this case, polyfluorenes exhibiting nematic mesophases were used to generate linearly polarized light [15-19].

Recently we have reported the synthesis of bisindenocarbazoles which are a new class of fused heterocycles. By introduction of different alkyl side chains the thermal properties of the bisindenocarbazoles can be tailored from crystalline materials to amorphous molecular glasses [20]. In this paper we report the synthesis of the first rod-like bisindenocarbazole derivative exhibiting a nematic mesophase.

2. Results and Discussion

2.1. Preparation of the Bisindenocarbazole Derivatives

Recently we reported the synthesis of novel electroactive bisindenocarbazoles from which depending on the alkyl substituents, both crystalline materials and amorphous molecular glasses are obtained [20]. In order to prepare a liquid crystalline bisindenocarbazole, the core molecule has to be extended by the introduction of aromatic side groups in order to increase the length of the molecule. For this purpose the bisindenocarbazole was first brominated in the 7- and 7'-position. After that it is possible to substitute the dibromobisindenocarbazole with different aromatic substituents via a Suzuki cross coupling. The synthesis of the bisindenocarbazole **1** is reported elsewhere [20]. In order to obtain the new building block **2**, the core molecule **1** had to be reacted with two equivalents of bromine. Kodomari et al reported that aromatic hydrocarbons like naphthalene and phenanthrene can easily be halogenated by alumina-supported copper(II) halides to give mono- or dihalogenated products [21]. By using this technique they were also able to brominate fluorene selectively in the 2- and 7-positions with high yields. We decided to adopt this method for the selective bromination of the bisindenocarbazole **1**. The halogenation was carried out with copper(II) bromide supported on alumina in carbon tetrachloride (Scheme 1). The selective bromination of the bisindenocarbazole in the 7- and 7'-position was proven by mass- and 2-dimensional NMR spectroscopy.

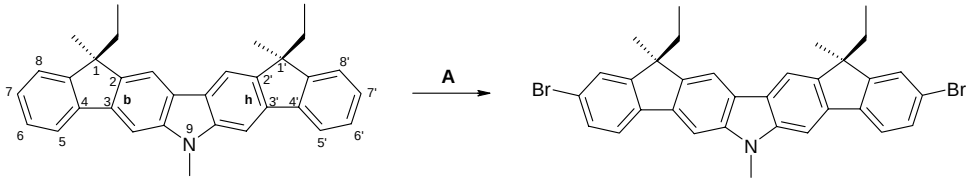

Scheme 1. *Synthesis of 7,7'-Dibromo-(1R, 1'S)-diethyl-(1S, 1'R)-dimethyl-bisindeno[3,2-b:2'3'-h]-9-methyl-carbazole. Note that the (R,S)-isomer of* ***1*** *has been used as starting material.*

Our approach to liquid crystalline bisindenocarbazoles was to react the novel building block **2** with different aromatic side groups. For this issue we used the Suzuki cross coupling reaction as it is a versatile method for unsymmetrical aryl-aryl couplings [22]. We decided to couple the brominated bisindenocarbazole **2** with alkylated phenyl, biphenyl and fluorene side groups. The preparation of the aromatic borolanes for the Suzuki cross coupling is shown in Scheme 2.

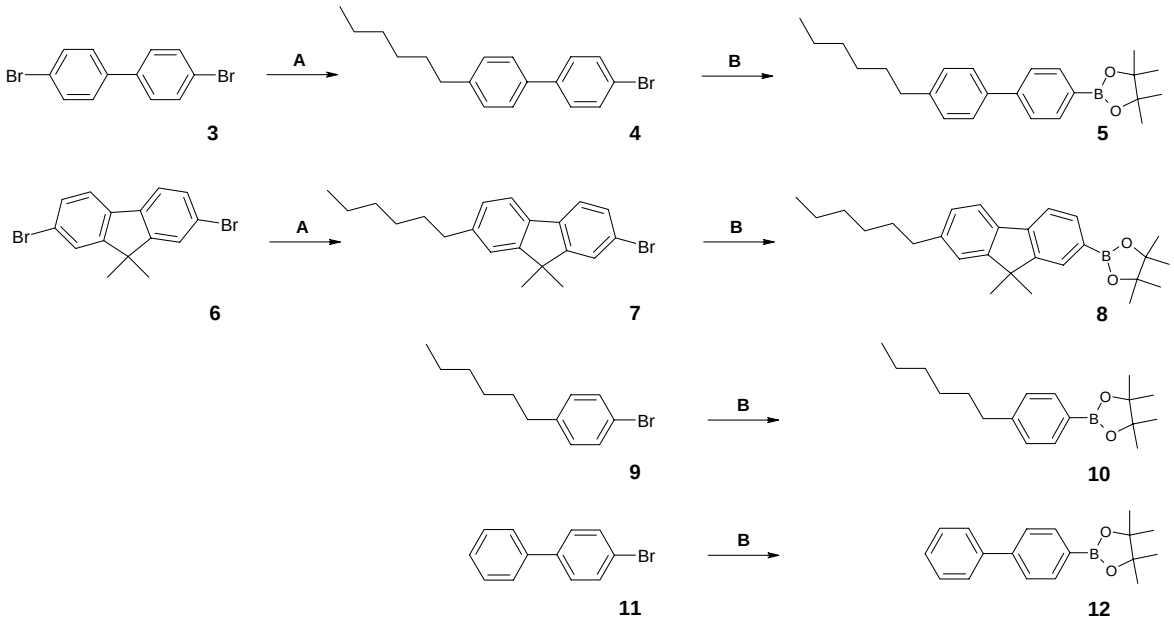

Scheme 2. *Synthesis of the borolane functionalized side groups for Suzuki cross-coupling.*

4,4'-dibromo-biphenyl (**3**) and 2,7-dibromo-9,9-dimethyl-fluorene (**6**) were monoalkylated by the reaction with one equivalent of *sec*-BuLi followed by the addition of 1-bromo-hexane. The alkylation runs statistically and non-, mono- as well as dialkylated products are formed. Nevertheless yields of almost 50 % were achieved with this synthetic approach after purification by column chromatography.

Step B in Scheme 2 describes the synthesis of the borolane compounds **5**, **8**, **10** and **12** which were used for the following Suzuki cross coupling reactions. For the borolane syntheses the starting compounds **4**, **7**, **9** and **11** were reacted with n-BuLi and 2-isopropoxy-4,4,5,5-tetramethyl-1,3,2-dioxaborolane in dry THF.

The aromatic borolanes **5**, **8**, **10** and **12** were coupled to the 7,7'-dibromo-bisindenocarbazole **2** using the Suzuki reaction. The reactions were carried out in a two-phase system of toluene and aqueous potassium carbonate, with trimethylbenzylammonium chloride as phase-transfer catalyst (PTC) (Scheme 3). Mixtures of $Pd(OAc)_2$ and $P(o\text{-tol})_3$ were used as catalyst.

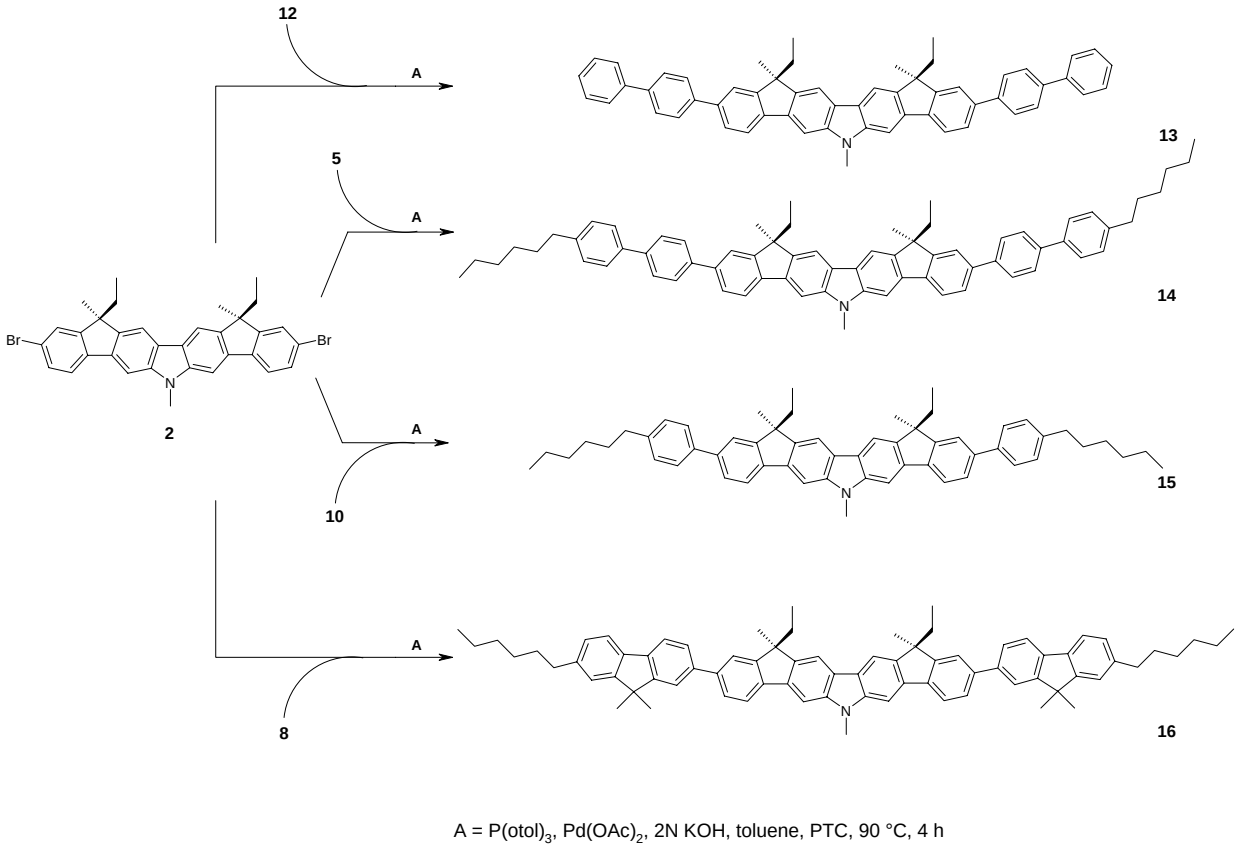

Scheme 3. *Preparation of the bisindenocarbazole derivatives* ***13-16*** *by Suzuki cross coupling.*

In the Suzuki reaction, yields up to 85 % were achieved after the purification of **13-16** by medium pressure chromatography (MPLC). The bisindenocarbazole derivatives **13-16** show excellent solubility in common organic solvents (e.g. THF, toluene, chloroform) what facilitates purification and processing of the compounds. The structures of the novel compounds were confirmed by IR, ^{1}H- and ^{13}C-NMR, mass spectrometry and elemental analysis. The synthetic procedures and the analytical data of all compounds are given in the experimental part.

2.2. Thermal Properties

The thermal properties of the bisindenocarbazole derivatives **13-16** were determined by thermogravimetric analysis (TGA), differential scanning calorimetry (DSC), polarized microscopy (POM) and with small angle x-ray scattering (SAXS).

We found that **15** with the 4-hexylphenyl side groups shows a liquid crystalline phase. Above 180 °C a nematic mesophase is observed by polarizing microscopy up to a clearing temperature at 251 °C. Upon cooling the typical Schlieren texture of the nematic mesophase appears at 250 °C and crystallization starts at about 165 °C. Polarizing microscope images are shown in Figure 1. In the DSC measurement **15** exhibits a melting transition at around 180 °C with an enthalpy of 12.4 kJ/mol and recrystallization at 165 °C (8.1 kJ/mol) upon cooling.

Further analysis by small angle X-ray scattering confirmed the existence of a nematic LC phase. The X-ray diffractogram of **15** in the nematic phase at 220 °C is shown in Figure 2. In the small angle region a Bragg peak was observed from which an average end-to-end distance of 34.5 Å at 220 °C can be calculated. This distance is a little bit shorter than the calculated length of the extended molecules (ca. 36 Å) which is consistent with a slightly tilted arrangement of the rigid-rod like bisindenocarbazole molecules in the nematic mesophase. From the broad wide angle Bragg peak a spacing of 5.6 Å is obtained. This peak reflects the average side-to-side distance of the rod-like molecules and is a typical value for a nematic LC phase.

The bisindenocarbazole derivatives with larger aromatic substituents show a different phase behaviour. **14** with the alkylated biphenyl and **16** with fluorene side groups form molecular glasses with glass transition temperatures (T_g) of 103 and 105 °C, respectively. In contrast, **13** with the non-alkylated biphenyl substituents is crystalline and melts at 331 °C under decomposition. The melting point of **13** was determined with coupled dynamic thermogravimetric (TGA) and differential thermal analysis (DTA).

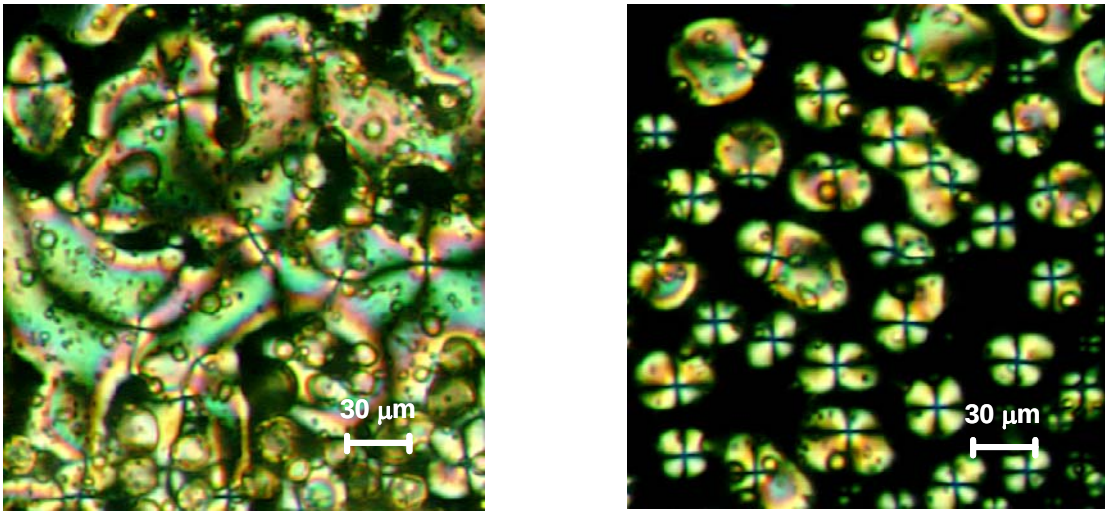

Figure 1. *Polarizing microscopy images of* ***15*** *on heating 220 °C (left) and upon cooling at 248 °C (right) under crossed polarizers.*

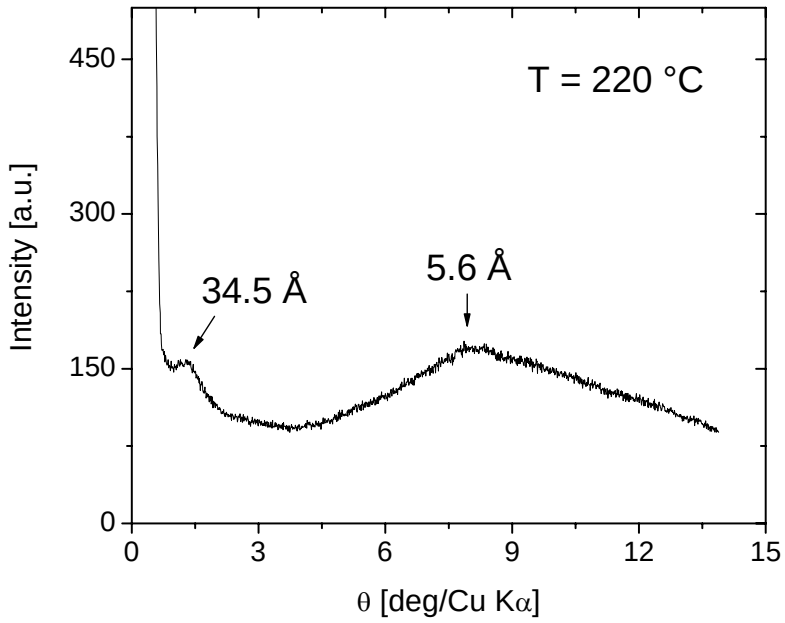

Figure 2. *X-ray diffractogram of the bisindenocarbazole derivative* ***15*** *at 220 °C.*

Thermogravimetric analysis proved the high thermal stability of the novel bisindenocarbazole derivatives. At a heating rate of 10 K/min decomposition of the novel materials starts above 300 °C in nitrogen atmosphere.

2.3. Optical Properties

The absorption and fluorescence spectra of the bisindenocarbazole derivatives **13-16** are shown in Figure 3 and 4. For comparison the absorption spectrum of the parent bisindenocarbazole **1** is also shown in Figure 3. The spectra of **14** with the 4-hexylbiphenyl and **16** with the fluorene substituents are very similar to the spectrum of **1**. This means that there is almost no conjugation between the bisindenocarbazole core and the fluorene or biphenyl side groups. In the case of **15** with the hexylphenyl substituents the situation is markedly different. The long wavelength absorption at 395 nm is the strongest peak and has a redshift of 16 nm compared to the bisindenocarbazole **1**, what means that in **15** the conjugation of the bisindenocarbazole core is somewhat extended to the phenyl substituents.
Until now we can not explain the differences in the absorption spectra of **15** compared to **14** and **16**. But it is striking that among the four bisindenocarbazole derivatives presented in this paper only **15** with the 4-hexylphenyl substituents shows a liquid crystalline mesophase whereas **13** is highly crystalline and **14** and **16** form molecular glasses.

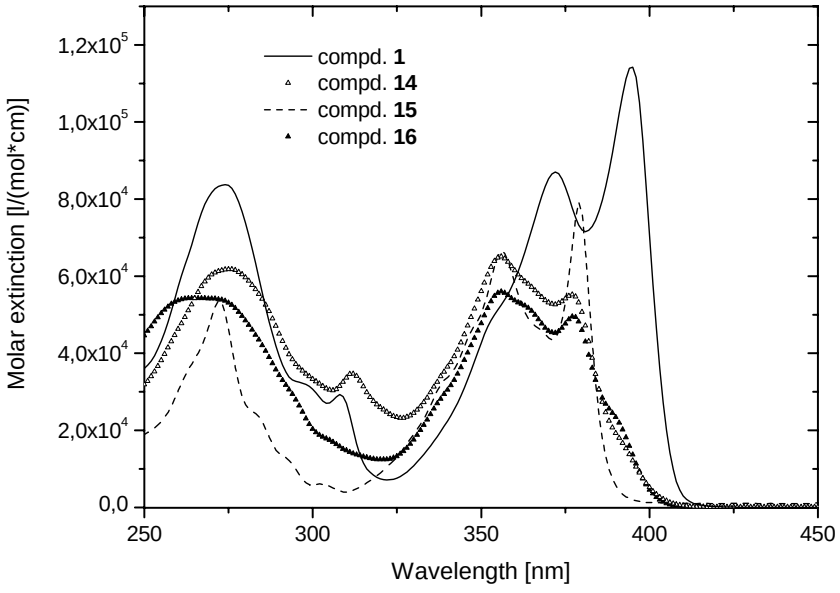

Figure 3. *Absorption spectra of the bisindenocarbzole* ***(1)*** *and of its derivatives* ***14***, ***15*** *(liquid crystalline), and* ***16****. All absorption spectra were taken from* 10^{-5} *M cyclohexane solutions.*

The new bisindenocarbazole molecules show a strong blue fluorescence. The maxima of emission of all four compounds are very similar and are at about 400 nm. The combined absorption and fluorescence spectra of **15** are presented in Figure 4. The results of the optical characterization are summarized in Table 1. The small Stokes shift of all four compounds is typical for the rigid structure of the bisindenocarbazole derivatives [23]. Among the four substituted bisindenocarbazoles, **15** which exhibits a nematic mesophase, has the smallest Stokes shift of 8 nm. For comparison, the planar bisindenocarbazole core compound (**1**) exhibits a Stokes shift of only 6 nm [20]. The derivatives with the larger substituents like the alkylated fluorenes **16**, apparently become more flexible. Compared to **15**, the Stokes shift of **16** is already 26 nm (Table 1).

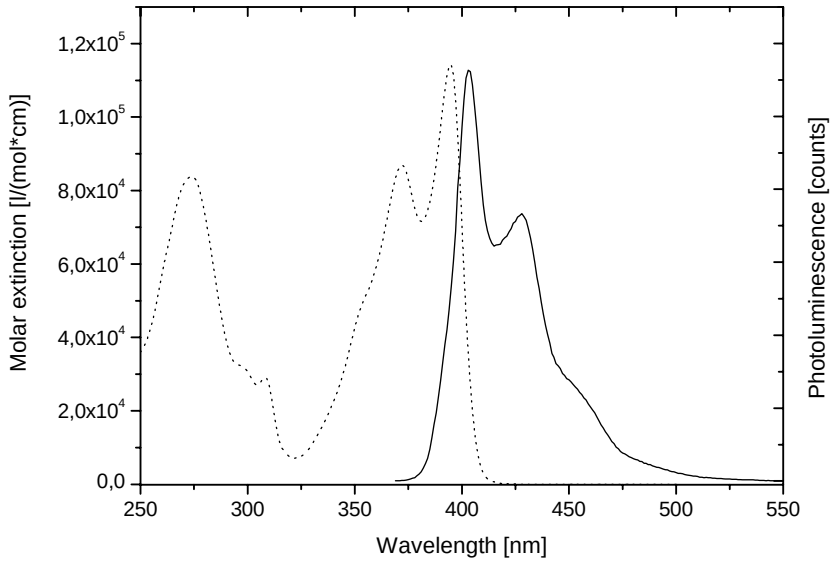

Figure 4. *Absorption and fluorescence spectra of bisindenocarbazole **15**. The absorption spectrum was taken from 10^{-5} M cyclohexane solution and the fluorescence spectrum was measured from 10^{-6} M cyclohexane solution with an excitation wavelength of 395 nm.*

In order to estimate the fluorescence quantum yield (Φ_f) of the bisindenocarbazole derivatives, the fluorescence of **13-16** was compared to the well known laser dye Exalite 428 [7,7''-bis(4-*t*-amylphenyl)-9,9,9',9',9'',9''-hexapropyl-2,2':7'2''-terfluorene], which has a quantum efficiency of 90 % in cyclohexane solution [24]. In order to minimize self-absorption it is necessary to measure the fluorescence from highly diluted solutions [25]. For the estimation of Φ_f, cyclohexane solutions of Exalite 428 and **13-16** with an optical density

of 0.1 were prepared. From these solutions fluorescence spectra were taken and by integration, the fluorescence quantum yield was calculated. With 56 %, the biphenyl substituted bisindenocarbazole derivative **13** gave the highest quantum efficiency (Table 1).

Table 1. *Optical properties of the bisindenocarbazole derivatives*

comp.	λ_{abs} [nm][1]	$\lambda_{max,flour}$ [nm][2]	λae [nm][3]	Stokes shift [nm]	Φ_f [%][4]
1	379	385	394	6	63
13	378	397	403	19	56
14	378	397	403	19	54
15	395	403	408	8	49
16	374	400	400	26	34

[1] Longest wavelength absorption maximum, measured in 10^{-5} M cyclohexane solution

[2] Fluorescence spectra taken from 10^{-6} M cyclohexane solution

[3] Absorption edge

[4] Fluorescence quantum yield (details see text)

2.4. Electrochemical Properties

The electrochemical stability of the bisindenocarbazoles was examined by cyclic voltammetry (CV). All measurements were carried out at 25 °C in CH_2Cl_2 solution containing 0.1 M tetrabutylammonium hexafluorophosphate ($TBAPF_6$) as supporting electrolyte with a glassy carbon working electrode. The oxidation potentials were measured vs. Ag/AgCl as the reference electrode [26]. Ten subsequent redox cycles were measured to check the redox stability of the novel bisindenocarbazole derivatives **13-16**. The CV curve of **15** (Figure 5) shows one quasireversible oxidation peak at 443 mV. Repeated oxidation and reduction cycles did not change the redox potential what is an evidence for the electrochemical stability of the material. **14-16** show identical behaviour in the CV experiments.

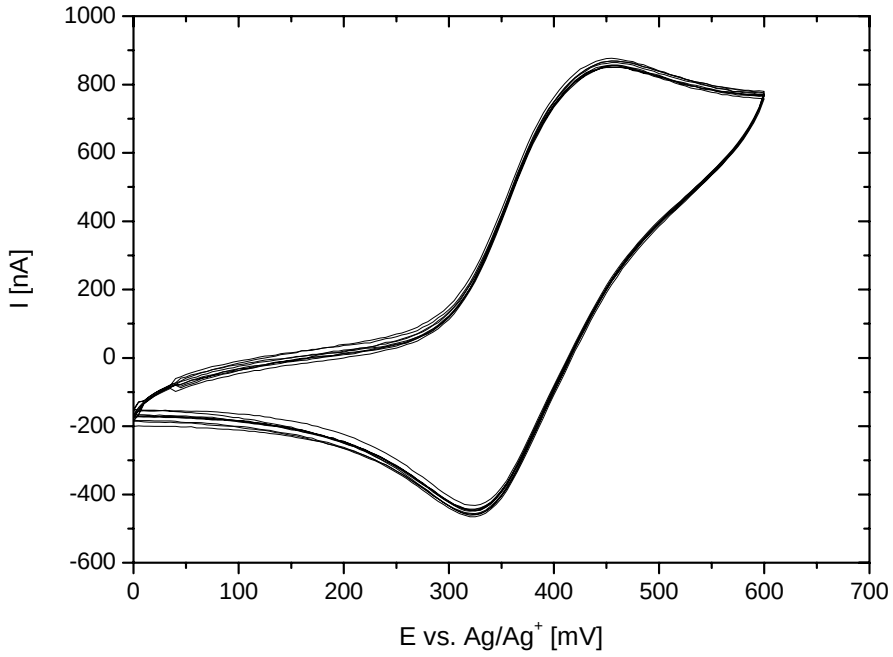

Figure 5. *Cyclic voltammetry curve of* ***15****, measured in dichloromethane at 25 °C at a scan rate of 50 mV/s vs. Ag/Ag*$^+$ *with* $TBAPF_6$ *as supporting electrolyte. In order to check the electrochemical stability 10 subsequent redox cycles were carried out.*

Taking -4.8 eV as the HOMO level for the ferrocene / ferrocenium redox system, HOMO values of about -5.4 eV were calculated for the bisindenocarbazole derivatives **13-16** [27]. With a band gap (ΔE) of 3.1 eV which was taken from the absorption spectra, LUMO values of -2.3 eV were estimated for the new bisindenocarbazole compounds. The different aromatic side arms have no distinct influence on the electrochemical properties of the novel materials.

3. Conclusions

We have presented the synthesis of four new bisindenocarbazole derivatives which were prepared by selective bromination of bisindenocarbazole in the 7- and 7'-position followed by subsequent Suzuki cross coupling reactions with alkylated phenyl, biphenyl and fluorene groups. From this new class of fused aromatics a liquid crystalline derivative is reported for the first time. The phenyl substituted bisindenocarbazole **15** exhibits a broad nematic phase between 180 °C and 250 °C. In contrast to **15**, the other bisindenocarbazole derivatives are crystalline (**13**) or form amorphous molecular glasses (**14, 16**). All target molecules exhibit high thermal stabilities above 300 °C and show excellent electrochemical stability in the CV experiments. HOMO and LUMO levels of -5.4 eV and -2.3 eV were determined for the novel bisindenocarbazoles. They display a strong blue fluorescence with quantum yields up to 56 % in solution.

Acknowledgments

The authors would like to thank Andrea Jahreis for helping to prepare the starting materials, Andreas Timme for the SAXS measurement and Günter Lattermann for fruitful discussions. We are grateful to the Deutsche Forschungsgemeinschaft (SFB 481) and the BMBF (POLITAG programme) for financial support.

4. Experimental

4.1. General

^{1}H-NMR spectra were recorded with a Bruker AC 250 (250 MHz) apparatus. All data are given as chemical shifts δ [ppm] downfield from $Si(CH_3)_4$. The IR spectra were recorded using a Bio-Rad Digilab FTS-40. The UV-VIS spectra were recorded with a Hitachi U-3000 spectrophotometer. Emission spectra were obtained from a Shimadzu spectrofluoro-photometer RF-5301PC. Mass spectra (MS) were recorded with a Finnigan MAT 8500 (70 eV) with a MAT 112S Varian. Thermogravimetric analysis (TGA) was performed on a Perkin Elmer TAS-409 at a heating rate of 10 K/min under N_2. For differential scanning calorimetry measurements (DSC) a Perkin Elmer Diamond DSC apparatus was used (heating/cooling rate: 10 K/min). Polarized microscopy was carried out with the Nikon

Diaphot 300 equipped with a Linkon hotstage. X-ray analysis was carried out with a Huber/Seifert Iso-Debyeflex 3003, using a Guinier diffractometer system (Cu K_α: 1,5418 Å) with a sealed tube for temperature dependent measurements. Cyclic voltammetry measurements (CV) were performed with a glassy carbon working electrode (0.2 mm) in a three-electrode potentiostat configuration from EG&G Princeton Applied Research.

All chemicals and reagents were used as received from Aldrich. Neutral alumina was purchased from ICN Biomedicals (MP Alumina N, Akt. I). Carbon tetrachloride was received from Merck. Tetrahydrofuran (THF) was distilled over potassium before use. The synthesis of *(1R, 1'S)*-Diethyl-*(1S, 1'R)*-dimethyl-bisindeno[3,2-b:2'3'-h]-9-methyl-carbazole (**1**) is reported elsewhere [20]. 4,4'-dibromo-biphenyl (**3**) was purchased from Aldrich and 2,7-dibromo-9,9-dimethyl-fluorene (**6**) was prepared as described in literature [28].

4.2. Preparation of Alumina Supported Copper(II) Bromide [21]

To a solution of copper (II) bromide (10 g) in distilled water (30 ml) neutral alumina (20 g) was added at room temperature. The water was evaporated at 80 °C under reduced pressure with a rotary evaporator. The resulting reagent was dried under high vacuum at 100 °C for 24 h and afterwards stored under argon.

4.3. Synthesis of the Bisindenocarbazole Building Block 7,7'-Dibromo-*(1R, 1'S)*-diethyl-*(1S, 1'R)*-dimethyl-bisindeno[3,2-b:2'3'-h]-9-methyl-carbazole (2).

A mixture of bisindenocarbazole **1** (0.38 g, 0.86 mmol), Al_2O_3-$CuBr_2$ (2.9 g) and carbon tetrachloride (80 ml) was stirred at 70 °C for 3 h. Afterwards the product mixture was filtered and the spent reagent was washed with dichloromethane (30 ml) before the solvents from the combined filtrate were evaporated under reduced pressure. Purification by column chromatography on silica gel with hexane/THF (10:1) as eluent yielded 0.4 g (78 %) of **2** as pale yellow solid. ^{1}H-NMR (250 MHz, $CDCl_3$): δ(ppm): 0.32-0.43(m, 6H), 1.61(s, 6H) 2.15(q, 4H), 3.93(s, 3H), 7.48(dd, 2H, J = 8.0 Hz and J = 1.5 Hz), 7.53(d, 2H, J = 1.5 Hz), 7.64(s, 2H) 7.68(d, 2H, J = 8.0 Hz), 8.04(s, 2H). ^{13}C-NMR (62.5 MHz, $CDCl_3$): δ(ppm): 8.93, 27.23, 29.41, 34.05, 50.88, 99.55, 113.95, 120.82, 120.89, 123.05, 126.27, 130.03, 137.72, 139.92, 141.77, 142.90, 154.73. MS (70 eV): *m/z* = 597/599/601 (M^+). Anal. Calcd for $C_{33}H_{29}Br_2N$ (599.4): C, 66.13; H, 4.88; N, 2.34. Found: C, 66.11; H, 4.87; N, 2.36.

4.4. Preparation of the Side Groups

4'-Bromo-4-hexyl-biphenyl (4).

2.5 g (8 mmol) 4,4'-dibromo-biphenyl were dissolved in 40 ml abs. THF under argon. The solution was cooled to -78 °C before 6.25 ml (8.1 mmol, 0.52 g) *sec*-BuLi (1.3 M solution in hexane) were added slowly. After stirring for 5 minutes, 1.2 ml (8.2 mmol) 1-bromohexane were added. The solution was allowed to warm to room temperature and stirred for 12 h before it was poured into 50 ml ice water. The reaction mixture was extracted with diethyl ether, the organic phase washed with water and dried over Na_2SO_4 before the solvent was evaporated. Purification by column chromatography on silica gel with hexane/THF (50:1) as eluent yielded 1.25 g (49 %) of **4** as colourless solid. ^{1}H-NMR (250 MHz, $CDCl_3$): δ(ppm): 0.89(t, 3H), 1.26-1.45(m, 6H), 1.60-1.71(m, 2H), 2.63(t, 2H), 7.37-7.48(m, 4H), 7.50-7.59(m, 4H). MS (70 eV): *m/z* = 317 (M^+).

2-Bromo-7-hexyl-9,9-dimethyl-fluorene (7) was prepared according to the procedure described for **4** yielding 47 % of **7**. ^{1}H-NMR (250 MHz, $CDCl_3$): δ(ppm): 0.88(t, 3H), 1.19-1.35(m, 6H), 1.47(s, 6H), 1.65(m, 2H), 2.67(t, 2H), 7.13(dd, 1H), 7.21(s, 1H), 7.42(dd, 1H), 7.54(m, 3H). MS (70 eV): *m/z* = 357 (M^+).

2-(4'-Hexyl-biphenyl-4-yl)-4,4,5,5-tetramethyl-[1,3,2]dioxaborolane (5).

0.85 g (2.7 mmol) of 4'-Bromo-4-hexyl-biphenyl (**4**) were dissolved in absolute THF under argon. The solution was cooled to -78 °C before 1.9 ml (3.0 mmol) n-BuLi (1.6M solution in hexane) were added dropwise. The reaction mixture was stirred for 10 min, before 0.8 ml (4.0 mmol) of 2-isopropoxy-4,4,5,5-tetramethyl-1,3,2-dioxaborolane were added. The reaction mixture was allowed to warm to room temperature and stirred for another 12 h before it was poured to ice water. The solution was extracted with diethyl ether, the organic phase washed with brine and dried with Na_2SO_4 before the solvent was removed. Purification by column chromatography on silica gel with hexane/THF (15:1) as eluent yielded 0.78 g (80 %) of **5** as white solid. ^{1}H-NMR (250 MHz, $CDCl_3$): δ(ppm): 0.88(t, 3H), 1.25-1.35(m, 8H), 1.36(s, 12H), 2.64(t, 2H), 7.24-7.27(m, 2H), 7.54(d, 2H), 7.60(d, 2H), 7.87(d, 2H). MS (70 eV): m/z = 364 (M^+).

2-(7-Hexyl-9,9-dimethyl-fluoren-2-yl)-4,4,5,5-tetramethyl-[1,3,2]dioxaborolane (8) was prepared according to the procedure described above (yield: 74 %). ^{1}H-NMR (250 MHz, $CDCl_3$): δ(ppm): 1.38(m, 3H), 1.24-1.35(m, 8H), 1.38(s, 12H), 1.49(s, 6H), 2.68(t, 2H), 7.16(d, 1H), 7.26(s, 1H), 7.67(d, 2H), 7.81(d, 1H), 7.86(s, 1H). MS (70 eV): m/z = 404 (M^+).

2-(4-Hexyl-phenyl)-4,4,5,5-tetramethyl-[1,3,2]dioxaborolane (10) was prepared according to the procedure described above. Purification by column chromatography on silica gel with

hexane/THF (20:1) as eluent yielded 85 % of **10** as colourless oil. ^{1}H-NMR (250 MHz, $CDCl_3$): δ(ppm): ^{1}H-NMR (250 MHz, $CDCl_3$): δ(ppm): 0.86(t, 3H), 1.18-1.26(m, 8H), 1.33(s, 12H), 2.62(t, 2H), 7.20(d, 2H), 7.73(d, 2H). MS (70 eV): m/z = 288 (M^+).

2-Biphenyl-4-yl-4,4,5,5-tetramethyl-[1,3,2]dioxaborolane (12) was prepared according to the procedure described above. Purification by column chromatography on silica gel with hexane/THF (10:1) as eluent yielded 76 % of **12** as white solid. ^{1}H-NMR (250 MHz, $CDCl_3$): δ(ppm): 1.36(s, 12H), 7.42-7.45(m, 3H), 7.62(d, 4H), 7.89(d, 2H). MS (70 eV): m/z = 280 (M^+).

7,7'-Di-(biphenyl-4-yl)-*(1R,1'S)*-diethyl-*(1S,1'R)*-dimethyl-bisindeno[3,2-b:2'3'-h]-9-methyl-carbazole (13).

0.1 g (0.17 mmol) of 7,7'-dibromo-bisindenocarbazole **2** and 0.1 g (0.37 mmol) of the borolane **12** were dissolved in 25 ml toluene. A 2M K_2CO_3 solution (6 ml) and 0.1 g of trimethylbenzylammonium chloride were added. The reaction mixture was degassed by three freeze/thaw cycles before 1.7 mg (7.3 x 10^{-6} mol) of palladium(II) acetate and 6.7 mg (2.2 x 10^{-5} mol) of tri-o-tolylphosphine were added under argon. The mixture was stirred for 4 h at 90 °C. The reaction mixture was poured to ice water, extracted with diethyl ether and dried with Na_2SO_4. After evaporation of the solvent, the crude product was purified by MPLC with an hexane/THF (20:1) as eluent at a pressure of 18 bar. 98 mg (77 %) of **13** were obtained as white solid. ^{1}H-NMR (250 MHz, $CDCl_3$): δ(ppm): 0.45(t, 6H), 1.64(s, 6H), 2.18(q, 4H), 2.94(s, 3H), 6.31(d, 2H), 6.91(t, 2H), 7.16(t, 2H), 7.37(t, 4H), 7.47(d, 4H), 7.55(d, 4H), 7.72-7.77(m, 8H), 8.16 (s, 2H). ^{13}C-NMR (62.5 MHz, $CDCl_3$): δ(ppm): 9.33, 27.14, 36.37, 109.21, 112.99, 117.51, 120.95, 122.87, 123.15, 123.28, 126.82, 127.40, 127.55, 127.93, 129.28, 131.41, 131.56, 138.22, 140.75, 141.52, 144.13, 153.30. MS (70 eV): m/z = 745 (M^+). IR (KBr): $\tilde{\nu}$ (cm^{-1}): 2960, 2921, 2850, 1635, 1486, 1398, 1341, 1008, 749. Anal. Calcd for $C_{57}H_{47}N$ (746.0): C, 91.77; H, 6.35; N, 1.88. Found: C, 91.69; H, 6.28; N, 1.92.

7,7'-Di-(4'-hexyl-biphenyl-4-yl)-*(1R,1'S)*-diethyl-*(1S,1'R)*-dimethyl-bisindeno[3,2-b:2'3'-h]-9-methyl-carbazole (14). Compound **14** was prepared by Suzuki cross coupling according to the procedure described for **13** and purified by MPLC with hexane/THF (25:1) at a pressure of 18 bar (yield: 81 %). ^{1}H-NMR (250 MHz, $CDCl_3$): δ(ppm): 0.38-0.47(m, 6H), 0.90(t, 6H), 1.27-1.42(m, 16H), 1.59-1.68(m, 6H), 2.17(q, 4H), 2.62(t, 4H), 2.92(s, 3H), 6.31(d, 2H), 6.88-6.95(m, 2H), 7.14-7.20(m, 2H), 7.30(s, 2H), 7.34-7.40(m, 4H), 7.52-7.57(m, 4H), 7.66(d, 4H), 7.73(d, 4H), 8.15(s, 2H). ^{13}C-NMR (62.5 MHz, $CDCl_3$): δ(ppm): 9.34, 14.49, 23.00, 27.97, 28.06, 29.35, 31.88, 32.13, 34.75, 36.00, 49.96, 112.94, 120.96, 122.82, 123.20, 123.30, 126.81, 127.19, 127.32, 129.33, 131.35, 131.50, 137.58, 137.86, 138.05, 140.65,

141.71, 142.82, 144.12, 153.30. MS (70 eV): m/z = 913 (M^+). IR (KBr): $\tilde{\nu}$ (cm^{-1}): 2959, 2925, 2854, 1497, 1457, 1342, 1006, 748. Anal. Calcd for $C_{69}H_{71}N$ (914.3): C, 90.64; H, 7.83; N, 1.53. Found: C, 90.40; H, 7.74; N, 1.79.

7,7'-Di-(4-hexyl-phenyl)-*(1R,1'S)*-diethyl-*(1S,1'R)*-dimethyl-bisindeno[3,2-b:2'3'-h]-9-methyl-carbazole (15). Compound **15** was prepared according to the procedure described for **13** and purified by MPLC with hexane/THF (30:1) at a pressure of 18 bar (yield: 79 %). ^{1}H-NMR (250 MHz, $CDCl_3$): δ(ppm): 0.33-0.41(m, 6H), 0.83(t, 6H), 1.18-1.32(m, 10H), 1.49-1.65(m, 12H), 2.09(q, 4H), 2.56(t, 4H), 3.89(s, 3H), 7.18(d, 4H), 7.50-7.57(m, 8H), 7.61(s, 2H), 7.79(d, 2H), 8.00(s, 2H). ^{13}C-NMR (62.5 MHz, $CDCl_3$): δ(ppm): 8.01, 13.10, 21.63, 26.42, 28.04, 28.38, 30.51, 30.75, 33.21, 34.63, 49.62, 98.37, 112.77, 118.73, 120.39, 121.77, 124.90, 125.96, 127.82, 137.40, 138.01, 138.95, 138.99, 140.74, 140.93, 142.53, 152.15. MS (70 eV): m/z = 761 (M^+). IR (KBr): $\tilde{\nu}$ (cm^{-1}): 2959, 2926, 2854, 1559, 1495,1345, 1260, 841. Anal. Calcd for $C_{57}H_{63}N$ (762.1): C, 89.83; H, 8.33; N, 1.84. Found: C, 89.72; H, 8.29; N, 1.95.

7,7'-Di-(7-Hexyl-9,9-dimethyl-fluoren-2-yl)-*(1R,1'S)*-diethyl-*(1S,1'R)*-dimethyl-bisindeno [3,2-b:2'3'-h]-9-methyl-carbazole (16). Compound **16** was prepared according to the procedure described for **13** and purified by MPLC with hexane/THF (30:1) at a pressure of 18 bar (yield: 85 %). ^{1}H-NMR (250 MHz, $CDCl_3$): δ(ppm): 0.37(m, 6H), 0.89(t, 6H), 1.33(m, 10H), 1.46(s, 12H), 1.58(m, 12H), 2.16(q, 4H), 2.66(t, 4H), 3.70(s, 3H), 7.13(dd, 2H), 7.20(s, 2H), 7.39(dd, 2H), 7.51-7.55(m, 6H), 7.68-7.73(m, 6H), 7.81(s, 2H), 8.14(s, 2H).

^{13}C-NMR (62.5 MHz, $CDCl_3$): δ(ppm): 9.35, 14.48, 23.01, 27.62, 28.10, 29.41, 29.48, 32.17, 34.67, 36.71, 47.10, 47.34, 50.04, 112.84, 120.30, 122.83, 123.28, 124.29, 125.51, 126.59, 126.70, 126.91, 127.23, 127.67, 129.83, 136.85, 137.01, 137.45, 139.37, 141.49, 143.00, 143.23, 153.28, 154.55. MS (70 eV): m/z = 993 (M^+). IR (KBr): $\tilde{\nu}$ (cm^{-1}): 2958, 2923, 2854, 1457, 1340, 1253, 821, 746. Anal. Calcd for $C_{75}H_{79}N$ (994.5): C, 90.58; H, 8.01; N, 1.41. Found: C, 90.46; H, 7.93; N, 1.52.

5. Literature

[1] Baude, P. F., Ender, D. A., Haase, M. A., Kelley, T. W., Muyres, D. V., Theiss, S. D., 2003, *Appl. Phys. Lett.*, **82**, 3964-3966.

[2] Sundar Vikram, C., Zaumseil, J., Podzorov, V., Menard, E., Willett Robert, L., Someya, T., Gershenson Michael, E., Rogers John, A., 2004, *Science*, **303**, 1644-1646.

[3] Wakim, S., Bouchard, J., Simard, M., Drolet, N., Tao, Y., Leclerc, M., 2004, *Chem. Mater.*, **16**, 4386.

[4] Wakim, S., Bouchard, J., Blouin, N., Michaud, A., Leclerc, M., 2004, *Org Lett.*, **6**, 3413-3416.

[5] Li, Y., Wu, Y., Gardner, S., Ong, B. S., 2005, *Adv. Mater.*, **17**, 849-853.

[6] Wu, Y., Li, Y., Gardner, S., Ong, B. S., 2005, *J. Am. Chem. Soc.*, **127**, 614-618.

[7] Adam, D., Schuhmacher, P., Simmerer, J., Haeussling, L., Siemensmeyer, K., Etzbach, K. H., Ringsdorf, H., Haarer, D., 1994, *Nature*, **371**, 141-143.

[8] Van De Craats, A. M., Warman, J. M., Fechtenkötter, A., Brand, J. D., Harbison, M. A., Müllen, K., 1999, *Adv. Mater.*, **11**, 1469-1472.

[9] Fechtenkötter, A., Saalwächter, K., Harbison, M. A., Müllen, K., Spiess, H. W., 1999, *Angew. Chem. Int. Ed.*, **38**, 3039-3042.

[10] Funahashi, M., Hanna, J., 2000, *Appl. Phys. Lett.*, **76**, 2574-2576.

[11] Sirringhaus, H., Wilson, R. J., Friend, R. H., Inbasekaran, M., Wu, W., Woo, E. P., Grell, M., Bradley, D. D. C., 2000, *Appl. Phys. Lett.*, 406.

[12] McCulloch, I., Heeney, M., Bailey, C., Genevicius, K., MacDonald, I., Shkunov, M., Sparrowe, D., Tierney, S., Wagner, R., Zhang, W., Chabinyc, M. L., Kline, R. J., McGehee, M. D., Toney, M. F., 2006, *Nature Materials*, **5**, 328-333.

[13] van Breemen, A. J. J. M., Herwig, P. T., Chlon, C. H. T., Sweelssen, J., Schoo, H. F. M., Setayesh, S., Hardeman, W. M., Martin, C. A., de Leeuw, D. M., Valeton, J. J. P., Bastiaansen, C. W. M., Broer, D. J., Popa-Merticaru, A. R., Meskers, S. C. J., 2006, *J. Am. Chem. Soc.*, **128**, 2336-2345.

[14] Huisman, B.-H., Valeton, J. J. P., Nijssen, W., Lub, J., ten Hoeve, W., 2003, *Adv. Mater.*, **15**, 2002-2005.

[15] Grell, M., Knoll, W., Lupo, D., Meisel, A., Miteva, T., Neher, D., Nothofer, H.-G., Scherf, U., Yasuda, A., 1999, *Adv. Mater.*, **11**, 671-675.

[16] Geng, Y., Chen, A. C. A., Ou, J. J., Chen, S. H., Klubek, K., Vaeth, K. M., Tang, C. W., 2003, *Chem. Mater.*, **15**, 4352-4360.

[17] Culligan, S. W., Geng, Y., Chen, S. H., Klubek, K., Vaeth, K. M., Tang, C. W., 2003, *Adv. Mater.*, **15**, 1176-1180.

[18] Aldred, M. P., Eastwood, A. J., Kelly, S. M., Vlachos, P., Contoret, A. E. A., Farrar, S. R., Mansoor, B., O'Neill, M., Tsoi, W. C., 2004, *Chem. Mater.*, **16**, 4928-4936.

[19] Whitehead, K. S., Grell, M., Bradley, D. D. C., Jandke, M., Strohriegl, P., 2000, *Appl. Phys. Lett.*, **76**, 2946-2948.

[20] Sonntag, M., Strohriegl, P., *Tetrahedron*, **2006**, *62*, 8103.

[21] Kodomari, M., Satoh, H., Yoshitomi, S., 1988, *J. Org. Chem.*, **53**, 2093-2094.

[22] Schlüter, A. D., 2001, *J. Polym. Sci. Part A: Polym. Chem.*, **39**, 1533-1556.

[23] Scherf, U., 1999, *J. Mater. Chem.*, **9**, 1853-1864.

[24] Kauffman, J. M., Litak, P. T., Novinski, J. A., Kelley, C. J., Ghiorghis, A., Qin, Y., 1995, *J. Fluorescence*, **5**, 295-305.

[25] Crosby, G. A., Demas, J. N., 1971, *J. Phys. Chem.*, **75**, 991-1024.

[26] Heinze, J., 1984, *Angew. Chem.*, **96**, 823-840.

[27] Pommerehne, J., Vestweber, H., Guss, W., Mahrt, R. F., Bässler, H., Porsch, M., Daub, J., 1995, *Adv. Mater.*, **7**, 551-554.

[28] Woo, E. P., Inbasekaran, M., Shiang, W., Roof, G. R., 1997, **WO 9705184**.

Bisindenocarbazole as new deep-blue emitter for OLED applications

Martin Sonntag, Michael Rothmann, Peter Strohriegl*

Macromolecular Chemistry I, University of Bayreuth, 95440 Bayreuth, Germany

Manuscript draft

Keywords

Bisindenocarbazole, blue organic light-emitting diode, combinatorial vacuum evaporation, doping, blue fluorescent emitter

Abstract

In this paper we describe a series of vapor-deposited blue organic light-emitting diodes (OLEDs), using a novel bisindenocarbazole emitter as dopant in different host materials. At first we have investigated the host/guest energy transfer by fluorescence and time resolved PL spectroscopy, using CBP, mCP and TCTA as matrix materials for the new dye. For the preparation of the OLED devices a combinatorial evaporation setup has been used. It was found that the bisindenocarbazole dye emits deep-blue light at color coordinates of x = 0.19 and y = 0.17. Turn on voltages of 5 V, luminance efficiencies up to 1.6 A and a brightness of 200 cd/m^2 were achieved, what shows that the bisindenocarbazole is a promising new blue fluorescent emitter for organic LEDs.

1. Introduction

Since the first organic light-emitting diode (OLED) was reported in 1987 by Tang and VanSlyke[1] great efforts have been made to optimize both materials and OLED devices. This has led to the first commercial full-color flat panel displays of the next generation.[2, 3] For this issue highly efficient red, green and blue emitting materials had to be developed. Up to now red[4] and green[5] electroluminescent devices with high efficiencies have been reported. However the performance of pure blue emitting devices remains a big challenge. A great variety of blue-fluorescent materials like anthracene[6] and distyrylarylene[7] derivatives and oligoquinolines[8] have been tested in OLEDs until now.

In order to increase the quantum efficiencies, OLEDs employing phosphorescent organometallic iridium complexes as blue emitting material were prepared. For example, quantum efficiencies of about 10.4 % could be reached with iridium (III)bis[(4,6-di-fluoropheny)-pyridinato-N,$C^{2'}$]picolinate (FIrpic).[9] But by using this class of materials for the preparation of blue OLEDs the device lifetime is lower than in the case of fluorescent emitters. Furthermore it was not possible to achieve stable OLEDs with a deep-blue phosphorescence emission so far. Ideally CIE (Commission International de L'Eclairage) color coordinates in the range of x = 0.16 and y = 0.16 are desired.[10] Since current blue light emitting devices still have some drawbacks, there is still a strong demand for the development of new high performance blue emitters.

Recently we have reported on a series of bisindenocarbazole derivatives which belong to a new class of fused heterocycles.[11] From these materials a strong blue fluorescence together with high quantum yields were obtained. For that reason we decided to use the 1,1-Dimethyl-1', 1'-dimethyl-bisindeno[3,2-b:2'3'-h]-9-sec-butyl-carbazole derivative (BIC 1) as blue emitter in multilayer organic LEDs. In order to avoid quenching of the electroluminescence (EL) in the device, the singulet emitter was doped into a host material by vacuum co-evaporation. For this issue 4,4'-dicarbazolyl-1,1'-biphenyl (CBP), 1,3-bis(9-carbazolyl)benzene (mCP) and 4,4',4"-tri(N-carbazolyl)triphenylamine (TCTA) were tested as matrix materials as they should be well suited for large band gap dyes. Details of the OLED performance with different matrix materials are presented in this article. The molecular structures of the OLED materials are shown in Scheme 1.

Blue emitter

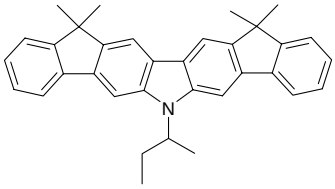

BIC 1

Host materials

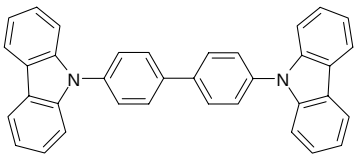

CBP

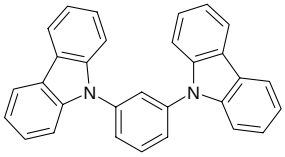

mCP

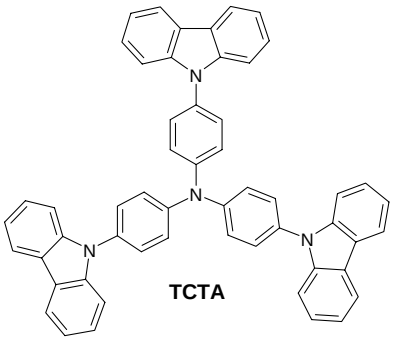

TCTA

Charge carrier injection and transport materials

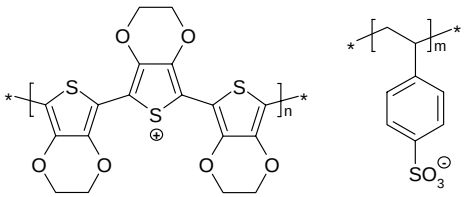

PEDOT : PSS

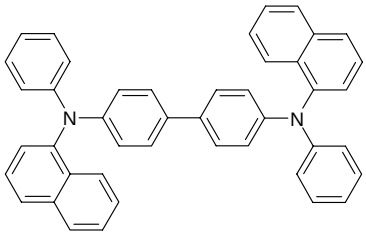

α-NPD

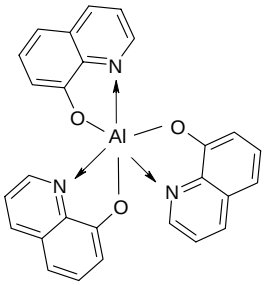

AlQ_3

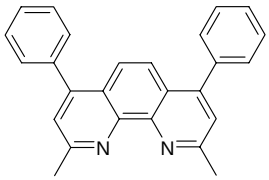

BCP

Scheme 1: *Molecular structures of all materials used in the OLED setups.*

2. Results and Discussion

Before the novel bisindenocarbazole was used as dopant in different host materials, we checked if the energy transfer from the host material to the fluorescent emitter works efficiently. For this purpose thin CBP films containing different concentrations of the blue dopant were prepared by vacuum co-evaporation. CBP was chosen for these preliminary tests as it is a very well known matrix material which is frequently used in organic LEDs. In order to find the ideal doping concentration, the emitter was co-evaporated in different amounts ranging from 0.1 % up to 10 % into the CBP host. Fluorescence spectra were taken from all films (Figure 1). By using an excitation wavelength of 297 nm only the matrix material is excited as the bisindenocarbazole has its absorption maximum at 350 nm. Due to the fact that fluorescence emission is detected exclusively from the emitter, it is assumed that an efficient energy transfer from the host (CBP) to the bisindenocarbazole is ensured.

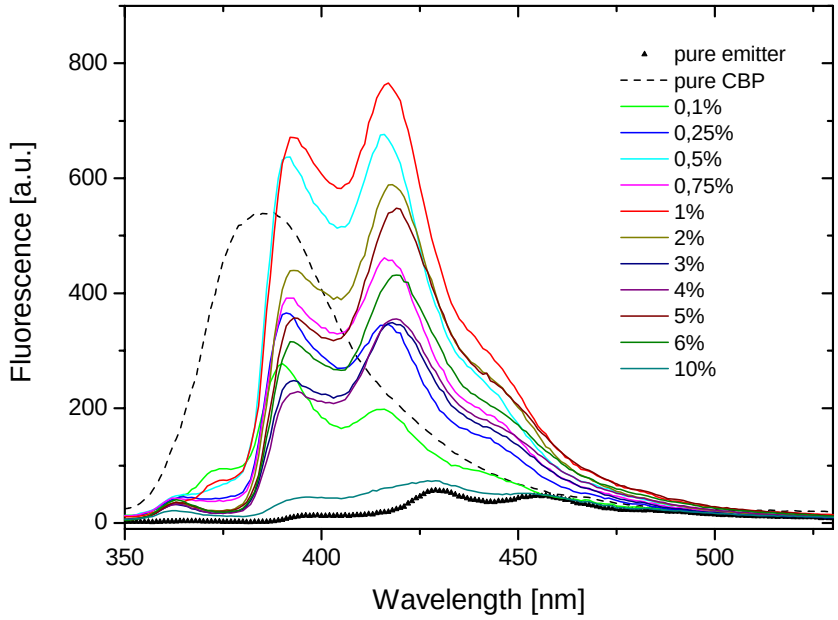

Figure 1. *Fluorescence spectra of thin CPB films containing different dopant concentrations. By using an excitation wavelength of 297 nm only the host material is excited as the absorption maximum of the dopant is around 350 nm. Fluorescence emission is exclusively detected from the emitter, meaning that an efficient energy transfer is ensured.*

Furthermore it was found that the highest fluorescence intensity is obtained at a doping concentration of 1 %. The fluorescence spectra of the different CBP/bisindenocarbazole mixtures are shown in Figure 1. Higher amounts of the emitter lead to a quenching of the fluorescence intensity (Figure 1 and 2).

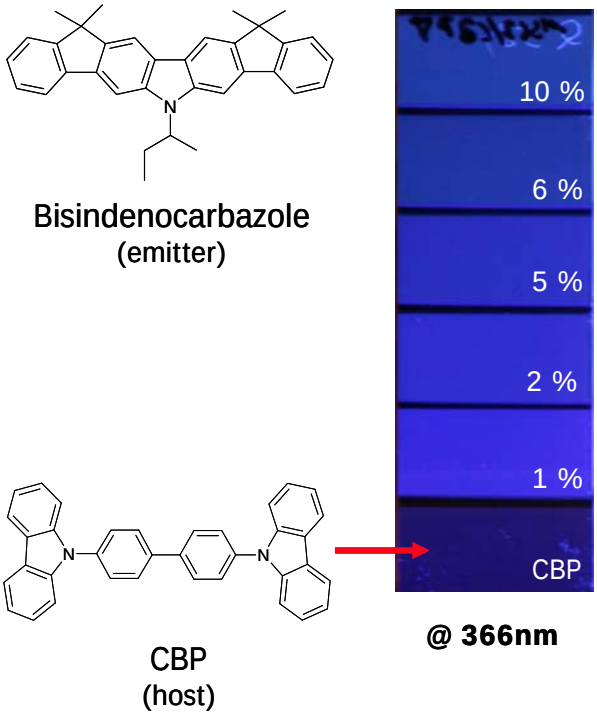

Figure 2. *Samples of different guest/host compositions irradiated with UV-light at 366 nm: The strongest fluorescence is observed at a doping concentration of 1 %. Higher amounts of emitter lead to quenching of the fluorescence intensity.*

In order to quantitatively analyze the energy transfer process, the photoluminescence (PL) intensity of the CBP matrix (λ_{em} = 370) was measured as a function of time for samples with different dopant concentrations. The decay curves are shown in the Figure 3. At doping concentrations lower than 0.1 % there is no PL lifetime dependence observed. The PL curves show that an efficient energy transfer is only obtained at doping concentrations of 0.1 % or higher. The average lifetime of the CBP donor in absence of an energy transfer is estimated from these data to be about τ_D=620 ps.

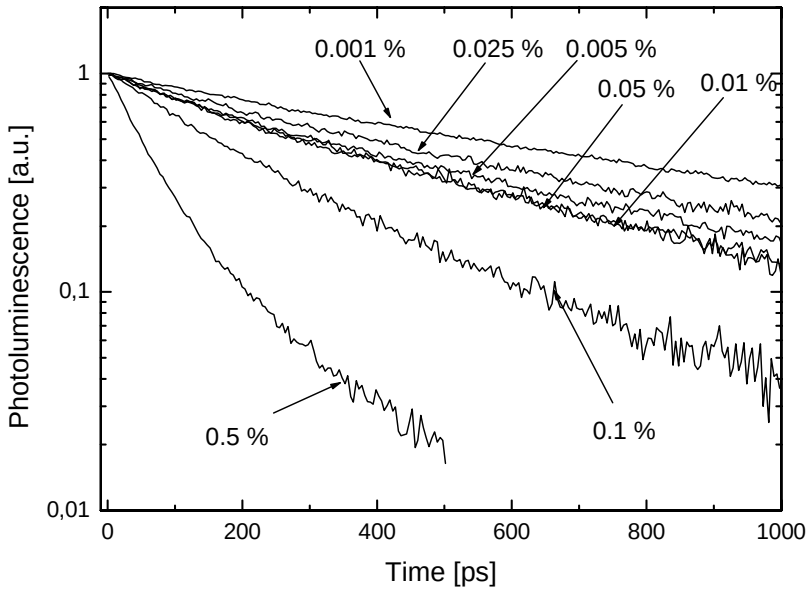

Figure 3. *Photoluminescence decay curves detected at wavelength λ = 370 nm (CBP emission). An efficient energy transfer is observed at doping concentrations of 0.1 % or higher.*

2.1. OLED setup with CBP matrix

As CBP is a well known matrix material for green and blue emitters[12] we used it as host for the first experiments with the new bisindenocarbazole emitter. Furthermore we decided to use a more complex multilayer OFET architecture to increase the device efficiency. On top of the ITO substrate a PEDOT film was coated to reduce the surface roughness and to improve the charge carrier injection. After that NPD was deposited as hole transport layer (HTL). Afterwards the emission layer was evaporated followed by an Alq_3 electron transport layer (ETL). Finally a thin LiF layer was introduced for an efficient electron injection followed by the aluminium cathode.[12, 13]

The OLED devices containing CBP as host material had the following structure; ITO/PEDOT (40 nm)/NPD (40 nm)/CBP:bisindenocarbazole (40 nm)/BCP (6, 12, 18 and 24 nm)/Alq_3 (40 nm)/LiF (1 nm)/Al (150 nm). As a result of the energy transfer experiments described before, a dye doping concentration of 1 % was chosen. Different film thicknesses of the 2,9-dimethyl-4,7-diphenyl-1,10-phenanthroline (BCP) hole blocking layer were evaporated in order to shift the recombination zone into the emitting layer. By using a combinatorial

evaporation technique, it was possible to prepare OLEDs with different blocking layer thicknesses in a single run. Figure 3 shows the schematic device architecture and the energy level diagram.

At a voltage of 3 V a current can be measured in the CPB based OLED device. The light turns on at 4.5 V. The delay between the turn on of the current and the light emission suggests that the charge carriers are still not perfectly balanced.[10] From these devices a maximum luminescence of 5000 cd/m^2 at 275 mA/cm^2 was measured. The device achieves maximum luminance efficiency as high as 2.87 cd/A at 62.19 mA/cm^2. Nevertheless electro-luminescence (EL) spectra of the OLEDs with hole blocking layer thicknesses of up to 18 nm show that the light emission is exclusively generated by Alq_3 (Figure 4). At a BCP layer thickness of 24 nm a shoulder appears at 438 nm which is an evidence for the emission of the bisindenocarbazole. An explanation for this observation might be the fact that the excitons are not confined in the CPB/emitter layer but may diffuse into the Alq_3 layer.

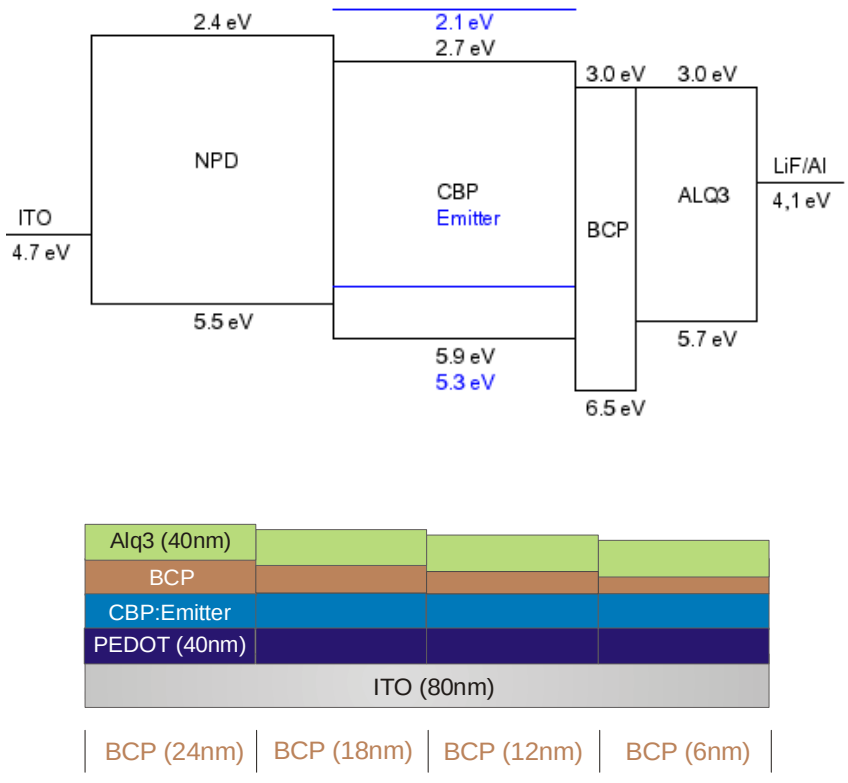

Figure 3. *Energy level diagram of the OLED containing CBP as host material doped with 1 % of the blue dye (above) and device architecture with different film thicknesses of the BCP hole blocking layer (below).*

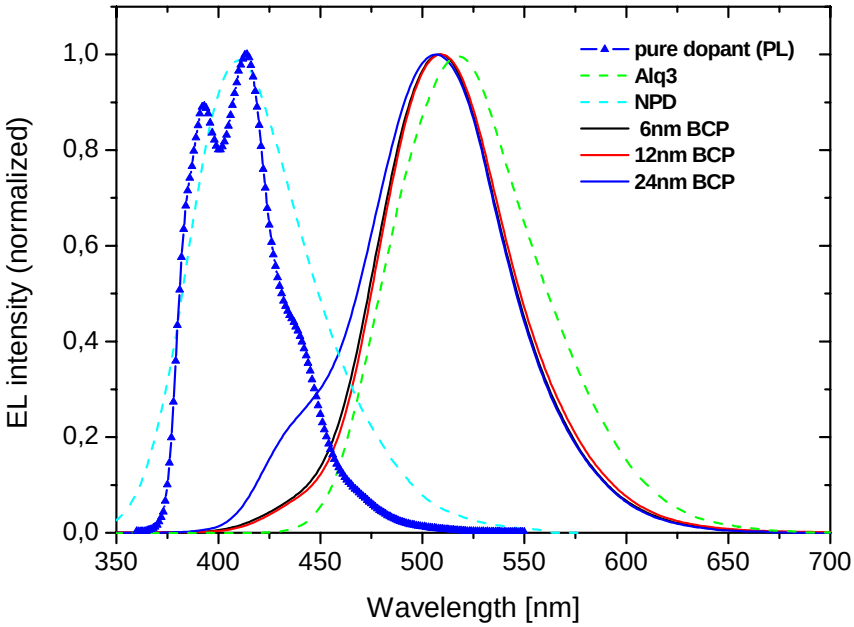

Figure 4. *EL spectra of OLEDs with different BCP layer thicknesses and CBP as host. An exclusive Alq_3 emission is observed up to a BCP thickness of 18 nm. Device setup: ITO/PEDOT (40 nm)/NPD (40 nm)/CBP:bisindenocarbazole (40 nm)/BCP (6, 12, 18 and 24 nm)/Alq_3 (40 nm)/LiF (1 nm)/Al (150 nm).*

2.2. OLED setup with mCP matrix

In order to increase the band gap between the dopant and the matrix, mCP was tested as second host material. The LUMO level of mCP is 0.3 eV higher than that of CBP. The devices containing mCP as host had an architecture similar to that of the OLED described before; ITO/PEDOT (40 nm)/NPD (40 nm)/mCP:bisindenocarbazole (40 nm)/BCP (6, 12, 18 and 24 nm)/Alq_3 (40 nm)/LiF (1 nm)/Al (150 nm). The energy level diagram of this setup is shown in Figure 5. Before the device was prepared, the guest/host energy transfer was checked by fluorescence spectroscopy as described before for the CBP/bisindenocarbazole system. From these experiments a dye doping concentration of 1% resulted in the highest PL intensity.

As in the case of the previous OLED setup, 1 % of the bisindenocarbazole emitter was co-evaporated into the mCP host material. Evaluation of the device characteristics proved that only green emission from the Alq_3 layer occurs.

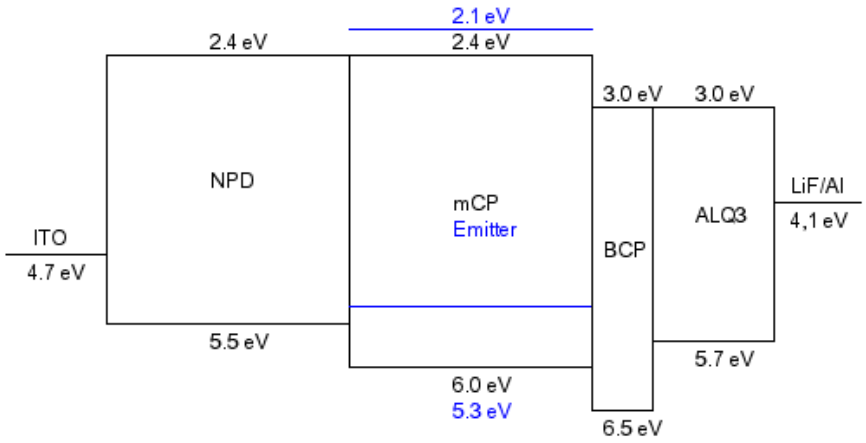

Figure 5. *Energy level diagram of the device consisting of ITO/PEDOT/NPD/mCP: bisindenocarbazole/BCP/Alq$_3$.*

2.3. OLED setup with TCTA matrix

Finally TCTA was tested as host material for the new emitter. The schematic energy level diagram and the device architecture of the TCTA/bisindenocarbazole system is depicted in Figure 6. Since TCTA does not sublime very well, we decided to deposit a 50 nm thick film from a 2 wt% toluene solution containing 1 % of the dopant on top of the PEDOT layer by spin-coating. The film was dried at 120 °C for 30 min under argon atmosphere. By adopting this method, an additional hole transport layer could not be included to the OLED. Devices containing TCTA as matrix material had the following structure; ITO/PEDOT (40 nm)/TCTA: bisindenocarbazole (40 nm)/BCP (10, 20, 30 and 40 nm)/Alq$_3$ (40 nm)/LiF (1 nm)/Al (150 nm).

By using this device architecture we were able to obtain a deep-blue emission at color coordinates of x = 0.19 and y = 0.17 from the bisindenocarbazole dopant. The EL spectra which were recorded from the OLEDs with TCTA as host material are presented in Figure 7. Only a small shoulder of an AlQ_3 emission is observed in the EL spectra. The shoulder becomes smaller by increasing the thickness of the hole blocking layer. A pure emission of the blue dye can be obtained at a BCP layer thickness of 40 nm. Luminance values up to

200 cd/m^2 at a current density of 100 mA/cm^2 and a maximum luminance efficiency as high as 1.60 cd/A was achieved with this series of devices. The turn on of the light emission was at 5 V. The luminance-voltage characteristics for different BCP thicknesses are shown in Figure 8. At voltages higher than 10 V the luminescence runs into saturation which is the reason that no higher brightness can be obtained from these OLEDs. The fact that the TCTA/emitter combination was spin-coated from solution on top of the PEDOT injection layer might have an inhomogeneous film surface as result. This fact could be an appropriate explanation for the low brightness of the OLED. As the emitting layer was deposited from solution it was not possible to use NPD as hole transport layer in this device setup. Therefore a large energy gap occurs between the ITO/PEDOT and the emitting layer and an efficient charge carrier injection is no longer ensured.

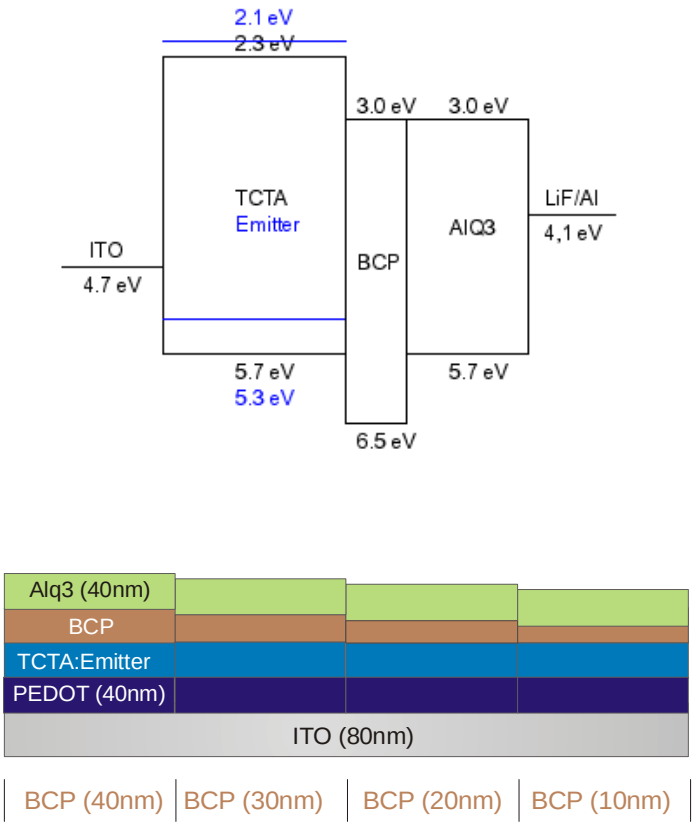

Figure 6. *Energy level diagram of the OLED containing TCTA as host material doped with 1 % of the blue dye (above) and device architecture with different BCP layer thicknesses (below).*

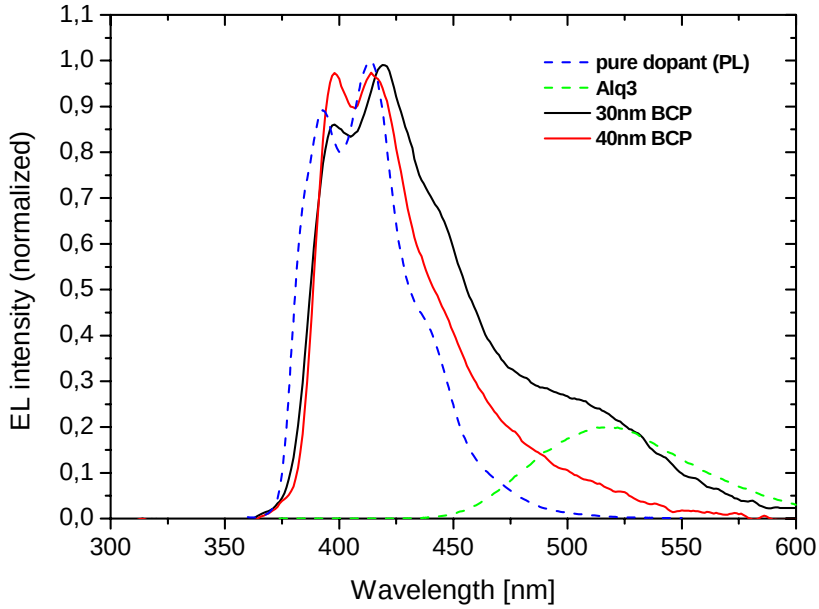

Figure 7. *EL spectra of the OLEDs with TCTA matrix and different BCP blocking layer thicknesses. For comparison the PL spectrum of the pure bisindenocarbazole emitter is added (blue dashed curve). Device setup: ITO/PEDOT (40 nm)/TCTA:bisindenocarbazole (40 nm)/BCP (10, 20, 30 and 40 nm)/Alq_3 (40 nm)/LiF (1 nm)/Al (150 nm).*

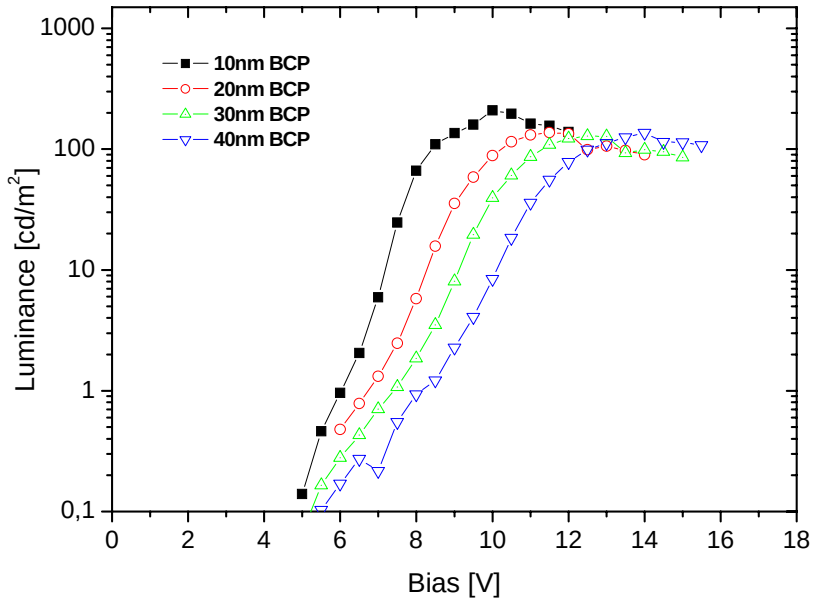

Figure 8. *Current-voltage characteristics of the OLEDs with TCTA matrix containing 1 % of the blue bisindenocarbazole as emitter. Device setup: ITO/PEDOT (40 nm)/TCTA:bisindeno-carbazole (40 nm)/BCP (10, 20, 30 and 40 nm)/Alq_3 (40 nm)/LiF (1 nm)/Al (150 nm).*

3. Conclusion

In this paper we present a new deep-blue fluorescent emitter for OLED applications. Three different host materials have been investigated together with the blue dye using doping concentrations of 1 % in all devices. The energy transfer from the host to the emitter was investigated by fluorescence spectroscopy and in the case of the CBP matrix, additionally by time resolved PL. The experiments proved an efficient energy transfer to the BIC 1 when CBP and TCTA were used as host materials. A combinatorial evaporation setup was used for the preparation of the OLEDs in order to dope the different host systems by co-evaporation of the guest material. Thus it was also possible to prepare step gradients of the hole blocking layers (BCP) in a single evaporation run. It was found that a pure, deep-blue emission at CIE coordinates of 0.19 and 0.17 can be obtained from the bisindenocarbazole emitter by using TCTA as host material at a BCP layer thickness of 40 nm. Luminance values of 200 cd/m^2 at a current density of 100 mA/cm^2 and a maximum luminance efficiency of 1.60 cd/A were obtained for the TCTA containing OLEDs. The turn on voltage is at 5 V. At driving voltages above 10 V the brightness runs into saturation what could be explained by the fact that the TCTA/emitter layer was solution processed and therefore no HTL could be used. Thus a huge mismatch of the HOMO energy levels of the ITO anode and the TCTA layer occurs and therefore an efficient charge carrier injection is no longer ensured. In future the TCTA/emitter layer should be prepared by evaporation in order to optimize the brightness of the LEDs.

Acknowledgements:
The authors would like to thank Ricardo Tubino and Jakub Mezyk (Universita Milano-Bicocca, Italy) for the time resolved PL measurements and the fruitful discussions. We are grateful to the Deutsche Forschungsgemeinschaft (SFB 481) and the BMBF (POLITAG program) for financial support.

4. Experimental

The time resolved photoluminescence (PL) measurements were performed by exciting the samples with third harmonic of a mode-locked Ti:Sapphire laser. The pulse duration time was 200 fs, and excitation wavelength $\lambda_{exc} = 279$ nm. The PL signal was temporally analyzed using a Hamamatsu streak camera. The measurements were carried out at room temperature under helium atmosphere.

For the OLED preparation, the ITO substrates were pre-cleaned with isopropanol before they were etched in oxygen plasma. A fresh PEDOT:PSS suspension (Baytron P VP.Al 4083, H. C. Starck) was diluted with 30 % of demineralized water and filtered through a 0.45 μm Teflon filter before it was spin-coated on top of the ITO substrate at 3000 rpm. Afterwards the films were baked at 150 °C for 5 min. The average PEDOT/PSS film thickness was 40 nm. The other thin films were fabricated by thermal vacuum deposition in a vacuum of less than 5×10^{-6} torr. In all devices single layers of electron and hole transport materials were evaporated with different thicknesses for comparison. The blue emitting layer was produced by the co-evaporation of the bisindenocarbazole emitter together with the different host materials in molar ratios of 1 %. The thickness of the films were recorded by quartz crystal monitors, which were calibrated with a Dektak profilometer. By using a combinatorial evaporation setup it was possible to prepare the hole blocking layers with different thicknesses in a single step, as described in the reference.[14] Finally 1 nm of LiF is evaporated as electron injection layer followed by a 150 nm thick aluminium layer as cathode. The device affords a light-emitting are of ~10 mm^2. The current-voltage (*I*-*V*) curves were characterized with a Keithley 2400 source measurement unit. The brightness was measured with a Konica Minolta luminance meter LS-100. The electroluminescence as well as the fluorescence spectra were taken with a Shimadzu spectrofluoro-photometer RF-5301PC. The CIE coordinates were measured with a Minolta chroma meter CS-100.

5. Literature

[1] Tang, C. W., VanSlyke, S. A., *Appl. Phys. Lett.*, **1987**, *51*, 913-915.

[2] Kido, J., Ikeda, W., Kimura, M., Nagai, K., *Jpn. J. Appl. Phys., Part 2*, **1996**, *35*, L394-L396.

[3] Montes, V. A., Li, G., Pohl, R., Shinar, J., Anzenbacher, P., Jr., *Adv. Mater*, **2004**, *16*, 2001-2003.

[4] Baldo, M. A., O'Brien, D. F., You, Y., Shoustikov, A., Sibley, S., Thompson, M. E., Forrest, S. R., *Nature*, **1998**, *395*, 151-154.

[5] Kawamura, Y., Goushi, K., Brooks, J., Brown, J. J., Sasabe, H., Adachi, C., *Appl. Phys. Lett.*, **2005**, *86*, 0711041-0711043.

[6] Shi, J., Tang, C. W., *Appl. Phys. Lett.*, **2002**, *80*, 3201.

[7] Hosokawa, C., Higashi, H., Nakamura, H., Kusumoto, T., *Appl. Phys. Lett.*, **1995**, *67*, 3853.

[8] Kulkarni, A. P., Gifford, A. P., Tonzola, C. J., Jenekhe, S. A., *Appl. Phys. Lett.*, **2005**, *86*, 611061-0611063.

[9] Tokito, S., Iijima, T., Suzuri, Y., Kita, H., Tsuzuki, T., Sato, F., *Appl. Phys. Lett.*, **2003**, *83*, 569-571.

[10] Tseng, R. J., Chiechi, R. C., Wudl, F., Yang, Y., *Appl. Phys. Lett.*, **2006**, *88*, 0935121-0935123.

[11] Sonntag, M., Strohriegl, P., *Tetrahedron*, **2006**, *62*, 8103-8108.

[12] Kwong, R. C., Nugent, M. R., Michalski, L., Ngo, T., Rajan, K., Tung, Y.-J., Weaver, M. S., Zhou, T. X., Hack, M., Thompson, M. E., Forrest, S. R., Brown, J. J., *Appl. Phys. Lett.*, **2002**, *81*, 162-164.

[13] Holmes, R. J., Forrest, S. R., Tung, Y. J., Kwong, R. C., Brown, J. J., Garon, S., Thompson, M. E., *Appl. Phys. Lett.*, **2003**, *82*, 2422-2424.

[14] Thelakkat, M., Schmitz, C., Neuber, C., Schmidt, H.-W., *Macromol. Rapid Commun.*, **2004**, *25*, 204-223.

Contributions to Conferences

Apart from the publications which are part of this thesis I gave contributions to the followingconferences:

Oral presentations:

Sonntag, M.
"New Carbazole Containing Materials for Organic Electronics"
Organic Electronic Summer School, Transport in carbon based conjugated materials, Fertilia (Sardinien), June 2005

Since my work was sponsored by the BMBF (POLITAG and OPAL project) and the European Union (EUROFET Network), I gave several talks on different project meetings all over Europe during the last years.

Poster presentations:

M. Sonntag, D. Hanft, P. Strohriegl
„New Carbazole Based Molecules for OFET Applications"
Fachgruppentagung makromolekulare Chemie der GDCh, Düsseldorf, March 2004

M. Sonntag, D. Hanft, P. Strohriegl
„New Carbazole Based Molecules for OFET Applications"
Winterschool on organic electronics (OEWS '04), Planneralm (Austria), March 2004

M. Sonntag, P. Strohriegl
"Novel Aromatic Amines for OFET Applications"
EUROFET mid term meeting, Strasbourg, September 2004

M. Sonntag, P. Strohriegl
„Novel Carbazole Based Materials for Optoelectronic Applications“
EUROFET meeting, ETH Zürich, March 2005

M. Sonntag, P. Strohriegl
“New Aromatic Amine Based Materials for Organic Electronics”
Organic Electronic Summer School, Transport in carbon based conjugated materials, Fertilia (Sardinien), June 2005

M. Sonntag, P. Strohriegl
“New Aromatic Amine Based Materials for Organic Electronics”
BASF International Summercourse, Ludwigshafen, July 2005

M. Sonntag, P. Strohriegl
“New Carbazole Containing Materials for Organic Electronics”
Bayreuther Polymer & Materials Research Symposium (BPS), Bayreuth, September 2005

Erklärung

Hiermit erkläre ich, dass ich die vorliegende Arbeit selbstständig verfasst und keine anderen als die von mir angegebenen Quellen und Hilfsmittel verwendet habe.

Ferner erkläre ich, daß ich weder anderweitig mit oder ohne Erfolg versucht habe, diese Dissertation einzureichen, noch eine gleichartige Doktorprüfung an einer anderen Hochschule endgültig nicht bestanden habe.

Bayreuth, 20. November 2006

Martin Sonntag